

مجلة

كلية المصطفى الجامعة

مجلة علمية محكمة نصف سنوية

تعنى بالدراسات والبحوث العلمية والإنسانية

العدد الخاص بالمؤتمر العلمي الدولي الخامس المدمج

(دور المؤسسات الحكومية وغير الحكومية في صناعة المستقبل

- رؤية واقعية في التغيير والإصلاح)

٢١-٢٢/آيار/٢٠٢٢

الرقم الدولي : ISSN2522-3097

Website: almustafauniversity.edu.iq

E-mail: info@almustafauniversity.edu.iq



وزارة التعليم العالي والبحث العلمي
كلية المصطفى الجامعة

وقائع المؤتمر العلمي الدولي الخامس المدمج

قال تعالى :

وَقُلْ اَعْمَلُوا فَسَيَرَى اللّٰهُ عَمَلَكُمْ وَرَسُولُهُ وَالْمُؤْمِنُونَ

برعاية معالي وزير التعليم العالي والبحث العلمي

(أ.د. نبيل كاظم عبد الصاحب) المحترم

وتحت شعار (دور المؤسسات الحكومية وغير الحكومية في صناعة المستقبل- رؤية واقعية في التغيير والإصلاح)

تقيم كلية المصطفى الجامعة مؤتمرها العلمي الدولي الخامس المدمج وذلك على قاعة فندق المنصور ميليا في تمام الساعة التاسعة من صباح يومي

السبت والاحد الموافق ٢١-٢٢/آيار/٢٠٢٢

هيئة التحرير:

- | | |
|--------------------------|--------------------------------|
| رئيساً | ١- أ.د هادي حسن جاسم |
| عضواً | ٢- أ.د سالم علي عباس |
| عضواً | ٣- أ.م.د عبد الأمير عبد العزيز |
| عضواً | ٤- أ.م.د علي عبد الرسول حمودي |
| عضواً | ٥- أ.م.د سهير إبراهيم حاجم |
| عضواً | ٦- أ.م.د خالد علي عبيد |
| عضواً | ٧- أ.م.د. أحمد زيدان محمد |
| عضواً | ٨- أ.م.د. أحمد طارق نعمان |
| عضواً | ٩- م.م. اسراء جواد كاظم |
| التصميم الداخلي والاعلام | ١٠- السيدة ايمان ليث اكرم |

اللجنة التحضيرية للمؤتمر :

- | | |
|----------------|----------------------------|
| / رئيساً | - د. خالد علي عبيد |
| / عضواً | - أ.د. أحمد ياسين عبد علي |
| / عضواً | - أ.د. قتيبة عباس حمد |
| / عضواً | - د. حسام ضياء كامل |
| / عضواً | - م.م. حسين قتيخان منسي |
| / عضواً | - أ.م.د.مكي مهدي عبد الحسن |
| / عضواً | - م.د. جمال كامل خضير |
| / عضواً | - د. علي حسين علي |
| / عضواً | - د. زياد طارق عبد الله |
| / عضواً | - م.م. إياد عبود عبد الحسن |
| / عضواً | - م.م. لمياء غاوي فجر |
| / عضواً | - م.م. مهند حسين سلمان |
| / عضواً | - م.م. عمر واثق طه |
| / عضواً | - م.م. اسراء جواد كاظم |
| / عضواً | - م.د.محمد عبد جواد كاظم |
| / عضواً | - م.م. طه رعد خليل |
| / عضواً | - م.م. منعم حسين علي |
| / عضواً | - الاستاذ مرتضى هادي عبد |
| / عضواً | - م.د.معتز محمد غازي |
| / المعلوماتية | - السيدة إيمان ليث أكرم |
| / مسؤول إعلامي | - الأستاذ حاتم المسعودي |

اللجنة العلمية للمؤتمر :

- أ.د. هادي حسن جاسم / عميد كلية المصطفى الجامعة
- أ.د. عبد جواد كاظم / عميد كلية النور الجامعة
- أ.د. مازن سمير الحكيم / عميد كلية الحكمة الجامعة
- أ.د. حيدر فخري هادي / عميد كلية بغداد للعلوم الطبية
- أ.د. أسامة سلمان التماري / كلية النور الجامعة
- أ.د. طلال خليفة سلمان / جامعة بغداد
- أ.د. حسن فاضل زعين / كلية المصطفى الجامعة
- أ.د. سالم علي عباس / كلية المصطفى الجامعة
- أ.د. ماجد صخي جابر / الجامعة التكنولوجية
- أ.د. نضال عبد الواحد علي / كلية المصطفى الجامعة
- أ.م.د. أحمد زيدان محمد / جامعة بغداد
- أ.م.د. سهير إبراهيم حاجم / كلية المصطفى الجامعة
- أ.م.د. أحمد طارق نعمان / كلية المصطفى الجامعة
- أ.م.د. علي عبد الرسول حمودي / كلية المصطفى الجامعة
- أ.م.د. عبد الأئمه بركة علي / كلية المصطفى الجامعة
- م.د. رائد كاظم محمد جواد / الجامعة المستنصرية / كلية الهندسة

قواعد النشر في المجلة

- ١- تخصص المجلة بنشر البحوث ذات التخصصات العلمية والإنسانية .
- ٢- تعرض البحوث المقدمة للمجلة على هيئة التحرير؛ لبيان ملاءمتها ويحق لهيئة التحرير أن تعتذر عن قبول البحث .
- ٣- يتم عرض البحث مسبقاً على لجنة السلامة اللغوية ولجنة السلامة الفكرية بالنسبة للتخصصات الإنسانية قبل إرسال البحث إلى التحكيم العلمي .
- ٤- تلتزم هيئة التحرير بإرسال البحوث إلى خبراء علميين من الاختصاص نفسه عدد (٢) وفي حالة الرفض من أحدهم يرسل إلى خبير ثالث لغرض الترجيح .
- ٥- تلتزم هيئة التحرير بعدم الكشف عن أسماء المحكّمين ، لضمان سرية التحكيم و لرفع، الرصانة العلمية وكذلك تكون المعلومات الخاصة بهوية الباحث في الصفحة الأولى من البحث فقط . وأن يلتزم الباحث بعدم الإشارة إلى هويته أو مكان عمله في ثنايا البحث .
- ٦- تكون حقوق الطبع للبحث ملكاً للمجلة عند قبوله للنشر، ولا يحق النقل والاقْتباس عنه إلا بعد الإشارة إلى المجلة .
- ٧- لا يجوز نشر أكثر من بحث للباحث في العدد الواحد .
- ٨- تحتفظ هيئة التحرير بحق أولوية النشر للبحوث مع مراعاة التنويع في النشر بحسب المحاور المعتمدة .
- ٩- ما ينشر في المجلة من بحوث ودراسات تعبّر عن رأي أصحابها ولا تعبر بالضرورة عن وجهة نظر هيئة تحرير المجلة أو وجهة نظر الكلية .

شروط النشر :

- ١- أن لا يكون البحث مشاركاً في مؤتمر أو ندوة علمية سابقاً أو مقمداً للنشر في مجلة علمية أخرى .
- ٢- يقدم البحث على قرص مدمج مع نسخة ورقية أو يرسل على البريد الإلكتروني: info@almustafauniversity.edu.iq
- ٣- أن لا يزيد عدد صفحات البحث عن ٣٠ صفحة .
- ٤- أن لا يزيد عدد المشتركين على ثلاثة باحثين في البحث الواحد .
- ٥- يطبع البحث على ورق (A4) ونوع الخط (Simplified Arabic) بالنسبة للبحوث باللغة العربية و(Times New Roman) بالنسبة للبحوث باللغة الانكليزية ويكون حجم الخط (١٤) للمتن والهامش (١٢) .

حقوق الطبع محفوظة لكلية المصطفى الجامعة

رقم الإيداع في دار الكتب والوثائق ببغداد : ٢٢٤٨ لسنة ٢٠١٧

اهداف المؤتمر :

- ١-تفعيل دور المؤسسات الحكومية وغير الحكومية في تقويم وتصحيح الواقع العراقي المتمثل بالجوانب السياسية والقانونية والاقتصادية .
- ٢-ايجاد الوسائل والسبل الكفيلة بتحقيق التكامل المنشود بين المؤسسات الحكومية وبين المؤسسات غير الحكومية في المجالات كافة .
- ٣-تشجيع المؤسسات كافة للانخراط في خدمة المجتمع وتقديم الخدمات والمتطلبات الكفيلة بتحقيق رفاهية افضل لافراد المجتمع .
- ٤-تفعيل وتشجيع القطاع الخاص لاذن دوره في عملية الاصلاح والتغيير والدفع بعجلة التقدم الاقتصادي .
- ٥-بيان دور المؤسسات الحكومية في الدفع بعملية الاصلاح والتغيير في المجالات كافة .
- ٦-اقتراح التشريعات والقوانين اللازمة ورفعها للجهات ذات العلاقة لاعتمادها واقرارها لغرض تحقيق متطلبات التغيير والاصلاح بشكل ينسجم مع طموحات افراد المجتمع العراقي .

محاور المؤتمر:

- محور الدراسات الطبية
- محور الدراسات الهندسية
- محور الدراسات الاقتصادية والإدارية
- محور الدراسات الإنسانية والتربوية
- محور دراسات العلوم الصرفة
- محور الدراسات الزراعية

كلمة المؤتمر:

بسم الله الرحمن الرحيم

والصلاة والسلام على اشرف خلق الله نبينا محمد وعلى آله المنتجبين واصحابه الغر
الميامين

السيد ممثل وزير التعليم العالي الدكتور المحترم

السادة رؤساء الجامعات وعمداء الكليات المحترمون

السادة الحضور من الباحثين والضيوف الكرام المحترمون مع حفظ المقامات والالقباب

السلام عليكم ورحمة الله وبركاته

ان التجديد العلمي يشكل عنصراً اساسياً في تطوير وبناء المجتمعات وتعد العملية التعليمية
ركناً اساسياً في هذا البناء ، اذا تساهم وبشكل فعال في تحقيق التنمية بكافة اشكالها ، سواء
كانت اقتصادية او بشرية او اجتماعية ، وعلى هذا الاساس فان الحرص على رصانة العملية
التعليمية يصب بالاساس على تطوير المجتمع وتاهيله لمواجهة متطلبات الحياة .

ومن هذا المنطق فقد سعت كلية المصطفى الجامعة وكلية النور الجامعة ان يكون من اهم
خطواتها هو تطوير الدور العلمي والمعرفي واكساب الطلبة المهارات النظرية والعملية
الحديثة ، وذلك باستخدام اساليب تعليمية متقدمة وضمن منهاج علمي رصين مع المحافظة
على التقاليد الجامعية والقيم التي تحفظ اصول العلم وتاريخه اذا بذلت جهوداً حثيثة من اجل
الارتقاء العلمي والريادة لرفع كفاءته الاساتذة والطلبة اسهاماً من الكلية في رفق سوق العمل
باحياجاته من الاختصاصات كافة . وقد تم استحداث عدد من الاقسام العلمية ضمن المعايير
المحلية والدولية التي يتطلبها سوق العمل كما سعت الكليتين المصطفى الجامعة و النور
الجامعة للحصول على مراتب علمية عالية وفق تصانيف الجودة المحلية والعالمية.

ولأجل المساهمة في معالجة المشكلات التي تواجه بلدنا العزيز عقد في الكليتين مؤتمرات
علمية عديدة محلية ودولية سلطت فيها الضوء على تحديد اهم المعوقات وتحديد طرق
واساليب معالجتها باسلوب علمي اعتمدت فيها البحوث العلمية التي قدمت في هذه المؤتمرات
واستكمالاً لهذه المسيرة العلمية جاء مؤتمرنا العلمي الدولي الخامس الموسوم (دور
المؤسسات الحكومية وغير الحكومية في صناعة المستقبل ، رؤية واقعية في التغيير

والاصلاح) وقد عقدنا مؤتمرا هذا ليكون منارا في التاكيد على اهمية المسؤولية المشتركة التي تقع على عاتق القطاع العام والقطاع الخاص في صناعة مستقبل مشرق للاجيال القادمة في بناء عراقنا العزيز.

وقد كان عدد البحوث المقبولة في المؤتمر اكثر من تسعون بحثا علميا في مختلف الاختصاصات والتي نامل ان تسهم في بناء عراق الرفاهية والتقدم .

وفي الختام نتقدم بالشكر والعرفان لجميع الحضور الكريم والباحثين والعاملين الذين اسهموا في انجاح هذا المؤتمر والسلام عليكم ورحمة الله وبركاته .

أ.د. هادي حسن جاسم

عميد كلية المصطفى الجامعة

ورئيس المؤتمر

منهاج المؤتمر العلمي الدولي الخامس

(دور المؤسسات الحكومية وغير الحكومية في صناعة المستقبل - رؤية واقعية في التغيير والإصلاح)

اليوم الاول السبت الموافق ٢٠٢٢/٥/٢١

ت	المنهاج	الوقت	الملاحظات
	ترحيب بالحضور الكرام	٩:٣٠	
١	النشيد الوطني	٩:٣٥	
٢	تلاوة أي من الذكر الحكيم	٩:٤٠	
٣	كلمة اللجنة العلمية	٩:٤٥	
٤	كلمة وزارة التعليم العالي والبحث العلمي	٩:٥٥	
٥	فيلم وثائقي عن كليتي المصطفى و النسور	١٠:٠٥	
			رئيس الجلسة أ.د. طلال خليفة العبيدي
٦	الجلسة الافتتاحية	١٠:٢٠	
			المحاضرين: د. احمد العباسي د. حسن المسعودي
٧	توزيع الدروع والشهادات	١٠:٤٥	
٨	فطور صباحي	١١:٠٠	
٩	معرض مشاريع التخرج ومعرض التشكيلي الفني	١١:٣٠	

منهاج المؤتمر

قاعة قرطبة - فندق المنصور ميليا

السبت ٢٠٢٢/٥/٢١ الساعة ١١:٤٥ ص

محور الدراسات الطبية	الجلسة الاولى
مقرر الجلسة أ.م.د. علاء كمال عبدالقادر	رئيس الجلسة أ.م.د. عمر جعفر عبدالحسن
عنوان البحث	اسم الباحث
دور الذكاء الاستراتيجي وانعكاسه على الفحص الضريبي للمكلفين في صناعة المستقبل	أ.م. فيصل سرحان عبود العزاوي مدرس سالي ابراهيم احمد
القطاع الخاص في العراق بين الية السوق وتدخل الدولة	أ.م.د حسين علي عبد أ.م.د علي عبودي نعمة م.م حيدر محمد كريم
دراسة تحليلية لتداعيات جائحة كوفيد- ١٩ على بعض المؤشرات الاقتصادية في العراق	م. د. فيصل غازي فيصل
مسؤولية الادارة العامة عن اعمالها التنفيذية	م.د علي حسين علي
أثر مبادرات النشاطات المجتمعية والانسانية في دعم النشاطات الاقتصادية- دراسة تحليلية في البنك (المركزي العراقي (٢٠١٥-٢٠٢١	د. مصطفى محمد ابراهيم م.م دنيا عامر عبد الامير

منهاج المؤتمر

الجلسة الاولى قاعة الدكتور غنية خماس الساعة ٩:٠٠ الى ١٠:١٥

اليوم الثاني ٢٠٢٢/٥/٢٢

الجلسة الاولى محور الدراسات الهندسية والعلمية		
مقرر الجلسة	رئيس الجلسة	
عنوان البحث	مكان الانتساب	اسم الباحث
A New 4-D Hyper Chaotic System: Design and Analysis	Computer Science Department, Mustansiriyah University	Sadiq A. Mehdi Anwar A. Hattab Huda R. Shakir
Analysis of Novel Five-Dimension Hyper Chaotic System	Computer Science Department College of Education, Mustansiriyah University,	Sarah S. Ahmed Sadiq A. Mehdi
Design of an unusual matching unit for a specific frequency band application	Al-Nisour University College, Baghdad, Iraq Computer Engineering techniques Department	Taha Raad Al-Shaikhli Jamal kamil Alrudaini, Ahmed Raed Al-Tameemi
تكنولوجيا التعليم الالكتروني في ظل مجتمع المعرفة: دراسة وصفية وتطبيقية	كلية النصور الجامعة	أ.م. رجاء جاسم محمد د. جمال كامل الرديني سرى خليل ابراهيم
Design and Implementation Cybersecurity Computing Architecture using for Better Throughput on FPGA	Al Nisour University College, Department of Computer Engineering Techniques,	Nada Qasim Mohammed Qasim Mohammed Hussein Maki Mahdi Abdulhasan Abdullah Ridha Faisal
Transmission Efficacy of Offset Pulse Position Modulation by Using Reed Solomon and LDPC	Middle Technical University, Electrical Engineering Technical College, Baghdad, Iraq	Ahmed Hasan Salman Mohamed Ibrahim Shuja'a Basman M. Al-Nedawe
Semigroup Based Ordinary Differential Equation Solution	Computer Engineering Techniques Al-Nisour University College	Ali Abdul Kadhum Ruhaima Dunya Mohee Hayder Jamal Kamil Kh. Abbas

Essentially Semismall Quasi-Dedekind modules and nonsingular modules	Computer Engineering, Al-mansur University College College of Education for pure science, Diyala University College of Computer science and Mathematics, Kufa University	Zahraa jawad kadhim Mukdad Qaess Hussain Heyam Khazaal Alkhayyat
New approach for image steganography	University of Al- Mustansiriyah, Iraq- Baghdad-Palestine Street	Ahmed A. Mohammed¹ Iman A. Saad² Hussein A. Hllal³
تفضيل الاختبار الالكتروني على التقليدي في مادة الحاسوب متوسطة نجلة للبنين انموذجاً	وزارة التربية، مديرية تربية بغداد الكرخ الثالثة/ ثانوية الشهيد أبو مهدي المهندس	م. م. اسراء حسين عبد الله

منهاج المؤتمر

الجلسة الثانية قاعة الدكتور غنية خماس الساعة ١٠:١٥ الى ١١:٣٠

اليوم الثاني ٢٠٢٢/٥/٢٢

الجلسة الثانية محور الدراسات الهندسية والعلمية		
مقرر الجلسة	رئيس الجلسة	
عنوان البحث	مكان الانتساب	اسم الباحث
A new approach for biodiesel production using heterogeneous catalyst	University of Baghdad/ Al-Khwarizmi College of Engineering/ Biochemical Engineering Dept	Alaa Kareem Mohammed Zahraa A. Alkhafaje sraa M. Rashid Yasmeen Salih Mahdi
Examination Applying ISO 9000 in Iraqi Construction Industry	College of education for girls, University of Thi-Qar	Noralhuda M. Azize
Effectiveness improvement of offset pulse position modulation system using reed-Solomon codes	Middle Technical University, Electrical Engineering Technical College, Baghdad, Iraq Middle Technical University, Technical Institute of Baquba, Diyala, Iraq	Ahmed H. Albatooosh Mohamed Ibrahim Shuja'a Basman M. Al-Nedawe
دور الذكاء الإستراتيجي وإنعكسه على الفحص الضريبي للمكافين في صناعة المستقبل رؤية واقعية في التغيير والإصلاح	جامعة ديالى كلية الإدارة والاقتصاد جامعة التقنية الوسطى كلية التقنية الإدارية	Asaad Sasaa Agrab ¹ , Abdalameer Zamil Latif ² . Ghaith hakim malik ³
Different Parameters Influence on Electrocoagulation Process	Chemical Engineering Department ,College of Engineering, University of Babylon	Abbas Salim ^a , Tahseen Ali Al-Hattab ^b , Huda Saeed Al-Barakat ^c

ديكور التصميم الداخلي و تحقيق المتعة الحسية للمتلقي	قسم التصميم الداخلي / العمارة و التصميم/ جامعة الشرق الاوسط عمان- الاردن	د. زينب عبد الباقي عبد العلي
Synthesis and Applications of (UPE/SiC) anti-Corrosion Nanocomposite Coating for Oil steel pipes	AL-Karkh University of Science, College of Energy and Environment Science ^{1,3} AL-Karkh University of Science, College of Science ²	Mohammed O. Kadhim ¹ Fadhil K. Farhan ² Faez Salim Abed ³
Enhancing the electrical conductivity and mechanical properties of the PVA electrospun polymeric film by adding a Silver nanoparticles	Al-mustafa University collage_ Dept. of Building and Cons. Engineering Technique	Shafaq Y. Abd ^{1,a}
STUDY AND OPTIMIZATION OF ELECTRO-FENTON TECHNOLOGY TO REDUCE	Chemical Engineering Department, College of Engineering, University of Baghdad	Rowaida N. Abbas^a and Ammar S. Abbas^b
PREDICTION ON THE CONDUCTION TO HEAT TRANSFER FOR PLANE-CHANNEL OF COMPLEX GEOMETRY	University of Thi-qar- College of engineering- Department of Petroleum and Gas engineering;	R.SHAKIER

منهاج المؤتمر

الجلسة الاولى قاعة الدكتور نهاد محمد عبد الوهاب الساعة ٩:٠٠ الى ١٠:١٥

اليوم الثاني ٢٠٢٢/٥/٢٢

الجلسة الاولى محور العلوم الانسانية		
مقرر الجلسة	رئيس الجلسة	
عنوان البحث	مكان الانتساب	اسم الباحث
التقاؤل غير الواقعي لدى الطلبة	كلية المصطفى الجامعة كلية التربية للبنات/جامعة بغداد	م.م. رسل ربيع زرع الله ا.م.د. أسماء عبدالحسين محمد
حقوق الانسان قبل ظهور الحماية الدستورية	قسم القانون - كلية النور الجامعة	م.م حيان ابراهيم حيدر الخياط
دور الاعلام التربوي في تحقيق الأمن النفسي الأسري		فاطمة محمد محمد طاهر شبيري
تنمية السياحة البيئية في هور الحمار والحويزة ، بالاستفادة من التجربة الإيرانية في تنمية الأهوار	جامعة البصرة/مركز دراسات البصرة والخليج العربي	أ.م.د. حسين قاسم محمد فرج الياسري
رؤية جغرافية في التخطيط التنموي المستدام للأحواض المائية الموسمية -أحواض شرق محافظة واسط وميسان (انموذجاً)	قسم الجغرافية/كلية التربية الأساسية/جامعتواسط مديرية تربية واسط/وزارة التربية الشركة العامة لموانئ العراق/وزارة النقل	أ.م.د. اباد عبد علي سلمان الشمري م.م.ناطق هاشم طوفان الشمري د. حسين كاظم عبد الحسين
التربية والتعليم في الإسلام		م. م. فاطمة حسين كاظم
الابعاد النظرية للمحاسبة الادارية البيئية ودورها في تخفيض التكاليف وتحقيق استدامة المنتج	جامعة بغداد /كلية الادارة والاقتصاد الجمهورية العراقية	الاستاذ الدكتور منال جبار سرور
حرفة الرعي في بلدية القبة- ليبيا خلال الفترة 2019/12/25) الي 2020/12/31)	جامعة درنة / فرع القبة قسم الجغرافيا - كلية الآداب	زهير محمد عبدالعاطي مسعود
دور المعلم في تعزيز الأمن الفكري	وزارة التربية، مديرية تربية بغداد الكرخ	م. د. جنان حسين علي م.د. مريم مجيد عبد الله

تأثير جودة الخدمة في تحسين عناصر التنمية السياحية دراسة تحليلية من وجهة نظر مديري الفنادق والاماكن السياحية في كربلاء	الجامعة المستنصرية / كلية العلوم جامعة كربلاء – كلية العلوم السياحية كلية الامام الاعظم الجامعة	م. محمد ثامر علي البياتي م. حيدر جابر جاسم الغيلاني م.م. مصطفى خضير حسين
---	---	--

منهاج المؤتمر

الجلسة الثانية قاعة الدكتور نهاد محمد عبد الوهاب الساعة ١٥:١٠ الى ١١:٣٠

اليوم الثاني ٢٠٢٢/٥/٢٢

الجلسة الثانية محور العلوم الانسانية		
مقرر الجلسة	رئيس الجلسة	
عنوان البحث	مكان الانتساب	اسم الباحث
دور المشاركة المجتمعية في صناعة المستقبل الجمعيات الأهلية النسائية العراقية انموذجاً		دكتورة فاطمة محمد محمد طاهر شبيري
تأثير الامتحان و التصحيح الالكتروني على التفكير وراء المعرفي لطلبة الدراسات العليا	كلية التربية البدنية وعلوم الرياضة / الجامعة المستنصرية	الأستاذ الدكتور ماهر محمد عواد العامري
واقع تطبيق مبادئ الحوكمة المصرفية في مصرف التنمية الدولي	معاون مدير البنك المركزي العراقي / بغداد	خالد زيدان عبدالهادي
دور المرأة في السلطة التشريعية في العراق	كلية القانون والعلوم السياسية / قسم العلوم السياسية	نور جتين شوكت
الضرر المباشر والعوامل المؤثرة في التعويض	قسم القانون / كلية النور الجامعة	م.م علي داود علي
نمط التعلم المفضل لدى طلاب كلية التربية البدنية وعلوم الرياضة في جامعة القاسم الخضراء وعلاقته بمتغيري الجنس واليد المستخدمة	جامعة القاسم الخضراء/كلية التربية البدنية وعلوم الرياضة	ا.م.د. بشار عبد اللطيف العبودي
أثر مبادرات النشاطات المجتمعية والإنسانية في دعم النشاطات الاقتصادية-		د. مصطفى محمد إبراهيم

اثر مواقع التواصل الاجتماعية بالمنظومة الثقافية والقيمية للشباب لتعزيز مفهوم الهوية الثقافية دراسة ميدانية	وزارة التربية -- المديرية العامة لتربية ديالى - قسم التعليم العام	د.حسين حسين زيدان د. هديل علي قاسم
دليل التنمية البشرية : الواقع ومؤشرات القياس " مع إشارة خاصة للعراق"	مركز دراسات البصرة والتربية قسم الدراسات الاجتماعية	أ.د. بشير هادي عودة الطائي
دور اصلاح الخدمة في معالجة سلوك شكوى الزبون (دراسة عملية في مصرف الرافدين في محافظة المثنى)	جامعة القادسية	أ.د. حسين علي عبدالرسول م. احمد منخي كشيبيش مرتضى طعمة سلطان

منهاج المؤتمر

الجلسة الاولى قاعة المؤتمرات الساعة ٩:٠٠ الى ١٠:١٥

اليوم الثاني ٢٠٢٢/٥/٢٢

الجلسة الاولى محور العلوم الطبية		
مقرر الجلسة	رئيس الجلسة	
عنوان البحث	مكان الانتساب	اسم الباحث
Assessment the influence of thyroid dysfunction on diagnostic type2 diabetes patients: Across sectional study	Osouledeen University college Baghdad	Mohammad Hasan Ali
Qualitative Detection of Staphylococcus aureus Enterotoxin in raw Iraqi milk	Department of Biology, College of Science, University of Babylon	Sura I. A. Jabuk
Allergens sensitization and Allergy modes among atopic diseases (Allergic rhinitis, Bronchial asthma and Atopic dermatitis) in Basrah province Through 2021-2022	Department of microbiology, College of medicine , University of Basrah Center of allergy and asthma diseases , basrah	Ihsan Edan Alsaimay Falih Hmood Mezban Hasan lateef jasim Abbas abduljabbar jerri Israa riyadh amer

	College of medicine , University of Basrah	
Detection and identification of bacterial species isolated from mobile phone among Al-Mustaqbal University College Community /Babil/Iraq	Dep. of Medical Physics , Al-Mustaqbal .University College, /Iraq Dep.of Dentistry\Iraq, Al-Mustaqbal University .College/Iraq Dep. of Medical physics /Iraq. Al-Mustaqbal .University college. /Iraq	Rawaa M. Mohammed¹, Mohammed F. Jubaz², Sara J.Ahmed³
دراسة التركيب الكيميائي لبذور الرمان وادخالها في اطالة العمر الخزن لاقراص البيروغ	قسم علوم الاغذية / كلية علوم الهندسة الزراعية / جامعة بغداد	ا.م.د.بيداء حافظ محمد ا.م.د. اشراق منير محمد علياء محسن غضبان
Practical Study of Some Antibiotics and Their Effect on Some Pathogenic Bacteria	Department of Biology; College of Science; Mustansiriyah University; Baghdad – Iraq, Department of Biology, Faculty of science and health, Koya University.	*Fatima Rammadan Abdul1, Maysoon K. Abbas2, Ihsan A. Raheem3 and Hanan T.subhi4
تحضير مصفوفات تراكيب أوكسيد الزنك النانوي على قواعد السيليكون بطريقة التحلل المائي الحراري	دائرة بحوث المواد- وزارة العلوم والتكنولوجيا ^{1,2} ³ جامعة الكرخ للعلوم / كلية علوم الطاقة والبيئة / قسم الطاقات المتجددة	محمد عبيد كاظم ³ محمد حسين علي ¹ علي جبر عداي ²
Spectrophotometric Determination of Lisinopril dihydrate using dye bleaching method in pure and pharmaceutical drugs	¹ Department of Chemistry, College of science , University of Mosul, Mosul, Iraq ² College of Agriculture and Forestry, university of Mosul, Iraq	Aws Maseer Nejres ^{1, a)} and Moath A. Najem ^{2, b)}
spectrophotometric of phenylpherine Hcl by oxidation and bleaching Alkali blue 6B	Department of Chemistry / College of Science University of Mosul, Mosul, Iraq	Ali M.Hussein ^{1a} and Nebbel S.Othman

Are COVID-19 infection and vaccination booster affecting ophthalmological infections	College of Medicine - of Basrah University Alshefaa general hospital - basrah Al-Mawani teaching hospital - Basrah	Ihasn E. AlSaimary Alzahraa Imad Hmood Imad H. AlMayah Alaa H. AlAsady
--	--	---

منهاج المؤتمر

الجلسة الثانية قاعة المؤتمرات الساعة ١٥:١٠ الى ٣٠:١١

اليوم الثاني ٢٠٢٢/٥/٢٢

الجلسة الثانية محور العلوم الطبية		
مقرر الجلسة	رئيس الجلسة	
عنوان البحث	مكان الانتساب	اسم الباحث
The side effects of shisha smoke on pregnant mice and their fetuses	Biology Department / College of Education for Pure Sciences / University of Mosul / Mosul / Iraq	Arwa Adress Alnuimy ¹ , Hani MallAlla Hamodi ²
دراسة تحليلية لتداعيات جانحة كوفيد-١٩ على بعض المؤشرات الاقتصادية في العراق	كلية جنات العراق للعلوم الإنسانية الاهلية	م. د. فيصل غازي فيصل
إصابة الرباط الصليبي الأمامي: والعودة إلى اللعب والاعتبارات الطويلة المدى	Al-Mustafa university collage	مرتضى هادي عبد
Assessment of the removal rate of bacterial biofilm or organic film simulating biofilm by a sodium hypochlorite irrigant delivered into flow cells	¹ Unit of Dentistry, Almustafa University College, Baghdad, Iraq.	Saifalarab Mohmmmed ¹
Effect of the Biological Drug Etanercept on levels of Interluekin 2, 17 in Psoriatic Patients	^{1,2} Department of Biology, College of Science, University of Baghdad, Baghdad,	Rasha Hussain Kuba ^{*1} , Ban Noori Al-Qadhi ² , and Ass. Prof. Dr. BasmanMedhat Fadheel ³

	Iraq ³ Department of Dermatology, College of Medicine, University of Baghdad, Baghdad, Iraq	
Evaluation of Salivary Profile among Adult Type 2 Diabetes Mellitus Patients	Mc.s in Oral Physiology, Dep. of Dentistry, Al-Mustaqbal University College/Iraq. Ph.D in Clinical Immunity and Microbiology , Dep. of Medical Physics , Al-Mustaqbal University college, /Iraq.	Mohammed F.Jubaz ¹ & Rawaa M. Mohammed ²
تحضير وتقييم فعالية المستخلص الكحولي من نبات الكرنب الهندي (اكليل الملك) كمبيد حشري فعال لحشرة الذباب الابيض	وزارة الصناعة والمعادن -هيئة البحث والتطوير الصناعي - مركز بحوث ابن البيطار كلية النور الجامعة -قسم الصيدلة	فلاح حسن أحميدي ^١ -فراس عزيز راهي ^٢ - فارس عبد الكاظم دخنه ^١ - عبد المجيد خطاب ^١ - وليد عبد الواحد حلو ^١ -سرى عدنان جابر
Knowledge regarding children's immunization among sample of Iraqi Mothers	*Middle Technical Univ., College of Health & Medical Technology; email: tabarknoori94@gmail.com ** Middle Technical Univ., College of Health & Medical Technology; email: prof.almzory@gmail.com ** Middle Technical Univ., College of Health & Medical Technology	Assistant Lecturer Tabarek A. Noori (MSc)* & Assistant Professor Khadija Shaban Hassan (MSc)** Zaman Jabbar Abd Al-Saied ***
Isolation of <i>Staphylococcus aureus</i> from gingivitis patients	Assistant lecturer of Department of medical laboratory tech, Al-Mustafa University College.	*Tuqa.A.KareemHameed **Wasan Q.Turki *** Noor A.Hanon

الفهرست

رقم الصفحة	البحوث	ت
المحور الهندسي		
٤	A New 4-D Hyper Chaotic System: Design and Analysis	١
١٨	A new approach for biodiesel production using heterogeneous catalyst	٢
٣٩	Design of an unusual matching unit for a specific frequency band application	٣
٤٩	Semigroup Based Ordinary Differential Equation Solution	٤
٦٠	Spectral features of the final Telecommunications Path devices	٥
٦٨	Effectiveness improvement of offset pulse position modulation system using reed-Solomon codes	٦
٨١	Design and Implementation Cybersecurity Computing Architecture using for Better Throughput on FPGA	٧
٩٧	Transmission Efficacy of Offset Pulse Position Modulation by Using Reed Solomon and LDPC	٨
١١٥	New approach for image steganography	٩
١٣٥	Advanced Seeded Region Growing for CBCT Image Reconstruction	١٠
١٥١	Some properties of complete intuitionistic fuzzy S-metric space	١١
١٧٠	A Double slot in a single Substrate Integrated Waveguide Antenna	١٢
١٧٨	Different Parameters Influence on Electrocoagulation Process	١٣
٢٠٢	Implementation of Digital Twin in Industrial 4.0 Technology	١٤
٢١٢	Enhancing the electrical conductivity and mechanical properties of the PVA electrospun polymeric film by adding a Silver nanoparticles	١٥
٢٣١	Software for teaching sign language based on image processing and machine learning	١٦

٢٤٠	The Role of Machine Learning Methods in Dealing with DDoS Attacks and Data Poisoning Cyberattacks	١٧
٢٥٦	STUDY AND OPTIMIZATION OF ELECTRO-FENTON TECHNOLOGY TO REDUCE COD IN REFINERY WASTEWATER USING MODIFIED ELECTRODES WITH PBO ₂ AND GRAPHENE BY THE TAGUCHI APPROACH	١٨
٢٨١	smart attendance student system using IoT RFID	١٩
٢٩٠	face recognition1 with A security system based on a neural network	٢٠
٢٩٧	Prediction on the Conduction to Heat Transfer for Plane-Channel of Complex Geometry	٢١
٣٠٧	Estimation of Heat Flow Properties on Inline-Channel Heat Sink	٢٢
٣١٩	Exploration of the General Algorithms and Standard Methods in TSP	٢٣
٣٣٥	Administrative creativity and its impact on improving employee performance (An exploratory study of the opinions of a sample of workers in the prefab factory / Kirkuk)	٢٤
٣٥٤	Calculating the slope in high-rise cylindrical and circular columns using the least squares correction method and producing a three-dimensional (3D) model.	٢٥



وزارة التعليم العالي والبحث العلمي
كلية المصطفى الجامعة

البحوث المشاركة في المؤتمر (المحور الهندسي)

ملاحظة: جميع البحوث خاضعة للاستلال الالكتروني

A New 4-D Hyper Chaotic System: Design and Analysis

Sadiq A. Mehdi ¹, Anwar A. Hattab ², and Huda R. Shakir ³

^{1,2,3} Computer Science Department, Mustansiriyah University -Iraq, Baghdad,
Iraq

sadiqmehdi71@uomustansiriyah.edu.iq¹

anwarabbas76@uomustansiriyah.edu.iq²

hudarashid@uomustansiriyah.edu.iq³

Abstract

In this study, a new four dimensional (4-D) hyper-chaotic system with ten positive parameters is introduced. The fundamental characteristics and dynamic behavior of the chaotic system are examined via equilibrium points, dissipativity, and the existence of a chaotic attractor, symmetry, Lyapunov exponents, and sensitivity to initial states. The result of the analysis shows that the new hyper-chaotic system include three-unstable equilibrium points, two non-negative Lyapunov exponents where the maximum Lyapunov exponents is 4.05761, and a Kaplan-Yorke dimension calculated as 3.06989, as well as the new system's waveform is non-periodic and very sensitive to the initial states. The novel system dynamics are simulated using the MATHEMATICA program.

Keywords: Hyper-chaotic, Four-dimensional, Waveform, Sensitivity to initial conditions, unstable.

1. Introduction

A non-linear dynamic system is known as a chaotic system [1], which has a number of feature like randomness, unpredictability, and sensitivity to initial states [2], [3]. Due to its chaotic characteristics, it is implemented in a wide variety of fields, like engineering science, lasers, encryption, mathematics, and biology [4], [5], [6]. Since Lorenz discovered the first chaotic attractor in 1963 while studying atmospheric convection [7], Several new chaotic systems have been suggested, including the Chen system, the Rössler system, and the Lü system [8], [9]. These systems are 3-D chaotic systems with one positive Lyapunov exponent. However, a hyper-chaotic system contains two or more positive Lyapunov exponents [10], and the dynamic behavior of a hyper-chaotic system is more complicated and difficult to predict [11], As a result, this problem can be addressed by utilizing higher-dimensional hyper-chaotic systems, which have increased unpredictability and randomness [12], [13], the hyper-chaotic system has been used in many fields, including information science, electronics, encryption, cryptosystems, physics, and secure communication [14]. In this study a new four-dimensional hyper-chaotic system is presented, and the dynamical behavior properties of the new system are investigated using Mathematica language.

2. Construction of New Four-dimensional Chaotic System

A mathematical model represents a novel four-dimensional autonomous system constructed via differential equation shown in Equation (1):

$$\begin{aligned} \frac{dx}{dt} &= -a x - b w + c y z + z e^y \\ \frac{dy}{dt} &= d y + e x - f x z - x e^z \\ \frac{dz}{dt} &= -g z + h x y \\ \frac{dw}{dt} &= -b w + i x z + j y z \end{aligned} \tag{1}$$

Where $x, y, z,$ and w represent the states of the system, $t \in \mathbb{R}$ and $a, b, c, d, e, f, g, h, i,$ and j are positive parameters of the system(1) shows a chaotic attractor in a new (4-D) chaotic system with parameter values of: $a=3.1, b=2.1, c=15.8, d=1.1, e=16.5, f=1.5, g=2.4, h=26.6, i=5.1,$ and $j=12.9,$ and the initial states of : $x(0)=0.2, y(0)=0.4, z(0)=1.5,$ and $w(0)=0.8.$ Figures1–8 illustrates the strange 3-D attractors of system (1), while Figures 9–16 show the strange 2-D attractors.

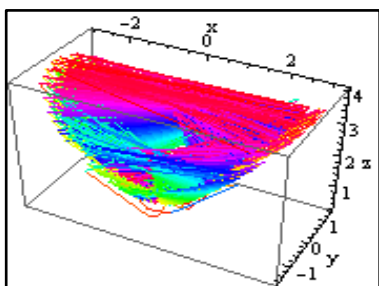


Figure (1): Phase portrait, in 3-D view (x-y-z)

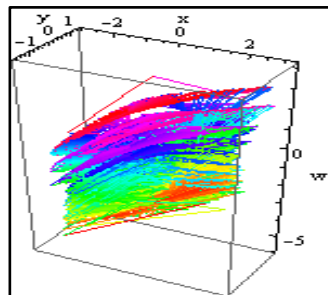


Figure (2): Phase portrait, in 3-D view (x-y-w)

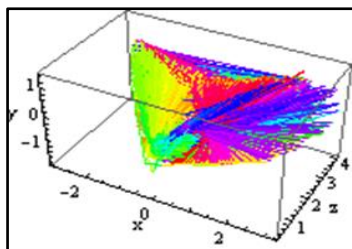


Figure (3): Phase portrait, in 3-D view (x-z-v)

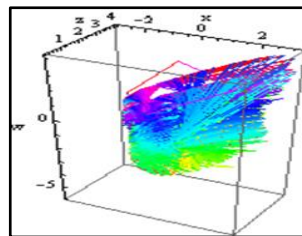


Figure (4): Phase portrait, in 3-D view (x-z-w)

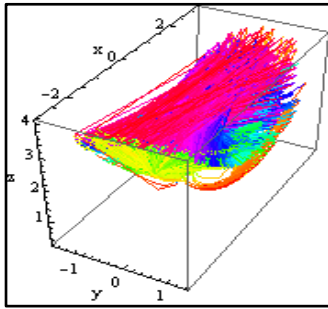


Figure (5): Phase portrait, in 3-D view (y-x-z)

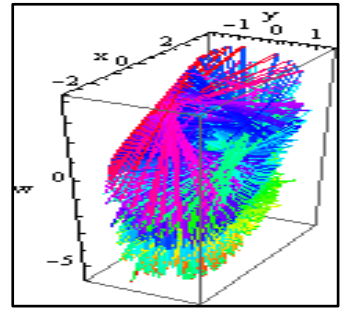


Figure (6): Phase portrait, in 3-D view (y-x-w)

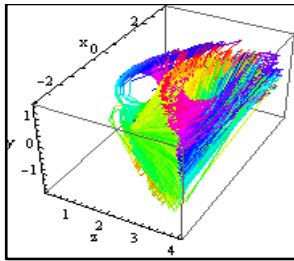


Figure (7): Phase portrait, in 3-D view (y-z-x)

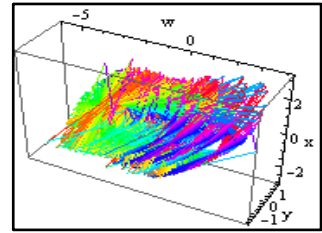


Figure (8): Phase portrait, in 3-D view (w-x-y)

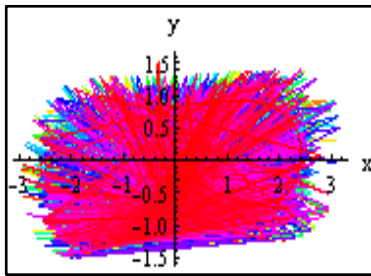


Figure (9): Phase portrait, in 2-D view (x-y)

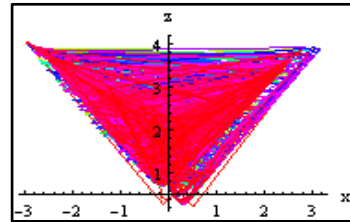


Figure (10): Phase portrait, in 2-D view (x-z)

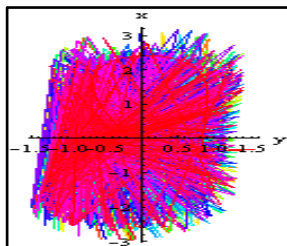


Figure (11): Phase portrait, in 2-D view (y-x)

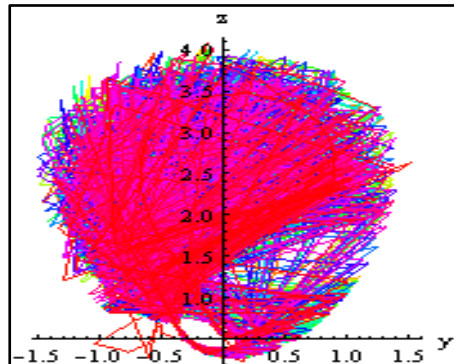


Figure (12): Phase portrait, in 2-D view (y-z)

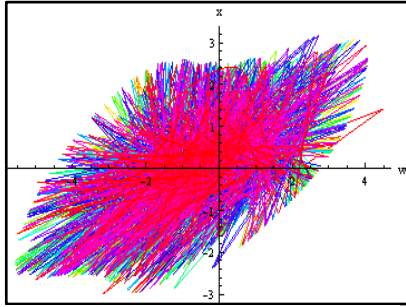


Figure (13): Phase portrait, in 2-D view (w-x)

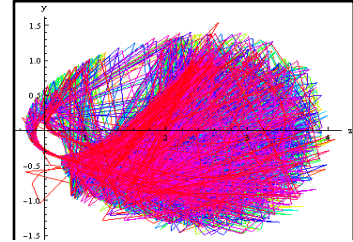


Figure (14): Phase portrait, in 2-D view (z-y)

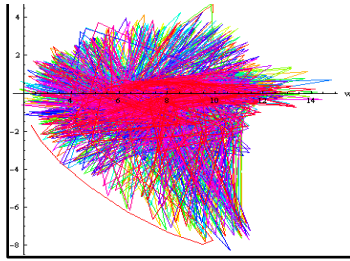


Figure (15): Phase portrait, in 2-D view (w-x)

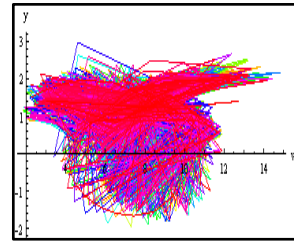


Figure (16): Phase portrait, in 2-D view (w-y)

3. Dynamic Analysis of New Chaotic System

The essential and complex dynamic behavior of the new system is investigated in this section and it has the following basic characteristics:

3.1. Dissipiativity

The system (1) can be described in vector formula as shown in equation (2):

$$f = \begin{cases} f_1 = \frac{dx}{dt} = -ax - bw + c y z + z e^y \\ f_2 = \frac{dy}{dt} = d y + e x - f x z - x e^z \\ f_3 = \frac{dz}{dt} = -g z + h x y \\ f_4 = \frac{dw}{dt} = -b w + i x z + j y z \end{cases} \quad (2)$$

Equation (3) illustrates the divergence of the vector field f on R4:

$$\nabla \cdot \mathbf{f} = \frac{\partial f_1}{\partial x} + \frac{\partial f_2}{\partial y} + \frac{\partial f_3}{\partial z} + \frac{\partial f_4}{\partial w} \quad (3)$$

Observe that $\nabla \cdot f$ indicates the average for which volumes vary under the flow Φ_t of f . Assume D is a smooth-boundary region in \mathbb{R}^4 , and assume $D(t) = \Phi_t(D)$, the image of D shown under Φ_t , and the time t of the flow of f . Also $V(t)$ represent the volume of $D(t)$. As a result of Liouville's theorem, we obtain:

$$\frac{dV}{dt} = \int_{D(t)} (\nabla \cdot f) dx dy dz dw \quad (4)$$

According to system (1), we obtained the following:

$$\nabla \cdot \mathbf{f} = \frac{\partial f_1}{\partial x} + \frac{\partial f_2}{\partial y} + \frac{\partial f_3}{\partial z} + \frac{\partial f_4}{\partial w} = -a+d-g-b < 0 \quad (5)$$

Because b and f constants are both positive.

Substituting equation (5) into equation (4) and simplifying it, we obtain:

$$\begin{aligned} \frac{dV}{dt} &= (-a + d - g - b) \int_{D(t)} dx dy dz dw dv du \\ &= (-a + d - g - b) V(t) \\ &= e^{-6.5} V(t) \end{aligned}$$

We get the unique solution by solving the first order linear differential equation, $V(t) = V(0) e^{(-a+d-g-b)t}$

$$= V(0) e^{-6.5t} \quad (6)$$

According to Equation (6), any volume $V(t)$ should drop exponentially quickly to zero over time. As a result, the dynamical system shown in (1) is a dissipative system. Because (1) is a dissipative system, all of its orbits are ultimately limited to a region of \mathbb{R}^4 with a volume of zero. As a result, asymptotic motion is settled on a system attractor (1).

3.2. Symmetry

When the coordinates $(x, y, z, \text{ and } w)$ are transformed into $(-x, -y, z, \text{ and } w)$, system (1) exhibits symmetry and invariance about the z -axis. The following illustrates the result:

$$x = -x, y = -y, z = -z, w = -w \quad (7)$$

So, we have:

$$-\frac{dx}{dt} = \frac{dx}{dt}, -\frac{dy}{dt} = \frac{dy}{dt}, \frac{dz}{dt} = \frac{dz}{dt}, \text{ and } \frac{dw}{dt} = \frac{dw}{dt} \quad (8)$$

According to Eq. (7) and Eq. (8), the result is obtained as follows:

$$\begin{aligned} -\frac{dx}{dt} &= ax + bw - cyz - ze^y \\ -\frac{dy}{dt} &= -dy - ex + f xz + xe^z \\ \frac{dz}{dt} &= -gz + hxy \\ -\frac{dw}{dt} &= +bw - ixz - jyz \end{aligned} \quad (9)$$

\Rightarrow

$$\begin{aligned} \frac{dx}{dt} &= -ax - bw + cyz + ze^y \\ \frac{dy}{dt} &= dy + ex - f xz - xe^z \\ \frac{dz}{dt} &= -gz + hxy \\ \frac{dw}{dt} &= -bw + ixz + jyz \end{aligned} \quad (10)$$

It's clear that the system (1) is constant by the coordinates transformation $(x, y, z, w) \rightarrow (-x, -y, z, w)$, which continues for every values of the parameters of the system. As a result, the system (1) exhibits rotation symmetry around the z -axis and w -axis, and any non-trivial trajectory of the system (1) should have a twin trajectory. The z -axis is also invariant under the system flow (1). As a result, this 4-D system may include symmetric pairings of attractors, like as strange attractors or limit cycles [15], [26].

3.3. Equilibrium Point

We could obtain system equilibrium (1) by solving nonlinear equations as follows:

$$\begin{aligned}
 0 &= -ax - bw + cyz + ze^y \\
 0 &= dy + ex - fxz - xe^z \\
 0 &= -gz + hxy \\
 0 &= -bw + ixz + jyz
 \end{aligned} \tag{11}$$

As a result, when the following system parameter values are selected: $a=3.1$, $b=2.1$, $c=15.8$, $d=1.1$, $e=16.5$, $f=1.5$, $g=2.4$, $h=26.6$, $i=5.1$, and $j=12.9$, three equilibrium points were found for the new hyperchaotic system as follows: $E_0\{x=0.484093, y=0.48761, z=2.6162, w=10.9121\}$,

Jacobian matrix of the system (1), let

$$f = \begin{cases} f_1 = \frac{dx}{dt} = -ax - bw + cyz + ze^y \\ f_2 = \frac{dy}{dt} = dy + ex - fxz - xe^z \\ f_3 = \frac{dz}{dt} = -gz + hxy \\ f_4 = \frac{dw}{dt} = -bw + ixz + jyz \end{cases} \tag{12}$$

$$J = \begin{bmatrix} \frac{\partial f_1}{\partial x} & \frac{\partial f_1}{\partial y} & \frac{\partial f_1}{\partial z} & \frac{\partial f_1}{\partial w} \\ \frac{\partial f_2}{\partial x} & \frac{\partial f_2}{\partial y} & \frac{\partial f_2}{\partial z} & \frac{\partial f_2}{\partial w} \\ \frac{\partial f_3}{\partial x} & \frac{\partial f_3}{\partial y} & \frac{\partial f_3}{\partial z} & \frac{\partial f_3}{\partial w} \\ \frac{\partial f_4}{\partial x} & \frac{\partial f_4}{\partial y} & \frac{\partial f_4}{\partial z} & \frac{\partial f_4}{\partial w} \end{bmatrix} \tag{13}$$

$$J = \begin{bmatrix} -a & cz + ze^y & cy + e^y & -b \\ e - fz - e^z & d & -fx - xe^z & 0 \\ hy & hx & -g & 0 \\ iz & jz & ix + jy & -b \end{bmatrix} \quad (14)$$

For equilibrium point $E_0\{x=0.484093, y=0.48761, z=2.6162, w=10.9121\}$, and $a=3.1, b=2.1, c=15.8, d=1.1, e=16.5, f=1.5, g=2.4, h=26.6, i=5.1$ and $j=12.9$.

Equation (15) shows the Jacobian matrix:

$$J = \begin{bmatrix} -3.1 & 15.8 * 2.6162 + 2.6162 * e^{0.48761} & 15.8 * 0.48761 + e^{0.48761} & -2.1 \\ 16.5 - 1.5 * 2.6162 & 1.1 & -16.5 * 0.484093 - 0.484093 * e^{2.6162} & 0 \\ 26.6 * 0.48761 & 26.6 * 0.484093 & -2.4 & 0 \\ 5.1 * 2.6162 & 12.9 * 2.6162 & 5.1 * 0.484093 + 12.9 * 0.48761 & -2.1 \end{bmatrix}$$

In order to get its eigenvalues, let $|\lambda I - J_0| = 0$, Therefore, the eigenvalues corresponding to the equilibrium $E_0(0.484093, 0.48761, 2.6162, 10.9121)$ are respectively obtained as follows: $\lambda_1 = 29.5015$, $\lambda_2 = -1.40835$, $\lambda_3 = 12.2049 + 9.81553 i$, $\lambda_4 = 12.2049 - 9.81553 i$.

Where i indicates the imaginary number unit. Therefore, at equilibrium point E_0 , the results display that λ_1 and λ_2 are a positive and negative real numbers, in addition, λ_3 and λ_4 becomes a pair of positive real-part complex conjugate eigenvalues. Therefore, equilibrium point E_0 is a saddle-focus point, so all of these equilibrium points are unstable. Hence, the hyperchaotic system is unstable [5], [17].

3.4. Lyapunov exponents and Lyapunov dimension

Calculating the Lyapunov exponent, according to nonlinear dynamical theory, is a quantitative measure of the sensitive dependency on the initial values. It's the average rate at which two adjacent trajectories diverge (or converge).

When the parameters of the system (1) are selected as: (a=3.1, b=2.1, c=15.8, d=1.1, e=16.5, f=1.5, g=2.4, h=26.6, i=5.1, and j=12.9), as well as the initial values as follows:

LE1= 4.05761, LE2= 0.347562, LE3= -3.94257 and LE4= -6.61896.

It could be seen that the maximum Lyapunov exponent is positive; pointing to that the system has chaotic properties. We see two positive Lyapunov exponent are LE1 and LE2, and the other two are negative As a result, the fractal dimension is a characteristic of chaos when the Kaplan-Yorke dimension is computed using Lyapunov exponents, and DKY is defined as follows [18]:

$$D_{KY} = j + \frac{1}{|L_{j+1}|} \sum_{i=1}^j L_i \quad (16)$$

Where J namely, is the first Lyapunov exponent, and j is the largest value of the i values that satisfy both $\sum_{i=1}^j L_i > 0$ and $\sum_{i=1}^{j+1} L_i < 0$ at the same time.

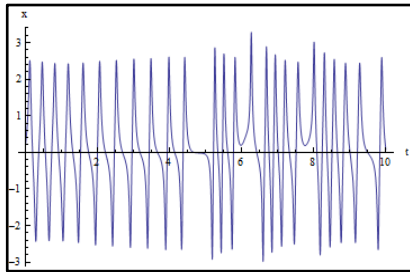
Lyapunov exponents may be used to show us that the L_i is in descending order, and DKY is our upper bound for system information dimension. For this new chaotic system, because the values of Lyapunov exponents is ten, so the j value is ten, and the Kaplan-Yorke dimension could be determined from the above because $L_1+L_2+ L_3 +L_4<0$ And $L_1+L_2+L_3>0$, the Lyapunov-dimension of a new chaotic system will be as follows:

$$\begin{aligned} D_{KY} &= j + \frac{1}{|L_{j+1}|} \sum_{i=1}^j L_i \\ D_{KY} &= 3 + \frac{1}{|L_{j+1}|} \sum_{i=1}^3 L_i = 3 + \frac{L_1+L_2+L_3}{L_4} \\ &= 3 + \frac{4.05761+0.347562-3.94257}{6.61891} \\ &= 3.06989 \end{aligned}$$

This means that the Lyapunov-dimension of system (1) is fractional, the novel system contains non-periodic orbits, and its neighboring paths diverge. Hence, the non-linear system is chaotic.

3.5. Waveform analysis

A chaotic system's waveform, as is well known, must be aperiodic. To show that the suggested system is chaotic, The time versus state plot derived from the MATHEMATICA simulation is shown in Figures (17–20). The time domain waveforms of $(x(t), y(t), z(t),$ and $w(t))$ are presented in Figures (17-20). The waveforms of $(x(t), y(t), z(t),$ and $w(t))$ are aperiodic. To distinguish between multiple periodic motions that exhibit complicated behavior and chaotic motions, the time domain waveform exhibits non-cyclical properties



Figure(17): Time versus x of the new chaotic system

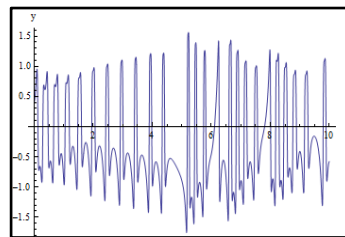
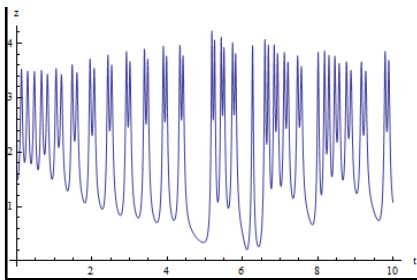
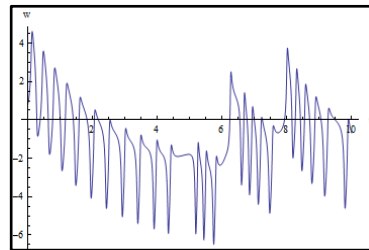


Figure (18):Time versus y of the new chaotic system



Figure(19):Time versus z of the new chaotic system

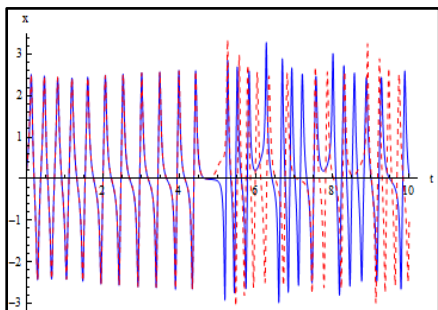


Figure(20):Time versus w of the new chaotic system

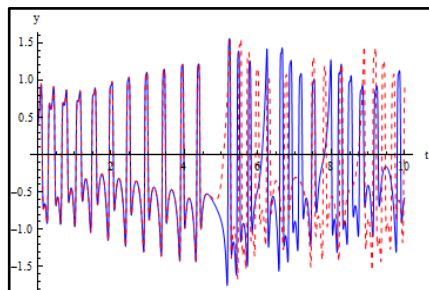
3.6. The Sensitivity to Initial Conditions

Long-term unpredictability is perhaps the most distinguishing aspect of a chaotic system. Basically, two varied initial states, regardless of their proximity, will eventually become significantly separated. Thus, for any initial state with a finite number of digits of precision, there will come a period in the future when no reliable predictions about the system's state can be made. The figures (21-24) demonstrate how the chaotic trajectories' evolution is highly sensitive to their initial value. The system's initial values are set of: $x(0)=0.2, y(0)=0.4, z(0)=1.5$ and $w(0)=0.8$.

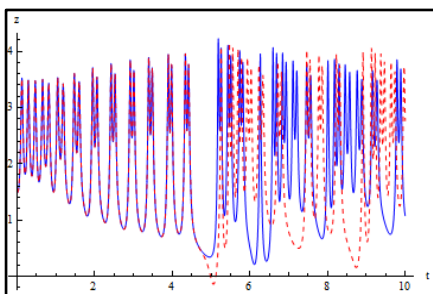
For the solid line and $x(0)=0.2$, $y(0)=0.4000000000000001$, $z(0)=1.5$ and $w(0)=0.8$, for the dashed line.



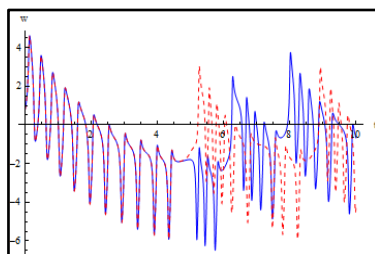
Figure(21): Sensitivity tests of the new system $x(t)$



Figure(22): Sensitivity tests of the new system $y(t)$



Figure(23): Sensitivity tests of the new system $z(t)$



Figure(24): Sensitivity tests of the new system $w(t)$

4. Conclusion

The essential properties and dynamical behavior of the chaotic system are analyzed to prove it is chaotic. Some of the basic characteristics of the system have been tested. The novel system exhibits chaotic behavior when the following parameters are selected: $(a=3.1, b=2.1, c=15.8, d=1.1, e=16.5, f=1.5, g=2.4, h=26.6, i=5.1, \text{ and } j=12.9)$, and initial conditions are set as: $x(0) = 0.2$, $y(0) = 0.4$, $z(0) = 1.5$, and $w(0) = 0.8$, Lyapunov The exponent values of the new system are: $LE1= 4.05761$, $LE2= 0.347562$, $LE3= -3.94257$, and $LE4 = -6.61896$, because it has two positive Lyapunov exponents, which means that the system is hyper chaotic. In addition, the new system includes three unstable equilibrium points, a fractal dimension of 3.06989, and a complicated chaotic attractor that is very sensitive to initial values. The new chaotic system can be used in many different applications, and it could also be used to encrypt information.

References

- [1] S. H. Yuningsih, Sukono, Kalfin, and A. T. Bon, "A new three-dimensional chaotic system with stable equilibrium and circuit design," *Proc. Int. Conf. Ind. Eng. Oper. Manag.*, no. 1963, pp. 3773–3779, 2021.
- [2] S. A. Mehdi and A. A. Kadhim, "Image Encryption Algorithm Based on a New Five Dimensional Hyperchaotic System and Sudoku Matrix," *Proc. 5th Int. Eng. Conf. IEC 2019*, pp. 188–193, 2019, doi: 10.1109/IEC47844.2019.8950560.
- [3] Q. Liu and L. Liu, "Color Image Encryption Algorithm Based on DNA Coding and Double Chaos System," *IEEE Access*, vol. 8, pp. 83596–83610, 2020, doi: 10.1109/ACCESS.2020.2991420.
- [4] C. H. Lien, S. Vaidyanathan, A. Sambas, S. Sampath, Sukono, and M. Mamat, "A new 3-D chaotic system with four quadratic nonlinear terms, its global chaos control via passive control method and circuit design," *IOP Conf. Ser. Mater. Sci. Eng.*, vol. 621, no. 1, 2019, doi: 10.1088/1757-899X/621/1/012013.
- [5] D. Lambić, "A new discrete-space chaotic map based on the multiplication of integer numbers and its application in S-box design," *Nonlinear Dyn.*, vol. 100, no. 1, pp. 699–711, 2020, doi: 10.1007/s11071-020-05503-y.
- [6] C. Ma, J. Mou, L. Xiong, S. Banerjee, T. Liu, and X. Han, "Dynamical analysis of a new chaotic system: asymmetric multistability, offset boosting control and circuit realization," *Nonlinear Dyn.*, vol. 103, no. 3, pp. 2867–2880, 2021, doi: 10.1007/s11071-021-06276-8.
- [7] F. Hannachi, "Analysis, dynamics and adaptive control synchronization of a novel chaotic 3-D system," *SN Appl. Sci.*, vol. 1, no. 2, 2019, doi: 10.1007/s42452-019-0175-3.
- [8] A. Sambas, M. Mamat, A. A. Arafa, G. M. Mahmoud, M. A. Mohamed, and W. S. M. Sanjaya, "A new chaotic system with line of equilibria: Dynamics, passive control and circuit design," *Int. J. Electr. Comput. Eng.*, vol. 9, no. 4, pp. 2336–2345, 2019, doi: 10.11591/ijece.v9i4.pp2365-2376.
- [9] C. K. V. V.-T. Pham, S. Vaidyanathan and S. J. T. Gotthans, "A Three-Dimensional Chaotic System with Square Equilibrium and No-Equilibrium," *Fract. Order Control Synchronization Chaotic Syst.*, pp. 1–877, 2017, doi: 10.1007/978-3-319-50249-6.
- [10] S. A. Mehdi and F. H. Abbood, "IMAGE ENCRYPTION BASED ON THE NOVEL 5D HYPER-CHAOTIC SYSTEM VIA IMPROVED AES ALGORITHM Sadiq," no. October 2020, 2018.
- [11] J. Zheng and L. F. Liu, "Novel image encryption by combining dynamic DNA sequence encryption and the improved 2D logistic sine map," *IET Image Process.*, vol. 14, no. 11, pp. 2310–2320, 2020, doi: 10.1049/iet-

- ipr.2019.1340.
- [12] S. E. El-Khamy and A. G. Mohamed, "An efficient DNA-inspired image encryption algorithm based on hyper-chaotic maps and wavelet fusion," *Multimed. Tools Appl.*, vol. 80, no. 15, pp. 23319–23335, 2021, doi: 10.1007/s11042-021-10527-6.
- [13] A. Khan and M. A. Bhat, "Hyper-chaotic analysis and adaptive multi-switching synchronization of a novel asymmetric non-linear dynamical system," *Int. J. Dyn. Control*, vol. 5, no. 4, pp. 1211–1221, 2017, doi: 10.1007/s40435-016-0274-6.
- [14] L. G. Dolvis, S. Vaidyanathan, K. Jacques, A. Sambas, Sukono, and M. Mamat, "A New 4-D Hyperchaotic System with Four-Scroll Hidden Attractor, Its Properties and Bifurcation Analysis," *IOP Conf. Ser. Mater. Sci. Eng.*, vol. 621, no. 1, 2019, doi: 10.1088/1757-899X/621/1/012014.
- [15] N. Wang, G. Zhang, L. Ren, and H. Bao, "Coexisting asymmetric behavior and free control in a simple 3-D chaotic system," *AEU - Int. J. Electron. Commun.*, vol. 122, p. 153234, 2020, doi: 10.1016/j.aeue.2020.153234.
- [16] S. Doubla Isaac, Z. T. Njitacke, and J. Kengne, "Effects of Low and High Neuron Activation Gradients on the Dynamics of a Simple 3D Hopfield Neural Network," *Int. J. Bifurc. Chaos*, vol. 30, no. 11, 2020, doi: 10.1142/S021812742050159X.
- [17] I. M. Batiha, R. B. Albadarneh, S. Momani, and I. H. Jebril, "Dynamics analysis of fractional-order Hopfield neural networks," *Int. J. Biomath.*, vol. 13, no. 8, pp. 1–17, 2020, doi: 10.1142/S1793524520500837.
- [18] W. San-Um and B. Srisuchinwong, "Highly complex chaotic system with piecewise linear nonlinearity and compound structures," *J. Comput.*, vol. 7, no. 4, pp. 1041–1047, 2012, doi: 10.4304/jcp.7.4.1041-1047.

A new approach for biodiesel production using heterogeneous catalyst

**Alaa Kareem Mohammed¹*, Zahraa A. Alkhafaje¹, Israa M. Rashid¹,
Yasmeen Salih Mahdi¹**

University of Baghdad/ Al-Khwarizmi College of Engineering/ ¹
Biochemical Engineering Dept.

Correspondence: dr.alaa@kecbu.uobaghdad.edu.iq; Tel.: *
009647718612291

Abstract: Biodiesel as an attractive energy source; a low-cost and green synthesis technique was utilized for biodiesel preparation via waste cooking oil methanolysis using waste snail shell derived catalyst. The heterogeneous alkaline catalyst was greenly synthesized from waste snail shells throughout a calcination process at different calcination time of (2-4) h and temperature of (750-950) °C. The catalyst was characterized for the best catalytic activity using XRD, BET, EDX, and FTIR. It was found that the optimum calcination conditions were 900°C, and 3.5 h, which resulted in 9.29 m²/g specific surface area and high catalytic activity. Then the transesterification of triglycerides was accomplished after studying the most affecting reaction variables, in designed experiments following central composite method, in the ranges of (10:1-30:1) MeOH: oil molar ratio, (3-11) wt% catalyst loading, (50-70) °C reaction temperature, and (2-6) h reaction time at five levels for each factor. The model optimization was set its parameters at 21.5 methanol molar ratio, 9.8 wt% catalyst loading, 4.8 h reaction time, and 62.2 °C reaction temperature, resulting in a mixture comprised of 95% esters content and 91 wt% yield of biodiesel product. Ensure the high potential of waste snail shells for use in the production of biodiesel.

Keywords: Transesterification reaction, Biodiesel production, Waste cooking oil, Green catalyst, Central composite Methodology.

1. Introduction

Biodiesel as a sustainable alternative energy source has received the attention and concerns for investigation and utilization in existing diesel engines [1], [2]. The manufacturing of biodiesel is generally accomplished by transesterification of triglycerides with short-chain alcohols in the presence of a suitable catalyst [3–6]. The production of biodiesel is restricted by both feedstock and catalyst availability [7], [8]. All vegetable oils and animal fats can be involved in the transesterification reaction but most of these refined vegetable oils are essential food chain constituents and their use for biodiesel synthesise is not preferred for competition with human food in addition to their high cost as they are refined oils [9], [10]. Consequently, non-edible oils or waste vegetable oils can successfully replace the high cost refined edible oils, waste frying oil appear as a premium feedstock for biodiesel preparation[11], [12]. The catalyzed transesterification reaction is usually accomplished using an alkaline catalyst, while the acid-catalyzed transesterification is not favorable due to long time and lower

conversion [13]. Many different types of alkaline catalysts are presented to mediate transesterification; homogeneous, or heterogeneous catalysts may be employed [14]. Each one has some merits and drawbacks to be considered in industrial production, started with the availability, activity, to the purification steps, and reusability access [15]. In general, the more desirable catalysts are heterogeneous alkaline, since they are widely available, separable, and easily recyclable [16]. Calcium oxide (CaO) shows good catalytic activity over other metal oxides in the production of biodiesel [17]. It can be derived from many different raw materials found in nature, such as waste eggshell, waste snail shell, waste seashell, animal bones, limestone, and many other sources based on calcium carbonate (CaCO₃) can be involved [18].

Chicken eggshell and dolomite solid catalyst were used to catalyze transesterification reaction [4], [18]. Another study used chicken bones derived catalyst to mediate transesterification reaction [19]. while Lasker et al (2018) prepared CaO catalyst from a waste snail shell for esters production from soybean oil [17]. The optimized reaction conditions for heterogeneous alkaline catalyzed methanolysis were studied by many researchers for high biodiesel yield and reported the best conditions in the range of (9:1-30:1) MeOH: oil molar ratio, (3-10) wt % loading of catalyst, (65-75) °C reaction temperature, and (1-8) h time of reaction [1], [19-22].

In a place where snails are used as a source of food, excessive quantities of depleted shells are emitted as waste which in turn resulted in a disturbed environment, therefore, the utilize of waste shells could develop large-scale production of biodiesel in such regions [17]. Therefore, the present work will investigate the potential of waste snail shells to catalyze the transesterification reaction of WCO with methanol targeted to produce biodiesel product.

2. Materials and Methods

2.1 Materials

The chemicals employed in this study were ethanol (Chem-Lab NV) 99.8%, methanol (Chem-Lab NV) 99.8%, KOH (Thomas Baker) 85%, phenolphthalein indicator (ph. ph), and methyl heptadecanoate (Sigma-Aldrich) 99.9%. whereas waste cooking oil and waste snail shells were collected locally.

2.2 Experimental methodology

2.2.1 Preparation and analysis of oil

The samples of waste cooking oil (WCO) were collected from local restaurants that are specifically waste sunflower oil (the most abundant oil locally) were initially purified from all waste insoluble particles via a filter paper (150 mm Ø), then dried at 120 °C for 6 h to remove water content. The WCO was identified by acid value of 4.05 mg KOH/g oil, the high acidity content was decreased to 0.95

mgKOH/g oil following the noncatalytic esterification procedure described in our previous work [23]. The collected WCO was analyzed for fatty acids composition by the technique of gas chromatography-mass spectrometry (GC-MS). The analyzed WCO was comprised of 78.85% linoleic acid, 10% oleic acid, 9.42% palmitic acid, and small amounts of docosapentaenoic, eicosenoic, and docosadienoic acids. The waste oil molecular weight was estimated using Eq. 1 and 2, where $M_{w_{av}}$ is the average fatty acids mixture molecular weight, f_i is the fatty acid mass fraction obtained from the analysis of GC-MS, M_{w_i} is the molecular weight of single fatty acid, and $M_{w_{oil}}$ is the estimated molecular weight of WCO [24]. The waste oil molecular weight was found to be 873.9 g/mol.

$$M_{w_{av}} = \frac{\sum f_i}{\sum \left(\frac{f_i}{M_{w_i}} \right)} \quad (1)$$

$$M_{w_{oil}} = 3 * M_{w_{av}} + 38.049 \quad (2)$$

2.2.2 Catalyst preparation and characterization

The waste snails were initially cleaned by washing with tap water several times, then boiled with distilled water for 1 h to remove all impurities of sand and organics. After that, it was dried for 6 h in an oven at 110 °C. The clean and completely dry snail shells were next crushed and pulverized in a grinder, then sieved at 180 µm mesh sieve and calcined under static air in a muffle furnace from (2-4) h calcination time, and (750-950) °C temperature range. After the calcination process, the prepared samples were stored immediately inside desiccator avoiding humidity and CO₂ interaction from the environment [17].

Several characterization methods were utilized to define the optimum calcination conditions. Starting with BET surface area analysis, followed by FTIR, besides to XRD, SEM, and EDX characterization analysis of the prepared snail shell catalyst.

2.2.3 Transesterification of WCO

The potential of prepared heterogeneous catalyst samples has been experimented in a transesterification reaction of WCO that was conducted by mixing 20 g of WCO with a designed amount of methanol and catalyst. The catalyst going on an activation step with methanol for 40 min stirring at 40 °C prior to oil addition. A rounded bottle 3-neck flask of 500 ml volume was used to carry out the reaction. Its three necks were connected to a reflex water-cooling condenser, thermocouple, and an overhead mixing agitator to provide the reaction an adequate mixing (the mixer was set at a constant mixing speed of 450 rpm), while the desired reaction temperature was maintained with the aid of heating mental.

2.3 Transesterification experimental design

Four variables at five levels were experimentally designed using central composite design (CCD) and studied to investigate the impact of reaction factors and their interactions at the heterogeneously catalyzed transesterification reaction of WCO with methanol [25], [26]. Statistica program (StatSoft USA 10, Inc.) experimental design software was used to design, analyze, and optimize, the affecting factors, as well as obtaining an empirical model representing the transesterification process using heterogeneous catalyst.

Table 1 presents the independent factors with their coded and actual levels selected for process optimization. The molar ratio of MeOH: oil (X_1), catalyst loading (X_2), reaction time (X_3), and reaction temperature (X_4) were used to optimize the dependent factor of reaction response fatty acid methyl ester% (FAME %) (X_5). The polynomial model in quadratic form is represented by Eq. 3 that is suggested based on analysis of variance (ANOVA) in coded factor terms, where; $b_0, b_1, b_2, \dots, b_n$ are constants [18].

$$X_5 = b_0 + b_1X_1 + b_2X_2 + \dots + b_nX_n + \sum b_{ik}X_iX_k + \sum b_{ii}X_i^2 \quad (3)$$

Table 1 independent parameters domain at the actual and coded levels

Independent factors	Symbol	Unit	Values of each variable				
			Coded value				
			$-\alpha$	-1	0	1	α
MeOH molar ratio	X_1	mol/mol	10	15	20	25	30
Catalyst loading	X_2	wt %	3	5	7	9	11
Reaction time	X_3	h	2	3	4	5	6
Reaction temperature	X_4	°C	50	55	60	65	70

2.4 Fatty acid methyl esters product analysis

After the transesterification reaction takes place and the time is finished, the mixture was moved to a separating funnel and left to settle overnight, three layers are formed, the upper layer (FAME) is separated off, dried from remaining methanol in an oven at 80 °C, then weighted and stored in a dark bottle for GC analysis. The GC analysis was accomplished following EN 14103 standard that is used to estimate chromatographically the methyl ester content (wt%) of biodiesel product originally obtained from vegetable oils that do not contain C_{17:0} (the used internal standard IS) in its composition (all vegetable oils). Equation 4 was employed to calculate the methyl esters content of the biodiesel product layer after transesterification process [27].

$$\text{Esters}\% = \frac{\sum A - A_{IS}}{A_{IS}} * \frac{(C_{IS} * V_{IS})}{m} * 100 \quad \dots (4)$$

Where V_{IS} : IS solution volume (ml), $\sum A$: total methyl esters peak area from C₁₄ to C_{24:1}, A_{IS} : IS peak area, C_{IS} : IS solution concentration (mg/ml), and m : biodiesel prepared sample mass (mg) [28].

3. Results

3.1 Catalyst characterization

The catalyst activity which is identified by its adsorption/desorption properties is enhanced at high specific surface area [8]. Therefore, the effect of calcination conditions was initially investigated for the best surface area, the temperature of calcination and time are significantly manipulating specific surface area and active sites of the prepared CaO catalyst as described in Figure 1. The specific surface area was found to be increased with the increase in calcination conditions due to the modification of sample composition during calcination. Gaseous CO₂ elimination at high calcination temperatures (750, 800, 850, 900, and 950 °C) causes the formation of pores at the catalyst surface [20]. Progressive increase in the surface area was observed at a calcination temperature of 750, 800, 850 °C for various calcination time without reaching the effective surface area, this is probably due to the decomposition of CaCO₃ into CaO is not complete yet, while the higher surface area was formed at 900 °C, 3.5 h when CaCO₃ was completely converted into CaO. However, prolonged heating did not result in higher surface area and lead to agglomeration in which the particles aggregate together and ending in sintered powder as it was observed at 950 °C. The obtained result is close to Lasker et al. (2018) [17] who obtained a close BET result (7 m²/g) of calcined snail shells at their optimized calcination conditions of 900 °C, 4 h, while

Nur Syazwani et al. [29] recorded the optimal surface area was only 3.88 m²/g for calcination conditions of 900 °C, 2 h.

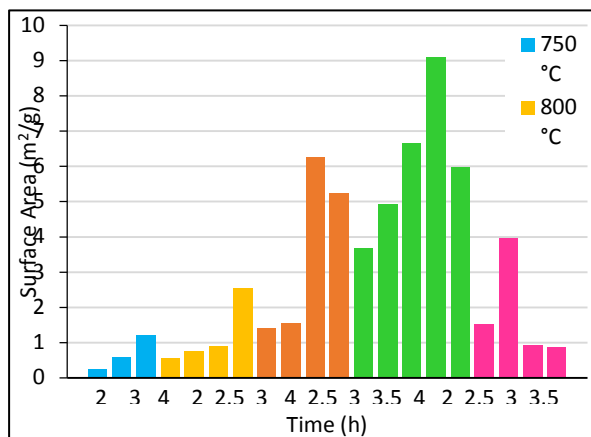


Figure 1. BET surface area analysis results for various calcination conditions of the

The raw and calcined snail shell XRD patterns are presented in Figure 2. It can be observed that the uncalcined snail shell revealed the crystalline nature of the catalyst and was dominated by the aragonite crystalline CaCO₃ phase. The intense peaks that belong to CaCO₃ can be observed at the strongest peaks of $2\theta = 27.26^\circ$, 33.18° , 36.19° , 37.93° , and 45.899° . CaCO₃ was subsequently converted into CaO with an increase in calcination temperature, and show the CaO patterns identification at 800, 850, and 900 °C this interesting result proves the transform of CaCO₃ into CaO for these degrees of calcination but the most affecting in transesterification reaction was 900 °C, this probably due to the elimination of gaseous CO₂ molecules is not accomplished and still adhere to the catalyst surface at a calcination temperature of 800 or 850 °C while completely eliminated at 900 °C, which was the end of CaCO₃ decomposition. The sharp and intense peaks of the calcined snail shell evidence the crystallinity structure of CaO catalyst. The obtained results are well matched with Laskar et al. (2018) [17] who reported similar XRD patterns for uncalcined and calcined snail shells, Boro et al. [30] also stated similar XRD patterns when calcined waste shells, whereas, Nur Syazwani et al. (2015) [29] found that all calcium carbonite was completely transformed into CaO during the calcination process of angel wing shells based on XRD analysis.

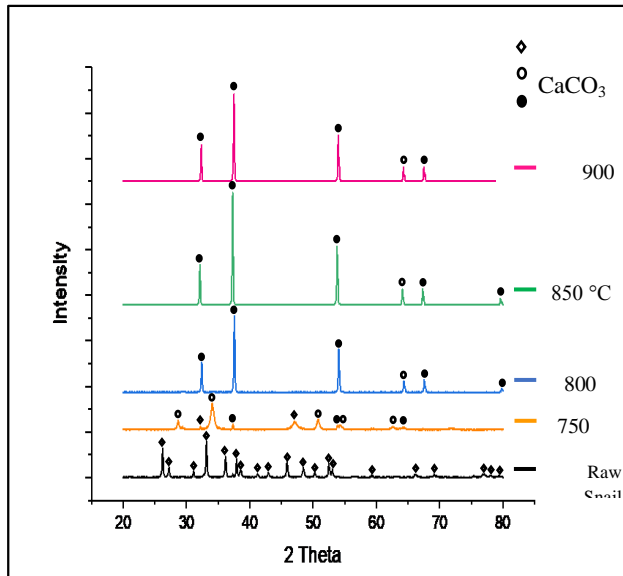
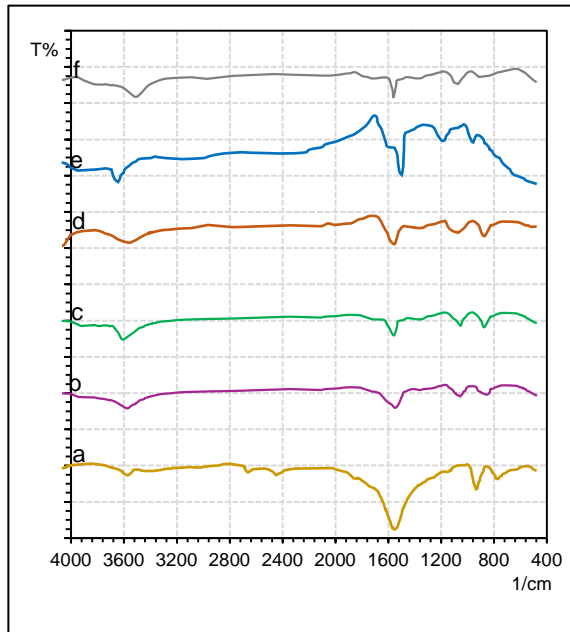


Figure 2. XRD patterns of raw and calcined snail shell powder

The raw and calcined snail shell powders were recorded with FTIR spectra to identify the absorption bands of presented functional groups. Figure 3 shows the FTIR patterns of the raw and calcined snail shell at different calcination temperatures. For raw snail shell in Figure 3 (a), the asymmetric molecules stretching of CO_3^{2-} is related to the major absorption band at 1480 cm^{-1} , while the observed absorption bands at 700 and 858 cm^{-1} are attributed to the in-plane and out-plane vibration modes band for CO_3^{2-} molecules, these peaks are attached to the existence of CaCO_3 in raw snail's powder. [31]. Whereas, the obtained peaks at 2375 and 2596 cm^{-1} are attributed to the organic matters presented in the shells [17], which completely disappeared after the calcination temperature of $750 \text{ }^\circ\text{C}$. The shift in the absorption bands that are ascribed with CO_3^{2-} to high energy in Figure 3 (b, c, d, e, and f) is attributed to the loss of carbonate ion and decrease in the mass of functional groups attached to CO_3^{2-} ions that conformed the decomposition of CaCO_3 to CaO throughout the calcination progress [18]. The presence of broad peaks at $3400\text{-}3600$ attributed to the formation of Ca(OH)_2 in the calcined samples and presence of humidity in the raw shells, this result demonstrates the tendency of highly active calcined snail shells to react with moisture content from the air and CO_2 molecules [11]. The obtained infrared spectra results agreed well with other research works [17], [18], [29].



at 3.5 h for **Figure 3.** FTIR results for (a) raw snail shell, as well as calcined snail shell (b) 750 °C, (c) 800 °C, (d) 850 °C, (e) 900 °C, and (f) 950 °C

Furthermore, the quantitative elemental composition analyzed by EDX confirmed the presence of calcium essential element at the appreciable quantity (74.9 wt%) (Figure 4), therefore, the snail shell is a worthy raw material in the catalyzed biodiesel production. Eventually, the snail shell derived catalyst shows its best catalytic activity at 900 °C and 3.5 h of calcination conditions.

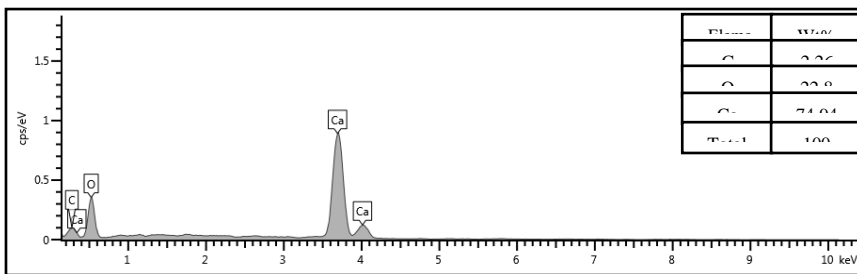


Figure 4. EDX elemental analysis of the prepared CaO catalyst

3.2 Design of experiments using CCD

The obtained experimental values of FAME content were compared with the predicted values estimated using CCD that is illustrated in Table. 2. The thirty design experiments ending in a close deviation of the predicted and actual response, that resulted in a coefficient of determination R_2 of 0.936 which approves the model accuracy, the closer R_2 value to unity, the model will be more accurate and gives predicted values closer to the actual response.

The model empirical equation is clearly presented in Eq. 5 that is representing the heterogeneously catalyzed transesterification reaction using waste snail shell derived catalyst.

$$\begin{aligned}
 X_5 &= -1037.6955 + 5.4907 X_1 + 7.8589 X_2 + 52.0691 X_3 + 29.3220 X_4 \\
 &+ 0.0026 X_1 X_2 - 0.0752 X_1 X_3 - 0.0190 X_1 X_4 - 0.2394 X_2 X_3 - 0.0395 X_2 X_4 \\
 &- 0.3008 X_3 X_4 - 0.0924 X_1^2 - 0.2201 X_2^2 - 3.0845 X_3^2 \\
 &- 0.2179 X_4^2
 \end{aligned}$$

Table 2 Transesterification reaction experimental design following CCD

run	MeOH molar ratio (X_1)	Cat. loading (wt%) (X_2)	Reaction time(h) (X_3)	Reaction temp.(°C) (X_4)	FAME% (wt%) (experimental)	FAME% (wt%) (predicted)	Residuals
1	15	5	3	55	57.750	56.848	0.902
2	25	5	3	55	62.458	62.256	0.202
3	15	9	3	55	66.124	64.548	1.576
4	25	9	3	55	70.983	70.062	0.921
5	15	5	5	55	74.932	73.900	1.032
6	25	5	5	55	77.750	77.805	-0.055
7	15	9	5	55	80.416	79.685	0.731
8	25	9	5	55	82.924	83.695	-0.771
9	15	5	3	65	78.924	74.777	4.147

10	25	5	3	65	81.083	78.290	2.793
11	15	9	3	65	85.052	80.895	4.157
12	25	9	3	65	86.858	84.514	2.344
13	15	5	5	65	88.416	85.813	2.603
14	25	5	5	65	89.624	87.823	1.801
15	15	9	5	65	93.192	90.017	3.175
16	25	9	5	65	94.753	92.132	2.621
17	10	7	4	60	70.991	76.413	-5.422
18	30	7	4	60	82.458	83.936	-1.478
19	20	3	4	60	76.625	79.887	-3.262
20	20	11	4	60	88.258	91.896	-3.638
21	20	7	2	60	59.958	64.740	-4.782
22	20	7	6	60	87.291	89.409	-2.118
23	20	7	4	50	55.625	54.443	1.182
24	20	7	4	70	72.725	80.807	-8.082
25	20	7	4	60	90.332	89.412	0.920
26	20	7	4	60	88.834	89.412	-0.578
27	20	7	4	60	89.572	89.412	0.160
28	20	7	4	60	89.362	89.412	-0.050
29	20	7	4	60	88.622	89.412	-0.790
30	20	7	4	60	89.752	89.412	0.340

3.3 ANOVA Results

The analysis of variance displayed in Table 3 records ANOVA evaluations. These results imply the effective parameters in the regression model by estimating its P-Value, it becomes significant when the P-Value is less than 0.05. Figure 5 also accommodates the significance estimation of variables in the linear, quadratic, and interacted forms, the Pareto chart of standardized effects clarifies the most significant from insignificant coefficients in the quadratic obtained model. It can

be observed that the most significant factor was the reaction temperature in its linear form (X_4), followed by the time of reaction (X_3), and subsequently by the quadratic reaction temperature term (X_4^2).

Table 3 ANOVA results of transesterification reaction findings

terms	SS	df	Mean square	F-value	P-value	Comments
X_1	84.893	1	84.893	5.58162	0.032085	significant
X_1^2	146.293	1	146.293	9.61857	0.007297	significant
X_2	216.324	1	216.324	14.22303	0.001848	significant
X_2^2	21.251	1	21.251	1.39721	0.255592	
X_3	912.889	1	912.889	60.02123	0.000001	significant
X_3^2	260.952	1	260.952	17.15727	0.000869	significant
X_4	1042.643	1	1042.643	68.55244	0.000001	significant
X_4^2	813.751	1	813.751	53.50304	0.000003	significant
$X_1 * X_2$	0.011	1	0.011	0.00072	0.978976	
$X_1 * X_3$	2.261	1	2.261	0.14863	0.705264	
$X_1 * X_4$	3.593	1	3.593	0.23623	0.633966	
$X_2 * X_3$	3.669	1	3.669	0.24124	0.630420	
$X_2 * X_4$	2.501	1	2.501	0.16445	0.690820	
$X_3 * X_4$	36.186	1	36.186	2.37920	0.143791	
Error	228.141	15	15.209			
Total SS	3542.781	29				

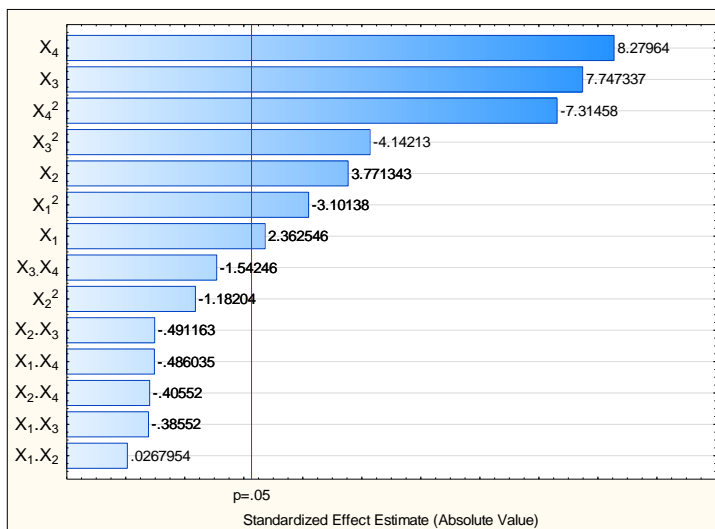


Figure 5. Standardized effects (Pareto chart) on system response of FAME %

3.4 Transesterification process optimization using CCD

The model accuracy was confirmed by transesterification variables optimization. The attained experimental value confirmed the validity of the model as shown in Table 4, the result was holding 0.499% error between the actual value obtained experimentally and the predicted data suggested by design software, the optimal FAME% was 95.1% which is corresponding to 90.94 wt% yield of biodiesel product.

Table 4 Transesterification reaction optimization following designed model

Process parameters (coded)	X_1	X_2	X_3	X_4	Predicted FAME %	Actual FAME %	Error %
Actual parameters	MeOH molar ratio	Catalyst (wt%)	loading	Reaction time (h)	Reaction temp. (°C)		
Optimal values	21.5	9.8	4.8	62.2	95.605	95.106	0.499

3.5. Transesterification parameters interactions

3.5.1. Effect of reaction temperature and time

The graphical results, shown in Figure 6 (a) and (b), present the 3D response surface and contours of the interactive effect of temperature and time. As supposed, the reaction conversion increases as the reaction temperature and time increase. Obviously can be observed from Figure 6 (a), the temperature is the most manipulating factor on transesterification, an increase in the reaction temperature resulted in high reaction conversion because the reaction molecules will be supplied with more energy, but a prolonged reaction temperature is not favorable. Temperature in the range of (60-66) °C is successive for reaction completion, while higher temperatures have a negative impact on transesterification, as the methanol molecules going to evaporate from the reaction mixture and resulted in an unstable molar ratio.

The effect of the reaction time is also of considerable effect as shown in Figure 6 (b). An increase in the methyl esters production is obtained at balanced conditions of time and temperature. (3.5-5.5) h reaction time is adequate, extended time do not help in increasing the conversion, because the reaction equilibrium is reached, temporarily minimize the range of temperature and time do not result in enhancing the biodiesel production.

The interactive reaction time and temperature are effective. From Figure 6 (b) at a time less than 3.5 h, the temperature is hardly affecting the reaction for high conversion, meanwhile, when the temperature is far from methanol boiling point, the reaction resulted in unfavorable conversion for all time range since the reaction requires its' enough time and appropriate temperature for completion.

The obtained results are well agreed with the literary works; the temperature was treated as an important variable to enhance biodiesel production [32], [33].

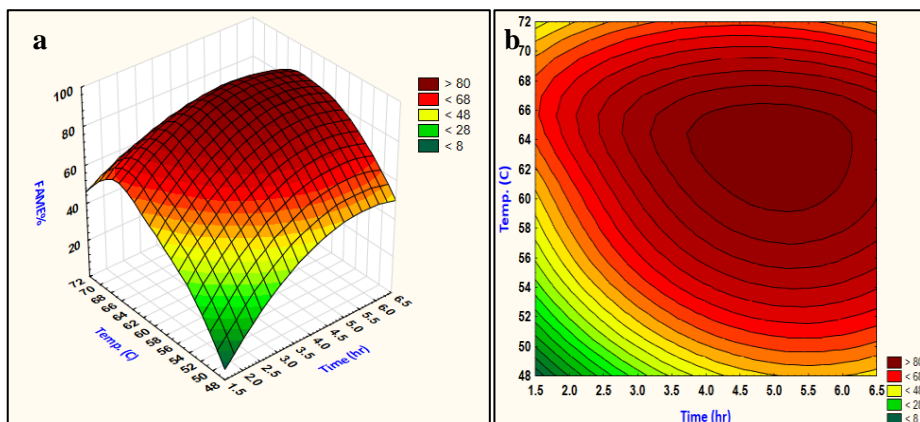


Figure 6. FAME 3D response as a function of reaction temperature and time (a) response surface (b) contour plot

3.5.2. Effect of molar ratio and catalyst loading

The effect of interactive molar ratio and catalyst loading is shown in Figure 7 (a) and (b) below. The 3D surface response in Figure 7 (a) indicated that the methyl esters production increases when increasing the methanol quantities as well as catalyst loading.

Excess methanol stoichiometry is used to shift the reaction toward completion, higher reaction conversion is promoted when a high alcohol ratio is employed, but excessive amounts of methanol makes glycerol recovery very difficult, and resulted in a dispersed glycerol layer with esters layer. Furthermore, a higher methanol molar ratio resulted in a dilution effect and cause the product of methyl esters to hold a large amount of alcohol which is unfavorable in the purification and recovery of the products [33]. Therefore, it is a fundamental variable in transesterification to be studied and optimized for certain production parameters of time, temperature, and catalyst concentration [33].

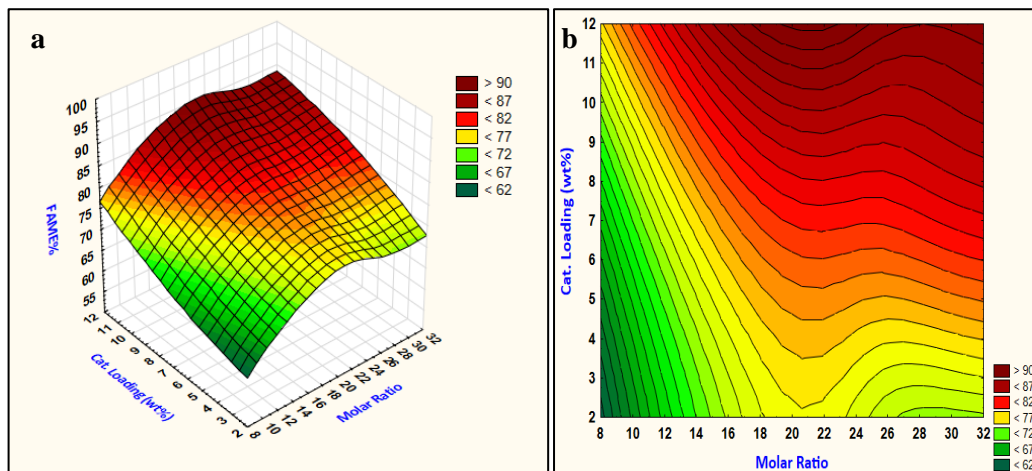


Figure 7. Reaction response of interactive molar ratio and catalyst loading (a) surface response and (b) contour plot

The catalyst concentration, on the other hand, is strongly affecting biodiesel production. When a high catalyst amount is applied, the reaction conversion increases but excessive addition resulted in the slurry formation and decreases the production of methyl esters as the viscosity of the mixture increases and leads to reduced diffusion between the reagents [18].

The interactive response of molar ratio and catalyst loading resulted in an interesting effect, the response shows that the molar ratio between (20-22) and catalyst loading in the range of (9-11) wt% resulted in maximum biodiesel production. As can be noticed from Figure 7 (b) the reaction conversion cannot be at a high level at less than 5.5 wt% catalyst loading and high molar ratio do not affect the reaction high conversion at these levels, otherwise, when the methanol molar ratio is less than 10 the catalyst loading has no change on the reaction conversion for high methyl esters production. These results agreed well with the reported results in other works [5], [18], [19].

4. Discussion

Authors should discuss the results and how they can be interpreted from the perspective of previous studies and of the working hypotheses. The findings and their implications should be discussed in the broadest context possible. Future research directions may also be highlighted.

5. Conclusions

The heterogeneously catalyzed transesterification reaction was statistically modeled and experimentally conducted using central composite design methodology. The catalytic activity of prepared CaO snail shell derived catalyst was investigated and exhibited an excellent catalytic activity in transesterification reaction at the optimized calcination conditions of 900 °C and 3.5 h. The synthesized catalyst was characterized by 9.29 m²/g specific surface area. Accordingly, the FAME product was obtained at high purity of 95% and biodiesel yield of 91% at the optimized reaction conditions of the molar ratio of 21.5:1 MeOH: oil, 9.8 wt% catalyst loading, 4.8 h reaction time, and 62.2 °C reaction temperature. The ANOVA study in transesterification reaction shows that the reaction temperature has the most significant effect on the reaction, followed by reaction time and catalyst loading, whereas, the molar ratio has the less significant effect from other reaction parameters in the studied range of transesterification conditions.

The low-grade biodiesel feedstocks specifically WCO and waste snail shell, were very adequate for biodiesel synthesis, and their employment could reduce the production cost, drop the struggle between food and fuel engineering, and develop a sustainable technology throughout recycling the wastes into a useful biodiesel product. Aid to improve citizens' awareness about the significance of recycling waste materials.

Acknowledgments: Special thanks and appreciation go to the department of biochemical engineering at AL Khwarizmi Engineering College in Baghdad University, for facilitating the accomplishment of this investigation.

Conflicts of Interest: The authors declare no conflict of interest. The funders had no role in the design of the study; in the collection, analyses, or interpretation of data; in the writing of the manuscript, or in the decision to publish the results.

References

- [1] A. Birla, B. Singh, S. N. Upadhyay, and Y. C. Sharma, "Kinetics studies of synthesis of biodiesel from waste frying oil using a heterogeneous catalyst derived from snail shell," *Bioresource Technology*, vol. 106, pp. 95–100, 2012, doi: 10.1016/j.biortech.2011.11.065.
- [2] J. L. Aleman-Ramirez, J. Moreira, S. Torres-Arellano, A. Longoria, P. U. Okoye, and P. J. Sebastian, "Preparation of a heterogeneous catalyst from moringa leaves as a sustainable precursor for biodiesel production," *Fuel*, vol. 284, no. August 2020, p. 118983, 2021, doi: 10.1016/j.fuel.2020.118983.
- [3] K. N. P. Rani, T. S. V. R. Neeharika, G. H. Vardhan, T. P. Kumar, and B.

- L. A. P. Devi, "The Kinetics of the Esterification of Free Fatty Acids in Jatropha Oil using Glycerol based Solid Acid Catalyst," *European Journal of Sustainable Development Research*, vol. 4, no. 2, pp. 1–11, 2020, doi: 10.29333/ejosdr/7594.
- [4] E. O. Ajala, M. A. Ajala, T. E. Odetoeye, F. A. Aderibigbe, H. O. Osanyinpeju, and M. A. Ayanshola, "Thermal modification of chicken eggshell as heterogeneous catalyst for palm kernel biodiesel production in an optimization process," *Biomass Conversion and Biorefinery*, 2020, doi: 10.1007/s13399-020-00636-x.
- [5] A. S. Yusuff and K. A. Bello, "Synthesis of fatty acid methyl ester via transesterification of waste frying oil by a zinc-modified pumice catalyst: Taguchi approach to parametric optimization," *Reaction Kinetics, Mechanisms and Catalysis*, vol. 128, no. 2, pp. 739–761, 2019, doi: 10.1007/s11144-019-01680-z.
- [6] F. Hassan, I. Aljbory, and T. Kassim, "An attempt to stimulate lipids for biodiesel production from locally isolated microalgae in Iraq," *Baghdad Sci J*, vol. 10, 2013, doi: 10.21123/bsj.10.1.97-108.
- [7] S. P. Silva, D. C. S. Sales, C. A. P. de Abreu, A. R. P. Schuler, and C. A. M. de Abreu, "Kinetics of the biphasic liquid–liquid transesterification of vegetable oils into biodiesel," *Reaction Kinetics, Mechanisms and Catalysis*, vol. 123, no. 2, pp. 529–542, 2017, doi: 10.1007/s11144-017-1322-8.
- [8] Y. C. Sharma, B. Singh, and S. N. Upadhyay, "Advancements in development and characterization of biodiesel: A review," *Fuel*, vol. 87, no. 12, pp. 2355–2373, 2008, doi: 10.1016/j.fuel.2008.01.014.
- [9] U. Kumar and P. Gupta, "Modeling and optimization of novel biodiesel production from non-edible oil with musa balbisiana root using hybrid response surface methodology along with african buffalo optimization," *Reaction Kinetics, Mechanisms and Catalysis*, vol. 130, no. 2, pp. 875–901, 2020, doi: 10.1007/s11144-020-01807-7.
- [10] R. Suresh, J. V. Antony, R. Vengalil, G. E. Kochimoolayil, and R. Joseph, "Esterification of free fatty acids in non- edible oils using partially sulfonated polystyrene for biodiesel feedstock," *Industrial Crops and Products*, vol. 95, pp. 66–74, 2017, doi: 10.1016/j.indcrop.2016.09.060.

- [11] S. E. Mahesh, A. Ramanathan, K. M. M. S. Begum, and A. Narayanan, "Biodiesel production from waste cooking oil using KBr impregnated CaO as catalyst," *Energy Conversion and Management*, vol. 91, pp. 442–450, 2015, doi: 10.1016/j.enconman.2014.12.031.
- [12] M. Afsharizadeh and M. Mohsennia, "Catalytic synthesis of biodiesel from waste cooking oil and corn oil over zirconia-based metal oxide nanocatalysts," *Reaction Kinetics, Mechanisms and Catalysis*, vol. 128, no. 1, pp. 443–459, 2019, doi: 10.1007/s11144-019-01622-9.
- [13] S. Sharma, V. Saxena, A. Baranwal, P. Chandra, and L. M. Pandey, "Engineered nanoporous materials mediated heterogeneous catalysts and their implications in biodiesel production," *Materials Science for Energy Technologies*, vol. 1, no. 1, pp. 11–21, 2018, doi: 10.1016/j.mset.2018.05.002.
- [14] A. H. Savameri, A. Izadbakhsh, and B. Zarenezhad, "Study of the performance of amino-functionalized ordered mesoporous carbon in the transesterification of soybean oil," *Reaction Kinetics, Mechanisms and Catalysis*, vol. 124, no. 1, pp. 247–264, 2017, doi: 10.1007/s11144-017-1333-5.
- [15] A. Navajas, I. Reyero, E. Jiménez-Barrera, F. Romero-Sarria, J. Llorca, and L. M. Gandía, "Catalytic performance of bulk and Al₂O₃-supported molybdenum oxide for the production of biodiesel from oil with high free fatty acids content," *Catalysts*, vol. 10, no. 2, pp. 1–14, 2020, doi: 10.3390/catal10020158.
- [16] S. Zhao *et al.*, "Experimental investigation on biodiesel production through transesterification promoted by the La-dolomite catalyst," *Fuel*, vol. 257, no. July, p. 116092, 2019, doi: 10.1016/j.fuel.2019.116092.
- [17] I. B. Laskar, K. Rajkumari, R. Gupta, S. Chatterjee, B. Paul, and L. Rokhum, "Waste snail shell derived heterogeneous catalyst for biodiesel production by the transesterification of soybean oil †," 2018, doi: 10.1039/c8ra02397b.
- [18] E. O. Ajala, M. A. Ajala, T. E. Odetoeye, and A. T. Okunlola, "Synthesis of solid catalyst from dolomite for biodiesel production using palm kernel oil in an optimization process by definitive screening design," *Brazilian Journal of*

Chemical Engineering, vol. 36, no. 2, pp. 979–994, 2019, doi: 10.1590/0104-6632.20190362s20180516.

[19] M. Farooq and A. Ramli, “Biodiesel production from low FFA waste cooking oil using heterogeneous catalyst derived from chicken bones,” *Renewable Energy*, vol. 76, pp. 362–368, 2015, doi: 10.1016/j.renene.2014.11.042.

[20] A. Buasri, N. Chaiyut, V. Loryuenyong, P. Worawanitchaphong, and S. Trongyong, “Calcium oxide derived from waste shells of mussel, cockle, and scallop as the heterogeneous catalyst for biodiesel production,” *The Scientific World Journal*, vol. 2013, 2013, doi: 10.1155/2013/460923.

[21] G. R. Moradi, M. Mohadesi, M. Ghanbari, M. J. Moradi, S. Hosseini, and Y. Davoodbeygi, “Kinetic comparison of two basic heterogenous catalysts obtained from sustainable resources for transesterification of waste cooking oil,” *Biofuel Research Journal*, vol. 2, no. 2, pp. 236–241, 2015, doi: 10.18331/BRJ2015.2.2.5.

[22] O. Ogunkunle, O. O. Oniya, and A. O. Adebayo, “Yield Response of Biodiesel Production from Heterogeneous and Homogeneous Catalysis of Milk Bush Seed (*Thevetia peruviana*) Oil ,” *Energy and Policy Research*, vol. 4, no. 1, pp. 21–28, 2017, doi: 10.1080/23815639.2017.1319772.

[23] Z. A. Alkhafaje, A. K. Mohammed, and I. M. Rashid, “Development of two-step noncatalytic esterification of waste cooking oil for biodiesel preparation,” *Reaction Kinetics, Mechanisms and Catalysis*, vol. 131, no. 2, pp. 645–659, 2020, doi: 10.1007/s11144-020-01873-x.

[24] A. Abdul, A. Budhwani, A. Maqbool, T. Hussain, and M. N. Syed, “Production of biodiesel by enzymatic transesterification of non-edible *Salvadora persica* (Pilu) oil and crude coconut oil in a solvent-free system,” doi: 10.1186/s40643-019-0275-3.

[25] S. V. Ghadge and H. Raheman, “Process optimization for biodiesel production from mahua (*Madhuca indica*) oil using response surface methodology,” *Bioresource technology*, vol. 97, no. 3, pp. 379–384, Feb. 2006, doi: 10.1016/j.biortech.2005.03.014.

[26] M. D. Souf, B. Ghobadian, G. Najaf, and S. M. Mousavi, “Optimization of

methyl ester production from waste cooking oil in a batch tri-orifice oscillatory baffled reactor,” *Fuel Processing Technology*, vol. 167, pp. 641–647, 2017.

[27] F. Munari, D. Cavagnino, and A. Cadoppi, “Determination of Total FAME and Linolenic Acid Methyl Ester in Pure Biodiesel (B100) by GC in Compliance with EN 14103,” in *Thermo Fisher Scientific*, Milan, Italy, 2007, pp. 1–4.

[28] European Committee for Standardization, “Fat and oil derivatives— Fatty Acid Methyl Esters (FAME)— Determination of ester and linolenic acid methyl ester contents,” *British Standard*, vol. 3, pp. 1–14, 2003.

[29] O. Nur Syazwani, U. Rashid, and Y. H. Taufiq Yap, “Low-cost solid catalyst derived from waste *Cyrtopleura costata* (Angel Wing Shell) for biodiesel production using microalgae oil,” *Energy Conversion and Management*, vol. 101, pp. 749–756, 2015, doi: 10.1016/j.enconman.2015.05.075.

[30] J. Boro, L. J. Konwar, A. J. Thakur, and D. Deka, “Ba doped CaO derived from waste shells of *T striatula* (TS-CaO) as heterogeneous catalyst for biodiesel production,” *Fuel*, vol. 129, pp. 182–187, 2014, doi: 10.1016/j.fuel.2014.03.067.

[31] Y. Li, Y. Jiang, and J. Gao, “Heterogeneous Catalyst Derived from Waste Shells for Biodiesel Production,” *Energy Sources, Part A: Recovery, Utilization, and Environmental Effects*, vol. 37, no. 6, pp. 598–605, 2015, doi: 10.1080/15567036.2011.588674.

[32] A. V. Veličković, O. S. Stamenković, Z. B. Todorović, and V. B. Veljković, “Application of the full factorial design to optimization of base-catalyzed sunflower oil ethanolysis,” *Fuel*, vol. 104, pp. 433–442, 2013, doi: 10.1016/j.fuel.2012.08.015.

[33] G. F. Silva, F. L. Camargo, and A. L. O. Ferreira, “Application of response surface methodology for optimization of biodiesel production by transesterification of soybean oil with ethanol,” *Fuel Processing Technology*, vol. 92, no. 3, pp. 407–413, 2011, doi: 10.1016/j.fuproc.2010.10.002.

Design of an unusual matching unit for a specific frequency band application

Taha Raad Al-Shaikhli, *Jamal kamil Alrudaini, Ahmed Raed Al-Tameemi

Al-Nisour University College, Baghdad, Iraq

Computer Engineering techniques Department

*Correspondence e-mail: jamal.k.eng@nuc.edu.iq

Abstract—This article is about an ideally selected band with a DC switching chain with two answers (Bandstop, allpass) using a designable static Matching circuit area with a fixed Matching circuit area using a folding ring resonator and a DC switching chain with a DC switching chain. It is provided to explain the isoelectric Matching circuit. This design's key concept, you can generate a response when the signal passes the resonator $C (\lambda / 4)$ or the two different methods that can change the 90phase shift. By removing the signal at this particular frequency. Another answer is that by blocking the signal line to the phase change resonator 270° , all the frequencies in the input are transmitted to the output, as the entire signal passes through 90 resonators.

1. INTRODUCTION

inverse and resonators ring done on multi-range, Many studies have been He has a lot to do and learn in the current circuits [1, 2]. memory matching [3, use of and ease communication section. He is in great demand for size, price a 4]. The main focus of this research project for validation is the development of The bandpass statistical matching circuit. compiled a of resonator ring multi-Bode is required for use in communication method Multiband Band stop Matching the adoption of As [5, 6]. signal bands unwanted cancel that selectively devices the demand for communication devices such as smart devices increases, circuits is increasing, which is the main matching miniaturization of these motivation for this study.

2. MINIATURIZED MATCHED BAND-STOP CIRCUIT

A small matching circuit design involving a high degree of deviation is considered [7]. Reference [8] proposes a new method, assuming that the multi-range noise suppression circuit technique is ideal at all frequencies. We also achieved high stops with low values of the q factor. The proposed method should be a cascade matching method to provide a multi-band storage function. You can see this in Figure 1. The need to cascade the measured response of the miniature multi-range matched notch circuit can be seen as a limitation. Because of these limitations, multi-lane blocking cannot be implemented when a large number of stopping lanes are required. Increasing the number of cascaded match circuits increases the overall size of the matching circuit, which counteracts the benefits it provides. Here, two built-in matching circuit prototypes suggested that the cascade could perform multi-range strip stops. The measured response is shown in Figure 2.



Figure. 1. Photograph of multiband band-stop Matching circuit design

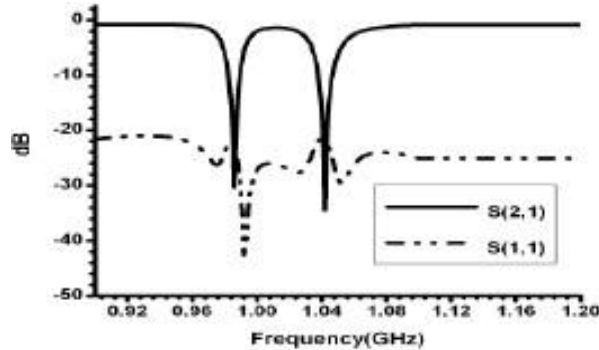


Figure. 2. Measured response for miniaturized multiband matched band-stop circuit

3. DUAL-MODE RING RESONATOR MATCHED BANDSTOP CIRCUIT

In the following analytical study, the authors demonstrated a dual-mode band-suppression matching circuit matched with a ring resonator. The design of the matching circuit is tuned between the 1 GHz full passband and the band trap. The structure of the two-mode ring resonator uses a perturbation stub to separate the resonant frequency or consists of two degenerate modes. A PIN diode is used as a switching element to switch between two operating states.

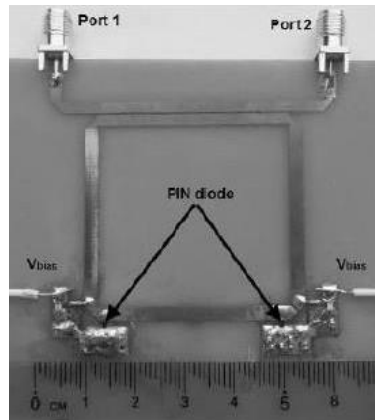


Fig. 3. Prototype of Reconfigurable Dual-Mode Ring Resonator Band Stop Matching circuit at 1GHz.

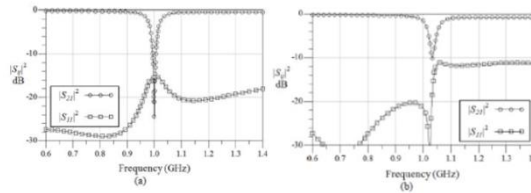


Figure. 4. Band-stop Response of Reconfigurable Matched Matching circuit (PIN Diode in OFF State) (a) simulation and (b) measurement

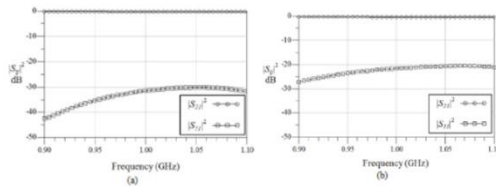


Figure. 5. All pass Response of Reconfigurable Matching circuit (PIN Diode in ON State) (a) simulation and (b) measurement.

This study has provided valuable insights into the design of a dual-mode ring resonator that can be reconfigured as needed. In this case, a PIN diode can be used as a switching element to change from bandpass to full pass. However, the illustrated design does not include the ability to operate a multi-band notch matching scheme.

4. RECONFIGURABLE MULTI-STATE COMPOSITE SPLIT-RING RESONATORS

The proposed design can be converted to multiple slowdowns and single-band configurations in a triple band. The reorganization will not function in the structure due to critical changes in the resonance frequency by separating individual SRRs. Accommodation using two accommodations used is achieved by using pin diodes without increasing the loss of administration, without requiring a complex displacement method, and using pin diodes to ground the SRR and connect the neighboring SRR. In Figure 6, two topologies are described.

The resulting two C3SRR topologies are versatile, allowing for a variety of configurations, small size, low power consumption, and insertion loss. The results also showed that the Matching circuit can perform any bandpass Matching circuit required in both topologies.

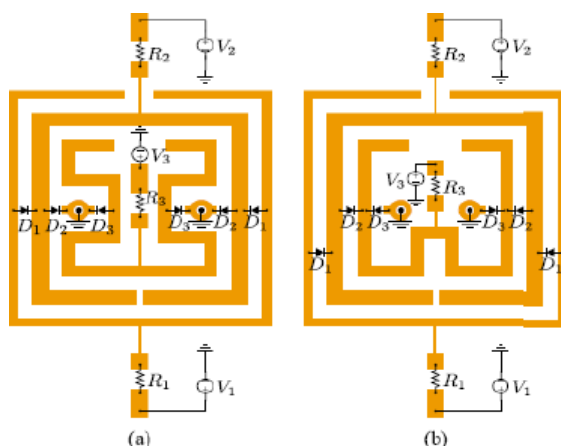


Figure. 6. C3SRRs with PIN diodes and dc bias circuit in (a) five-state topology, and (b) seven-state topology. Input feeds are omitted.

5. MULTIBAND SPLIT-RING RESONATOR BASED PLANAR INVERTED-F ANTENNA FOR 5G APPLICANTS

This paper [3] achieves high data rates by focusing on multiple frequency bands such as 6GHz, 10GHz, 15GHz, 28GHz, and 38GHz in 5G wireless networks. 10 GB/USD A failed industry can cover these remote lanes where multi-lane areas do a much more difficult job. A new multi-division resonator has been developed. It consists of an EP, a parasitic inertial element, a rectangular parasitic element, and a resonator tubing (RPO). The 8 GHz band cut and 10 GHz resonance were created as split-ring resonators and inverse L resonator inserts. The concept was

Comparative analyses of modeled using Ansys Electromagnetic Suite 17 software. and calculated effects were made. They usually match well. simulated

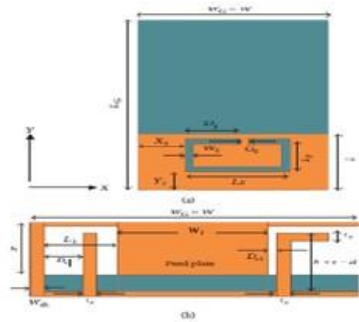


Figure 7. The geometry of an SRR based PIFA, (a) Top view, (b) Side view

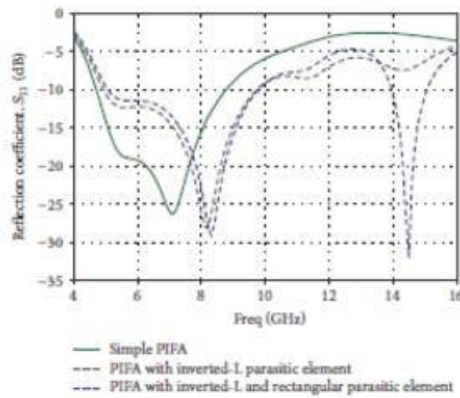


Figure. 8. The magnitude of the simulated reflection coefficient of the PIFA with and without the inverted-L and rectangular-shaped parasitic strips.

6. DESIGN OF MULTIBAND MATCHED BAND-STOP CIRCUIT USING T-SHAPE RESONATOR NETWORK SYSTEM

bandpass blocking A previous study [9-12] developed a multiband matched circuit matching using a T-shape resonator network. The microwave notch scheme A bands. bandwidth into wider communication system front-end can divide the Simulation methods are resonator. T-shaped circuit using a matching bandpass created using the advanced simulation design environment of this design software

(ADS) and FR4 boards [13]. This project can isolate the project from the real world. The signal of interest at the desired frequency in the interfering signal.

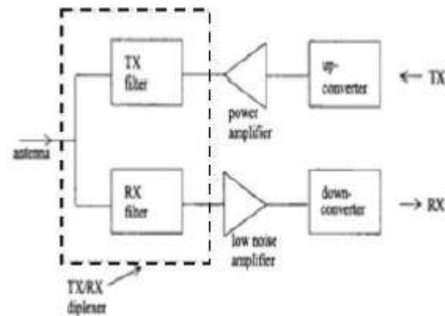


Figure. 9. RF front end of the cellular base station system

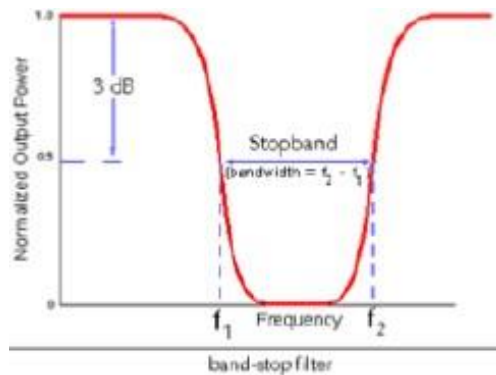


Figure. 10. Band-stop frequency response with lower cut-off frequencies, f_1 and upper cut-off frequencies, f_2

7. MINIATURIZED MULTI-BAND MATCHING CIRCUIT USING CIRCULAR SPLIT-RING RESONATOR AND NULL GAP SEPARATIONS BETWEEN ALL PARALLEL LINES

“Small multiband Matching circuit using split-ring resonator and sharing zero gaps between all parallel lines” [14]. In this article, we present a novel Matching

circuit for multiband stopband loaded with short metamaterial circuits. First, two Matching circuits loaded with stubs and an open ring resonator (ORR) are inspected and compared. In terms of miniaturization, ORRs move to lower frequencies and lower frequencies, creating additional effects. Analyze equivalent Matching circuits and other features of LC circuit models. A matching circuit with a pair of TsRPs was prototyped and weighed.

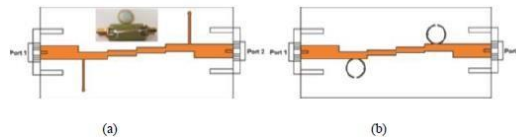


Figure. 11. Design of the Matching circuits. (a) With Stubs. (b) With ORRs cells.

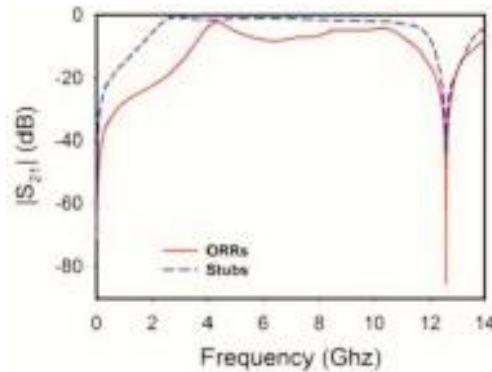


Figure. 12. Electrical responses of the two Matching circuits with Stubs and ORRs.

8. DESIGN OF MULTI-BAND BANDSTOP MATCHING CIRCUIT

The proposed structure includes an ESCAPE resonator and metropole feeder formed on an FR4 substrate with a dielectric and substrate thickness of 4.3. Feedline impedance 100 ohms. This circuit contains a centralized resonator. The loaded component is added to the transmission line focus. Transmission lines can be homogeneous or inadequate. It could also be a microstrip or other unbalanced transmission line.

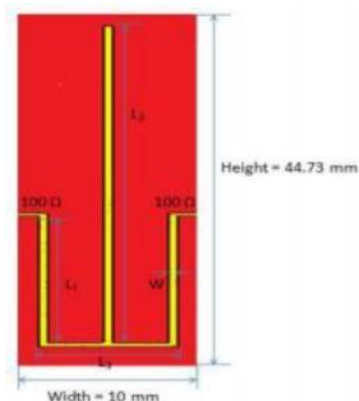


Fig. 13. The layout of the designed multi-band BSF

Table 1. Simulated Results of the Proposed Multi-Band Band stop Matching circuit.

Parameter	Simulation
Center frequency (GHz)	1.1, 3.2, 5.4 and 7.5
Insertion loss , (dB)	-0.01, -0.03, -0.24 and -0.15
Return loss , (dB)	-43.44, -45.34, -39.66 and -36.81
Group delay	Less than 0.5 in pass band

Synthesis of a multi-band blocking channel (MSBC) with an E-shaped resonator. The circuit has four stopbands at 1.1 GHz, 3.2 GHz, 5.4 GHz, and 7.5 GHz with adjustable focal frequency and bandwidth. Multiband is achieved by E-formed resonators. The acceptable design of stop-pass matching circuits finds applications in modern communication technology.

CONCLUSION

Previous studies are useful for smaller matching circuits constituting multi-band scores, but may further improve the proposed design.

References

- [1] M. Ninic, B. Jokanovic and P. Meyer, "Reconfigurable Multi-State Composite Split-Ring Resonators," in *IEEE Microwave and Wireless Components Letters*, vol. 26, no. 4, pp. 267-269, April 2016, doi: 10.1109/LMWC.2016.2537790.
- [2] G. Eason, B. Noble, and I. N. Sneddon, "On certain integrals of Lipschitz-Hankel type involving products of Bessel functions," *Phil. Trans. Roy. Soc. London*, vol. A247, pp. 529-551, April 1955. (*references*)
- [3] J. Clerk Maxwell, *A Treatise on Electricity and Magnetism*, 3rd ed., vol. 2. Oxford: Clarendon, 1892, pp.68-73.

- [4] I. S. Jacobs and C. P. Bean, "Fine particles, thin films and exchange anisotropy," in *Magnetism*, vol. III, G. T. Rado and H. Suhl, Eds. New York: Academic, 1963, pp. 271–350.
- [5] K. Elissa, "Title of paper if known," unpublished.
- [6] R. Nicole, "Title of paper with only first word capitalized," *J. Name Stand. Abbrev.*, in press.
- [7] Y. Yorozu, M. Hirano, K. Oka, and Y. Tagawa, "Electron spectroscopy studies on magneto-optical media and plastic substrate interface," *IEEE Transl. J. Magn. Japan*, vol. 2, pp. 740–741, August 1987 [Digests 9th Annual Conf. Magnetism Japan, p. 301, 1982].
- [8] M. Young, *The Technical Writer's Handbook*. Mill Valley, CA: University Science, 1989.
- [9] Ahmed, Badiia Ait, Otman Aghzout, Azzeddin Naghar, and Ana V. Alejos. 2020. "Miniaturized Multi-Band Stopband Filter Using Circular Split Ring Resonator and Null Gap Separations between All Parallel Lines." *Progress In Electromagnetics Research C* 106(September):137–50. doi: 10.2528/PIERC20072504.
- [10] B. A. Adoum and P. W. Wong, "Miniaturized multiband matched band-stop Filter," 2011 IEEE International RF & Microwave Conference, Seremban, Negeri Sembilan, 2011, pp. 29-32, doi: 10.1109/RFM.2011.6168688.
- [11] Joshi¹, A., & Bhatia, D. Analysis and Design of Multi-Band Bandstop Filter.
- [12] Hassan, Nornikman, Mohd Khairy Ismail, Badrul Hisham Ahmad, Zahriladha Zakaria, Nurul Syahira Nordin, Mohd Khairy Zahari, and Mohd Fareq Abdul Malek. 2018. "Design of Multiband Matched Band- Stop Filter Using T-Shape Resonator Network System." *Journal of Theoretical and Applied Information Technology* 96(23):7760–70.
- [13] Ishfaq, Muhammad Kamran, Tharek Abd Rahman, Hassan Tariq Chattha, and Masood Ur Rehman. 2017. "Multiband Split-Ring Resonator Based Planar Inverted-F Antenna for 5G Applications." *International Journal of Antennas and Propagation* 2017:1–8. doi: 10.1155/2017/5148083.
- [14] M. K. Zahari, B. H. Ahmad, N. A. Shairi and Peng Wen Wong, "Reconfigurable dual-mode ring resonator matched bandstop Filter," 2012 IEEE Symposium on Wireless Technology and Applications (ISWTA), Bandung, 2012, pp. 71-74, doi: 10.1109/ISWTA.2012.6373880.

Semigroup Based Ordinary Differential Equation Solution

Ali Abdul Kadhum
Ruhaima
Computer
Engineering
Techniques
Al-Nisour University
College
Baghdad, Iraq
ali.abd.eng@nuc.edu.
iq

Dunya Mohee Hayder
Medical Physics
Madent Alelm University
College
Baghdad, Iraq
dunyamoheehaydee@mauc.edu.
iq

*Jamal Kamil Kh.
Abbas
Computer Engineering
Techniques
Al-Nisour University
College
Baghdad, Iraq
Jamal.k.eng@nuc.edu.
iq
currency

Corresponding e-mail: Jamal.k.eng@nuc.edu.iq

Abstract: In this paper, the work of a standard framework and a new current system to solve the problem of moderate control of the quadratic optimal line using a Semigroup approach. This program uses an algorithm to solve such problems that was introduced and used in other examples solved using this new algorithm to achieve limited solutions.

Keywords: ODE, linear quadratic, semigroup, operator, Banach space, Riccati .

I. Introduction

The one-parameter rebel theory of linear operators in Banach space began with the generative theory of Hille-Yosida in 1948 and reached a climax in E. Hille and Philips' 1957 program "Semigroups and Functional Analysis". In the 1970s and 1980s, the idea reached some degree of maturity. Some basic definitions

Definition 1.1 [1]

Let X be the Banach space. One parameter family $S(t): \mathbb{R}^+ \rightarrow \mathcal{L}(X)$ $0 < t < \infty$ The number of bounded linear operators from X to X is a symbolic group of bounded linear operators for X if $S(0)=I$. where I stand for the equality operator with respect to X .

$S(t+s) = S(t).S(s)$ for every $t, s \geq 0$

Also the linear operator A defined in the

domain. $D(A) = \left\{ x \in X : \lim_{t \rightarrow 0} \left(\frac{S(t)x - x}{t} \right) \text{ exist} \right\}$

By $Ax = \lim_{t \rightarrow 0} \left(\frac{S(t)x - x}{t} \right), x \in D(A)$

It is defined as the minimal generator of the rebel $S(t)$.

Definition 1.2 [1]

Let X be a Banach space, and let $S(t)$ be a bounded operator on X . $S(t)$

$$\lim_{t \rightarrow 0} \|S(t) - I\|_{\mathcal{L}(X)} = 0$$

Definition 1.3 [2]

Let H be a Hilbert space. Minimal generator A is called dissipation. if $\operatorname{Re} \langle Ax, x \rangle_H \leq 0$ for all $x \in D(A)$.

a. Infinite dimensional linear quadratic controller problem [3]

Consider the dynamic system

$$\dot{x} = A_0 x(t) + Bu(t) \quad (1)$$

$x(0)$ is given, let H be real Hilbert space

$A: D(A_0) \subseteq H \rightarrow H$ is infinitesimal generators of C_0 -semigroup $S(t)$ and A_0 is closed linear operator with dense domain such that for all $x \in D(A_0)$.

$$A_0x = \lim_{t \rightarrow 0} \frac{S(t)x}{t}$$

$S(t)$: strongly continuous semigroup of operator A_0

B : bounded linear operator $H_u \rightarrow H$, where H_u stand for Hilbert spaces for control input(space) and $u(\cdot)$ Is an element of $L_2((0, T); H_u)$.

The optimal control theory (Known as "the linear quadratic regulator problem (LQR)" is to find u in $L_2((0, T); H_u)$ so as minimize the cost functional:

$$q(u) = \int_0^T \left\{ \langle Qz(t), z(t) \rangle + \int_0^T \langle u(t), u(t) \rangle \right\} dt \quad (2)$$

Q : Linear bounded nonnegative, definite operator for the Hilbert space cap H to itself.

b. Theorem [4]

Assume that A_0 is a minimal generator of strongly continuous inverse $S(t)$ over Hilbert space H , and assume that $\pi(t)$ for each $t, 0 \leq t \leq T$ is a linear bounded operator for H in H , strongly continuous at $0 \leq t \leq T$. Then the equation

$$\frac{d}{dt} \langle x(t), y \rangle = \langle x(t), (A_0 + \pi(t))' y \rangle \quad ; y \in D(A_0) \quad x_0(0) \text{ is given} \quad (3)$$

has a unique continuous solution $x(t), 0 \leq t \leq T$ and

$$x(t) = \Phi(t, s)x(s); \quad t \geq s \geq 0;$$

c. Optimal control problem in infinite time

This section introduces the optimal control problem for infinite time. Let H and U be Hilbert spaces endowed with inner product $\langle \cdot, \cdot \rangle_H$ and $\langle \cdot, \cdot \rangle_U$, respectively

$$\left\{ \langle u, v \rangle_H = \int_a^b u(x)v(x)dx \right\}$$

Let $Q: H \rightarrow H$ and $J: U \rightarrow U$ be bounded linear operators with the following properties:

i) the operator J is a positive definite operators on U

ii) the operator Q is a positive definite operators on H

Consider the following optimal control problem (LQR) :

Find $u \in L_2((0, \infty); U)$ such that u minimize

$$\mathfrak{J}(z_0, u) = \int_0^\infty \left\{ \langle Qz(t), z(t) \rangle_H + \langle Ju(t), u(t) \rangle_U \right\} dt \quad (4)$$

Subject to

$$\frac{dz(t)}{dt} = A_0z(t) + Bu(t) \quad \text{on } H \quad (5)$$

$$z(0) = z_0$$

(6)

Where A_0 and B are defined.

II. computational algorithm for solving infinite dimensional LQR problem.

Step 1 (main problem)

Let H and U be Hilbert spaces endowed with inner product $\langle \cdot, \cdot \rangle_H$ and $\langle \cdot, \cdot \rangle_U$, respectively $\left\{ \langle u, v \rangle_H = \int_a^b u(x)v(x)dx \right\}$

Let $Q: H \rightarrow H$ and $J: U \rightarrow U$ be bounded linear operators with the following properties:

i) the operator J is a positive definite operators on U

ii) the operator Q is a positive definite operator on H

Consider the following optimal control problem (LQR) :

Find $u \in L_2((0, \infty); U)$ such that u minimize

$$\mathfrak{J}(z_0, u) = \int_0^\infty \{ \langle Qz(t), z(t) \rangle_H + \langle Ju(t), u(t) \rangle_U \} dt \quad (7)$$

Subject to

$$\frac{dz(t)}{dt} = A_0 z(t) + Bu(t) \quad \text{on } H \quad (8)$$

$$z(0) = z_0$$

(9)

Where A_0 and B , Q and J are defined as follow

$A_0: D(A_0) \subseteq H \rightarrow H$, the closed linear operator A_0 with dense domain infinitesimal generators of C_0 -semigroup $S(t)$

B : bounded linear operator $H_u \rightarrow H$ where $H_u \equiv L_2((0, \infty); U)$

Step 2 (Generating of semigroup)

Let V be a subspace of H such that $D(A_0) \subseteq V \subseteq H = H^* \subseteq V^* \subseteq D(A_0')$. Where $*$ stand for the dual space. Let $S(t)$ be a C_0 -semigroup defined on V with infinitesimal generator A_0 .

Step 3 (choosing the finite dimensional subspaces)

Finite dimensional subspace should be selected such that $V_N \subseteq V^*$. Since V_N is finite dimensional, it is span of a finite number of basis functions in V .

Step 2.1 (choosing the finite dimensional operators)

Define suitable operators that approximate A, B, Q and J of main problem,

Let A_N, B_N, Q_N and J_N the approximate operators to A, B, Q and J respectively can be selected such that

The operator $A_N: V_N \rightarrow V_N$ generate a C_0 -semigroup on V_N

The operator $B_N: U \rightarrow V_N$ is bounded.

The operator $Q_N: V_N \rightarrow V_N$ is bounded and semidefinite.

The operator $J_N: U \rightarrow U$ is bounded and positive definite.

Step 2.2 (Define the orthogonal projection)

Let P_N denote the orthogonal projection as $P_N: H \rightarrow V_N$. By restricting the bilinear form $a(\cdot, \cdot)$ to V_N , we have

$A_N: V_N \rightarrow V_N$ such that $a(x, y) = \langle A_N x, y \rangle$ for all $x, y \in V_N$.

To define the operators B_N, Q_N and J_N , we utilize the projection operator P_N as

$B_N: U \rightarrow V_N$ such that $B_N = P_N B$.

$Q_N: V_N \rightarrow V_N$ such that $Q_N = P_N Q$.

Step 2.3 (matrix approximation of linear operators)

One of most important finite approximation is the matrix approximation of suitable linear operators, be the basis of V_N defined a $N \times N$ matrix to be:

$[M_N] = [\langle b_i, b_j \rangle_H]_{i,j=1}^N$; where the notation $[.]$ is standing of matrix representation, and $\langle \cdot, \cdot \rangle$ is standing for a suitable inner product. Notice that $[M_N]$ is a symmetric matrix. The matrix representation for approximate operators A_N, A_N', B_N, Q_N can be done as follow:

Find the suitable basis $b_i, i = 1, \dots, N$ from the subspace V_N , M_N -inner product on R^N by

$$\left\langle \begin{bmatrix} a_1 \\ \vdots \\ a_N \end{bmatrix}, \begin{bmatrix} c_1 \\ \vdots \\ c_N \end{bmatrix} \right\rangle = [a_1 \quad \dots \quad a_N] [M_N]^T \begin{bmatrix} c_1 \\ \vdots \\ c_N \end{bmatrix}, \text{ for all } \begin{bmatrix} a_1 \\ \vdots \\ a_N \end{bmatrix}, \begin{bmatrix} c_1 \\ \vdots \\ c_N \end{bmatrix} \in R^N$$

The matrix representation of the operator A_N with respect to the basis vector $\{b_i\}_{i=1}^N$ and M_N -inner product of the matrix $[A_N]$ defined by

$$\left\langle A_N \sum_{i=1}^N a_i b_i, \sum_{j=1}^N c_j d_j \right\rangle = \left\langle [A_N] \begin{bmatrix} a_1 \\ \vdots \\ a_N \end{bmatrix}, \begin{bmatrix} c_1 \\ \vdots \\ c_N \end{bmatrix} \right\rangle_{N \times N}, \text{ for all } \begin{bmatrix} a_1 \\ \vdots \\ a_N \end{bmatrix}, \begin{bmatrix} c_1 \\ \vdots \\ c_N \end{bmatrix} \in R^N$$

The matrix representation of $[A_N]'$ is given by

$$[A_N]' = [M_N]^{-1} [A_N]^T [M_N]$$

The matrix representation of the operator Q_N with respect to the basis vector $\{b_i\}_{i=1}^N$ and M_N -inner product of the matrix $[Q_N]$ defined by

$$\left\langle Q_N \sum_{i=1}^N a_i b_i, \sum_{j=1}^N c_j d_j \right\rangle = \left\langle [Q_N] \begin{bmatrix} a_1 \\ \vdots \\ a_N \end{bmatrix}, \begin{bmatrix} c_1 \\ \vdots \\ c_N \end{bmatrix} \right\rangle_{N \times N}, \text{ for all } \begin{bmatrix} a_1 \\ \vdots \\ a_N \end{bmatrix}, \begin{bmatrix} c_1 \\ \vdots \\ c_N \end{bmatrix} \in R^N$$

Note that U is finite dimensional. Thus the operator $B: U \rightarrow H$ is an operator of finite rank, this implies that there exist vector $f_i \in H, i = 1, \dots, m$ such that

$$B \begin{bmatrix} u_1 \\ \vdots \\ u_m \end{bmatrix} = \sum_{i=1}^m f_i u_i \quad \forall \begin{bmatrix} u_1 \\ \vdots \\ u_m \end{bmatrix} \in R^m$$

In this case $[B_N] \in R^{m,n}$

The matrix representation of B_N is the matrix given by

$$\langle B_N \begin{bmatrix} u_1 \\ \vdots \\ u_m \end{bmatrix}, \sum_{j=1}^m c_j b_j \rangle = \langle [B_N] \begin{bmatrix} u_1 \\ \vdots \\ u_m \end{bmatrix}, \begin{bmatrix} c_1 \\ \vdots \\ c_N \end{bmatrix} \rangle_{M \times N}, \quad \text{for all } \begin{bmatrix} u_1 \\ \vdots \\ u_m \end{bmatrix} \in R^m,$$

$$\begin{bmatrix} c_1 \\ \vdots \\ c_N \end{bmatrix} \in R^N$$

Furthermore

$$[B_N]' = [B_N]^T [M_N]$$

Step 3 (finite approximate of **LQR** problem)

Consider the above problem where $U = R^m$. The main problem is then approximated as follows:

Find $u_N \in L^2((0, \infty); U)$ so that

u_N minimizes the following cost functional

$$\mathfrak{J}(z_{0,N}, u_N(\cdot)) = \int_0^\infty \{ \langle Q_N z_N(t), z_N(t) \rangle_H + \langle J_N u_N(t), u_N(t) \rangle_U \} dt$$

Subject the following dynamical control system

$$\begin{aligned} \frac{dz_N(t)}{dt} &= A_N z_N(t) + B_N u_N(t) \quad \text{on } H \\ z_N(0) &= z_{0,N} \end{aligned}$$

Where A_N, B_N are defined in step 3

So in matrix representation in step 3 for our problem we write the matrix linear quadratic regular problem ($[LQR_N]$)

Find $[u_N(t)] \in L^2((0, \infty); R^N)$ such that $[u_N]$ minimizes

$$\begin{aligned} \mathfrak{J}([z_{0,N}], [u_N(\cdot)]) \\ = \int_0^\infty \{ \langle [Q_N][z_N(t)], z_N(t) \rangle_{M_N} + \langle [J_N][u_N(t)], [u_N(t)] \rangle_U \} dt \end{aligned}$$

Subject to

$$\frac{d[z_N(t)]}{dt} = [A_N][z_N(t)] + [B_N][u_N(t)] \quad \text{on } R^N$$

Where $[A_N], [B_N], [Q_N], [J_N]$ are defined in step 3.3

Step 5 (finding the algebraic Riccati equation(ARE))

Theorem (1) [5]

Consider the above optimal control problem where the operators are satisfying the following conditions:

The operator J is positive definite operator on U . The operator Q is positive semidefinite operator on H . The closed linear operator A_0 with dense domain is

infinitesimal generators of C_0 -semigroup $S(t)$ and the operator B is bounded linear operator. Suppose the semigroup $S(t)$ is exponentially stable. Then there is a unique control $u_0(t)$ minimizing which has the form

$$u_0(t) = -B'\pi(t)z_0(t)$$

Where

$$\pi(t)z_0(t) = \int_t^\tau S(s-t)Jz_0(s)ds$$

Where $z_0(t)$ is the unique continuous solution of

$$\langle z_0(t), y \rangle = \langle z_0(0), y \rangle + \int_0^t \langle z_0(s), (A_0 + \pi)'y \rangle ds, \quad y \in D(A_0').$$

π is bounded linear operator mapping ($\pi: H \rightarrow H$) and characterized as the unique solution of

$$0 = \langle Qz, y \rangle + \langle \pi z, A_0 y \rangle + \langle A_0 z, \pi y \rangle - \langle B\pi z, J^{-1}B'y \rangle$$

The Algebraic Riccati equation for the system is defined as follows

$$\langle Qz, y \rangle + \langle \pi z, A_0 y \rangle + \langle A_0 z, \pi y \rangle - \langle B\pi z, J^{-1}B'y \rangle = 0$$

$$\langle (Q + A_0\pi + \pi A_0 - \pi B J^{-1} B' \pi)z, y \rangle = 0$$

But z and y does not equal to zero. Hence

$$(Q + A_0'\pi + \pi A_0 - \pi B J^{-1} B' \pi) = 0$$

Or $A_0'\pi + \pi A_0 - \pi B J^{-1} B' \pi + Q = 0$ (this equation called Algebraic Riccati Equation (ARE))

Then the optimal control is $u(t) = -J^{-1}B'\pi z(t)$ and hence is a solution of feedback

$$\dot{z}_N = A_N z_N + B_N u_N, \text{ on using the semigroup}$$

$$\dot{z} = Az + B(-B'\pi z) = Az - \pi z$$

$$= Az - \int_t^\tau S(s-t)'Jz(s)ds$$

On using the theorem (1) on the system we get the following ARE

$$A_N'\pi_N + \pi_N A_N - \pi_N B_N J_N^{-1} B_N'\pi_N + Q_N = 0$$

On using the hypotheses of the theorem (1) (LQR_N) is transformed into solving the following matrix equation

$$[M_N]^{-1}[A_N]^T[M_N][\pi_N] + [\pi_N][A_N] - [\pi_N][B_N][J_N]^{-1}[B_N]^T[M_N][\pi_N] + [Q_N] = 0$$

Step 6 (finding the Optimal Control operator)

Define the bounded linear operator $K: H \rightarrow U$ where K defined as $K = J^{-1}B'\pi$, such that $A_0 - BK$ generates an exponentially stable semigroup on H . We get the optimal control:

$$u(t) = -J^{-1}B'\pi z(t) \quad 0 \leq t \leq \infty$$

If the system () - () satisfy the hypotheses of theorem (). The optimal control u_N is defined as

$$u_N(t) = -K_N z_N(t) \equiv -J_N^{-1}B_N'\pi_N z(t)$$

The optimal control $u = -J^{-1}B'\pi z$ can be approximated by

$$u_N = -J_N^{-1} B_N' \pi_N z \equiv -K_N z_N$$

The optimal control for $[(LQR_N)]$ is become:

$$\begin{aligned} [u_N(t)] &= -[K_N][z_N(t)] \equiv -[J_N^{-1}][B_N]'[\pi_N][z(t)] \\ &= -[J_N^{-1}][B_N]^T[M_N][\pi_N][z(t)] \end{aligned}$$

$$\text{Let } [P_N] = [M_N][\pi_N]$$

$$[A_N]^T [P_N] + [P_N][A_N] - [P_N][B_N][J_N^{-1}][B_N]^T [P_N] + [M_N][Q_N] = 0$$

Then the optimal control () can be rewritten as follows

$$[u_N(t)] = -[J_N^{-1}][B_N]^T [P_N][\pi_N][z_N(t)]$$

$$\text{Where } [\pi_N] = [M_N]^{-1}[P_N]$$

III. Convergence of the Riccati and feedback optimal control operator

In this section we provide the frame work for proving of the Riccati $\pi_N \rightarrow \pi$

$$\text{Let } H = L^2(0,1), \quad V = H_0^2(0,1) \quad \text{and } U = R^m$$

Let A, B, Q and J satisfy the hypotheses in the theorem(4.1) and consider the following problem (#)

$$\frac{dy}{dt} = Ay(t) + Bu(t) \quad \text{on } H$$

$$y(0) = y_0$$

Together with associated performance measure

$$\bar{\mathfrak{J}}(y_0, u) = \int_0^\infty \{ \langle Qy(t), y(t) \rangle_H + \langle Ju(t), u(t) \rangle_U \} dt$$

Consider the following optimal control problem(#) minimize $\bar{\mathfrak{J}}(y_0, u)$ over $u \in L^2((0, \infty); U)$ subject to (3) (5). The problem(1) is approximated by a sequence of approximate problem. Let $V_N, N = 1, 2, \dots$ be a sequence of finite dimensional subspace of $V \subseteq H$ and P_N be the orthogonal projection operators $P_N: H \rightarrow V_N$ under the H inner product. Let $S_N(t)$ be the seq. of C_0 -semigroup defined on V_N with infinitesimal generator $A_N \in \mathcal{L}(V_N)$ and $S_N(t)'$ denote the respective adjoint semigroup. Additionally, let $B_N \in \mathcal{L}(U, V_N)$ and $Q \in \mathcal{L}(V_N)$

The following approximate optimal control problem (1) has been considered as follows

Consider the problem (1): minimize the following objective function

$$\bar{\mathfrak{J}}(y_{0,N}, u_N) = \int_0^\infty \{ \langle Q_N y_N(t), y_N(t) \rangle_{V_N} + \langle J_N u_N(t), u_N(t) \rangle_U \} dt$$

Over $u_N \in L^2((0, \infty); U)$ subject to

$$\frac{dy_N}{dt} = A_N y_N(t) + B_N u_N(t) \quad \text{on } H$$

$$y_N(0) = P_N y_0$$

We shall say that the function $u_N \in L^2((0, \infty); U)$ is admissible control for initial state $y_N(0)$ if $\bar{\mathfrak{J}}_N(y_N(0), u_N)$ is finite. Bancks and Kunish theorem (Vurgin)

establishes sufficiency for the convergences of $\pi_N \rightarrow \pi$ using the following assumptions:-

H1) for each $y_N(0) \in V_N$, there exists a control $u_N \in L^2((0, \infty); U)$ for $(\#^N)$, and any admissible control for $(\#^N)$ derives the state to zero asymptotically.

H2)

i) for each $z \in H$; $S_N(t)P_N z \rightarrow S(t)z$, with convergence uniform in t on bounded subsets on $[0, \infty)$.

ii) for each $z \in H$; $S'_N(t)P_N z \rightarrow S'(t)z$, with convergence uniform in t on bounded subsets on $[0, \infty)$.

iii) for each $u \in U$; $B_N P_N u \rightarrow B u$
and for each $u \in U$; $B'_N P_N u \rightarrow B' u$

iv) each $z \in H$; $Q_N P_N z \rightarrow Q z$

C1) each $z \in V$; the exist an element $z \in V_N$ such that $\varepsilon(N) \rightarrow 0$ as $N \rightarrow \infty$.

C2) the pair (A, B) is stabilizable

C3) There exist a bounded operator $K: H \rightarrow U$ the stabilizes (A, B) . Furthermore, there exist an integer N_0 such that for $N \geq N_0$, the order (A_N, B_N) is stabilizable by K .

Theorem (2) (Banks-Kunich) [6, 7]

Suppose (H1) and (H2) and (C1)-(C3) holds and suppose that $J > 0, Q > 0, Q_N > 0$. Then there exit an unique Riccati operator π and π_N associated with $(\#)$ and $(\#^N)$ on H and V_N respectively such that if P_N denote the orthogonal projection into V_N then

$$\begin{aligned} \pi_N P_N z &\rightarrow \pi z & \forall z \in H \\ S_N(t) P_N z &\rightarrow S(t) z & \forall z \in H \\ u_N(t) &\rightarrow u(t) & \forall u \in U \end{aligned}$$

With these statement holding uniformly in t on compact subsets of $[0, \infty)$. Here, $S_N(t)$ and $S(t)$ are the semigroup generated by $A_N - P_N B_N J^{-1} B_N^{-1} P_N \pi_N$ and $A - B J^{-1} B' \pi$ and $u(t)$ and $u_N(t)$ are the optimal feedback for $(\#)$ and $(\#^N)$ respectively and π_N is positive definite Riccati operator that solve ARE

$$A'_N \pi_N + \pi_N A_N - \pi_N B_N J_N^{-1} B'_N \pi_N + Q = 0$$

Now when we construct (LQR_N) , then they will be the feedback gains $K_N = J_N^{-1} B'_N P_N \pi_N$ converge to $K = J^{-1} B' \pi$, the resulting feedback gain for (LQR) , specially we want $\|K - K_N\|_{L(H,V)} \rightarrow 0$

Remark

$$\begin{aligned} \pi_N P_N z &\rightarrow \pi z & \forall z \in H \\ S_N(t) P_N z &\rightarrow S(t) z & \forall z \in H \\ u_N(t) &\rightarrow u(t) & \forall u \in U \\ A_N z &\rightarrow A z & \forall z \in H \\ K_N &\rightarrow K \end{aligned}$$

The approximate optimal control is $u_N = -K_N z_N = -J_N^{-1} B'_N \pi_N z_N$

The approximate optimal solution is

$$\dot{z}_N = A_N z_N + B_N u_N \quad ; z(0) = z_0$$

$$\dot{z}_N = A_N z_N - B_N K_N z_N$$

$$\dot{z}_N = (A_N - B_N K_N) z_N$$

Hence $z_N \rightarrow z$

and

$$\mathfrak{J}(z_{0,N}, u_N(\cdot)) \rightarrow \mathfrak{J}(z_0, u_N(\cdot))$$

Example: simple problem

Let H and U be a Hilbert spaces endowed with inner product $\langle \cdot, \cdot \rangle_H$ and $\langle \cdot, \cdot \rangle_U$, respectively. Let $Q: H \rightarrow H$ and $J: U \rightarrow U$ be a bounded linear operator with the following properties

The operator J is a positive definite operator on .

The operator Q is a positive semidefinite operator on .

Consider the following optimal control problem (LQR):

Find $u_N \in L^2((0, \infty); U)$ such that u minimize

$$\mathfrak{J}(z_0, u) = \int_0^\infty \{ \langle Qz(t), z(t) \rangle_H + \langle Ju(t), u(t) \rangle_U \} dt$$

Subject to

$$\frac{d}{dt} \begin{bmatrix} v(t) \\ w(t) \end{bmatrix} = \begin{bmatrix} \mu & R \\ 0 & -\mu \end{bmatrix} \begin{bmatrix} v(t) \\ w(t) \end{bmatrix} - \begin{bmatrix} p \\ q \end{bmatrix} u(t)$$

$$z(0) = z_0 \quad \text{in } H.$$

Where A , B , Q and J are defined as follow:

$A: D(A) \subseteq H \rightarrow H$; the closed linear closed operator A with dense domain is infinitesimal generator of C_0 -semigroup $S(t)$.

$B: H_u \rightarrow H$ bounded linear operator; where H_u instead of $L^2((0, \infty); U)$ where $R > 0, \mu > 0$ and p, q are not both zero.

If we define $A = \begin{bmatrix} \mu & R \\ 0 & -\mu \end{bmatrix}$ and $B = \begin{bmatrix} p \\ q \end{bmatrix}$ then the linear system can be written as

$$\frac{d}{dt} \begin{bmatrix} v(t) \\ w(t) \end{bmatrix} = A \cdot \begin{bmatrix} v(t) \\ w(t) \end{bmatrix} - B \cdot u(t)$$

Where $p \neq 0$ and $q \neq 0$ and $R > 0, \mu > 0$

So we use the theorem (3)

Then the positive definite solution π of ARE

$$A'\pi + \pi A - \pi \pi B B' \pi + Q = 0$$

Is given by

$$\pi(\mu, p, R) = \begin{bmatrix} \frac{\mu + \sqrt{\mu^2 + p^2}}{p^2} & \frac{R}{p^2} \\ \frac{R}{p^2} & \frac{R^2 - p^2}{2\mu p^2} \end{bmatrix}$$

As R become large, the matrix A become more non normal

Moreover $p \geq 1 \quad \lim_{R \rightarrow \infty} \|\pi(\mu, p, R)\| = \infty$

Thus, the *ARE* can become ill-condition for large value of R .

However when $R \rightarrow 0$ the matrix A become normal (self-adjoint) and when $R = 0$

$$\pi(\mu, p, 0) = \begin{bmatrix} \frac{\mu + \sqrt{\mu^2 + p^2}}{p^2} & 0 \\ 0 & \frac{R^2 - p^2}{2\mu p^2} \end{bmatrix}$$

References:

- [1] Ammon Pazy, “ Semigroups of linear operators and applications to partial differential equations “, Springer -Verlag , New-York 1978.
- [2] A.V. Balakrishnan, “Applied Functional Analysis”, 1976
- [3] Klaus Engel, “one parameter semigroups for linear evolution equations”, 2000.
- [4] Eric D. Vurgin , “ On approximation and optimal control of non-normal distributed parameter system”, PhD Thesis, Blacksburg, Virginia, USA, 2004.
- [5] J.S. Gibson “The Riccati integral equations for optimal control problems in Hilbert spaces “ , SIAM J. , control and optimization , 1981.
- [6] [Banks, 84] Banks and Kunisch, “The Linear regulator problem for parabolic system “, SIAM J. , control and optimization, 1984.
- [7] Svatopluk Fucik , “ Solvability of Nonlinear Equations and boundary value problem”, D. Reidel Publishing Company, Dordrecht, 1980.

Spectral features of the final Telecommunications Path devices

Abdullah Qays Taher
Islamic University,
Department of Computer
Engineering Techniques,
Kufa str. , Najaf, Iraq 5400
abdallahqays@gmail.com

Ali Ihsan Alanssari
Al Nisour University
College,
Department of Computer
Engineering Techniques,
Baghdad, 10036, Iraq
ali.ih.eng@nuc.edu.iq

*Jamal Kamil Alrudaini
Al Nisour University College,
Department of Computer
Engineering Techniques,
Baghdad, 10036, Iraq
Jamal.k.eng@nuc.edu.iq

Mustafa Kalil Ibrahim
Al Nisour University College,
Department of Computer
Engineering Techniques,
Baghdad, 10036, Iraq
Mustafa.kh.eng@nuc.edu.iq

Volodymyr Pyliavskiy
O.S. Popov Odessa National
Academy of
Telecommunications
Odesa, Ukraine
Department of Radio and
Television Broadcasting
v.pilyavskiy@ukr.net

*Correspondence e-mail: jamal.k.eng@nuc.edu.iq

Abstract –Approaches to assessing color fidelity in standard, high, and ultrahigh definition television systems and related applications, depending on the spectral characteristics of video cameras, are considered. An assessment of the error of color reproduction of cameras, in which colorimetry CIE 1931 is embodied, is given concerning cameras, in which colorimetry of 2006 is embodied, and it is shown that the transition from using colorimetry CIE 1931 to the use of colorimetry 2006 did not to a noticeable increase in color fidelity. An assessment of the color reproduction of real cameras is given and it is shown that a “standard” camera with a linear matrix [TECH 3355], in comparison with an “ideal” camera, provides practically undistorted color rendition; cameras with other spectral characteristics should be used for HDTV and UHDTV.

Keywords – camera, color perception model, equal-contrast color space, end-to-end video path “light to light”, spectral response, color rendering, CIECAM02, CAM02-USC

1. INTRODUCTION

The main difference between the progress of TV systems and other video applications is the tendency to move to new levels of image quality and create new functionalities for the systems. In this case, a special place is occupied by the fidelity of color rendering, which depends on the colorimetric characteristics of the systems as a whole and their components, which determines the colorimetric quality of the image.

When it comes to colorimetric quality, one should proceed from the assessment of color fidelity in the through path “from light to light” [1–3]. The main color distortions occur on the transmitting and receiving sides, namely, they arise due to the possible imperfection of the spectral composition of the studio lighting source and imperfection of the spectral characteristics of the camera. Also, as the colorimetric errors introduced by the reproducing device, and the errors that can be introduced by digital image processing on the transmitting and receiving sides. Among the most critical factors is the imperfection of the spectral characteristics of the sensitivity of the channels of the primary colors of the camera. This means that when assessing the fidelity of color reproduction, one cannot abstract from the spectral characteristics of the reflection of objects in the scene and operate only with their color coordinates. That is why in [1], special attention is paid to the spectral composition of objects and a comparison of color distortions of optimal colors and examples of real colors in the form of a combination of Gaussian functions of the radiation wavelength given. It is shown that there can be changes depending on metamerism.

To be able to quantitatively judge the color fidelity of TV cameras, it is necessary to be able to compare the characteristics of real cameras with the characteristics of ideal cameras. The spectral properties of the channel (R, G, B) should provide undistorted color reproduction regardless of the spectral composition of the object.

2. CAMERA COLOR CHARACTERISTICS

In this paper, we determine the spectral characteristics of the ideal camera and the spectral characteristics of the UHF system in terms of CIE 1931 colorimetry for standard (HDTV), high definition (HDF), and ultra-high definition (UHF) television systems. CIE 2006 Perspectives of colorimetry and examples of color reproduction error estimation - on the discrepancy of ideas about the undistorted color reproduction. Also provided is an example evaluating the distortion of the Color Checker color set introduced by an optimally tuned "standard" SDTV camera compared to an ideal camera.

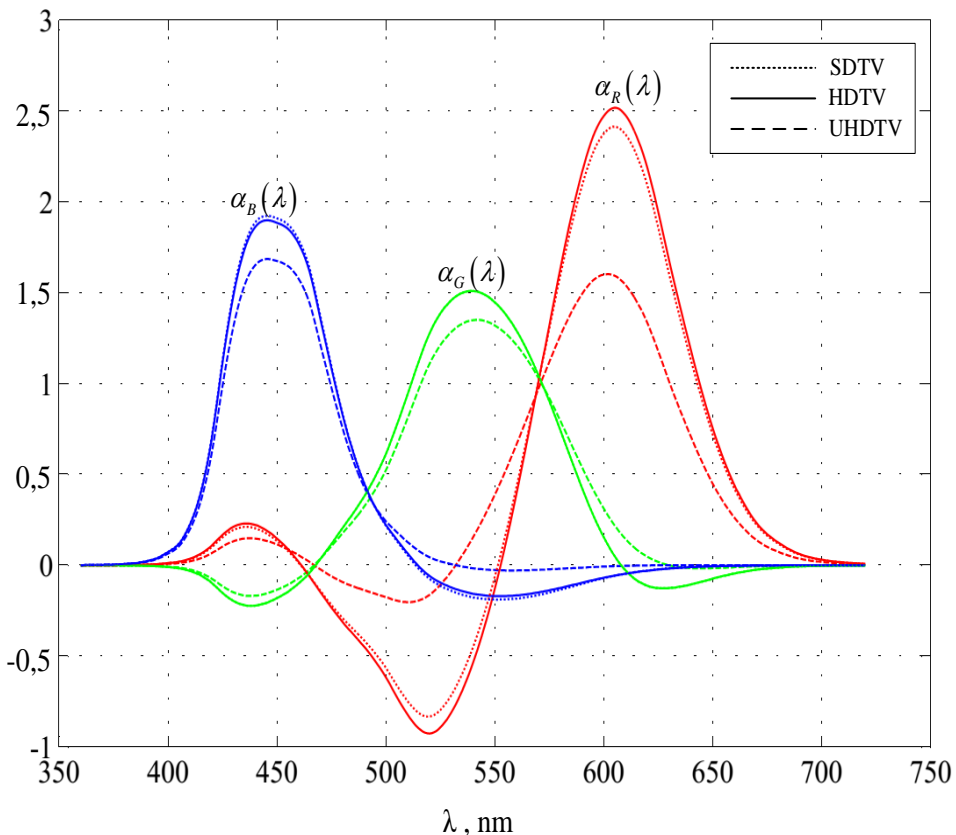


Figure 1 - Comparison of the spectral characteristics of the sensitivity of the channels of the primary colors, ideal from the point of view of colorimetry CIE 1931, cameras TSCH, HDTV, HDTV

The difference in these characteristics leads to a color rendering error introduced by the camera, in which the colorimetry of 1931 is implemented about the camera, in which the more perfect colorimetry of 2006 is implemented. Where are the vectors of the spectral characteristics of the sensitivity of the channels of the primary colors of the TV cameras? Index F denotes colorimetry belonging to 2006.

Colors differ in brightness and therefore refer to different levels of image lightness. For the Color Checker set, the signals of the primary colors do not exceed the interval $\overline{0;1}$, i.e., they can all be transmitted by the UHDTV system. For a set of optimal colors for some colors, the signals of the primary colors exceeded one level; therefore, normalization was introduced into their brightness, as a result of which the signal levels were limited by the interval $\overline{0;1}$. The color points of both sets are shown in Figure 2.

This difference in characteristics causes color errors that occur in cameras implementing the 1931 colorimeter and in cameras implementing the more advanced 2006 colorimeter. Where is the spectral characteristic vector of the camera's primary color channel sensitivity? Index F indicates a colorimetric reference to 2006.

Colors vary in brightness, so they represent different levels of image brightness. The primary color signal does not exceed the interval for the Color Checker set $\overline{0;1}$. In other words, it can all be transmitted on a UHDTV system. When choosing the optimal color for some colors, the signal of the primary color exceeded one level. Therefore, normalization was introduced in the brightness as a result of the signal level being limited by the interval $\overline{0;1}$. The two sets of color points are shown in Figure 2.

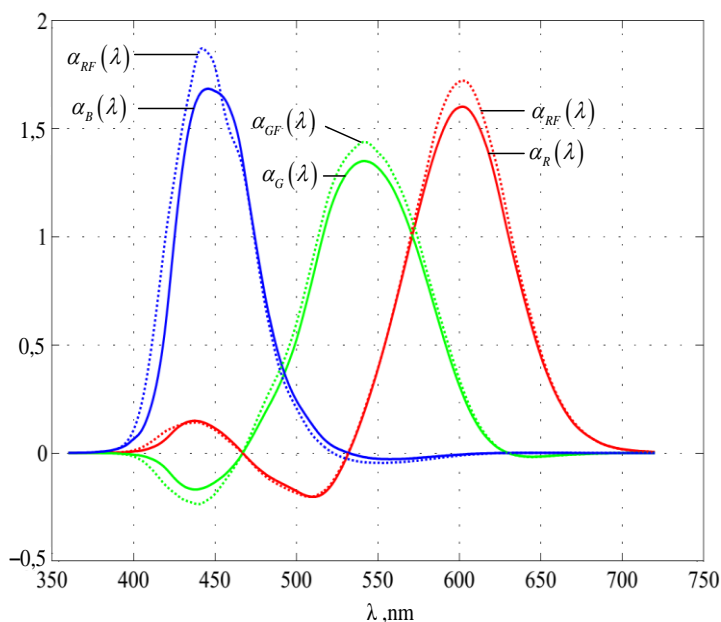


Figure 2 - Comparison of the spectral characteristics of the sensitivity of the channels of the primary colors of the UHDTV camera, ideal from the point of view of colorimetric CIE 1931 and 2006

An estimate of the color distortion of a “standard” camera relative to an ideal one. B TECH 3355 [4] presents an assessment of the color fidelity for a “standard camera”, the characteristics of which are obtained as a result of averaging modern SDC cameras. For the “standard camera” in [4, 5], the resulting spectral characteristics were calculated taking into account the linear matrix, which brought the resulting spectral characteristic as close as possible to the ideal one, and an estimate of the color shift concerning the original colors was given for two models linear, i.e. without taking into account gamma transformations, and nonlinear, i.e. taking into account gamma transformations. In this case, in [4], the chromaticity shifts are taken as occurring due to the imperfection of the spectral characteristics of the camera together with nonlinear transformation, and matrix optimization is applied to compensate for them.

3. EXPERIMENTAL RESULTS

In the present work, another approach is taken as the original one, which consists of the fact that successive gamma transformations with c on the transmitting side $\gamma_1 = 0,45 = \frac{1}{2,2}$ and the receiving side lead to the reproduction of colors and

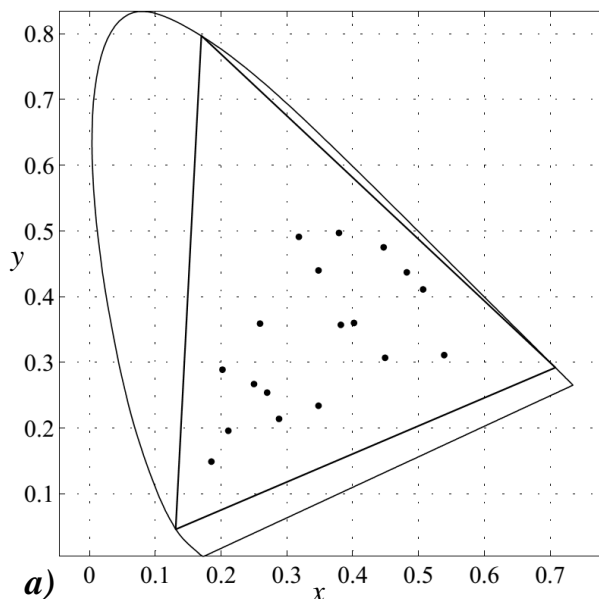
luminance halftones, perceived by observers as the best. Therefore, as a criterion for the fidelity of color reproduction, it seems preferable to evaluate the chromaticity shift about the colors determined for the case of using an ideal camera and using successively both nonlinear gamma transformations. Such a comparison is given in Figure 3, which follows the use of a camera with the characteristics of a “standard” camera with a linear matrix [4]. Figure 3 provides practically undistorted color rendition.

This conclusion can be extended to the HDTV system, taking into account the proximity of the colorimetric systems standardized for the HDTV and HDTV systems and are consistent with the data of [4] for the HDTV system.

In the present work, another approach is taken as the original one, which consists of the fact that successive gamma transformations with c on the transmitting side

$\gamma_1 = 0,45 = \frac{1}{2,2}$ and $\gamma_2 = 2,4$ and on the receiving side lead to the reproduction of colors and luminance halftones, perceived by observers as the best. Therefore, as a criterion for the fidelity of color reproduction, it seems preferable to evaluate the chromaticity shift about the colors determined for the case of using an ideal camera and using successively both nonlinear gamma transformations. Such a comparison is given in Figure 3, which follows the use of a camera with the characteristics of a “standard” camera with a linear matrix [4]. Figure 3 provides practically undistorted color rendition.

This conclusion can be extended to the HDTV system, taking into account the proximity of the colorimetric systems standardized for the HDTV and HDTV systems and are consistent with the data of [4] for the HDTV system.



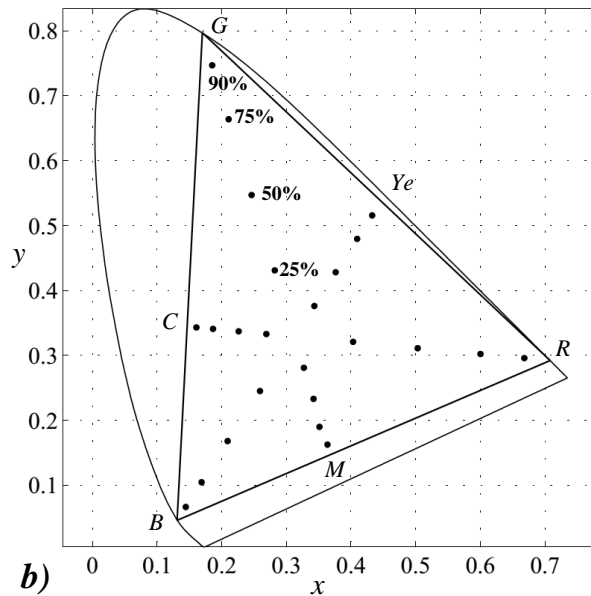


Figure 3 - Chromaticity points of the colors of the Color Checker set (a) and the set of optimal colors (b) as a function of the chromaticity coordinates of the CIE 1931 color space.

4. DISCUSSION AND CONCLUSIONS

The paper presents a study of the spectral characteristics of cameras standardized in the ITU systems of SDTV, HDTV, and UHDTV in terms of their influence on the colorimetric image quality as one of the main factors.

The method of colorimetric calculations recommended by SMPTE [4] was used to study the spectral characteristics of the sensitivity of the channels of the primary colors of ideal cameras that provide undistorted color rendition. These formulas and the tables of values of spectral characteristics of the sensitivity of the channels of the primary colors of ideal cameras built on them can be used in further research and development.

The assessment of color distortions of an ideal camera, in which the CIE 1931 colorimetry is implemented, about the ideal camera, in which the CIE 2006 colorimetry is implemented, was carried out for a set of colors specified by the spectral characteristics of the reflection of the test objects: The Color Checker set, which has found application for assessing the image quality for various video applications, including for assessing the characteristics of TV cameras. The assessment showed that the color rendering error does not exceed approximately 2

CIE units, i.e., its level is below the level of error of colorimetric instruments and below the threshold for the visibility of color change. Thus, it can be predicted that the transition to the use of the CIE 2006 colorimetry instead of the 1931 CIE colorimetry will not lead to a noticeable improvement in the quality of color rendering in television and similar systems. The presented estimates of the fidelity of color reproduction for the “standard” SDTV camera, defined in [4, 5], in comparison with the ideal camera, show that in a system with gamma correction on the transmitting side and gamma conversion in a reproducing device, a camera with the characteristics of a “standard” Cameras with a linear matrix provide practically undistorted color reproduction, if we take the converted image with the resulting index as optimal, and compare the evaluated image with it. The presented estimates of the colorimetric characteristics and signals for the colors of the Color Checker set, as well as the proposed set of optimal colors, can be used to implement the metrological base for assessing the color fidelity in the end to end television path “from light to light”, as well as for the calculated assessment of the colorimetric image quality.

References:

- [15] Pilyavskiy V.V. Evaluation of color reproduction in the path of a high-definition television system using signals from color stripes / V.V. Pilyavsky // News of higher educational institutions of Russia. Radio electronics. - No. 3. - 2014. - P.26–33
- [16] Gofaizen O.V. Problem questions of TV colorimetry / O.V. Gofaizen, V.V. Pilyavskii // Digital technologies, 2014. - №. 16. - P. 104-110
- [17] Gofaizen O.V. New directions in the progress of methods for assessing image quality in the end-to-end video path of digital TV systems “from light to light”. Gofaizen // 69th Science and Technology Conference of the Professors and Teacher Warehouse, Science, Postgraduate and Student. ONAT n.a O.S. Popov. - Odesa, 5–7 breast, 2014 p.
- [18] TECH 3355. Method for the assessment of the colorimetric properties of luminaires. The television lighting consistency index (TLCI-2012). FTV-LED. Geneva, April 2013
- [19] Pilyavskiy V., Vorobienko P. (2021) Theory of Color Constancy of Multimedia Images. In: Ilchenko M., Uryvsky L., Globa L. (eds) Advances in Information and Communication Technology and Systems. MCT 2019. Lecture Notes in Networks and Systems, vol 152. Springer, Cham. https://doi.org/10.1007/978-3-030-58359-0_24 University Science, 1989.

Effectiveness improvement of offset pulse position modulation system using reed–Solomon codes

1 st Ahmed H. Albatoosh

Middle Technical University, Electrical
Engineering Technical College,
Baghdad, Iraq
bbc0042@mtu.edu.iq

2 nd Mohamed Ibrahim Shuja'a

Middle Technical University, Electrical
Engineering Technical College,
Baghdad, Iraq
drshujaa@mtu.edu.iq

3 rd Basman M. Al-Nedawe

Middle Technical University, Technical
Institute of Baquba,
Diyala, Iraq
b.al-nedawe@mtu.edu.iq

Abstract—Currently, the pulse position modulation (PPM) schemes are suffering from bandwidth application where the line rate is double that of the initial data rate. Thus, the offset pulse position modulation (OPPM) has been suggested to rectify this concern. Several attempts to improve the OPPM can be found in the open literature. This study focuses on the utilization of Reed Solomon (RS) codes to enhance the forward error correction (FEC) bit error rate, which is not yet explored. The performance of errors of the uncoded OPPM was compared to the one used by RS coded OPPM using the number of photons per pulse, the transmission's efficacy, and bandwidth growth. The results demonstrate that employing FEC coding would increase the system's error performance especially when the RS is operating at its optimum Parameters. Specifically, when operating with a Code Rate that is equivalent to or even more 0.7, the OPPM with RS code outperforms the uncoded OPPM where the OPPM with MLSD needs only 1.2×10^3 photons per pulse with an ideal coding rate of about $\frac{3}{4}$.

Keywords—*Offset pulse position modulation, Forward error correction, Reed Solomon*

1. Introduction

The modulation and coding of the transmitter are widely used to guarantee that information is conveyed effectively and reliably. A modulating signal that represents the message and a carrier wave that is suited for the application are commonly utilized in modulation. Specifically, a modulator adjusts the transmitted signal in a systematic manner as a response to expected changes in the modulating signal [1]. Due to the reduced sign ratio, digital pulse position modulation (PPM) has a great sensitivity for encrypting huge data bits [2].

Fig. 1 depicts a diagram of OPPM transceiver. Information is conveyed via digital PPM by shifting the location of the pulse within $N = 2^M$ slots as represented in Fig. 1. M is the number of bits to be coded. The idea of a sign bit is employed in offset PPM, the amount of slots utilized in a single frame is less than half the amount of a digital PPM system (2^{M-1}) [3]. Ahfayd et al. [4] approved that OPPM runs at half the speed of a digital PPM line while becoming more sensitive at low bandwidth. In other words, OPPM has been presented as a solution to solve the issue of pulse position modulation bandwidth extension. OPPM enhances the sensitivity by >3.1 dB beyond the digital PPM, and it also outperforms multiple PPM in terms of precision. OPPM signifies by a common returning of the codeword positions to the starting point where the initial series is used. The least

significant bit (LSB) is therefore changed with one in the next iteration [5]. Afterwards, the following code words in the sequence will be generated as a result of deleting one of the least important considerations digits to the most significant bit (MSB).

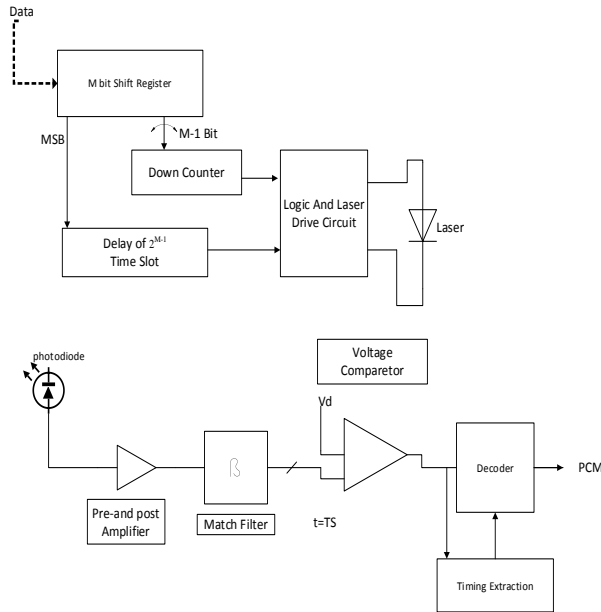


Fig. 1 A schematic diagram of an OPPM transceiver (Adapted from [1])

Several studies can be found in the open literature that focused on to improving the analysis of OPPM in comparison to PPM using several approaches. In this regard, a modulation scheme, dicode pulse position modulation (DiPPM) for optical wireless communications utilizing intensity modulation with direct detection (IM/DD) has been introduced by Wang et al. [6]. They proposed the Automatic Repeat Request (ARQ) technique to address OPPM error causes. This in turn showed an improvement of 3 dB in the PER performance for DiPPM due to the implementation of ARQ when an error is spotted.

Charitopoulos and Sibley [7] affirmed that the frame error rate performance of OPPM can be increased due to applying the ARQ technique while discovering an error.

Ray et al. [8] provided a novel performance assessment of an OPPM system employing a Gaussian impulse response graded index plastic optical fiber. The major goal of this study is to anticipate how sensitivity, inaccuracy, the number of photons needed, threshold voltage, and the influence of intersymbol interference would vary as the number of data bits encoded at a rate of 1 Gbit/s increases. The bandwidth-utilization efficiency is determined after a detailed information theory examination. The comparison is made to equivalent digital PPM and multiple PPM methods, and it is also demonstrated that offset PPM outperforms nonreturn-to-zero on-off keying by 7.5 dB.

Ray et al. [5] proposed the spectral features of an offset PPM sequence for the first time. The results demonstrate high frequency components at both the frame rate and the slot rate when return-to-zero pulses are utilized. The slot clock required to renew the signal can be obtained by extracting this component. Offset PPM can be said to have the greatest frame component.

Al-Nedawe et al. [9] utilized backward error correction to enhance the effectiveness of error in a dicode pulse position modulation system.

Using a commercial high power white single LED (30 W) and the new coding method, Ahfayd et al. [4] assessed the performance of a visible light communication (VLC) system based on OPPM. Through the simplest transceiver circuits, data at 11 Mbps has been conducted across a distance of 1 m with zero-bit error rate (BER) and 18 Mbps with 1.15×10^{-6} of BER.

The bit-error rate (BER) of the OPPM system can be increased significantly utilizing a priority decoding mechanism without requiring further bandwidth expansion, according to Farhat et al. [10]. The OPPM system was proposed on FPGA using VHDL, along with priority decoding. The BER results of the traditional and modified OPPM are compared in this study, revealing a considerable improvement in the BER of priority decoding OPPM.

A precise review of the previous studies would ascertain that the utilization of the Reed Solomon (RS) codes in improving the OPPM has not been yet investigated. Thu, this study comes to justify this concern by introducing the main concept of RS coded OPPM system with a thorough comparison between the performance of transmission's efficacy, bandwidth growth, and the performance of errors of the uncoded OPPM and the RS coded OPPM system via a simulation.

2. OPPM Error Source

As notified by Sibley [11], both digital PPM and OPPM are susceptible to three distinct forms of detecting errors: wrong-slot, erasure and false alarm as show in Fig. 2. In the occasion of a noise, a wrong-slot error occurs, a recorded pulse's rising edge would enable the pulse to act in time slots next to each other. The pulse is recognized at the middle of the time slot width to reduce this mistake T_s . Thus, mistakes are created when the edge moves by $T_s/2$ [12].

Erasure mistakes happen when there is a lot of noise sufficiently high that the voltage of the peak signal falls below the threshold value. Consequently, the pulse will be vanished and there're this voltage becomes noisy as a result to crossing the threshold with false alarms. The voltage can also be presented as a signal in the slots around the one holding a pulse due to Inter-Symbol Interference.

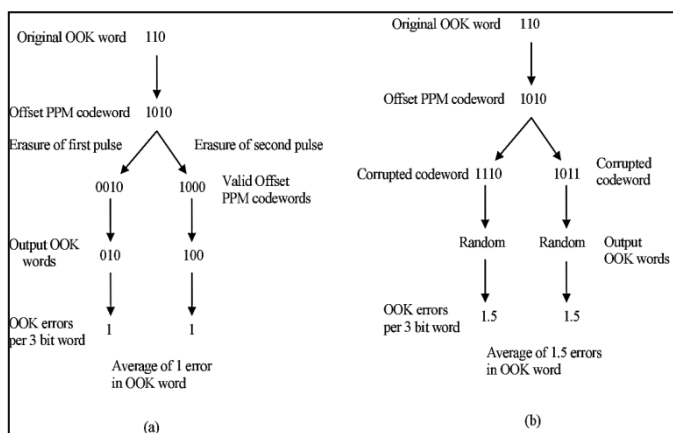


Fig. 2 Effect of (a) erasures and (b) false alarms on the decoding of offset PPMs (Adapted from [11])

3. Reed-Solomon error correction

Reed-Solomon are error-correcting codes that have a variety of communication networks and storage applications. In several systems, Reed-Solomon codes can be considered as a super method to repair faults. Thus, this study presents the Reed-Solomon encoding to resolve the errors that plague the OPPM. Reed-Solomon encoding augments a chunk of digital data that contains additional redundant bits. Basically, there is a possibility of having faults during transmission due a number of reasons. Reed-Solomon decoder can decode each

block in order to fix errors and recover the data from the start. The number and kind of repairable errors are governed by the Reed-Solomon code's characteristics. Cryan and Elmighani [13] endorsed Reed-Solomon decoder as a subclass BCH codes of linear block coding. With s-bit symbols, a RS code is written as RS(n,k).

In terms of the likelihood of a channel symbol mistake, the likelihood of receiving an incorrect sign decoded by RS, P_E can be written in the following way:

$$P_E \approx \frac{1}{2^{m-1}} \sum_{j=t+1}^{2^m-1} j \binom{2^m-1}{kj} p^j (1-p)^{2^m-1-j} \dots (1)$$

t is the code's symbol-error-correction capacity. Each signal includes m bits. The binary likelihood of mistake is connected to the decoded symbol outage probability [14].

$$P_{eb} = \frac{2^{M-1}}{2^M-1} P_E \dots (2)$$

4. Simulation System Design

The ideal parameters of an RS code with an OPPM structure were explored using slope detection and central detection methods. Nevertheless, it is necessary to create an acceptable model of a system in order to execute an effective simulation. A system model defines the links between intake and output outflow parameters. The receiver system, also known as the FEC system of communication, is depicted schematically in Figure 3 and also is based on the RS code for error correction.

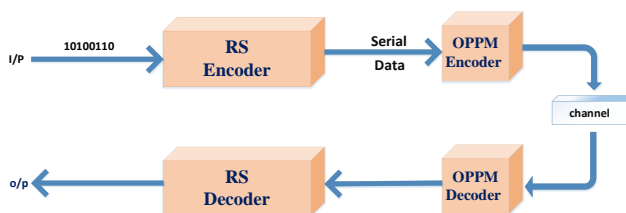


Fig. 3 Flow Sender and Receiver System Design

5. Results and Discussion

The primary goal of this part is to look into the effect of per-pulse photons (b) in the OPPM coded format with a variable speed. Slope and central sensing techniques are also used, and coding speeds are used to describe them. Apart from M values between 3 and 5, the quantity of photons is usually determined using a $2M$ codeword length. It's worth noting that when the RS coding rate rises, so does the RS coding rate (b). This is because of a constant association between the number of data symbols and the RS coding rates. When using the slope's bandwidth detection approach, b is relative to standardized. This is also due to the fact that the output signal is dependent on the slope detecting technology.

The change of b for an OPPM utilizing the RS coding rate at various normalized bandwidths is depicted in Fig. 4. It's worth noting that the rate of mechanism failure was kept to a bare minimum. In addition, as shown in Fig. 4, b is the number of persons normalized bandwidths is inversely related to the number of people. The smallest b confirms the greatest normalized bandwidth. Furthermore, as the RS coding rate increases, b increases exponentially. Understanding the importance of minimizing b is crucial in this regard, as it allows you to produce the appropriate code rate when using an RS code and increase the device's maximum performance.

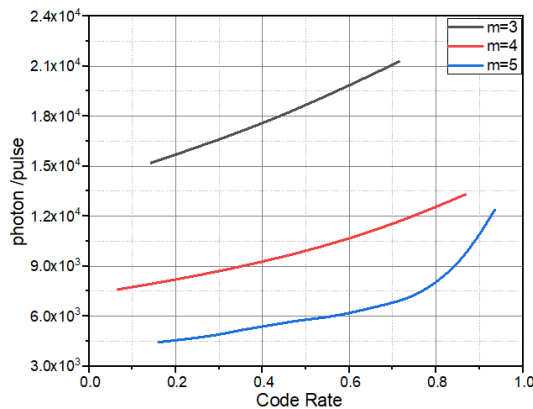


Fig. 4 Number of photons against the RS coding rate for variable normalization bandwidths

Figure 5 specifies the transmission efficiency of the coded OPPM system versus RS code rates for multiple fibers with normalized bandwidths. Figure 5 shows that for most normalized bandwidths, the best transmission effectiveness is around 0.6 of the RS coding rate. Higher RS coding rates of around 0.7 were found to provide the best transmission efficacy at narrower normalized bandwidths. Understanding the link between transmission effectiveness and code rate is critical, because efficacy started to drop once the ideal code rate is reached. Specifically, while the coding rate has increased, the number of unrecorded symbol errors has enlarged as well. Consequently, the efficiency of the system and its ability to communicate rectified symbols are impaired. In this circumstance, the amount of redundancy and the rate of redundancy surpass the prime coding rate. On the other hand, higher fiber normalized bandwidths, have effectively increased transmission efficiency. The implications of reducing b utilizing RS codes in order to boost the OPPM's transmission efficacy is seen in Figs. 5 and 6.

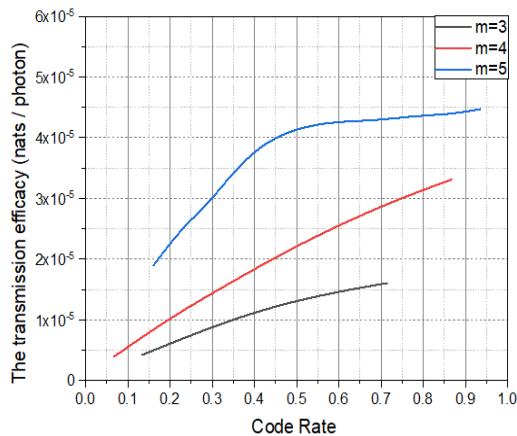


Fig. 5 The effectiveness of a coded OPPM system in transmitting data versus RS code rates

Fig. 6 compares the amount of photons in each pulse for the code OPPM method to the RS Code for a variety of normalized fiber bandwidths (f_n). For any given normalized bandwidth, the photons in each pulse have a positive relation with the RS Code Rate. As the Code Rate climbs, so does the number of photons in a given bandwidth.

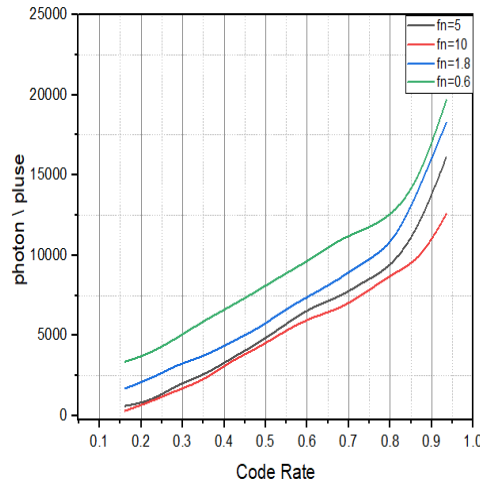


Fig. 6 The number of photons against the RS coding rate at different normalized bandwidths

Fig. 7 shows the relationship between OPPM transmission efficiency utilizing the RS coding scheme and the RS Code Rate for various fiber bandwidths (fn) normalized to the OPPM data rate. Using an optimal value of 0.7 for the Code rates tends to improve overall efficiency. The coded OPPM with RS coding yielded the desired transmission efficiency for the low dispersive channel.

$$\alpha = \frac{0.1874 T_b}{f_n} \dots\dots\dots (3)$$

T_b is the PCM bit-time

$$\rho = \frac{r \ln 4}{b} \dots\dots\dots (4)$$

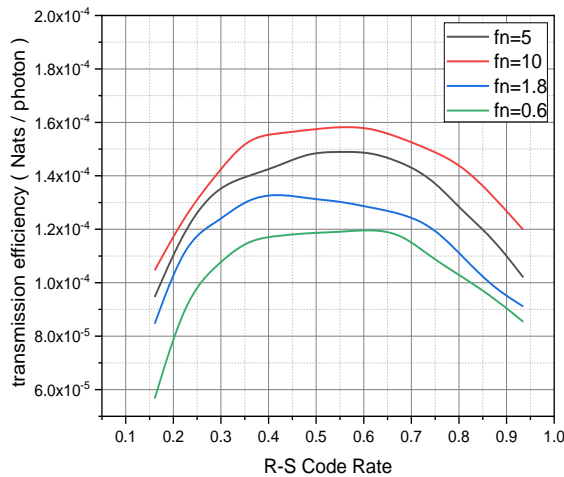


Fig. 7 The transmission efficiency against RS coding rate for variable normalized bandwidths

The transmission efficiency of uncoded and coded OPPM systems as a function of normalized bandwidth can be seen in the Fig. 8. The coded OPPM adopting RS coding provides a higher transmission efficiency while functioning in a low dispersive channel. This is attributable to the fact that the redundancy symbols in the RS coding need additional bandwidth.

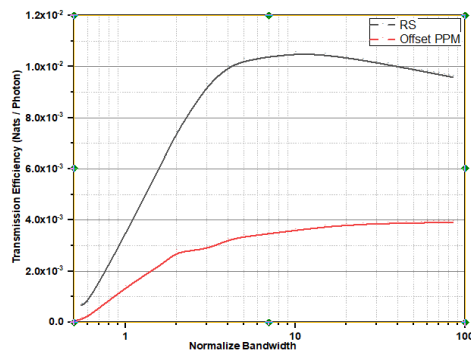


Fig. 8 RS coding rate and OPPM transmission efficiency against the normalized bandwidths

Fig. 9 shows the comparison between RS and OPPM. Because OPPM has the highest number of errors, it will deliver more error-free data to the recipient. Every communication system's primary purpose is to receive data with the fewest possible errors; the BER is defined by the modulation method used

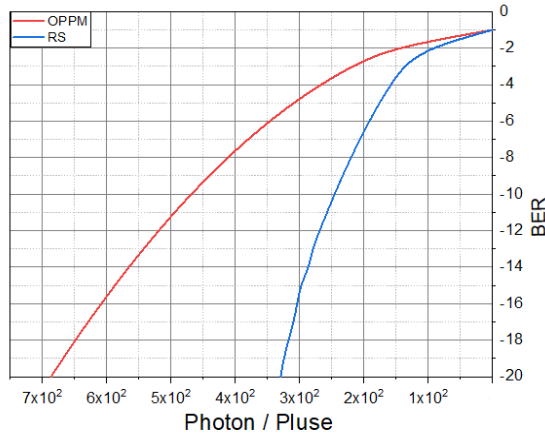


Fig. 9 Relationship between the number of photons for OPPM and RS versus bit error rate

6. Conclusions

OPPM was used to explore the transmission effectiveness, bandwidth increase, and quantity of photon required per pulse of Reed Solomon codes. The OPPM programmed mechanism surpasses the uncoded system in general. The acquired signal was evaluated using two improved slope and center detection practices in order to meet the study's principal goal. It might be claimed that using RS codes to reduce the number of photons is a good idea, as this considerably boosted the OPPM's transmission effectiveness. The machine's performance has also been increased by raising the RS codeword. More crucially, the research identified the best RS coding rates for high and low standardized fiber bandwidths, resulting in the highest transmission efficiency.

References

- [1] M.J. Sibley, "Analysis of offset pulse position modulation-a novel reduced bandwidth coding scheme" *IET optoelectronics*, vol. 5, no. 4, pp.144-150, 2011.
- [2] I. "Garrett, August. Digital pulse-position modulation over dispersive optical fibre channels" In Int. Workshop on Digital Communications, Tirrenia, Italy (pp. 15-19), 1983.
- [3] I. Garrett, "Pulse-position modulation for transmission over optical fibers with direct or heterodyne detection" *IEEE transactions on communications*, vol. 31, no. 4, pp.518-527, 1983.
- [4] M.H. Ahfayd, M.J. Sibley, P.J. Mather, P.I. Lazaridis, "Visible light communication based on offset pulse position modulation (Offset-PPM) using high power LED" XXXIInd General Assembly and Scientific Symposium of the International Union of Radio Science (URSI GASS) (pp. 1-4). IEEE, 2017.
- [5] I. Ray, M.J. Sibley, P.J. Mather, "Spectral characterisation of offset pulse position modulation" *IET optoelectronics*, vol. 9, no. 6, pp.300-306, 2015.
- [6] H. Wang, G. Cheng, X. Sun, T. Zhang, "September. Performance analysis of dicode pulse position modulation for optical wireless communications" International Conference on Wireless Communications, Networking and Mobile Computing (pp. 3027-3030). IEEE, 2007.
- [7] R. Charitopoulos, M.J. Sibley, "Experimental coder/decoder of dicode pulse position modulation" University of Huddersfield. 2009.
- [8] I. Ray, M.J. Sibley, P.J. Mather, "Performance analysis of offset pulse-position modulation over an optical channel" *Journal of lightwave technology*, vol. 30, no. 3, pp. 325-330, 2011.
- [9] B.M. Al-Nedawe, A.M. Buhafa, M.J. Sibley, P.J. Mather, "November. Improving error performance of dicode pulse position modulation system using forward error correction codes" 21st Telecommunications Forum Telfor (TELFOR) (pp. 331-334). IEEE, 2013.

- [10] Z.A. Farhat, M.H. Ahfayd, P.J. Mather, M.J. Sibley, "Improved BER for offset pulse position modulation using priority decoding over VLC system" *Wireless Days (WD)* (pp. 1-4). IEEE, 2019.
- [11] M., Sibley, "Performance analysis of a dicode PPM system, operating over plastic optical fibre, using maximum likelihood sequence detection" *IEE Proceedings-Optoelectronics*, vol. 152, no. 6, pp.337-343, 2005.
- [12] H. Joki, J. Paavola, V. Ipatov, "September. Analysis of Reed-Solomon coding combined with cyclic redundancy check in DVB-H link layer" 2nd International Symposium on Wireless Communication Systems (pp. 313-317). IEEE, 2005.
- [13] R.A. Cryan, J.M.H.M.O. Elmighani, "Reed-solomon coded optical PPM employing PIN-FET receivers" In *Proceedings of ICC/SUPERCOMM'94-1994 International Conference on Communications* (pp. 126-130). IEEE, 1994.
- [14] C. Fu, C. Gong, N. Huang, J. Luo, Z. Xu, "Concatenated RS-LDPC Coding for Water-to-Air Visible Light Communication Through Wavy Water Surface" 13th International Conference on Wireless Communications and Signal Processing (WCSP) (pp. 1-5). IEEE, 2021.
- [6] L. Shu D.J. Costello "Error Control Coding Fundamentals and Application" London, Prentice-Hall, Inc.,1983
- [10] M.J. Sibley," Dicode pulse-position modulation: a novel coding scheme for optical-fibre communications" *IEE Proceedings-Optoelectronics*, vol. 150, np. 2, pp.125-131, 2013.
- [17] H. Bartz, S. Puchinger, "Fast Decoding of Interleaved Linearized Reed-Solomon Codes and Variants" arXiv preprint arXiv:2201.01339, 2022.

Design and Implementation Cybersecurity Computing Architecture using for Better Throughput on FPGA

Nada Qasim Mohammed 1 , Qasim Mohammed Hussein 2 Maki Mahdi
Abdulhasan 3 , Abdullah Ridha Faisal 4

Ali Abdul Kadhim Ruhaima 5

Email: nadaqasim99@gmail.com ; kassimalshamry@yahoo.com
;maki.a.eng@nuc.edu.iq, ali.abd.eng@nuc.edu.iq,

Abdullah.r.eng@nuc.edu.iq

Abstract—This paper presents an efficient parallelism architecture that uses a dual-computing engine architecture to better throughput using both spatial and temporal parallelism on FPGA technology. This architecture will enhance the performance in terms of operating frequency and throughput and reduces the power consumption that meets applications with huge data processing such as Internet of Things .in this design, two boards are used, "DE1_Soc and NEEK board" with Altera Quartus Prime 18 for synthesis and simulation. The proposed design architecture gives better resource usage and throughput through fewer hardware redundancies using a frequency of 600MHZ with 64 bits for each engine from the dual-engine. Furthermore, the proposed architecture implementation results show the reduction in the time delay by 40 % and achieves a throughput of 153.6 Gb/s

Index Terms— Field programmable gate array, embedded system design, spatial parallelism, AES encryption/decryption, Low power Architecture, Internet of thing

I. Introduction

In this digital age, cyberspace has become an arena for Management, social services, education, marketing, business, and entertainment in everyday life. This was accompanied by an increasing in threats and breaches cybersecurity to access, steal, damage, or change the information or during storage or transmission over networks [1]. To secure these data need executing complex cybersecurity algorithms, such as AES algorithm, that requires high computing power, which makes sequential processing inefficient. Therefore, it is necessary to use parallel processing to execute these algorithms to obtain the most conceivable computational power of operations and throughput [2]. Various approaches have

Manuscript received Month Day, 2016; revised Month Day, 2016.

This work was supported by the Foundation Name under Grant No. XXXXXX.

Corresponding author email: author@hostname.org.

doi:10.12720/jcm.v.n.p-p

been introduced to deal with the complex computation problem to achieve low cost in hardware (area and power consumption) and high-speed performance. One approach is to invest parallelism in the spatial domain to perform tasks in parallel execution by using several processing units to use parallel features of functional units. This parallelism will take less time to execute the processing of operations; the most important features that should be considered when choosing parallel processing are reconfigurability, cost, power consumption, and time processing [3, 4].

Field-programmable gate arrays (FPGAs) have most of these features and more characteristics, which are suitable for implementing architectures with high parallelism, reliability, and flexibility [5]. In concern of security, cryptography plays a vital role in protecting information in cybersecurity protection. High-security cryptography algorithms that achieve information secrecy and integrity require high computational capabilities to increase the speed of operation and throughput. For example, AES is a good cryptography algorithm to ensure cybersecurity, and there is no practical attack against it [6]. Nevertheless, this algorithm requires high computational power to execute its operations. Therefore, a significant amount of research has been conducted on hardware implementation of the AES algorithm using FPGA. These implementations on hardware aim to achieve increased throughput and operating frequency, in addition to lower power dissipation, decreased latency and less area occupation

In this study, a hardware implementation of an efficient architecture is performed on the FPGA using spatial and temporal parallelism to obtain better throughput with a high operating frequency and fewer hardware redundancies. DE1 and neek-board devices are used in designing and implementing a dual-computing engine architecture using spatial and temporal parallelism. In this architecture, each color image is split into two equal parts, and each part is executed in one of the two engines concurrently. Deep pipelining is used to execute instructions of each engine independently. Encrypted color images using the AES cryptography algorithm were adopted to implement the proposed architecture". The remainder of this paper is organized as follows. in section 2 the literature survey is presented. Section 3 discusses the system specifications for the hardware implementation of the proposed architecture. Section 4 provides the results and discussion, and Section 5 includes concludes of this paper

II. Literature survey

Various architectural designs have been implemented on FPGA families to achieve many advantages, such as increased operating frequency, better throughput, decreased latency, lower power dissipation and lesser area, these approaches aim to optimize the power and increase the processing speed for many algorithms and applications. For example, several studies proposed a memory-based architecture design with less time and less complex. However, these architectures design requires more access time and more area, in addition to consumes more power [7-9].

In [10], the authors] proposed a mathematical and analytical model of the application's throughput in real time, using a low-latency Bloom filter on an FPGA, to obtain high-performance real-time information. In [11], a hardware design for the AES algorithm using a pipelined architecture was introduced. It delivers 2.29 GB/s encryption throughput at 56 MW of power consumption in 0.18- μ m CMOS technology.

partial parallelism to perform a fully stochastic simulation using FPGA architecture has been harnessed by [12]. As a result, the architecture, which presented, is faster than the existing simulator designed and implemented using FPGA with over 12-30 times that meet design requirements. Furthermore, to reduce the area of the crypto core, AES encryption and decryption were combined in [13]. from literature survey, one can conclude that memory-based architecture and combinational logic models consume more power and occupy more areas. In contrast, a composite field such as the Galois field model consumes significantly less power.

In [14], the author proposed FPGA architecture for parallel connected components analysis. It is based on partitioning the image into several vertical image slices, each slice processed in parallel. They used a coalescing unit collects information of components spanning these slices.

To produce high accuracy and throughput, Min, J. J., Salih, M. H eta al proposed new embedded data acquisition unit using spatial parallelism on DE0-Nano Field Programmable Gate Array board. In this proposal, through spatial

parallelism, Up to 7 input channels processed concurrently. The design of the system increases the operating frequency up to 1GHz. [15],[16] introduced the design of an AES algorithm using Xilinx SysGen, implemented on Nexys4, and simulated it using Simulink. It consumes 121 slice registers, and its operating frequency is 1102.536 MHz, and the system throughput is 14.1125 Gbps. MATLAB was used to generate keys. In [17], proposed approach sub-kernel parallelism that based on the correlation between execution semantic of FPGAs and OpenCL parallelism abstraction to decouple the actual computation from data access of memory. This overlaps the computation of current threads with the memory access of future. The achieving of implementing this kernel parallelism is 7% increase in power consumption which increases the speed 2X and reduces the overall energy consumption more than 40%., with only 3% increase in utilization of resources. In [18], Neelima and Brindha elaborated a parallelism architecture using the Quartus FPGA device to explore the parallelism within the mix column in the AES algorithm. This architecture reduces the area by 30% and a 5% delay. Graded and Deshpande [19] discussed a composite field arithmetic SBox to improve the delay performance. In their work, composite field arithmetic AES SBox, pipelined SBox, LFSR-based SBox and direct compute SBox were presented. In [20], a triple-key AES on a Spartan 3E FPGA kit was proposed. The researchers mentioned their results to optimize the delay of 4.221ns in the outcome and 1.55w in total power consumption.

[21] used the entire pipeline and parallel computing features of the FPGA to optimize the high-performance AES encryption algorithm. Then, [22] proposed pipeline techniques to implement the AES algorithm on an FPGA to increase the AES encryption speed. They used the Xilinx "Spartan-3A/3AN FPGA Starter Kit" to implement the AES algorithm. The implementation results of the proposed algorithms were good.

In [23], the proposed implementation of the AES] algorithm on FPGA uses a multistage pipeline and resource sharing to secure and provide low power and area for networks of IoT applications. Meanwhile, the authors in [24] proposed an architecture on the Xilinx Spartan FPGA series to implement AES-128 to minimize the area and reduce hardware utilization. From the obtained results, the reduced area was 67%, and the delay increase was 69%.

In [25], the authors presented a high performance computing architecture that exploited FPGAs as "full-fledged peers" within a distributed system instead of attached to the computer central processing. The resultant of hardware implementation gives improves the latency to 25% versus a software-based transport, the computing throughput increased 10%.

In order to get high-performance computing domain, the authors presented a workflow for semi-optimal FPGAs for network structure applications by takes advantage of the FPGA key characteristics. They implemented their design for three representative applications on a Xilinx Alveo U280 FPGA. The implementation using the low-level circuit elements results showed 2× energy savings [26].

In [30], Authors introduced lightweight block cipher architecture to ensure security against attacks of malicious that make used of pseudo random number with good random statistical features This architecture utilizes dual-port read-only memory to generate the 80-bit key from 64-bit of input. The operating frequency of the generator architecture was 612.208 MHz using a Virtex 5

III. SPATIAL AND TEMPORAL PARALLELISMS

Data partitioning strategies significantly aid in data processing techniques to improve performance by using parallel processing systems [27]. Spatial parallelism allows duplication of tasks that can be processed via specific modules using many engines. These tasks were performed simultaneously in different physical locations.

In the spatial parallelism mechanism, the main task is divided into several regions, and then each region is processed by processing element independently [28]. This hardware duplication reduces the processing speed and increases throughput by processing multiple tasks at times. Therefore, using spatial parallelism as a solution merits attention to process many tasks simultaneously via different processing models unless there are no resource conflicts. Significantly, the flexibility of spatial computation performance is available in reconfigurable platforms [29]. The spatial parallelism features are explored and used at many construction levels of the system, starting with the system interconnection to the entire functional unit features to improve the system's throughput. Therefore, it is considered as a potential solution in parallel system design, and many techniques

use spatial parallelism techniques to execute complex algorithms; one explores the parallelism features on FPGA. [5].

In temporal parallelism can be used pipelined to reduce the total cycle's number to process the file, which makes the system faster. Also in the case, the number of system cycles will reduce by using the parallel processing technique which is based make the processor work as more than one processors to achieve the task processing faster as possible.

IV. The proposed Architecture

The proposed architecture is designed to work with efficient parallelism that able us to use it for any image processing process by modifying only small part of it. the details of it as following:

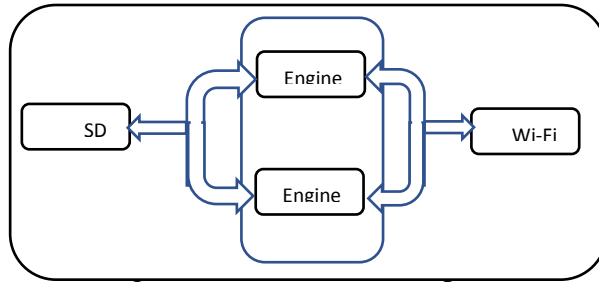
A. Architecture Specifications

The top-level design of the proposed system, presented in Figure "1", illustrates the design of dual engine cybersecurity computing architecture using a spatial parallelism and a temporal parallelism on an FPGA, depends on using a DE1_SoC board connected with a NEEK board through Wi-Fi in each DE1_Soc (Server) and NEEK board (Client).

The presented design implement makes use of the spatial parallelism on the FPGA technique for processing, simultaneously, four parts of the input image; each performs a specific function.

The architecture consists of three parts, which are explained in detail, figure 1.

- SD cards: The design used a Micro SD card interface to read and store the reading images. SD card is 2 Gb for NEEK board and 4Gb for DE1_SoC.
- Two engines: They process the data in parallelism manner simultaneously. The engine consists of the necessary operation of the encryption/decryption processing unit, on-chip mem, sync, and time/multi-clock units. The processing in each engine depend on using pipelining architecture.
- The Wi-Fi controller transfers images between two boards: DE1-SoC and NEEK boards. Both boards had the same TLDs. Wi-Fi in DE1_SoC operates as (Server) and Wi-Fi in NEEK operates as (Client), so the transmission will be easy.



B. Engine Top Level Design

Each engine includes five Part. This section explains in detail the top-level design of each machine, as shown in Figure 2. The design contains the following parts:

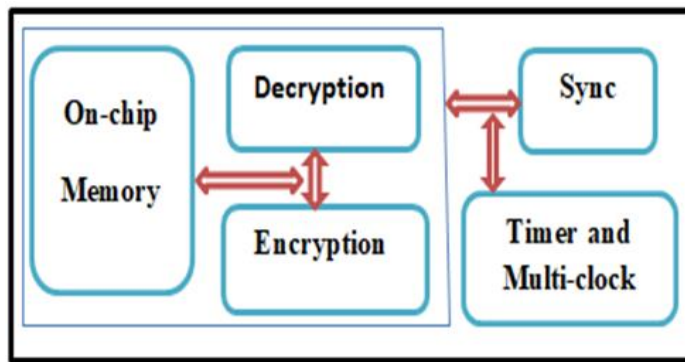


Fig.2. Engine Top-level Design

- On-Chip Memory: The DE1-SoC computer includes a 256 KB memory that is implemented inside the FPGA chip, which organized into 64 K × 32 bits. Memory is used as a pixel buffer for storing the image when encrypting and storing the image during decryption.
- Encryption/ decryption: This part performs the encryption or decryption process programs depending on the aim of the execution. The symmetric block cipher AES was used to encrypt the images. In AES, all arithmetic operations are performed over a finite field GF(28). It takes a key length of 128 bits and 128 bits' plain text block size.
- Sync: This part of the design uses the timer scheduler of all operations/tasks inside each engineer, and uses master and multi block

generators to synchronize all transmissions.

- Timer and multi clock: This part generates the necessary clocks and timers for different operations. Some of the subunits work with different watches, such as 1GHz, 1.3GHz, and 600MHZ. Sub-units are those in TLD and use different frequencies

C. Images encryption process

To encrypt the image, or any type of image processing, the following steps are performed:

Image's preparing: This step includes two steps. The first step is reading the image. Images have different types of gray or color of any size. After reading, the image will be split vertically into two equal segments, as figure 3.

- Each segment is transferred to one of the two images.
- Each engine executes the encryption/ decryption process using AhghggES-128 bit simultaneously.
- After finishing the encryption/ decryption process, the processed data return to SD card and store these data after merging the two segments.



(a) Original Image

(b) Image Splitting

Fig 3: Image splitting operation

D. Image decryption process

To decrypt the encrypted image as in Figure 1, the same steps are repeated in 3.3, except there is a changing in the function of the encoder/decoding part, where the program that related to the decryption process is executed

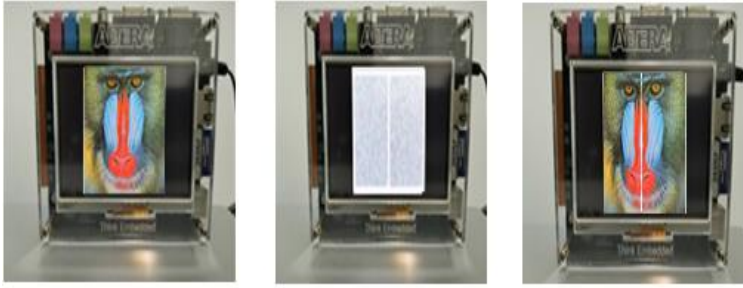
V. IMPLEMENTATION AND RESULTS ANALYSIS

The proposed design is implemented on DE1_Soc(server) and NEEK board(client) connected using Fi-Wi on both boards, and the software is Altera Quartus Prime 18 for synthesis and simulation. The AES version is a 128-bit block used to encrypt images. Firstly, before encryption process, each image is divided into two equal parts, and each two parts are processed by one engine of the architecture. After processing the image, the next image will be read. Each part is processed in $1.66 * 10^{-6}$ seconds. Figure 4 include original images examples and their encrypted and decrypted by using spatial and temporal parallelism with dual engines

Through the results obtained from the implementation of the architecture, the application of the spatial parallelism principle can enable modules of the system to process multiple input data at the same time to achieve multiple outputs, thus decreasing the complexity of overall system and increasing the utilization of the module. After executing the proposed architecture implementation, the final results were displayed on the LCD touch screen.

The experimental results show the architecture efficiency in terms of increasing the processing speed and high throughput. In contrast, NEEK showed the desired results even there is a noise was present within the input system signals Furthermore, one can be concluded that spatial parallelism is a good solution for systems that require real-time processing features, especially embedded system

. In this paper architecture, one can overcome some issues that faces systems resources constrains, such as memory size within the system, speed, and power consumption represent real challenge, which are faced many embedded systems



(a) Original Image (b)Encryption Image (c)Decryption Image

Fig4: Encryption and decryption processes

The hardware implementation results were shown that the throughput become 153.6 Gb/s which is faster than the results obtained from implementation this system using software. The proposed system supported with the ability to flexibility, reconfigurability, and reliability of the FPGA

The novelty of the proposed algorithm can be summed up in the following: Achieve the parallelism in two approaches spatial and temporal. In the spatial domain, it creates multiple engines to handle different files at the same times. Whereas in temporal domain, it uses deep pipelining by dividing every engine to sub modules to process and execute different executing tasks. In the security part, the dividing/encryption/decryption /collecting of files remain as original with minimum data corruption

Table 1. Comparison with others work for Frequency and Throughput

Design	Device	Frequency MHz	Throughput (Mbps)
Our architecture	SoC and Neek board	600	153.6 Gbps
[11]	a Virtex-II	159.210	1.941
[16]	Nexys4 Xilinx	112.536 MHz	14.1125 Gbps
[19]	Virtex-4 XC4VLX200	112.37	14,383
[20]	Spartan 3E FPGA kit	77.6	867.34
[24]	Spartan-3 XC300s	67.75	8672

VI.CONCLUSION

This study demonstrates the ability of the proposed architecture to perform the AES algorithm in spatial and temporal parallelism with high productivity. Within the Altera® Nios "II" Embedded Evaluation Kit, Cyclone "III" Edition many good features was harnessed to implement our design of this paper, such as the LCD touch screen, the switch inputs and "LEDs".

. The implementation results conformed high throughput of the system for different frequencies with a maximum frequency of 600 MHZ with 64 bits in each engine with a throughput equal to 76.8 Gb/s, which means that the throughput will become 153.6 Gb/s in all systems,

Therefore, the power consumption of the proposed design was significantly less. It can make use of these frequencies processing to be sent to platforms for IoT devices, which is defused, and shown on the LCD touch screen. All these results can be done with a resource utilization of low hardware.

ACKNOWLEDGEMENTS

This work was not funded by any part. I would like to thank my supervisors Dr.Amiza Amir and Dr..Muataz Hameed , UniMAP staff, my family, and everyone who supported me to make this work

REFERENCES

- [1] Guma'a, Omar Sapti, Qasim Mohammed Hussein, and Ziyad Tariq Mustafa Al-Ta'i. "Q-NTRU Cryptosystem for IoT Applications." *Journal of Southwest Jiaotong University* 54, no. 4 (2019).
- [2] Mohammed, Nada Qasim; Hussein, Qasim Mohammed; Sana, Ahmed M; Khalil, Layth A.A Hybrid Approach to Design Key Generator of Cryptosystem, *Journal of Computational and Theoretical Nanoscience*, Volume 16, Number 3, March 2019, pp. 971-977(7).
- [3] Nada Qasim Mohammed, Muataz H. Salih, Rafikha Aliana, Qasim Mohammed Hussein and Noor Aldeen A. Khalid, Design and implementation Image Processing functional units using spatial parallelism on FPGA, *ARNP Journal of Engineering and Applied Sciences*, Vol. 13, No. 15, 2018. PP. 4514-4520
- [4] Rami M. Aldahdoo, Parallel Implementation and Analysis of Encryption Algorithms, master thesis, Al-Azhar University-Gaza, 2018.
- [5] Nada Qasim Mohammed, Muataz H. Salih, Rafikha Aliana, Qasim Mohammed Hussein and Noor Aldeen A. Khalid, FPGA Implementation of Multiple Processing algorithms using spatial parallelism, *ARNP Journal of Engineering and Applied Sciences*, VOL. 13, NO. 15, 2016, PP.4556-4562.
- [6] William Stallings, *Cryptography and network security principles and practice*, seventh edition, published by Pearson Education Limited, 2017.
- [7] Good and Benaissa (2005) T. Good & M. Benaissa., Very small FPGA application-specific instruction processor for AES. *IEEE Trans. Circuits System*, 2006. pp- 1477–1486.
- [8] Harshali Zodpe and Ashok Sapkal, An efficient AES implementation using FPGA with enhanced security features, *Journal of King Saud University – Engineering Sciences* 32, 2020, PP. 115–122
- [9] Chow CT, Tsui LSM, Leong PS, Luk W, Wilton JSE, Dynamic voltage scaling for commercial FPGAs. *Proceedings, IEEE International Conference*, 2005, pp-173-180.
- [10] S. R. Chalamalasetti and M. Margala Throughput Analysis for a High-Performance FPGA-Accelerated Real-Time Search Application, *International Journal of Reconfigurable Computing*,2012(1), 2012, 16 pages.

- [11] Sirin Kumari M, Mahesh Kumar D, Rama Devi Y. High throughput-less area-efficient FPGA Implementation of block cipher AES algorithm. International Conference On Advanced Computing, Communication and Networks, volume 2011; pp 484–489
- [12] Thomas David B. and Amano Hideharu.. A fully pipelined FPGA architecture for stochastic simulation of chemical systems. IEEE 23rd international conference on field programmable logic and applications *FPL), Portugal , 2013
- [13] M. Rajeswara Rao; R. K. Sharma, FPGA implementation of combined AES-128, 8th International Conference on Computing, Communication and Networking Technologies (ICCCNT), 2017
- [14] Michael J. Klaiber , Donald G. Bailey , Silvia Ahmed , Yousef Baroud , Sven Simon, A high-throughput FPGA architecture for parallel connected components analysis based on label reuse, International Conference on Field-Programmable Technology (FPT) , IEEE Xplore 2014. 2013, DOI: 10.1109/FPT.2013.6718372
- [15] Min, J. J., Salih, M. H., Ng, Z., Kho, T., Woo, Y. S., & Yee, F. (2016). Design and implementation of embedded DAQ using spatial parallelism on FPGA for better throughput. 2016 3rd International Conference on Electronic Design (ICED). doi:10.1109/iced.2016.7804652.
- [16] Mane and Mulani , P. B. Mane and A. O. Mulani, High-Speed Area Efficient FPGA Implementation of AES Algorithm, International Journal of Reconfigurable and Embedded Systems Vol. 7, No. 3, November 2018, pp. 157-165.
- [17] Suhas Ashok Shiddibhavi, EMPOWERING FPGAS FOR MASSIVELY PARALLEL APPLICATIONS, Mater thesis, The University of North Carolina at Charlotte, 2018.
- [18] Neelima S., Brindha R. (2018) FPGA-Based Implementation of AES Algorithm Using MIX Column. In: Anguera J., Satapathy S., Bhateja V., Sunitha K. (eds) Microelectronics, Electromagnetics and Telecommunications. Lecture Notes in Electrical Engineering, vol 471. Springer, Singapore., 2018.
- [19] Ming Wong, M. L. Dennis Wong, Cishen Zhang, and Ismat Hijazin, Circuit and System Design for Optimal Lightweight AES Encryption on FPGA, IAENG International Journal of Computer Science, 45:1, IJCS_45_1_10, 2018.

- [20] Fazal Noorbasha, Y.Divya, M.Poojitha, K.Navya, A.Bhavishya, K. Koteswara Rao and K Hari Kishore, FPGA Design and Implementation of Modified AES Based Encryption and Decryption Algorithm, Volume-8 Issue-6S, 2018, pp.132-136
- [21] Chen H.Y. and YU SC, FPGA Implementation and Design of a Hybrid Chaos-AES Color Image Encryption Algorithm, MDP journal, Vol. 12, issue 2, 2019.
- [22] Mohamed Nabil, Ashraf A. M. Khalaf and Sara M. Hassan, Design and implementation of pipelined and parallel AES encryption systems using FPGA, Indonesian Journal of Electrical Engineering and Computer Science Vol. 20, No. 1, 2020, pp. 287-299.
- [23] P. Rajasekar & H. Mangalam, Design and implementation of power and area optimized AES architecture on FPGA for IoT application, Vol 47, issue 1, 2020
- [24] C. Arul Murugan, P. Karthigaikumar & Sridevi Sathya Priya, FPGA implementation of hardware architecture with AES encryptor using sub-pipelined S-box techniques for compact applications, Journal for Control, Measurement, Electronics, Computing and Communications, Vol. 61, No. 4, 2020. pp. 682-693
- [25] Lant, J., Navaridas, J., Luján, M., & Goodacre, J. (2020). Toward FPGA-Based HPC: Advancing Interconnect Technologies. IEEE Micro, 40(1),2020, 25-34.
- [26] K. Kamalakkannan, I. Z. Reguly and S. A. Fahmy High-Level FPGA Accelerator Design for Structured-Mesh-Based Explicit Numerical Solvers, arXiv:2101.01177v2 [cs.AR] 7 Jan 2021
- [27] Zhao C, Zhao Y, Meng L, et al. The key technological issues of parallel spatial database management system for parallel GIS, [J]. Computer Knowledge & Technology,47(4): 205. PP1265-1270.
- [28] Behera, Ranjan Kumar, Kumar, Deepak, & Pandey, K. S. . Concept, Design and Performance Evaluation of VLVIW Processor. International Journal of Scientific Engineering and Technology 2(7), 2013
- [29] Yousif, Muataz H. Salih, L. A. Hassnawi, Mahmoud A. M. Albreem, Mays Q. Seddeq and Hiba M. Isam Design and Implementation Computing Unit for Laser Jamming System using Spatial Parallelism on FPGA, 2015 IEEE International Conference on Signal and Image Processing Applications (ICSIPA), 2015.

- [30] T. Kowsalya, R. Ganesh Babu, B. D. Paramesh Chari, Anand Nayyar and Raja Majid Mehmood, Low Area PRESENT Cryptography in FPGA Using TRNG-PRNG Key Generation, Computers, Materials & Continua, vol.68, no.2, 2020.pp 1447-1465

Transmission Efficacy of Offset Pulse Position Modulation by Using Reed Solomon and LDPC

1st Ahmed Hasan Salman¹, 2nd Mohamed Ibrahim Shuja'a^{2,3}, 3rd Basman M. Al-Nedawe³

{bbc0042@mtu.edu.iq¹, drshujaa@mtu.edu.iq², b.al-nedawe@mtu.edu.iq³}

Middle Technical University, Electrical Engineering Technical College, Baghdad, Iraq^٢ & ^١

³ Middle Technical University, Technical Institute of Baquba, Diyala, Iraq

ABSTRACT

An innovative performance study of an offset pulse-position modulation (OPPM) scheme is presented in this work with reed Solomon and low-density parity-checking (LDPC). For the very first time, this work aims to solve the OPPM error problem by including Forward Error Correction (FEC). In order to generate a bandwidth-efficient modulation technique, Reed Solomon (RS) is utilized in combination with multi-level coding and trellis-based waveform shaping. When the RS is operational at its optimal settings, the findings indicate that applying FEC coding can increase the system's bit error rate. The standard best rates for different fiber normalization bandwidths for the greatest transmission efficiency will be researched. Low-density parity-checking (LDPC) is utilized in combination with RS in this instance. Comparing the outcomes of the two error correction procedures before to and after the transmission and determining the transmission efficiency. OPPM was used to study the transmitting efficacy, channel extension, as well as the needed number of photons per pulse of Reed Solomon and LDPC codes in this article. When compared to RS and LDPC, offset PPM has the most errors, hence the former will deliver more error-free data to the receiver.

Keywords:

OPPM

FEC

RS

LDPC

Transmission Efficiency

1. INTRODUCTION

Modulation and coding are processes carried out at the transmitter to ensure that information is sent efficiently and reliably. Two waveforms are used in modulation, a modulating signal that represents the message and a carrier wave that is appropriate for the application. A modulator changes the

carrier wave systematically in response to changes in the modulating signal [1]. We usually demand that modulation be a reversible operation, so that the message may be recovered using the corresponding demodulation procedure. a part of an analog modulating signal and the modulated waveform formed by changing the amplitude of a sinusoidal carrier wave this is the amplitude modulation (AM) that you're probably acquainted with from radio broadcasts and other uses [2]. Frequency modulation (FM) or phase modulation can also be used to imprint a message on a sinusoidal carrier (PM). Continuous-wave (CW) modulation is the umbrella term for all sinusoidal carrier's modulation schemes. The carrier frequency of most long-distance transmission systems is significantly higher than the modulating signal's highest frequency component [3]. Because it has a low mark-to-space ratio, digital pulse position modulation (PPM) is very good at encoding big data words because it doesn't have a lot of marks. [4].

2. MOSELING AND PROPOSED SYSTEM DESIGN

I. Offset Pulse Position Modulation (OPPM)

Sibley suggested Offset Pulse Position Modulation (OPPM) in 2010, OPPM is a new type digital pulse position modulation (DPPM) that works at about half of the speed of a digital PPM acceptable rates while increasing sensitivity at low bandwidth [5]. OPPM presented a solution to the problem of pulse position modulation bandwidth extension (PPM). The offset PPM improves sensitivity by >3.1 dB over digital PPM, and it also has superior sensitivity than multiple PPM. At the start, the first sequence is utilized when all codeword locations have been reset to zero. In the second sequence, the least significant bit (LSB) is discarded in favors of one. By moving one digit from the least significant towards the most significant, the following code words in the sequence will produce (MSB) [6]. The spectrum properties of OPPM, MPPM, and truncated PPM were compared and studied [7]. OPPM produces distinct lines DPPM does not have a strong frame element frame recurrence rate, but OPPM does. The OPPM technique converts pulse code modulation (PCM) three-bit codewords to four-bit codewords. On the other hand, DPPM, has a line rate of $2^M / M$ percent of the M-bits are the signal bits in the fundamental PCM rate. illustrates how to convert 3 bits of PCM into OPPM and DPPM codewords **Tab1**. For words 100 PCM, the method is comparable to that of DPPM; Just with

Offset PPM is there a differential., no pulse is broadcast for 000 PCM. The MSB is stripped the PCM term and is delays by 2^{M-1} time slots by decoder and offset PPM coder.

PCM (dataword)	OPPM codeword	DPPM codeword
000	0 000	0000 0001
001	0 001	0000 0010
010	0 010	0000 0100
011	0 100	0000 1000
100	1 000	0001 0000
101	1 001	0010 0000
110	1 010	0100 0000
111	1 100	1000 0000

Tab. 1 PCM TO OPPM AND DPPM TRANSFORMATION

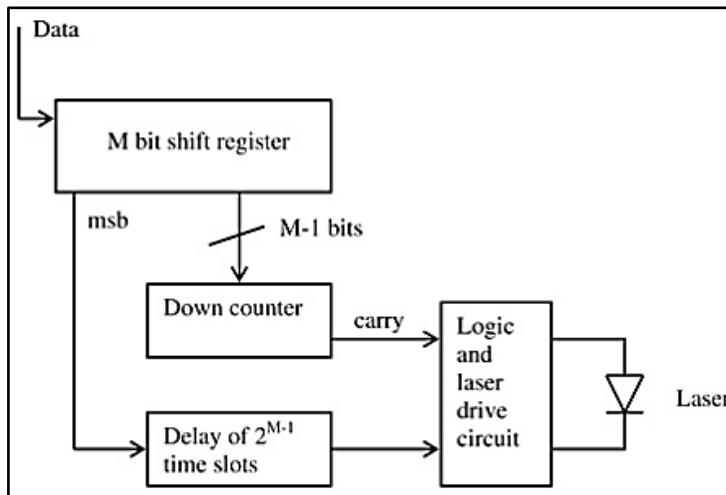


Fig.1 System for OPPM coding and transmission (M. J. Sibley, 2011)

For the first time, PPM was successfully implemented on a VLC system with a 'warm' 30W LED, reaching a data throughput of 11 Mbps having zero errors in transmission over a 1 m space that is free. [8]. Wang, Cheng, Sun, and Zhang [9] proposed the Automatic Repeat Request (ARQ) technique to address OPPM error causes. They demonstrated that OPPM has built-in error checking capabilities, and that by applying the

ARQ technique when an error is discovered, the frame error rate performance of OPPM may be increased [10].

II. OPPM Error Source

OPPM, like digital PPM, there are three different types of detecting failures: incorrect slot, erase, and false alarm [11]. When noise on a recorded pulse's rising edge causes the pulse to appear in adjacent time slots, this is known as a wrong-slot mistake. The likelihood of an incorrect slot mistake is computed in the following manner:

$$P_s = 0.5 \operatorname{erfc} \left(\frac{Q_s}{\sqrt{2}} \right) \dots\dots\dots (1)$$

Where
(2)

$$Q_s = \frac{T_s \operatorname{slope}(td)}{2\sqrt{(n\sigma^2)}} \dots\dots\dots$$

T_s is the slot time, t_d is the pulse that was slop received at the moment of decision, and n^2 is the noise with a mean square delivered detectors at the upper limit. The pulse is detected in the middle of the time slot width T_s to reduce this mistake. When the edge moves by $T_s/2$, mistakes are created [12].

Erasure errors occur when noise levels are high enough to cause the peaked voltage applied to the signal below

the cut-off point, as a consequence of which a pulse is lost. The likelihood of something happening is given by:

$$P_s = 0.5 \operatorname{erfc} \left(\frac{Q_s}{\sqrt{2}} \right) \dots\dots\dots (3)$$

Where T_s / R denotes the amount of noise that is unrelated bits per time frame, τ_R denotes the point in time when auto correlation has shrunk considerably, and Q_t denotes the time at which the auto correlation has become small.

$$Q_s = \frac{(V_{pk} - v_d)}{2\sqrt{(n\sigma^2)}} \dots\dots\dots (4)$$

v_{pk} Which describes the transmitter voltage level of a Specific time slot and the decision voltage is represented by v_d

On this voltage, there is noise. may trigger a threshold crossover occurrence if there is no pulse, resulting in false alarms. There may be a signal voltage in the slots around the one holding a pulse due to Inter-Symbol Interference [13].

$$P_s = \frac{T_S}{\tau_R} 0.5 \operatorname{erfc} \left(\frac{Q_S}{\sqrt{2}} \right) \dots \dots \dots (5)$$

Per time slot, the number of uncorrelated noise samples is represented by the ratio T_s / τ_R , where τ_R is the moment when the time series produces the minimal value.

$$Q_s = \frac{(V_d - v_{isi})}{\sqrt{(n\sigma^2)}} \dots \dots \dots (6)$$

The signal voltage level at a specific time slot is represented by VISI, which is dependent on the fault occurrences.

III. Reed-Solomon error correction

Error-correcting codes such as Reed-Solomon codes are used. dependent on blocks that have a variety of applications in communications networks and storage.[14] In several systems, Reed-Solomon codes are employed to repair faults. The Reed-Solomon encoder augments a chunk of digital information with extra "duplicate" bits. For a variety of causes, errors can arise during transmission and storage. The Reed-Solomon decoder examines every block, attempting to rectify and recover the beginning data [15]. The number and kind of repairable errors are governed by the Reed-Solomon code's characteristics. BCH codes are a subclass of RS codes, which are blocks that are linear digits. With s-bit symbols, a Reed Solomon code is written as RS(n,k) [16].

A Reed Solomon code is used in this paper. RS is offered in this study as a remedy to the error causes that plague the OPPM.in terms of the likelihood of a channel symbol failure, P_E may be written in the following way based on the Symbol-error likelihood encoded by Reed-Solomon:

$$P_E \approx \frac{1}{2^m - 1} \sum_{j=t+1}^{2^m - 1} \binom{2^m - 1}{j} P^j (1 - P)^{2^m - 1 - j} \dots\dots\dots (7)$$

The code's ability to rectify symbol errors is t, and each signal is formed composed of m bits. The likelihood of a decoded symbol outage is proportional to the probability of a binary mistake. [17].

$$P_{eb} = \frac{2^{m-1}}{2^m - 1} P_E \dots\dots\dots (8)$$

The scheme has associated characters like n and k, which can be written as Reed Solomon utilises m-bit symbols in his coding.

$$0 < k < 2^m + 2 \dots\dots\dots (9)$$

The 'k' in this instance denotes to the number of characters in the information that would be decoded throughout the data transmission process using Reed Solomon codes. The value 'n_{RS}' denotes the overall sum of characters that are used in the codes contained in the block that contains the codes. It is feasible to create the greatest code essential with the shortest distance (d_{min}) covered Reed Solomon decodes the encoder's instructions incoming and outgoing bit system are used to just about any code in a linear format as demonstrated below, Reed Solomon Codes can fix t or less types of transmission stream problems [18].

$$t = [(d_{min} - 1) / 2] = [(n - k) / 2] \dots\dots\dots (10)$$

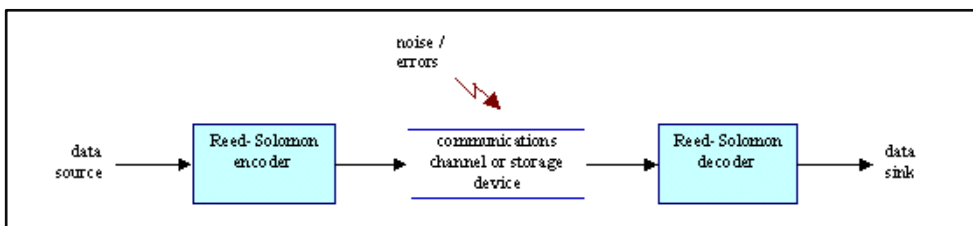


Fig.2 Reed Solomon Coding Scheme (Riley & Richardson, 1998)

IV. low-density parity-check

In information theory, a linearly fault correcting code (LFCC) is a low-density parity-check (LDPC) used to deliver information through a chaotic

communication system [19]. bipartite graph's subclass is used to create an LDPC. LDPC codes are ability coding, this implies that there are designs that allow the noise limit for a symmetrical memoryless channel to be set very close to the theoretical maximum to be reached. The noisy thresholds provide an upper limit for channel noise below which the risk of data loss is maintained to a minimum. Iterative belief propagation methods may be used to decode LDPC codes in a fashion that is demonstrated to their block length. [20]. LDPC codes are increasingly being employed in applications that need accuracy in the face of corrupting noise. effective and highly economical transmission of information throughput or a network with a restricted return channel. As a result, the device variable's temporal variation ($v_o(t)$) is mathematically expressed as:

$$v_o(t) = b\eta q R_T \frac{\omega_c}{2} \exp(\alpha^2 \omega^2) \times \exp(-\omega_c t) \operatorname{erfc}[\alpha \omega_c - (\frac{t}{2\alpha})]$$

..... (11)

η is the quantum efficiency of the detector, The electrical charge is denoted by the letter q , R_T is the receiver's mid-band transimpedance, and ω is the obtained change in the Gaussian pulse. [21].

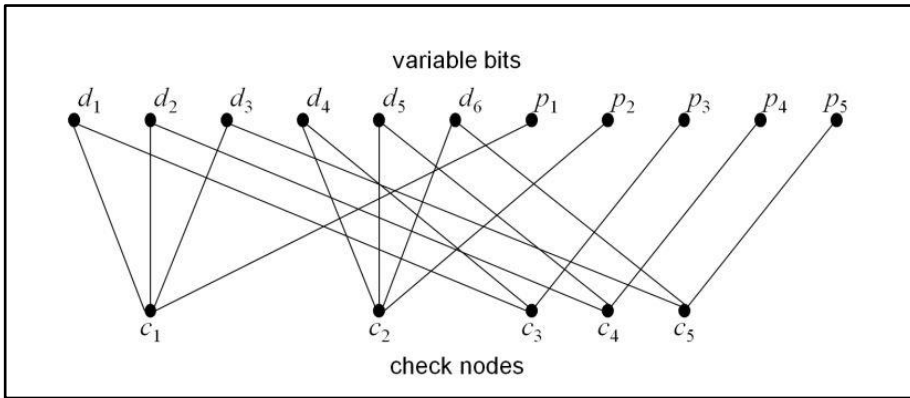


Fig. 3 Graphical representation of LDPC codes

There are a variety of design tools that can be used to represent LDPC codes. The Tanner graph[fig.3] is one of them, and it provides an excellent graphical depiction of LDPC codes. It not only gives a thorough representation of the code, but it also aids in the description of the decoding procedure.[22]

Anner graphs are bipartite graphs, which means they have two disjoint groups of nodes.

There are two sorts of nodes are Variable Nodes (VND) and Check Nodes (CN) (CND).

Variable Nodes: These are the nodes that represent the code bits. As a result, one VND represents each of the n columns of the H matrix.

Check Nodes: These are the nodes that represent the code limitations. As a result, each of the m rows of the H matrix is represented by a single CND [23].

If $H_{ij}=1$, each "variable node" V_i will link to a "check node" C_j , as seen below:

$$H = \begin{pmatrix} 0 & 1 & 0 & 1 & 1 & 0 & 0 \\ 1 & 1 & 1 & 0 & 0 & 1 & 0 \\ 0 & 0 & 0 & 0 & 0 & 0 & 1 \\ 1 & 0 & 1 & 1 & 0 & 1 & 0 \end{pmatrix}$$

There are two types of LDPC codes: regular and irregular. Each column of H in the normal LDPC codes has precisely V ones, and each row of H contains exactly C ones [24]. As a result, a normal LDPC code is defined just by the values of V and C [25]. The H-Matrix is used to encode the LDPC codes. This H-Matrix may be created in two ways for a normal LDPC code Gallager's method and MacKay and Neal method [26].

Discussion of findings

The major goal of this section is to study the influence of the number of photons in a pulse (b) on the OPPM coded format when slope and central detection systems are utilized at various coding speeds. Apart from examining M values between 3 and 5, the photon count is mostly determined using a 2M codeword length. It is critical to note that when the RS coding rate increases, (b) increases proportionately. This is because the amount of data symbols and the RS coding speeds are proportional. When the slope detection technique is utilized, b is also proportional to the standardized bandwidth. This is also because the resulting signal is very reliant on the slope detecting technique.

2.1 Number of photons versus RS code

Fig. 3 illustrates the change of **b** for an OPPM using the RS coding rate at various normalized bandwidths. It's worth noting that the fault rate of the system was kept to a minimal. In addition, as seen in Figure 3, **b** is inversely related to the number of standardized bandwidths. The maximum normalized bandwidth is corroborated by the lowest **b**. In addition, when the RS coding rate rises, **b** grows exponentially. In this regard, understanding the relevance of minimizing **b** is critical in order to create the ideal in the context of the application of an RS code rate and accelerate the maximum performance of the device. The transmission effectiveness of the coded OPPM system versus RS coding rates normalized bandwidths for numerous fibers could be seen in Fig. 3. For the broadest possible range of normalized bandwidths,

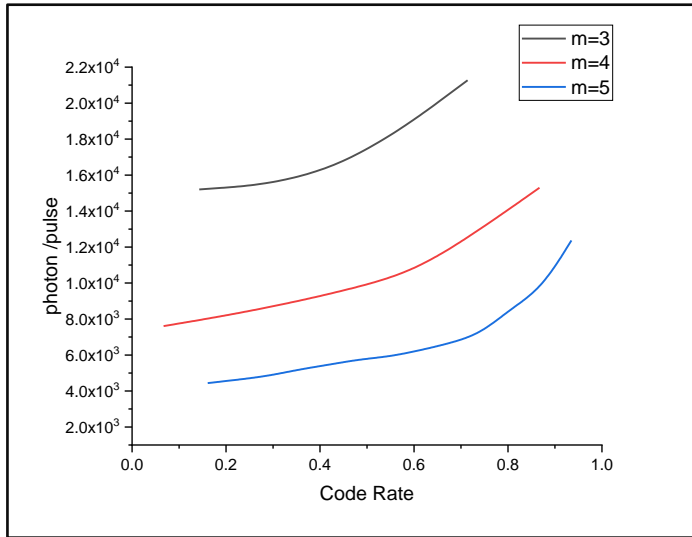


Fig. 3 Photons per second vs RS coding rate at various normalization bandwidths

3.2 Transmission Effectiveness

Fig. 4 reveals that the best transmission efficiency is about 0.6 of the RS coding rates. but, with narrower normalized bandwidths, the highest transmission efficiency was seen at roughly 0.7 RS coding rate. It is vital to understand that the transmission effectiveness and the code rate are exponentially related since the efficacy is effectively zero once the

optimal code rate is reached. In other words, as the pace of coding has increased, uncoded symbol errors have increased even more. As a consequence, the effectiveness of the system and ability to transmit symbols that have been rectified is reduced. In this example, both the amount and rate of redundancy exceed the optimal coding rate. On the other side, increased fiber normalized bandwidths have successfully increased transmission efficiency. Figures 3 and 4 illustrate the critical nature of lowering b via the use of RS codes in order to boost the OPPM's transmission effectiveness.

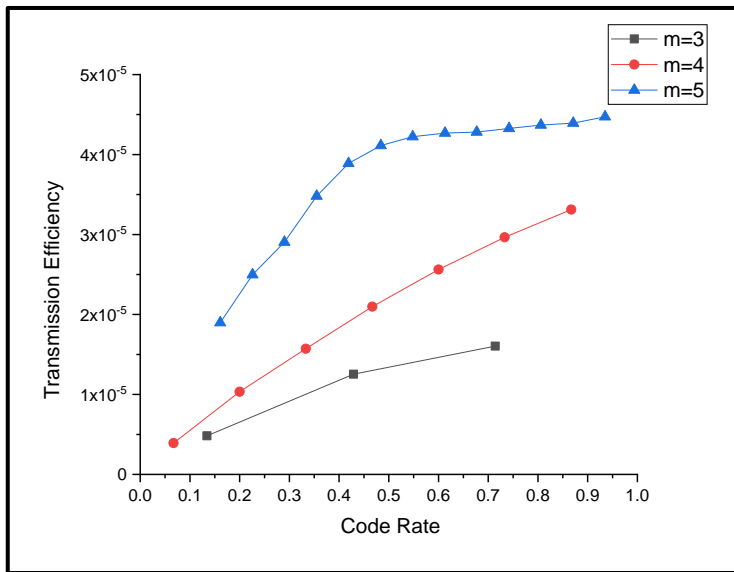


Fig. 4. The effectiveness of transmission code OPPM system against RS code rates

3.3 Number of photons versus RS code

For many normalized fiber bandwidths (f_n), **Fig. 5** depicts the evolution of the quantity for the coded OPPM system in photons per pulse vs RS Code The rate. For every given normalized bandwidth, there is a straight positive connection between the RS Code and per-pulse photon count Rate. For a certain bandwidth, As the Code Rate increases, the quantity of photons rises.

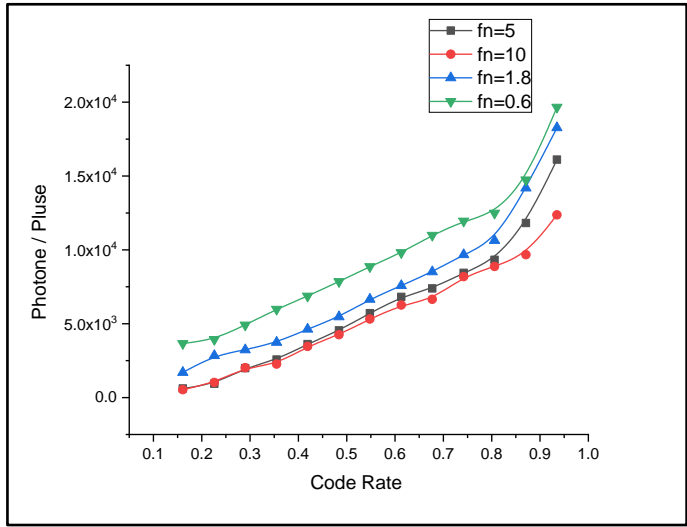


Fig. 5. The number of photons varies with the RS coding rate at different normalized bandwidths.

3.4 Efficiency of transmission vs RS coding rate at various normalized bandwidths

The link between the OPPM transmission efficiency using the RS code scheme and the RS Code Rate (f_n) for different Normalized fiber bandwidths to the OPPM data rate is shown in **Fig. 6**. The usage of an optimal code rate of 0.7 tends to improve overall efficiency. For the low dispersive channel, the coded OPPM with RS coding achieves the best transmission efficiency.

$$\alpha = \frac{0.1874 T_b}{f_n} \dots\dots\dots (12)$$

T_b is the PCM bit-time

$$\rho = \frac{r \ln 4}{b} \dots\dots\dots (13)$$

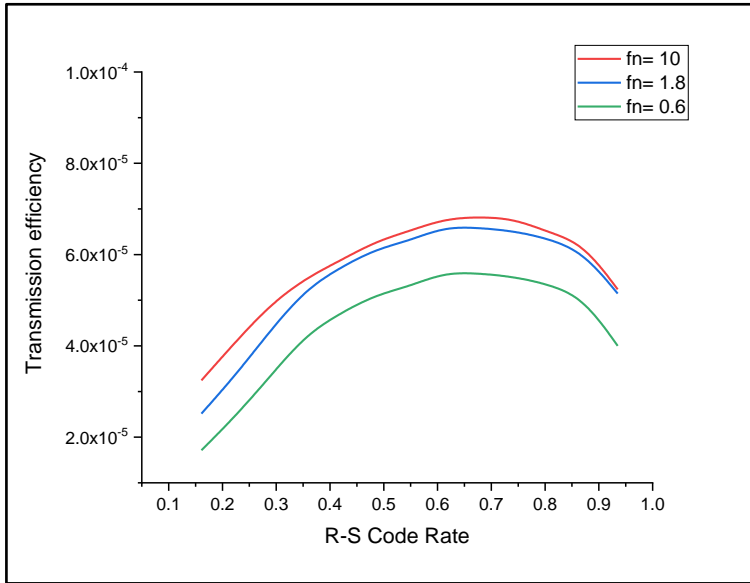


Fig. 6 Efficiency of transmission vs RS coding rate at various normalized bandwidths

3.5 At various normalized bandwidths, the transmission efficiency of RS code rate, OPPM, and LDPC

Fig 7 demonstrates the transmission efficiency of uncoded and coded OPPM systems as a function of normalized bandwidth. When working in a low dispersive channel, the coded OPPM employing RS coding and LDPC achieves a greater transmission efficiency. This is owing to the fact that the RS code requires more bandwidth as a result of the redundancy symbols.

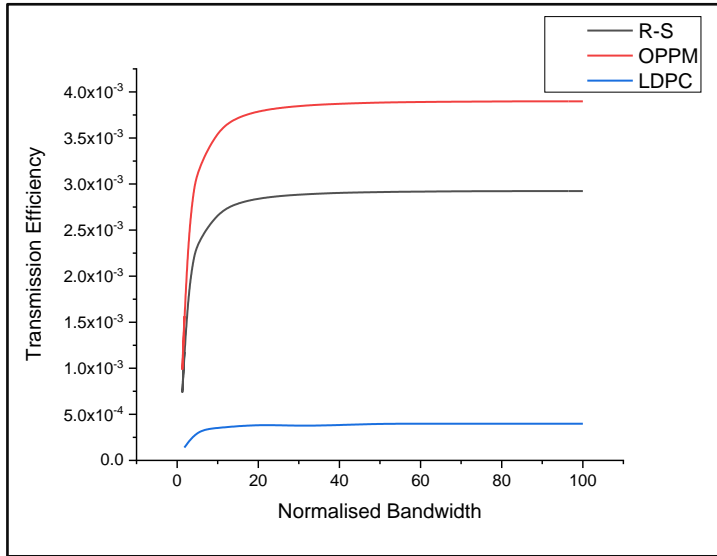


Fig. 7 Transmission efficiency of the RS code rate, the OPPM and the LDPC code rate at various normalized bandwidths

3.6 different number of photons for OPPM, RS and LDPC versus different Bit error rate

Fig.8 In compared to RS and LDPC, offset PPM has the highest number of mistakes, as a result, the predecessor will deliver more data that is error-free to the receiver. The primary goal of every communication system is to receive sent data with the fewest possible mistakes; the BER is determined by the modulation technology chosen.

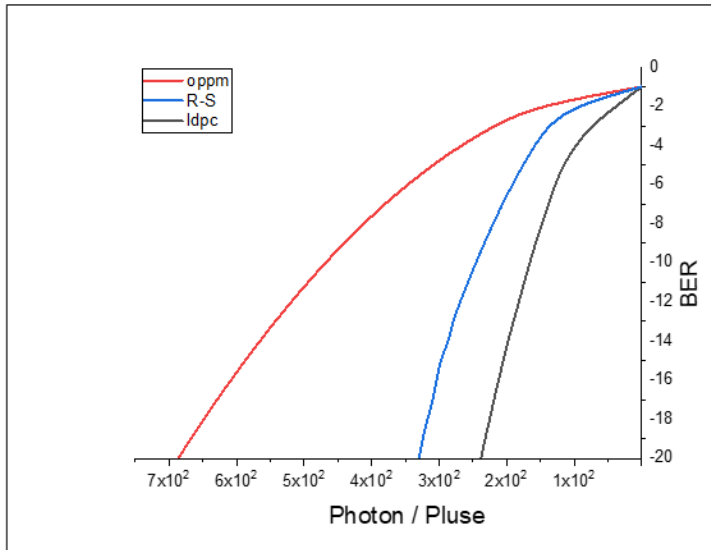


Fig. 8 different number of photons for OPPM, RS and LDPC versus different Bit error rate

4. Conclusions

Using OPPM, this article studied the transmission effectiveness, bandwidth expansion, and number of photons needed per pulse of Reed Solomon and LDPC codes. By and large, the programmed mechanism of the OPPM surpasses the uncoded system. The acquired signal was measured using two enhanced slope detection and central detection techniques to accomplish the study's primary objective. One may claim that by lowering the amount of photons sent through RS codes and LDPC, the OPPM's transmission effectiveness will be greatly increased. Additionally, increasing the LDPC codeword and RS may increase the performance of the machine. Furthermore, the research determined the ideal LDPC coding rates for high and low standardized fiber bandwidths, resulting in the highest possible transmission efficiency.

REFERENCES

- [1] M.J. Sibley, ' Analysis of offset pulse position modulation-a novel reduced bandwidth coding scheme' IET optoelectronics, vol.5 pp,144 -150,2011
- [2] Hreshee, S. S. (2020). Automatic recognition of the digital modulation types using the artificial neural networks. International Journal of Electrical & Computer Engineering (2088-8708), 10(6).
- [3] Garrett, I.: 'Digital pulse-position modulation over dispersive optical fiber channels. International Workshop on Digital communications, Tirrenia, Italy, 15–19 August 1983
- [4] Garrett, I.: 'Pulse-position modulation for transmission over optical fibers with direct or heterodyne detection', IEEE Trans., 1983, COM- 31, pp. 518–527
- [5] Ahfayd, M. H., Sibley, M. J., Mather, P. J., & Lazaridis, P. I. (2017, August). Visible light communication based on offset pulse position modulation (Offset-PPM) using high power LED. In 2017 XXXIInd General Assembly and Scientific Symposium of the International Union of Radio Science (URSI GASS) (pp. 1-4). IEEE.
- [6] Ray, I., M.J. Sibley, and P.J. Mather, Spectral characterization of offset pulse position modulation. IET optoelectronics, 2015. 9(6): p. 300-306.
- [7] Ahfayd, M.H., et al. Visible Light Communication Based on Offset Pulse Position Modulation (Offset-PPM) Using High Power LED. in Proceedings of the XXXIInd International Union of Radio Science General Assembly & Scientific Symposium (URSI GASS), (Montreal, 19-26 August 2017). 2017. IEEE
- [8] H. Wang, G. Cheng, X. Sun, and T. Zhang "Performance analysis of dicode pulse position modulation for optical wireless communication," in International Conference on Wireless Communications, Networking and Mobile Computing, 2007, pp. 3027–3030
- [9] L. Shu, and D. J. Costello, "Error Control Coding Fundamentals and Application", London, Prentice-Hall, Inc.,1983

- [10] R. A. Charitopoulos, and M. J. Sibley, "Experimental coder/decoder of dicode pulse position modulation," presented at School of Computing and Engineering Researchers' Conf. University of Huddersfield, UK, Dec. 2009
- [11] Sibley, M.J., Dicode pulse-position modulation: a novel coding scheme for optical-fiber communications. IEE Proceedings Optoelectronics, 2003. 150(2): p. 125-131.
- [12] Sibley, M., 2005. Performance analysis of a dicode PPM system, operating over plastic optical fiber, using maximum likelihood sequence detection. IEE Proceedings Optoelectronics, 152(6), 337-343
- [13] Joki, H., Paavola, J., & Ipatov, V. (2005, September). Analysis of Reed-Solomon coding combined with cyclic redundancy check in DVB-H link layer. In 2005 2nd International Symposium on Wireless Communication Systems (pp. 313-317). IEEE
- [14] Egorov, S., & Markarian, G. (2003). Error correction beyond the conventional error bound for Reed-Solomon codes. JOURNAL OF ELECTRICAL ENGINEERING-BRATISLAVA-, 54(11/12), 305-310.
- [15] Lone, F. R., Puri, A., & Kumar, S. (2013). Performance comparison of Reed Solomon code and BCH code over Rayleigh fading channel. arXiv preprint arXiv:1307.6930.
- [16] R. A. Cryan, and J. M. Elmirghani, "Reed-Solomon Coded Optical PPM Employing PIN-FET Receivers," IEEE International Conference on Communications New Orleans, 1994, pp. 126-130
- [17] Al-Nedawe, B. M. (2014). Microelectronic Implementation of Dicode PPM System Employing RS Codes (Doctoral dissertation, University of Huddersfield).
- [18] Fang, Y., Bu, Y., Chen, P., Lau, F. C., & Al Otaibi, S. (2021). Irregular-mapped photograph LDPC-coded modulation: A bandwidth-efficient solution for 6G-enabled mobile networks. IEEE Transactions on Intelligent Transportation Systems.

- [19] Raju, P., & Prasad, P. S. (2017). Design of an LDPC Decoder and Its Performance. *International Journal of Electrical and Electronics communication*, 1(1).
- [20] Hasan, F. S., Mosleh, M. F., & Abdulhameed, A. H. (2021). FPGA implementation of LDPC soft-decision decoders based DCSK for spread spectrum applications. *International Journal of Electrical & Computer Engineering* (2088-8708), 11(6).
- [21] Yazdani, R., and Ardakani, M., 2007. An efficient analysis of finite-length LDPC codes. In *2007 IEEE International Conference on Communications* (pp. 677-682). IEEE.
- [22] A. Orlitsky and J. Zhang, "Finite-length analysis of LDPC codes with large left degrees," in *Proceedings of the International Symposium on Information Theory*, 2002.
- [23] Dai, L., Fang, Y., Yang, Z., Chen, P., & Li, Y. (2021). Protograph LDPC-coded BICM-ID with irregular CSK mapping in visible light communication systems. *IEEE Transactions on Vehicular Technology*, 70(10), 11033-11038.
- [24] Bhooshan, S. (2022). Pulse Modulation. In *Fundamentals of Analogue and Digital Communication Systems* (pp. 355-396). Springer, Singapore.
- [25] Hussein, Y. M., Mutlag, A. H., & Al-Nedawe, B. M. (2021, June). Comparisons of Soft Decision Decoding Algorithms Based LDPC Wireless Communication System. In *IOP Conference Series: Materials Science and Engineering* (Vol. 1105, No. 1, p. 012039). IOP Publishing.
- [26] Mohamed I. Shujaa and Laith Falah Mohammed Hassan, 2018. Adaptive Filter for a Memory HPA Distortion in OFDM Signals. *Journal of Engineering and Applied Sciences*, 13: 6225-6231.

New approach for image steganography

**Ahmed A.
Mohammed¹**

¹ University of Al-
Mustansiriyah, Iraq-
Baghdad-Palestine
Street, P.O. Box:
14022.

[amohamm@uomustan
siriya.edu.iq](mailto:amohamm@uomustan
siriya.edu.iq)

Iman A. Saad²

² University of Al-
Mustansiriyah, Iraq-
Baghdad-Palestine Street,
P.O. Box: 14022.

[eman_abduljabbar@uomust
ansiriya.edu.iq](mailto:eman_abduljabbar@uomust
ansiriya.edu.iq)

Hussein A. Hllal³

³ University of Al-
Mustansiriyah, Iraq-
Baghdad-Palestine Street,
P.O. Box: 14022.

[huseinabed342@uomust
ansiriya.edu.iq](mailto:huseinabed342@uomust
ansiriya.edu.iq)

Abstract

Image steganography is a mean to conceal the existence of secret information in a non-secret audio, which is referred to as cover media. Different from cryptography, the steganography focuses on hiding the secrecy of the information rather than obfuscating it. Additionally, the complex nature of the cover media makes it harder for the attacker to expose the hidden information. In this paper, we propose a new method to hide secret image in an audio file. The proposed method for images steganography is based on embedding the confidential information in an audible part of the sound files. Additionally, for the purpose of increasing the difficulty for the intruder to gain access to the secret information, the technique of random sample location was utilized to initiate the process of hiding the secret information. Experimental results proved that our proposed method is effective and efficient due to the imperceptibility aspect of the human hearing of the resultant audio file, which is referred to as stego file. The performance of the proposed method was tested using two common fidelity measurements, Peak-Signal-to-Noise-Ratio (PSNR) and Mean-Square-Error (MSE).

Keyword : *steganography, hiding information , image processing,LSP.*

I. INTRODUCTION

Information protection is considered as one of the essential interests for any organization. So, this has prompted the attention of the researchers to concentrate their effort in the field of information security [1]. Basically, cryptography has been utilized as a secure and authoritative transmission. However, the encrypted data may raise suspicion for intruders of potential existence of a confidential information [2][3][4]. As a result, this suspicious may prompt the unauthorized person to exert an effort to obtain the confidential information; this is considered as the main weakness of the cryptography. On the other hand, steganography [5] represents another

technique to keep the important information secure. Steganography is different than cryptography via concealing the secret information from the intruders [6]. In general, steganography utilizes several types of digital objects as host media known as 'cover media' to hold the secret information such as image, text, video and audio [7][6]. In fact, steganography can provide three aspects that are not

included in cryptography; these aspects are security, robustness and capacity [8]. Security is concerned to prevent the intruder to discover the hidden data, robustness is concerned with the altering of the hidden information and the capacity is related with the amount of data that can be embedded in the host or cover media. Of all cover media, image steganography has been considered as the most widely types of steganography used to hide secret information. Nowadays, another trend of using audio files as a cover media to hide secret information have appeared which is known as audio steganography. It provides huge capacity that allows a big amount of secret information to be concealed in the cover media.

In this paper, we propose a new method to hide digital image in digital audio. The huge number of samples in the digital audio files makes it a preferred candidate as a cover media to hide even a big image size in them. This aspect overcomes the limitations of the embedding capacity and decrease suspiciousness. On the other hand, the most important things that should be taken in our account are where and how to embed our secret information. So, in our proposed method, the area in which the information is hidden is randomly determined and difficult to predict by the intruders.

1. Letritures Review

Due to diverse technologies integrated in digital image steganography in the last decade, a significant achievement in terms of performance have been occurred, i.e. the emergence of an effective algorithms for concealing informations. In this section, we briefly describe some of the previous work related to digital image steganography.

Naidu, Prasad and Mamatha (2014) [9] presented their work on audio steganography. In their work, the secret message is converted to binary representation using ASCII form. Then, the produced ASCII representation is embedded in digital audio samples utilizing some certain rules. Using LSB encoding scheme, if the value of the first 2 MSBs of the sample are equal (both are zeros or ones), the first LSB will be replaced with the secret message bit; otherwise, if the first 2 MSBs are 0 1 or 1 0, the second LSB is replaced with the secret message bit.

Tayel, Gamal and Shawky (2016) [10] presented their work to hide secret audio file in another audio file using Least Significant Bit (LSB) technique. In [10], the technique is applied on two cards of programmed with arduino (1.0.5) program

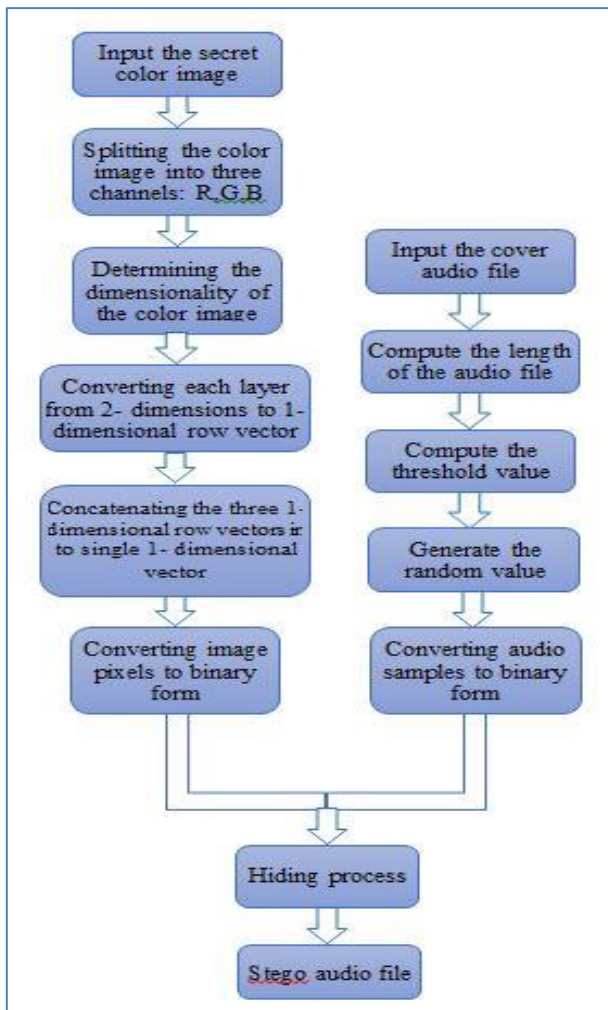
[11] using sound samples (8,16 or 24) bits. The first card is used to convert the analogue audio signal to digital form using analog to digital converter (A/D) and replace the most Significant Bit (MSB) of the audio cover file and the audio secret file producing the stego-file. The stego-file is then transmitted to the second card which is utilized as a receiver to convert it back to analogue form using digital to analogue converter (D/A). The second card replaces the four Least Significant Bits (LSB) of the stego-file with the Most Significant Bits (MSB) of the secret audio file.

Mligy, Nasef and Eid [12] proposed their audio steganography method utilizing a hybrid between Least Significant Bit (LSB) and the modification of phase coding. The authors have stated that their method will benefit from the advantages of the two techniques to enhance the efficiency of their proposed audio steganography method. In the modified phase coding, the Fast Fourier Transform (FFT) is applied to whole signal instead of breaking it into smaller segments. Then, the fraction number of the phase part produced from applying the FFT is converted to binary representation and the binary representation of the secret message is embedded in it using LSB technique. In the reconstruction part of the hybrid method, the audio signal is reconstructed by applying the Inverse Fast Fourier Transform (IFFT) to the magnitude part resulted from the FFT technique and the phase part (after embedding the secret message in it) producing the stego-audio file.

Gupta and Shama (2013) [13] proposed their steganography method to hide image file in audio file using Discrete Wavelet Transform (DWT) and Least Significant Bits (LSB). In [13], the audio signal is converted to frequency domain by applying DWT to it. The converted samples in frequency domain are then converted to binary form. Hence, each sample is represented in 16-bits. The audio samples in the frequency domain are then segmented into 8×8 blocks and the image bits are embedded utilizing 3 LSBs in the audio samples to produce the audio stego-file. In the extraction process, the audio stego-file is converted to frequency domain using DWT. The higher frequency components are also segmented into 8×8 blocks similarly in embedding process and taking the 3 LSBs for each sample to re-extract the original secret image.

Vani and Prasad (2013) [14] in their work proposed a hybrid security system utilizing cryptography and steganography techniques. In cryptography part, they adopted Hopfield chaotic neural network to encrypt the secret plain text. The Hopfield chaotic neural network can be viewed in [15] [16]. The produced encrypted text is then more secured via hiding it in an audio file utilizing Double-

Density Discrete Wavelet Transform (DD DWT) in which the audio signal is transformed via applying one scaling function and two wavelets. To this sake, DD DWT is implemented utilizing one low pass filter and two high pass filters and the audio signal is decomposed utilizing these three filters to produce one low frequency sub-band and two high frequency sub-bands. The encrypted secret message is then embedded in the two high frequency sub-bands using LSB technique.



I. The proposed system

The proposed system that embeds color image in an audio file consists of many stages utilizing several techniques. Our system provides a method of embedding and extracting data (color image) through multiple hiding and retrieving stages in a multimedia represented by mono wave file. The proposed system is divided into two subsystems. The first one is designated to achieve hiding process, while the other one is to retrieve (or extract) the original data.

3.1. Hiding process

The general outline of the hiding process is depicted in figure (1) below which explains the main stages of hiding the secret image in a mono audio

file. The following sections will explain the function of each stage.

• First stage:

This stage includes the process of reading the cover media (audio file) and the secret message (color image). The audio signals used in this work are standard digital mono audio signals using sampling frequency of 1 to 32000MHz with 16-

bits PCM encoding. The resulted data is one-dimensional signal (row vector) consisting of digital samples each with 16-bits. The secret message is color image in JPEG file format. Each pixel is represented by three channels; each channel represents a distinct color (red, green or blue) each with one byte. Thus, each pixel is represented in three bytes, one byte (8-bits) for each channel. So, each luminance pixel in a color image is represented using 24-bits.

• **Second stage:**

This stage determines the length of the cover media (audio file) as well as the dimensionality of the secret message (color image). Then, each channel (which represents a certain color) is converted from 2-dimensional array to 1-dimensional row vector resulting in three vectors. The three vectors are then concatenated into 1-dimensional vector.

Figure (1). The general outline of the hiding process

• **Third stage:**

In this system the secret image is embedded in the audible samples and ignoring inaudible ones. So, this stage is to distinguish which part is audible that can hold secret message without affecting the human auditory system (HAS) from the inaudible part (that represents noise or crackle) of the audio signal. This process can be performed by comparing the audio samples with the threshold value. If the audio sample is greater than the threshold value, the sample can be considered as audible and the secret data can be concealed in it, otherwise it is considered as inaudible sample and will be ignored. The threshold value is used in the hiding process in later stage. The threshold value is computed using the following equation:

$$thr = \text{ABS}(\sigma/x) \quad \text{.....(1)}$$

Where, σ is the standard deviation of the audio signal and x is a variable representing the threshold factor.

The thresholding process is explained in the following algorithm.

• **Fourth stage:**

In this stage the randomize value is generated which represents the beginning of the locations where the secret message (color image) will be concealed. The randomize value will be tested; it should be less than the length of the signal. If this condition is false, the randomize value will be regenerated again.

• **Fifth stage:**

The main goal of this stage is to determine if there is enough space available in the cover media (digital audio samples) that can be utilized to embed the secret information. The achievement of this process is by computing the number of bytes to hold the secret information (color image). This task can be performed by determining the size of the secret information that needs to be hidden. On the other hand, the number of values that can be used in the cover media should be computed. So, if the absolute value of the digital samples of the audio signal greater than the threshold value started from the value after the location that determined by the randomize value, it will be used. This number of the samples should be at least twenty-four times greater than the number of bytes in the color image. This is because the color image consists of three channels (Red, Green and Blue), each pixel in these channels occupies 8-bits (one byte). So, $8\text{-bits} \times 3 = 24$. If this condition is true, the embedding process will be takenplace in the next stage. Otherwise, a new randomize value will be regenerated and this process is repeated again.

• **Sixth stage:**

The essential task of this system is the concealing process in which the binary representation of the image pixels is distributed in the audio signal samples. In this context, the embedding (concealing process) will be started from the sample location which is equal to the randomize value generated previously. In the previous stages, both decimal values of the image pixels and audio signal samples were converted to the binary form. The 1-LSB coding . is used to distribute the binary bit planes of the image pixels in the audio signals. In 1-LSB coding method, each pixel in each channel (channel R, channel G or channel B) will be distributed in 8audio samples. So, each luminance pixel in the color image (including three bytes; one byte in each of the channel R, channel G and channel B) is distributed in 24 samples in the audio signals. It is worth noting that, not all audio samples will be used to hide the secret message, rather the audio samples whose absolute value greater than the threshold value (obtained from equation 1) will be utilized to conceal the secret image. This step is very important for human

auditory system (HAS) by ensuring that all the secret information will be concealed in the audible parts of the audio signal and ignoring the inaudible ones. By completing this stage, the stego-file is produced which is the same type of the original cover file.

3.2. Extracting process

The general structure of the extraction process is depicted in figure (2) explaining the main stages of extracting the secret image from the stego-audio file. The following sections will explain the function of each stage.

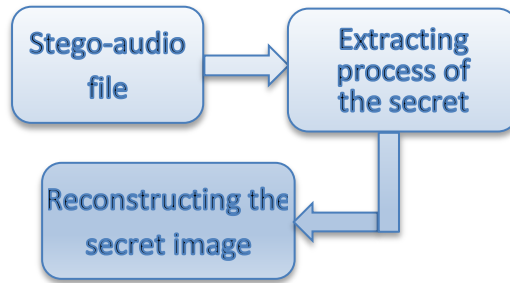


Figure (2). The general structure of extraction process

- **First stage:**

The extraction subsystem begins by reading the stego-audio file that holds the secret message. This process will be yielding a mono audio file which is represented by one dimensional audio signal consisting of sample values each with 16-bits PCM encoding.

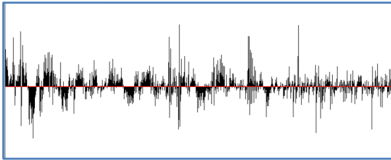
- **Second stage:**

In this stage the same randomize value and the threshold generated in the hiding subsystem will be used in the extraction process. Similar to the hiding process, the randomize value represents the first sample in which the secret message is hidden and the threshold value determines the audible parts which are used to embed the secret message (color image) than the inaudible parts which are not used in the hiding process.

4. Experimental results

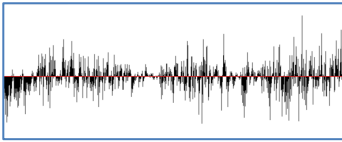
This section presents the experimental results of the proposed image steganographic method using the test materials represented by four audio wave

files as cover media and four different color images as secret messages. The original audio files used as cover media to hide the image files are shown in figure (3) a,b,c,d, while the image files utilized as secret messages to be hidden in the cover media are shown in the figure (4) a,b,c,d.



(a) Sound1

(b) Sound2



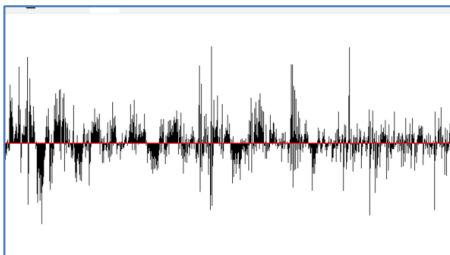
(c) Sound3

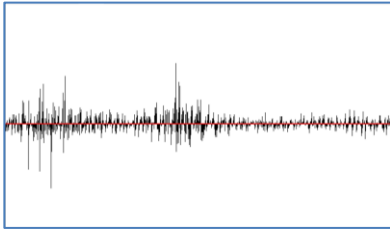
(d) Sound4

Figure (3). The Original audio signals

Figure (4). The Original images

All the audio signals have the same time duration which is one minute length and all





images are in JPEG file format with (256×256 pixels). The experiments were performed using the personal computer with the following properties: Intel core i7 processor with 2.4 GHz speed, 16 G RAM and Microsoft Windows 10 operating System. The code of the system was written in VB.NET Programming language with the environment of visual Studio. Net. The experimental results have been measured in terms of two metrics which are Peak-Signal-to-Noise-Ratio (PSNR) and Mean-Square-Error (MSE) Both metrics were used to analyze the difference between the original (before the secret message was embedded) and the stego audio signal (after embedding the secret message). The PSNR is defined as the following formula:

$$PSNR = 10 \times \log_{10} \left(\frac{255}{MSE} \right) \dots \dots \dots (2)$$

Where MSE is the mean square error.

The higher value of the PSNR represents the good quality of the audio signal. The MSE is defined as the following formula:

$$MSE = \frac{1}{n} \sum_{i=1}^n ||C_{aud}(i) - S_{aud}(i)||^2 \dots \dots \dots (3)$$

Where n is the total number of the samples in the audio file, $C_{aud}(i)$ is the ith sample value of the cover audio signal and $S_{aud}(i)$ is the ith sample value of the stego audio signal. For a good quality of the signal, MSE should be remained at the minimum value.

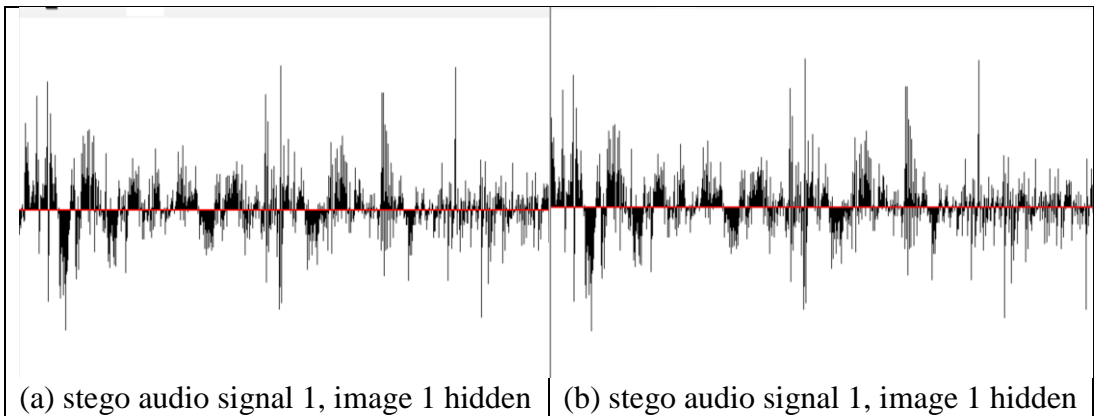
4.1 Performance results

The experimental analysis of the proposed image steganographic method is presented in this section. The color images (secret messages) are selected as the input images and embedded in the cover audio files and transmitted, and then the images (secret messages) get extracted by the receiver.

The following section 4.1.1 shows the results of hiding the four images in each audio file while fixing the threshold factor. In section 4.1.2, the impact of changing the threshold factor is tested.

4.1.1 Hiding all images in each audio file

Our proposed system was evaluated when hiding the four secret images in each audio file. In other word, the secret color images 1, 2, 3 and 4 get embedded in the cover audio signal 1 and cover audio signal 2 and so on. These results were obtained by fixing the threshold factor ($x=1$). Figure (5) a,b,c,d, below shows the resulted stego audio signal 1 containing color image 1, stego audio signal 2 containing color image 2, stego audio signal 3 containing color image 3 and stego audio signal 4 containing color image 4.



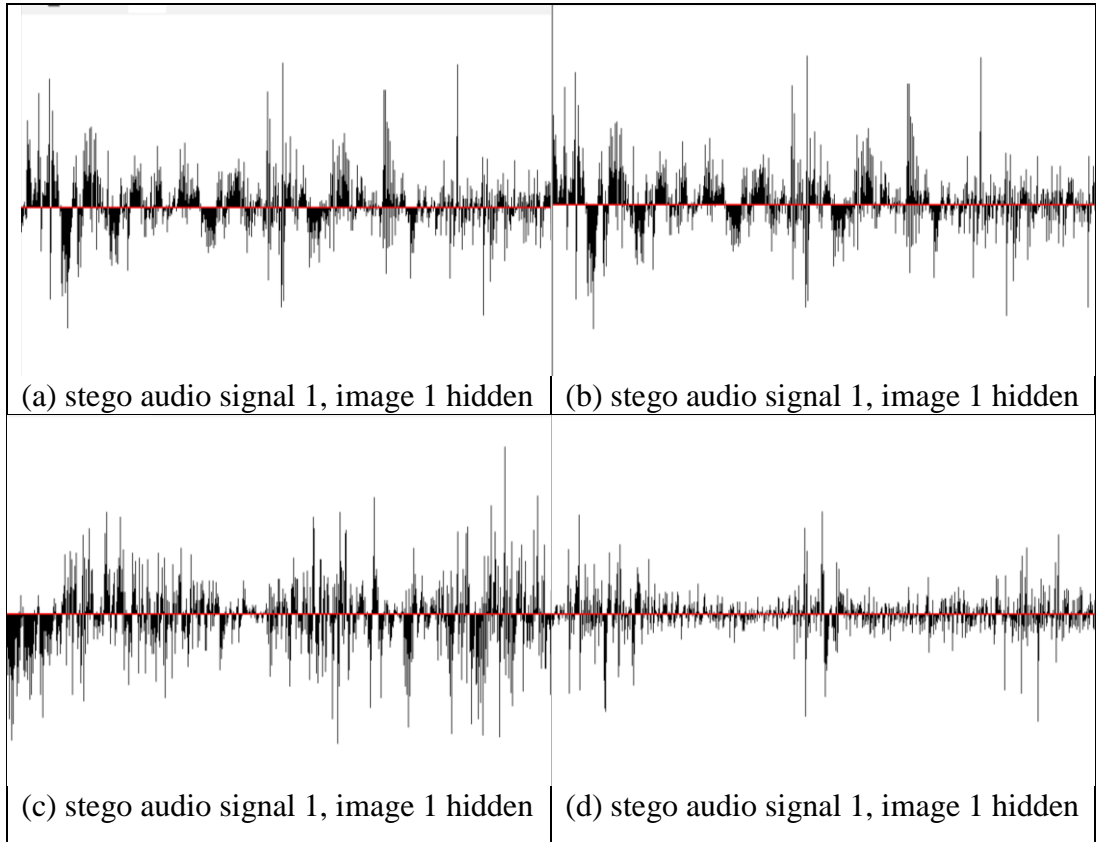


Figure 5. (a) Stego audio signal 1 containing image 1; (b) stego audio signal 2 containing image 2; (c) stego audio signal 3 containing image 3 and (d) stego signal 4 containing image 4.

Table (1), below shows the performance of the proposed image steganographic system in terms of PSNR and MSE.

Table (1): performance of the process steganography

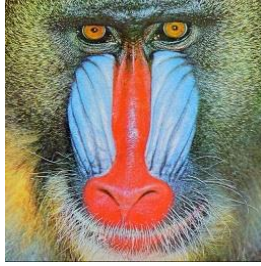
Stego audio	Secret Image	PSNR	MSE
Sound 1	Image 1	38	1.001
	Image 2	45	١.٠000
	Image 3	36	0.١000

	Image 4	50	0.9000
Sound 2	Image 1	30	0.0010
	Image 2	45	0.0100
	Image 3	44	0.5000
	Image 4	45	0.0300
Sound 3	Image 1	30	0.1000
	Image 2	44	0.1000
	Image 3	30	0.2000
	Image 4	50	0.1000
Sound 4	Image 1	38	1.0010
	Image 2	45	1.0000
	Image 3	49	0.1000
	Image 4	50	0.07777

From the results presented in the table (1) above, it is difficult to determine which audio signals gave the best results. However, what can be noticed is that the best results were obtained when hiding image 4 in audio file 1, audio file 3 and audio file 4 as they gave the highest values of PSNR and low values of MSE in most cases. In contrast, we noticed that the worst results were given by images 1 and 3 as they gave the lowest PSNR values and the highest MSE values in most cases. The clear exception in the results is that image 3 gave the second best result with the audio signal 4.

4.1.2 Changing the threshold factor (x)

The effect of the threshold value on the system's performance is evaluated in this experiment. The threshold factor is evaluated using equation (1). In this experiment, the threshold value depends on the variable (x). In this context, this factor controls the samples that will contribute to the concealment of the secret information. As illustrated in section (3.1), the



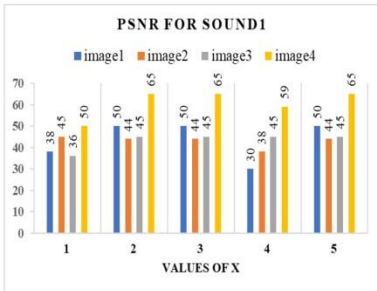


Figure 6. Effect of changing threshold factor (x) on MSE for sound1

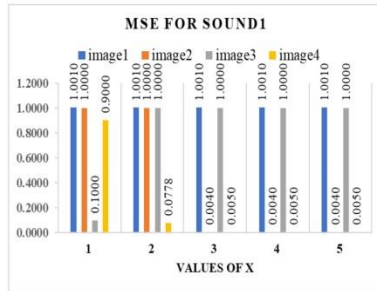


Figure 7. Effect of changing threshold factor (x) on MSE for sound1

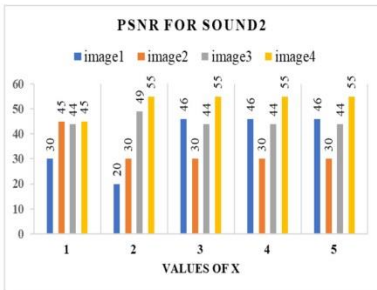


Figure 8. Effect of changing threshold factor (x) on PSNR for sound2

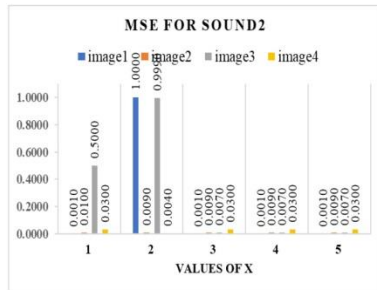


Figure 9. Effect of changing threshold factor (x) on MSE for sound2

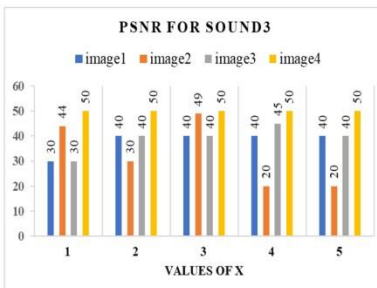


Figure 10. Effect of changing threshold factor (x) on PSNR for sound3

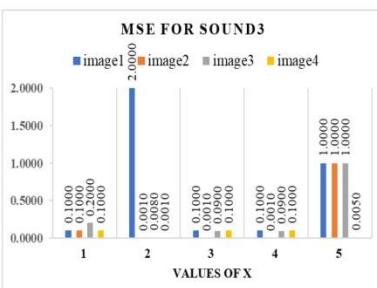


Figure 11. Effect of changing threshold factor (x) on MSE for sound3

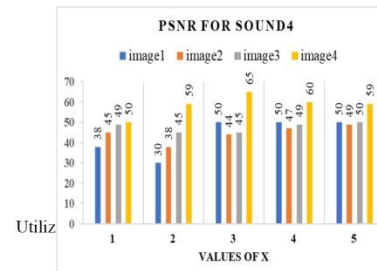


Figure 12. Effect of changing threshold factor (x) on PSNR for sound4

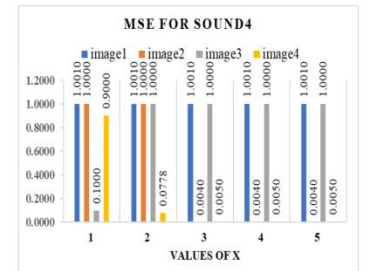


Figure 13. Effect of changing threshold factor (x) on MSE for sound4

the figures that image 4 has given the best results. On the other side, sound 1 has given the best results as it has the highest PSNR values, followed by sound 4. For the effect of changing the threshold factor (x), the threshold factor (x) is determining by which (σ) will be divided. So, the bigger value of the threshold factor (x) the smaller the threshold value will be and the more samples will be available to embed the secret bits. However, this is not definitely true because of the random value that is generated which represents the starting position in which the secret information will be hidden. A range of x values (1-5) is evaluated in this experiment to determine the best operational value. PSNR and MSE values for all images embedded in four sound signals were calculated for each value of threshold vector to find out the relation between the system performance and the x value. Throughout this range of x , the results have shown the highest values of PSNR when x values are 2-5. These results have been found in most cases. However, the only exception was found with sound 3 when high values of PSNR are equal to all values of x . This represents the worst results obtained from the four sound signals. Utilizing MSE measurement, it is also noticed that image 4 has given the best results as it has the lowest values of MSE. On the other side, sound 2 has given the best results as it has the lowest values of MSE values in most cases, followed by sound 3. As the effect of changing the values of x it is found that the lowest values for MSE were obtained by increasing the values of x . the clear exception was found with sound 3 when the highest values for MSE were found for most images with the highest values of x . The selected range of change for x values is obviously affecting the high performance of the image steganography system. The optimal choice for the x value was around the middle of the evaluated range (about 3) because it reveals the highest values of PSNR when using any of the sound signals.

4.1.3 Comparing the proposed method with other published techniques

The proposed method for image steganography is compared with some state-of-the-art methods that utilize different techniques. The comparison is conducted by utilizing a fidelity criterion common to all the considered methods, which is "PSNR". As shown in Table 2, the PSNR of the proposed method is higher than the other methods which depicts the superior performance of our method over the other methods.

Table 2: PSNR of the proposed method

Methods	PSNR
S.K. Bandyopadhyay, B. Datta [19]	54.7
D.Pal, N.Ghashol [20]	64.4402
Gomez-Coronel, S.L., Escalante-Ramirez, B., Acevedo-Mosqueda, M.A. and Mosqueda, M.E.A., 2014 [21]	60
Rekik, S., Guerchi, D., Selouani, S.A. and Hamam, H., 2012 [22]	54.37
Shahadi, H. and Jidin, R., 2011 [23]	60
Proposed method	65

5. CONCLUSION

In this paper a new image steganography system was proposed and evaluated. It is an effective and efficient way to transfer image file while maintaining the confidentiality and non-disclosing of its existence. The main idea of the proposed method is to hide secret information by randomly determining locations in the audible parts of the audio files while neglecting the inaudible areas. The performance of the proposed image steganography system was evaluated by using four audio files as cover media and four color images as secret information. A broad range of experiments were performed to improve the fidelity criteria of the resultant audio file (stego file). At last, the conducted results were compared with results of other publications.

ACKNOWLEDGEMENTS

The author(s) would like to thank Mustansiriyah Univeristy (www.uomustansiriyah.edu.iq) Baghdad-Iraq for its support in the present work.

REFERENCES

1. Kumar, S., Singh, A., & Kumar, M. (2019). Information hiding with adaptive steganography based on novel fuzzy edge identification. *Defence Technology*, 15(2), 162-169









2. Swetha, V., Prajith, V., & Kshema, V. (2015). Data hiding using video steganography-a survey. *International Journal of Science, Engineering and Computer Technology*, 5(6), 206.
3. Maniriho, P., & Ahmad, T. (2019). Information hiding scheme for digital images using difference expansion and modulus function. *Journal of King Saud University-Computer and Information Sciences*, 31(3), 335-347
4. Prasad, S. and Pal, A.K., 2017. An RGB colour image steganography scheme using overlapping block-based pixel-value differencing. *Royal Society open science*, 4(4), p.161066.
5. Chan, C.K. and Cheng, L.M., 2004. Hiding data in images by simple LSB substitution. *Pattern recognition*, 37(3), pp.469-474.
6. Sahu, A. K., & Swain, G. (2019). High fidelity based reversible data hiding using modified LSB matching and pixel difference. *Journal of King Saud University-Computer and Information Sciences*
7. Taha, A., Hammad, A. S., & Selim, M. M. (2020). A high capacity algorithm for information hiding in Arabic text. *Journal of King Saud University-Computer and Information Sciences*, 32(6), 658-665
8. Dutta, H., Das, R. K., Nandi, S., & Prasanna, S. M. (2020). An overview of digital audio steganography. *IETE Technical Review*, 37(6), 632-650
9. Naidu, K. T. R., Prasad, T. V. S. G., & Mamatha, P. G. (2014). An Approach of Robust High Capacity Audio Steganography and Cryptography Using LSB Algorithms. *International Journal of Engineering Trends and Technology (IJETT)*, 9(10), 521-524.
10. Tayel, M., Gamal, A., & Shawky, H. (2016, January). A proposed implementation method of an audio steganography technique. In 2016 18th international conference on advanced communication technology (ICACT) (pp. 180-184). IEEE.
11. Web site: <https://www.arduino.cc/en/software>
12. Meligy, A. M., Nasef, M. M., & Eid, F. T. (2016). A hybrid technique for enhancing the efficiency of audio steganography. *International Journal of Image, Graphics and Signal Processing*, 8(1), 36.

13. Gupta, N., & Sharma, N. (2013). Hiding Image in Audio using DWT and LSB. *International Journal of Computer Applications*, 81(2).
14. Geetha, B., Vani, E. and Prasad, V., 2013. A Hybrid Model for Secure Data Transfer in Audio Signals using HCNN and DD DWT. *IJACSA* International Journal of Advanced Computer Science and Applications, 4(7), pp.202-208.
15. Yu, W., & Cao, J. (2006). Cryptography based on delayed chaotic neural networks. *Physics Letters A*, 356(4-5), 333-338.
16. Geethavani, B., & Prasad, E. V. High Secure Image Steganography Based on Chaotic Neural Network. *IJCSNS*, Volume13, (3).
17. Shete, K.S., Patil, M. and Chitode, J.S., 2016. Least significant bit and discrete wavelet transform algorithm realization for image steganography employing FPGA. *International Journal of Image, Graphics and Signal Processing*, 8(6), p.48.
18. Sharma, V.K., Srivastava, D.K. and Mathur, P., 2018. Efficient image steganography using graph signal processing. *IET Image Processing*, 12(6), pp.1065-1071.
19. S.K. Bandyopadhyay and B.Datta, "Higher LSB Layer Based Audio Steganography Technique" *The International Journal on Electronics & Communication Technology IJECT*, Vol. 2 (4), 2011.
20. D. Pal and N. Ghoshol, "A robust audio steganography scheme in time domain," *International Journal of computer Applications*, vol.80 (15), October 2013.
21. Gomez-Coronel, S.L., Escalante-Ramirez, B., Acevedo-Mosqueda, M.A. and Mosqueda, M.E.A., 2014. Steganography in audio files by hermite transform. *Applied Mathematics & Information Sciences*, 8(3), p.959.
22. Rekik, S., Guerchi, D., Selouani, S.A. and Hamam, H., 2012. Speech steganography using wavelet and Fourier transforms. *EURASIP Journal on Audio, Speech, and Music Processing*, 2012(1), pp.1-14.
23. Shahadi, H. and Jidin, R., 2011. High capacity and resistance to additive noise audio steganography algorithm. *International Journal of Computer Science Issues (IJCSI)*, 8(5), p.176.

24. Applications, 76(22), pp.24091-24106.

BIOGRAPHIES OF AUTHORS

The recommended number of authors is at least 2. One of them as a corresponding author.

	<p>Ahmed A. Mohammed    received the B.Sc. in computer science from Al-Mustansiriyah University, Higher diploma in Iraqi Commission for Computers and Informatics (ICCI)/ Informatics Institute for Postgraduate Studies Software Engineering and M.sc. in Computer Science – Image processing in Iraqi Commission for Computers and Informatics (ICCI)/ Informatics Institute for Postgraduate Studies Software, Baghdad, Iraq, in 1992, 1999 and 2004. He received The Ph.D. degree in IT from Deakin University, Melbourne, Australia in 2018.</p> <p>Currently, he is a lecturer in Al-Mustansiriyah University. His research interest includes: image and multimedia processing, Pattern recognition, face recognition and facial attributes classification. and its applications. He can be contacted at email: amohamm@uomustansiriyah.edu.iq.</p>
	<p>Hussein A. hilal    received the B.Sc. and M.Sc. degrees in computer science from university of technology 2015 and al imam alsadiq university respectively, He has been a good of computer and image processing in computer and Technology, He has authored or coauthored refereed journal and conference papers, 2 and one edited books. His research interests include the applications of artificial intelligence, data security, cloud computing and control. He can be contacted at email: huseinabed342@uomustansiriyah.edu.iq</p>

Advanced Seeded Region Growing for CBCT Image Reconstruction

Shimaa Janabi*, Shaimaa Shukri Abd Alhaleem, Israa Jwad Kazim

Computer Technical Engineering Department, Almustafa University College,
Bagdad, Iraq

Corresponding author email: shimaa.cte@almustafauniversity.edu.iq*

Abstract— Cone-beam computed tomography (CBCT) is a powerful imaging tool for reconstructing three-dimensional (3D) images of scanned objects. CBCT provides image reconstruction. During the restoration phase, two research methods are used: analytical and iterative. In spite of being superior to analytical reconstruction schemes, iterative reconstruction schemes are not routinely used in clinical applications. This paper reduces the reconstruction time of iterative algorithms by restricting their reconstruction to a specific region of interest. The seeded region growing segmentation process creates this region. This procedure is validated using the “ART” algorithm. Simulated results show that this method improves image quality while decreasing “ART” reconstruction time.

Keywords— “ART”, Cone beam computed tomography, Iterative Reconstruction, Seeded region growing, Segmentation

Introduction

It produces nondestructive cross-sectional pictures of scanned objects [1]. However, while the benefits of CT are well documented, the hazards are mounting [2]. Analytical reconstruction techniques, including the FBP algorithm, have been around for a long time. Reduced radiation dose may cause streak aberrations and increased picture noise [3]. No radiation is used in the new IR CT procedures [4]. Early CT scanners employed iterative reconstruction methods. They were not employed clinically due to computational constraints. Those algorithms were initially marketed in 2009. Modernized radiology [5]. Simplicity trumps calculation in this strategy. These strategies are used when many projections cannot be acquired or is limited. While not perfect, this procedure does enhance image quality [6]. Iterative “ART” was coupled with two additional iterative techniques in 2007. Their effort began with the slow development of the weight matrix. MATLAB was used for the calculations. The authors struggled to create the weight matrix and apply the algorithms. Because these algorithms are slow, they employed little phantom images to compensate. Then there's [8]'s method for segmenting CT images. Less than reliable and effective, their recommended procedure was segmented. [9] tested five basic algebraic reconstruction techniques. Algebraic approaches can produce a picture from faulty or missing data. Further algebraic refinement may yield a CT breakthrough. To aid radiologists in early disease diagnosis, [10] suggested a segmentation technique to reliably segment CT images. [11] surveyed image segmentation techniques. Their

work focuses on image segmentation and its application in diverse investigations. This method has various advantages over previous segmentation methods, according to their research. [12] compared and contrasted various segmentation algorithms. In CT, [13] researched and improved IR radiation reduction methods. IR algorithms increase image quality, noise, signal-to-noise ratio, and contrast-to-noise ratio when compared to the FBP algorithm. recommended segmenting lung CT images. The method proposed in this research can be used to segment medical images. [15] compared IR and FBP results. Infrared techniques reduced noise while keeping resolution.

IN THE SEEDED REGION GROWING SEGMENTATION PROCESS, A USER-DEFINED REGION OF A 3D CBCT SCAN OF A HUMAN CHEST VOLUME IS GENERATED. PRELIMINARY COMPARISON WITH THE STANDARD ALGORITHM PRECEDES ACCELERATION.

Reconstruction of the iterative image

By assuming an initial guess image, they mimic the forward projections of the original CT device acquisition. To calculate the update, these forward estimates are compared to the CT device's actual projections. As a result, the image is improved until the forward projections and measurements agree. This is achieved by first discretizing the image into pixels as shown in Fig. 1 [1], [17].

For example, (1) shows how to relate the image-pixels to the projections using linear equations [1].

$$\begin{aligned}
 x_1 + x_2 + x_3 &= p_1 \\
 x_4 + x_5 + x_6 &= p_2 \\
 x_7 + x_8 + x_9 &= p_3 \\
 x_3 + x_6 + x_9 &= p_4 \\
 x_2 + x_5 + x_8 &= p_5 \\
 x_1 + x_4 + x_7 &= p_6 \\
 2(\sqrt{2} - 1)x_4 + (2 - \sqrt{2})x_7 + 2(\sqrt{2} - 1)x_8 &= p_7
 \end{aligned}
 \tag{1}$$

$$(\sqrt{2})x_1 + (\sqrt{2})x_5 + (\sqrt{2})x_9 = p_8$$

$$2(\sqrt{2} - 1)x_2 + (2 - \sqrt{2})x_3 + 2(\sqrt{2} - 1)x_6 = p_9$$

This system may be rewritten in matrix-form, as shown by (2):

$$AX = P \quad (2)$$

Where $X = [x_1, x_2, \dots, x_9]^T$, $P = [p_1, p_2, \dots, p_9]^T$ and (A) is the system's coefficient-matrix. If the inverse-matrix exists (A^{-1}) of (A) , (3) gives the reconstructed-image [1].

$$X = A^{-1}P \quad (3)$$

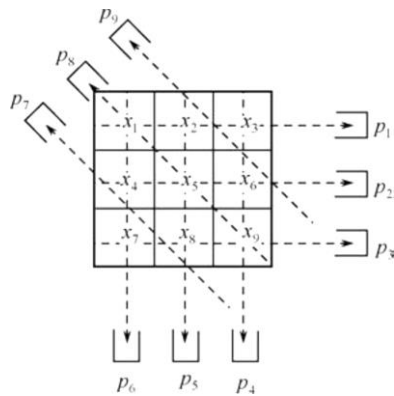


Figure 1. A system of linear-equations [1].

Because the matrix (A) is too large to store in a computer, it is built row-by-row. Any iterative change to (A) is ineligible. Instead, we use (A) and its transposed-matrix. According to math, which means that all IR methods test the reconstruction progression (x) , which is zero, and updating it according to the IR

algorithm used. IR-algorithms are based on (six) main steps shown in Fig. 2. Following the CT-protection measurements, a preliminary guess-image is created, followed by simulated-projections. The next step links virtual projection data to CT scanner predictions. To update an approximate image with anomalies, the IR algorithm's update-equation is used. This image correction method is repeated until the algorithm meets a pre-defined requirement. The final image is formed when this condition is met [5].

The “ART”-Algorithm

The “ART” algorithm works by having the approximate image satisfy a single equation at a time. The “ART”-algorithm was the first used in CT. This algorithm modifies the image after each projection ray. (4) [1] shows how to create the algorithm symbolically.

$$x^{next} = x^{current} - \text{Backproject}_{ray} \left\{ \frac{\text{Project}_{ray}(x^{current}) - \text{Measurement}_{ray}}{\text{Normalization Factor}} \right\} \quad (4)$$

To simplify the equation, the initial guess picture is ($x^{current}$), the updated initial guess image is (x^{next}), the simulated projections of the initial guess image are ($\text{Project}_{ray}(x^{current})$), (Measurement_{ray}) are the measured projections data acquired from the CT scanner and a matrices of (1's) is ($\text{Normalization Factor}$).

The “ART” algorithm only accepts input from one beam (i.e., projection-ray). That is, it adds pixels to a straight line and compares the total to the calculated projection along that ray. The variance between the estimated projections derived from the image calculation and the moving X-ray beam is used to update the original map. As a result, “ART” is also known as ray-by-ray reconstruction [18].

Fig. 3 depicts a projection-beam (P_i) with diameter ($\Delta\xi$) flowing across tissue. The pixel size is determined by (b). (5) is used to calculate the weight (a_{ij}) [18].

$$a_{ij} = (\text{illuminated area of pixel } j \text{ by ray } I) / (\text{total area of pixel } j) \quad (5)$$

The “ART” algorithm image restoration process is summarized in the following stages [18]:

1. A first guess picture ($X^{current}$) is proposed.
2. Equation (6) is used to correct the initial guess graphic.

$$X^{next} = X^{current} - \lambda \frac{A_i X^{current} - p_i}{\|A_i\|^2} A_i^T \quad (6)$$

(λ) is the relaxation vector, which is normally selected to be (1), (p_i) are the calculated estimates, and (A_i) is the matrix contribution factor along the i th ray. $\|A_i\|^2 = \sum_j a_{ij}^2$. Is the squared number of the i th ray's "contribution variables."

3. Beginning with the second step, continue the preceding stages.

Region Growing

Region-Growing segmentation divides an image into larger regions based on predefined parameters. This phase's key segmentation condition is homogeneity. A homogeneity criterion could be assigned using a gray level, a color, a form, or another pre-defined criterion [19]. The region growing segmentation process is [20]:

1. Consolidating pixels into areas.
2. A method of dividing an image into parts.
3. An iterative search technique that separates and merges regions.

The region merging process merges similar regions. The merging process creates initial regions in the image, then compares them to see if they are similar, if so, they are merged. Replicate until no more regions merge [21]. Heterogeneous regions are recursively split [20]. Area splitting divides a picture into disjointed regions that are coherent within themselves. For this, the area of interest is first considered as the entire image. If all pixels in the region meet a resemblance constraint, the area of interest corresponds to an image region. In this case, the region of interest is divided into four equal sub-areas. So on until no more splitting happens.

separately, splitting and combining did not work well. this improves performance [21]. divide and combine regions iteratively for the best segmentation. this technique divides an image into arbitrary unconnected regions that are then merged to meet a pre-defined constraint

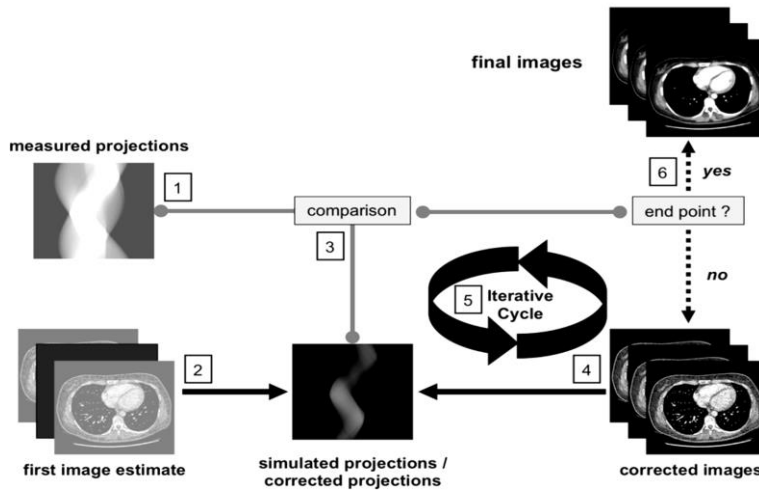


Figure 2. The principal steps of IR-algorithms [5]

Seeded Region Growing

A semi-automatic region merger, seeded region growing [20]. The area starts with one or more seeds, each one comprising one or more pixels. It is possible to place the seeds manually or automatically (ROI). After that, if the intensity of the neighboring pixels is less than a threshold value, they are applied to the growing area. The process is repeated, but this time the growing area mean value is compared to the adjacent pixel intensity. When the rising area has no ins. The algorithm is finished when no pixels adjacent to the growing area have an amplitude greater than a threshold value [22].

Seeds can be started in various ways. The simplest solution is to start only one seed per ROI [22].

The initial seed point and the target threshold are used in the region growing process. This is how iterative seeded region growing works [23]:

1. A seed point is chosen (P_i).

2. If the difference between the initial seed point's pixel intensity and its nearby points is less than the threshold (T_t), the neighboring point is categorized into a cluster termed.

3. The cluster's boundary is recomputed (C_i), and the new boundary points are placed as new seed points.

4. Repeat steps 2 and 3 until the desired threshold is attained.

To extend the region, add adjacent pixels that match the similarity criteria (see Fig. 4). That's how all the pixels are assigned.

Segmentation creates a segmented and binary image from an input. This mask picture is used to recreate the desired pixels selected in the seeding procedure. Fig. 5 shows three phantom mask binary images.

These three phantoms show the seeded region expanding method's adaptable skills in segmentation. The segmented image and mask are the same size.

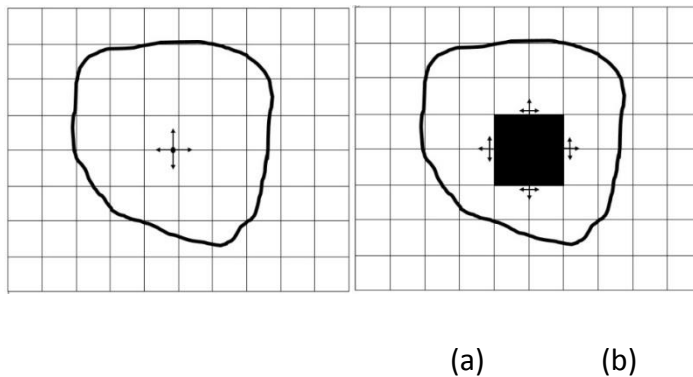


Figure 4. Seeded region growing (a) First step in region growing (b) The growing process.

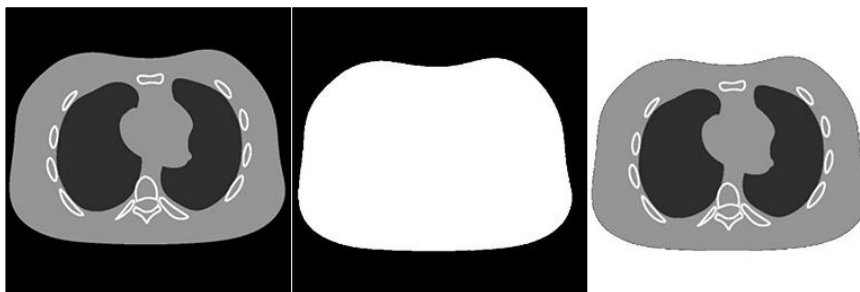


Figure 5. Phantom images (a) Original image, (b) Mask image, (c) Segmented Image

Simulating the Proposed Reconstruction-Algorithm

By pre-processing the 3D CBCT scan image with seeded area expanding, this article minimizes the reconstruction time of the iterative "ART" approach. This minimizes the number of pixels that must be recreated during the iterative algorithm's reconstruction phase. Additionally, the time savings and picture quality of the rebuilt image are evaluated. This investigation is conducted using MATLAB simulations. This enhancement is implemented as follows:

1. A 3-D CBCT scan of a human chest volume is created.
2. The seed point and initial threshold value for the seeded region growing algorithm are chosen. In this step, we will create a segmented test image and a binary mask for it. This mask will restrict the subsequent reconstruction process to only reconstruct the desired pixels where the mask equals (1), and ignore all other pixels (0).
3. Measure the segmented image projections.
4. Create an initial-guess image for iterative reconstruction. The generated image is the same size as the test image.
5. The iterative reconstruction relaxation parameter (λ) and number of iterations are defined.
6. Stimulate the initial guess projections.
7. The "ART" algorithm performs iterative reconstruction. To determine the correction, this algorithm compares the estimated and measured estimates.
8. The iterative reconstruction procedure updates each algorithm's picture based on step's iteration count (5).

Simulation Results and Discussions

CBCT uses the X-ray attenuation coefficient distribution to obtain cross sectional images of the scanned object.

Our simulated algorithm's results show our solution's efficiency in terms of time reduction and image quality

improvement. Despite its superiority over the analytical method, this algorithm's long restoration time prevents its use in medical image reconstruction.

It uses a 3D chest scan to validate and test the simulated algorithms. As shown in Fig. 6, these images are MATLAB-based

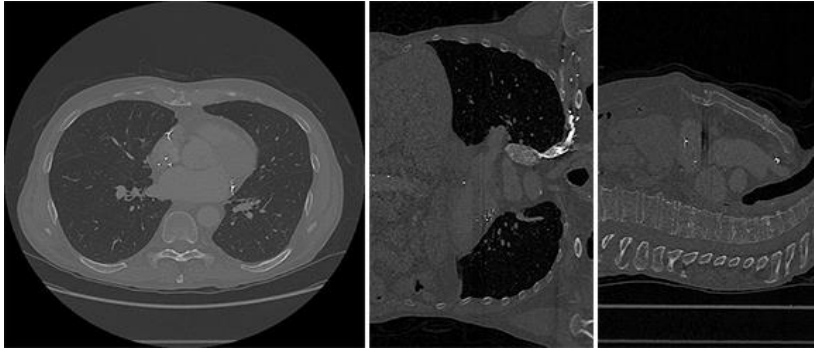


Figure 6. MATLAB 3D chest volume test image in the (X, Y, and Z) direction.

The computer simulation of the iterative reconstruction algorithm “ART” using a CBCT scanner starts with defining the test image's pixel count. The number of acquired projections is (400) at (3600) degrees around the scanned object. This image's initial seeds and gray level are chosen for the seeded region growing algorithm. It will remove all unnecessary pixels from the test image and segment the lung parenchyma as shown in Fig. 7.

Input test picture binary mask is also possible (see Fig. 8). Use this mask for subsequent steps. If the mask contains 0's (black), the reconstruction process ignores them, and processes them if the mask contains 1's (white).

It is now time to collect the measured projection data for the test head phantom image. This step generates 400 projections. A CBCT scanner rotating (3600) degrees around the scanned object generates those projections. A sinogram is a collection of projections collected from various angles during a CT scan. Using the mask from Fig. 8 speeds up the projection generation step. This step allows subsequent reconstruction to focus on the desired pixels only, reducing reconstruction time.

Make a guess image the same size as your segmented test image. This parameter is 1 and the iterations are set to (250). The amount of iterations does not

influence the image quality. Make a one-size matrices of the initial guess picture. This matrix yields a factor (6).

The next step is to begin the iteration loop, which continues until the desired number of iterations is reached. Figure 10 shows the final reconstruction.

Various image quality tests are applied to the test images to verify the reconstruction's precision. 1 shows the results.

Table 1 compares the reconstructed image to the segmented image before reconstruction. The proposed “ART” algorithm reconstructs the test image in (90.659426) seconds. Comparing these results to the standard “ART” algorithm. The initial “ART” algorithm takes 170.792048 seconds to run. The original algorithm takes much longer to reconstruct than our proposed algorithm. Table 2 shows the standard “ART” image quality estimation parameters.

Comparing the image quality parameters of the two “ART” algorithms (tables 1 and 2). using our approach to the “ART” algorithm, we see an increase in (PSNR and SC), which is a sign of good image quality. this means that the image reconstruction is better and the “NMSE, RMSE, MD, and NAE” are lower than the traditional algorithm. by reconstructing the CBCT image of a human lung, we have shown the effectiveness of our proposed method in reconstructing certain regions in the scanned object the results show that our method reduced reconstruction time and improved image quality.

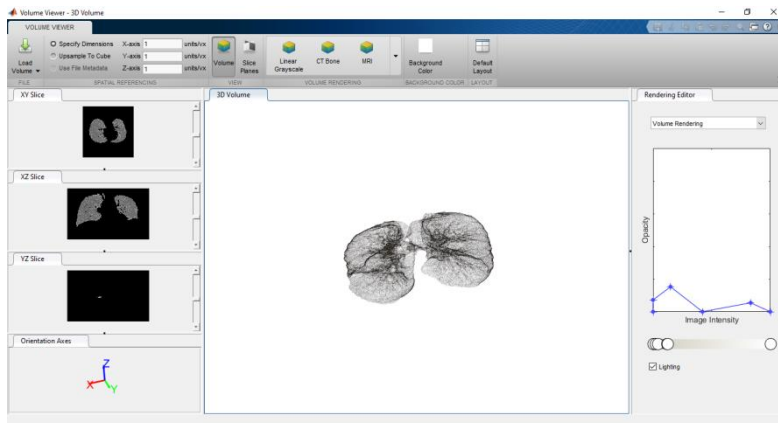


Figure 7. The segmented lung parenchyma.



Figure 8. The binary masks of the segmented test image.

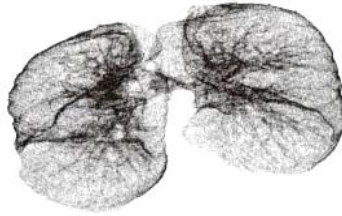


Figure 10. The reconstructed phantom-image using the proposed “ART”-algorithm.

TABLE 1. Image quality measurements using the proposed “ART” algorithm.

“NMSE”	0.00031935
“RMSE”	0.0165
“PSNR”	35.8524
“SC”	0.9999
“MD”	0.1622
“NAE”	0.0098

TABLE 2. Image quality measurements using the traditional “ART” algorithm.

"NMSE"	0.00054649
"RMSE"	0.0245
"PSNR"	32.8225
"SC"	0.9552
"MD"	0.2086
"NAE"	0.0533

Conclusion

This paper's approach could be used to recreate CBCT images. This technique is used to reduce the reconstruction time of iterative algorithms. The iterative approach's success was measured by "RMSE, PSNR, MD, NAE, NMSE, and SC". This approach uses seeded area dependent image segmentation reconstruction to reconstruct image segmentation for the iterative "ART" algorithm.

1. Comparing the suggested method to the traditional "ART" algorithm reduced reconstruction time by 61.2983 percent.
2. The proposed enhancement method to the "ART" algorithm improved the "PSNR and SC" of the reconstructed image as shown in Tables 1 and 2. Other image quality measures "RMSE, NMSE, MD, and NAE" decreased, indicating a better reconstruction with less error.

Our method may be tested on other cone-beam CT images. Proposing alternative methods or using an empirical and iterative reconstruction method known as a hybrid-algorithm may help speed up iterative CT image restoration.

REFERENCES

- [١] G. L. Zeng, Medical image reconstruction: a conceptual tutorial. Springer, 2010.
- [٢] J. P. Sheppard, T. Nguyen, Y. Alkhalid, J. S. Beckett, N. Salamon, and I. Yang, "Risk of brain tumor induction from pediatric head CT procedures: a systematic literature review," Brain tumor Res. Treat., vol. 6, no. 1, pp. 1–7, 2018.
- [٣] A. Tabari, R. Lo Gullo, V. Murugan, A. Otrakji, S. Digum"ART"hy, and M. Kalra, "Recent advances in computed tomographic technology," J. Thorac. Imaging, vol. 32, no. 2, pp. 89–100, 2017.
- [٤] W. Stiller, "Basics of iterative reconstruction methods in computed tomography: A vendor-independent overview," Eur. J. Radiol., vol. 109, pp. 147–154, 2018.
- [٥] M. J. Willeminck and P. B. Noël, "The evolution of image reconstruction for CT—from filtered back projection to "ART"ificial intelligence," Eur. Radiol., vol. 29, no. 5, pp. 2185–2195, 2019.
- [٦] A. K. Louis, "Exact cone beam reconstruction formulae for functions and their gradients for spherical and flat detectors," Inverse Probl., vol. 32, no. 11, p. 115005, 2016.
- [٧] W. S. Van Hemelryck Tessa, G. Maggie, B. K. Joost, and S. Jan, "The implementation of iterative reconstruction algorithms in MATLAB," Master's thesis, Dep"ART"ment of Industrial Sciences and Technology~..., 2007.
- [٨] Y. Chen, Z. Wang, W. Zhao, and X. Yang, "Liver segmentation from CT images based on region growing method," in 2009 3rd International Conference on Bioinformatics and Biomedical Engineering, 2009, pp. 1–4.
- [٩] M. Brooks, "A survey of algebraic algorithms in computerized tomography," UOIT, 2010.
- [١٠] N. Mesanovic, M. Grgic, H. Huseinagic, M. Males, E. Skejic, and M. Smajlovic, "Automatic CT image segmentation of the lungs with region growing algorithm," in 18th international conference on systems, signals and image processing-IWSSIP, 2011, pp. 395–400.

[١١] S. Kamdi and R. Krishna, "Image Segmentation and Region Growing Algorithm," *Int. J. Comput. Technol.*, vol. 2, 2012.

[١٢] C. Panchasara and A. Joglekar, "Application of image segmentation techniques on medical reports," *Int. J. Comput. Sci. Inf. Technol.*, vol. 6, no. 3, pp. 2931–2933, 2015.

[١٣] M.-L. Aurumskjöld, *Optimisation of image quality and radiation dose in computed tomography using iterative image reconstruction*. Lund University, 2017.

[١٤] B. A. Skourt, A. El Hassani, and A. Majda, "Lung CT image segmentation using deep neural networks," *Procedia Comput. Sci.*, vol. 127, pp. 109–113, 2018.

[١٥] H. Kawashima, K. Ichikawa, T. Takata, H. Nagata, M. Hoshika, and N. Akagi, "Performance comparison of ultra-high-resolution scan modes of two clinical computed tomography systems," *Med. Phys.*, vol. 47, no. 2, pp. 488–497, 2020.

[١٦] K. Mueller, R. Yagel, and J. J. Wheller, "Fast and accurate projection algorithm for 3D cone-beam reconstruction with the Algebraic Reconstruction Technique ("ART")," in *Medical Imaging 1998: Physics of Medical Imaging*, 1998, vol. 3336, pp. 724–732.

[١٧] A. C. Kak and M. Slaney, *Principles of computerized tomographic imaging*. SIAM, 2001.

[١٨] T. Knopp and T. M. Buzug, *Magnetic p"ART"icle imaging: an introduction to imaging principles and scanner instrumentation*. Springer Science & Business Media, 2012.

[١٩] C. Shuhan, W. Ben, L. Jindong, and H. Xuelong, "Semantic image segmentation using region-based object detector," in *2017 13th IEEE International Conference on Electronic Measurement & Instruments (ICEMI)*, 2017, pp. 505–510.

[٢٠] C. Sun, T. Bednarz, T. D. Pham, P. Vallotton, and D. Wang, *Signal and image analysis for biomedical and life sciences*. Springer, 2015.

[٢١] M. Sonka, V. Hlavac, and R. Boyle, Image processing, analysis, and machine vision. Cengage Learning, 2014.

[٢٢] J. C. Russ, The image processing handbook. CRC press, 2006.

[٢٣] E. A. Zanaty and S. F. El-Zoghdy, "A novel approach for color image segmentation based on region growing," Int. J. Comput. Appl., vol. 39, no. 3, pp. 123–139, 2017.

[٢٤] W. Wang and Y. Lu, "Analysis of the mean absolute error (MAE) and the root mean square error (RMSE) in assessing rounding model," in IOP conference series: materials science and engineering, 2018, vol. 324, no. 1, p. 12049.

Some properties of complete intuitionistic fuzzy S-metric space

بعض خصائص الفضاء المترى الضبابي S الحدسي الكامل

Amani E. Kadhm 1 , Rasha A. Ali 2

University of Middle Technical, College of Technical Engineering Baghdad, Baghdad,
Iraq 1 , College of Physical

Education and Sports Science – Al jadiriya, University of Baghdad. Baghdad, Iraq 2

E-mail: amh_2090@yahoo.com 1 , E-mail: Rasha.stat@gmail.com 2 , +964-750-532-
5595

اماني التفات كاظم ١ ، رشا عبد الحسين علي ٢

الجامعة التقنية الوسطى، كلية التقنية الهندسية بغداد ، بغداد، العراق¹ ، كلية التربية البدنية
وعلوم الرياضة الجادرية ، جامعة بغداد، بغداد، العراق²

Abstract:

By introduce S –

metric space and some of properties aim of this paper to prove at fixed point theorem by using fuzzy S – metric space while intuitionistic fuzzy S – metric space in schauder

fixed point theorem while think through a few sample while application of some theorems in

intuitionistic fuzzy S –

metric space and readers benefit from it in proving other theories in fixed point in intuitionistic fuzzy S – metric space

Keywords: S-metric space, bounded S-metric space, closed S-metric space

الخلاصة

من خلال تقديم الفضاء المترى S وبعض الخصائص تهدف هذه الورقة لاثبات نظرية النقطة الثابتة باستخدام الفضاء المترى S الضبابي الحدسي وتطبيق بعض النظريات الخاصة بالفضاء المترى الضبابي S .

1. Introduction

S. Gahler, introduced the 2 –

metrische Raume und iher tepeloische struktur, Math

Nachr. in (1963) [1], B. C. Dhage, introduction of Generalized metric spaces mappings with fixed point, Bull. CalcuttaMathaSoc. in(1992)[2], In(2003)we study Proc. Internat conf. Fixed Point Theory and Applications in some results concerning D –

metric spaces[3], and also D – metric spaces from metric by S. V. R. Naidu,

K. P. R. Rao, N. Srinivas a Rao, introduced the generation of Spaces andthe topology of

D – metricspaces, In (2004)[4] and In (2005). Z Mustafa, A New structure for Generalized Metric spaces with Applications to Fixed point Theory[5].

introduction in (2006) Z. Mustafa, B. Sims, A new approach to generalized metric spaces[6],

In(2007) study by S. Sedghi, K. P. R. Rao, Noshabe, we such that for

Sixweekly compatible mappings in D^ , H. zhometric spaces in common fixed point*

theorems [7] and S. Sadghi, N. shobeu, study in fixed point theoryby common fixed point

Theorem in D^ metric spaces, [8]. In (2008) introduced*

fixed point theory for Some common fixed point theorems for mapping on

complete G – Metric spaces, by Z. Mustafa, H obiedat, F. Awawden, and

study fixed point theorem in fixed point Theory for contractive mappings

satisfying ϕ maps in G metric spaces,

In (2010)and such that fixed pointheory in Property p in G metric spaces

, by R. chagh, T. kalian, A, Rani B.E. Rhoades, [9].

Introduced in (٢٠١٢)[10], S. Sedghi, N. Shobe, A. Aliouche, A Generalization of fixed point theorem in S-metric spaces, Introduced in (2014) some properties of S-metric Spaces and fixed point by shoban Sedghi, I. Altun, N. shobe [11], Introduced common fixed point theorem for the R-weakly commuting mappings in S-metric spaces [12], In (2016) by Jong K. Kimy shaban Sedghi, A. Gholidahuch, M. Mehdi Rezaee, fixed point theorems in S-metric space[13] In(2021) *Suzuki Type of common fixed point Theorems in S – fuzzy metric spaces* by M. Jeyaraman and S. Sowndrarasan[14]

2- Preliminaries

Contains of this section definition of fuzzy s – metric space, intuitionistic

Fuzzy S – metric space and results from example and theorem.

Definition (2.1), [10]: A function $S : W^3 \rightarrow [0, \infty)$ is said to be an S-metric on X when X be a nonempty set. If to any $a_1, a_2, a_3, v \in W$,

$$1) (S(a_1, a_2, a_3) \geq 0),$$

$$2) (S(a_1, a_2, a_3) = 0) \text{ if and only if } a_1 = a_2 = a_3$$

$$3) (S(a_1, a_2, a_3) \leq (S(a_1, a_1, v) + S(a_2, a_2, v) + S(a_3, a_3, v)))$$

Then say is S – metric – space by the pair (W, S) .

Definition (2.2), [10]: if $K : W \times W \times W \rightarrow [0, \infty)$ a nonempty set of W be a function such that the conditions to any $a_1, a_2, a_3 \in W$

$$1) \text{if } 0 = [K(a_1, a_2, a_3)], \text{ When } a_1 = a_2 = a_3$$

$$2) [K(a_1, a_1, a_2) > 0] \text{ } \forall \text{ To any } a_1, a_2 \in W \text{ with } (a_1 \neq a_2)$$

$$3) [(K(a_1, a_2, a_3) \geq K(a_1, a_1, a_2))] \text{ } \forall \text{ To any } a_1, a_2, a_3 \in W \text{ when } (a_1 \neq a_2)$$

$$4) (K(a_2, a_3, a_1)) = (K(a_1, a_2, a_3)) = (K(a_1, a_3, a_2)) = \dots$$

5) $[K(a_1, a, a)) + (K(a, a_2, a_3))] \geq [K(a_1, a_2, a_3)]$ to any $a_3, a_1, a, a_2 \in W$

Is called me a K -metric space If job K called me in general metric or a $-K$ metric on W Then couple (W, K) .

Lemma (2.1), [10]: let $S(x, x, y) = (y, y, x)$ (X, S) be an S -metric space. Then we have (X, S) bean S -metric space $x, y \in X$

Lemma (2.2), [14]:

when $(X, S, *)$ bean S – fuzzy metric – space if there exist sequence $\{X_n\}$ & $\{Y_n\}$ such that $\lim_{n \rightarrow \infty} x_n = x$ and $\lim_{n \rightarrow \infty} y_n = y$ then

$\lim_{n \rightarrow \infty} S(x_n, x_n, y_n, t) = S(x, x, y, t)$ to any $y, x \in X$

Definition (2.3), [15] let $*: [0,1] \times [0,1] \rightarrow [0,1]$ be a binary operation is a continuous t -norm

Then $*$ satisfy then the condition:

a) \square $*$ Is associative & commutative

b) \square $*$ is continuous,

c) $q = q * 1$ For all $[0,1] \in q$

d) $[(s * t) \geq (q * r)], s \geq q$ and $(t \geq r)$ to each $t, s, q, r \in [0,1]$.

Definition (2.4), [15]: let binary operation $\diamond: [0,1] \times [0,1] \rightarrow [0,1]$ is a continuous t – conorm if $*$ satisfies the following conditions:

1) \diamond is commutative and associative,

2) \diamond is continuous,

3) $a \diamond 0 = 0$ for any $a \in [0,1]$,

4) $(a \diamond b) \leq (c \diamond d)$ whenever $(a \leq c)$ and $(b \leq d)$ for all $d, c, b, a \in [0,1]$.

Definition (2.5), [14]: $(W, S, *)$ is A3-tuple called fuzzy S - metric -space if $*$ is a continuous t – norm , spot non-empty set is X , and S fuzzy set

on $W^3 \times [0, \infty)$ such that the following condition for

each $p, q, o > 0, a_1, a_2, a_3, a \in W$

$$1) (S(a_1, a_2, a_3, p) > 0);$$

$$2) (S(a_1, a_2, a_3, p)) = 1 \text{ Then } a_3 = a_2 = a_1;$$

$$3) [S(p\{a_1, a_2, a_3\}, p)] = [S(a_1, a_2, a_3, p)]$$

$$4) S(a_1, a_2, a_3, q + o + p) \geq S(a, a_2, a_3, p) * S(a_1, a_2, a, q) * S(a_1, a, a_3, o) \text{ (Tetrahedral inequality)}$$

$$5) S(a_1, a_2, a_3, \cdot) : (0, \infty) \rightarrow [0, 1] \text{ is continuous.}$$

Definition (2.6), [14]: when a rotation $\{w_l\} \rightarrow W$ & $(W, S, *)$ be an S-fuzzy metric-space $w \in W$. Then $p > 0$?

1) When to any $\gamma > 0$ to find $c_0 \in C$ A sequence in $\{w_l\}$ is said to be convergent to W such that $S(w_l, w_l, w, p) > 1 - \gamma$ for all $l \geq c_0$.

2) To all $\gamma > 0$ and there exist $c_0 \in C$, $\{w_l\}$ a sequence is told to become a Cauchy sequence if such that $1 - \gamma < S(w_k, w_l, w_l, p)$ to all $k, l \geq c_0$.

3)

In S – fuzzy metric –

space is told complete if any Cauchy sequence is convergent.

Lemma (2.3): when $*$ is a continuous t – norm & \diamond is a continuous t – connorm, then:

a) For every $a_1, a_2 \in [0, 1]$, if $(a_2 > a_1)$ there are $a_4, a_3 \in [0, 1]$, $a_5, a_6 \in [0, 1]$ such that $(a_3 * a_5 * a_1) \geq a_2$, $(a_2 \diamond a_4 \diamond a_6) \leq a_1$.

b) When $a_3, a_1, a_2 \in [0, 1]$ such that $a_1 \leq (a_2 * a_2 * a_2)$ & $(a_3 \diamond a_3 \diamond a_3) \leq a_1$

Definition (2.7):

A three told $(W, M, *)$ is fuzzy S – metric – space Where $*$ is a

continual t – norm W is a nonempty group & $M = W^3 \times [0, \infty) \rightarrow [0, 1]$ which

is a mapping such that any estate $a_1, a_2, a_3, a \in W$

$$1) 0 = M(a_1, a_2, a_3, 0)$$

- 2) $1 = (M(a_1, a_2, a_3, p)), \text{ to any } p > \infty \Leftrightarrow a_3 = a_1 = a_2;$
- 3) $(M(a_3, a_2, a_1, p)) = (M(a_1, a_2, a_3, p)), \text{ then } p > 0;$
- 4) $(M(a_1, a_2, a_3, \cdot)): [0, \infty) \rightarrow [0, 1]$ is left continuous
- 5) $\lim_{p \rightarrow \infty} (M(a_1, a_2, a_3, p)) = 1$
- 6) $(M(a_1, a_2, a_3, t+s+r)) \geq (M(a_1, a_2, a, p)) * (M(a_2, a_3, a, s)) * (M(a_3, a_1, a, r)), \text{ then } o, q, p > 0$

When $(W, M, *)$, the open ball $B_x(q, p)$ for $p > 0$ with center $a_1 \in W$ and radius $q \in (0, 1)$ is defined as

$$\text{The } B_x(q, p) = \{a_3, a_2 \in W \mid (M(a_1, a_2, a_3, p)) > 1 - q\} \quad \dots (1)$$

A fuzzy S-metric M is a nearness suit to Hausdorff topology on W induced by family name $\{B_x(q, p) \mid a_1 \in W, r \in (0, 1), p > 0\}$

Example (2.1): be continuous t-norm is $a * b * c = abc$, $a * b * c = \min(a, b, c)$ then it is fuzzy S-metric space

Definition (2.8): A triple (W, N, \diamond) is fuzzy S-metric -space is Where \diamond issue continuous t -conorm, W issue nonempty group, $N = W^3 \times [0, \infty) \rightarrow [0, 1]$ is a mapping out let such that that properties of to any $a_1, a_2, a_3, a \in W$

- 1) $N((a_1, a_2, a_3, 0)) = 1$
- 2) $p > 0, 0 = N((a_1, a_2, a_3, p)), \Leftrightarrow a_3 = a_1 = a_2;$
- 3) $p > 0, N((a_3, a_2, a_1, p)) = N((a_1, a_2, a_3, p))$
- 4) $Is \text{ left continua } (N(a_1, a_2, a_3, \cdot)): [0, \infty) \rightarrow [0, 1]$
- 5) $0 = \lim_{p \rightarrow \infty} (N(a_1, a_2, a_3, p))$
- 6) $(N(a_1, a_2, a_3, p+q+o)) \leq [N(a_1, a_2, a, p) \diamond N(a_2, a_3, a, q) \diamond M(a_3, a_1, a, o)], \forall p, q, o > 0.$

Then (W, N, \diamond) , that $D_w(q, p)$ open ball for $p > 0$ when $w \in W$, radius $p \in (0, 1)$ is says that

$$\text{The } D_w(q, p) = \{a_3, a_2 \in W \mid (N(a_1, a_2, a_3, t)) < p\} \quad \dots (2)$$

In fuzzy S-metric N then the family name $\{D_w(q, p) \mid w \in W, q \in (0, 1), p > 0\}$ is a nearness suit to an induced by Hausdorff topology in W .

Example (2.2): A continuous t- conorm issue $[a_1 \diamond a_2 \diamond a_3 = \min(a_1 + a_2 + a_3, 1)]$,
 $[a_1 \diamond a_2 \diamond a_3 = \max(a_1, a_2, a_3)]$

And then it is fuzzy S-metric space. Any fuzzy S-metric space $(W, M, *)$ that couple (M, N) is said at intuitionistic fuzzy S-metric on Q . is an intuitionistic fuzzy S – metric space to that $(W, M, 1 - M, *, \diamond)$, satisfy t-norm $*$, t-conorm \diamond are with,

$$\text{i.e. } 1 - [(1 - a_1)(1 - a_2)(1 - a_3)] = [a_1 \diamond a_2 \diamond a_3] \text{ to any } a_1, a_2, a_3 \in W .$$

Then $(W, M, N, *, \diamond)$ be an intuitionistic fuzzy S- metric space. For $p > 0$ the open ball $G_w(q, p)$ and center $w \in W$ and radius $q \in (0, 1)$ is defined by

$$G_w(q, p) = \{a_3, a_2 \in W \mid [M(a_1, a_2, a_3, p) > 1 - q], [N(a_1, a_2, a_3, p) < q]\} \quad \dots (3)$$

Remark seen able be trivial.

$[G_w = B_w \cap D_w]$ When B_w, D_w get at **(1) & (2)** respectively

Then $*, \diamond$ are with a continuity t-norm, t-conorm generates a topology $T_{(M, N)}$, $\{G_w(q, p) \mid w \in W, q \in (0, 1), p > 0\}$ we have issue said to be the (M, N) - topology $A \in T_{(M, N)}$ to any $\forall w \in W, p > 0, q \in (0, 1)$ satisfy $G_w(q, p) \subset A$. We donate the (M, N) - uniformity (or generated by M and N the uniformity) by $U_{(M, N)}$.

$U_{q, p}, q \in (0, 1), p > 0$ The family when is a base for this uniformity

$$U_{(q, p)} = \{(a_1, a_2, a_3) > W^3 : [M(a_1, a_2, a_3, p) > 1 - q], [N(a_1, a_2, a_3, t) < q]\} ?$$

Definition (2.9): at spot group in W , continue $t - norm$ is $*$, a continue $t - conorm$ is \diamond & M, N are fuzzy group on $W^3 \times [0, \infty)$ A 5 - tuple $(W, M, N, *, \diamond)$ is called to institute an intuitionistic fuzzy $S - metric$ space (i. f. s. m. s) such that to every $a_1, a_2, a_3, a \in W$, $0 < p, q, o$

- 1) $1 \geq [N(a_1, a_2, a_3, p)] + [M(a_1, a_2, a_3, p)]$
- 2) $0 = [M(a_1, a_2, a_3, p)]$
- 3) $1 = [M(a_1, a_2, a_3, p)]$ if $a_3 = a_1 = a_2$
- 4) $[M(a_3, a_2, a_1, p) = M(a_1, a_2, a_3, p)]$
- 5) $[M(a_1, a_2, a, p) * M(a_2, a_3, a, o) * M(a_3, a_1, a, q)] \leq [M(a_1, a_2, a_3, p + o + q)]$
- 6) $M(a_1, a_2, a_3, .) : R^3 \times [0, \infty) \rightarrow [0, 1]$
- 7) $\lim_{p \rightarrow \infty} M(a_1, a_2, a_3, p) = 1$
- 8) $1 = N(a_1, a_2, a_3, .)$
- 9) $0 = [N(a_1, a_2, a_3, p)]$ if and only if $a_1 = a_2 = a_3$
- 10) $[N(a_3, a_2, a_1, p)] = [N(a_1, a_2, a_3, p)]$
- 11) $[N(a_1, a_2, a_3, p + o + q)] \geq [N(a_1, a_2, a, p) \diamond M(a_2, a_3, a, o) \diamond N(a_3, a_1, a, q)]$
- 12) $[N(a_1, a_2, a_3, .) : R^3 \times [0, \infty) \rightarrow [0, 1]$ Is right continuous.
- 13) $\lim_{w \rightarrow \infty} N(a_1, a_2, a_3, p) = 0$

Then (M, N) is called an intuitionistic fuzzy $S - metric$ on W .

An alternative definition of convergent and Cauchy sequence in intuitionistic fuzzy S -metric space is given next.

Remark (2.1): let $(W, M, N, *, \diamond)$ at intuitionistic fuzzy S -metric space, $N(a_1, a_2, a_3, \diamond)$ issue not- increasing & $M(a_1, a_2, a_3, *)$ issue not-decreasing to any $a_3, a_2, a_1 \in W$

Definition (2.10): when intuitionistic fuzzy S - metric space in $(W, M, N, *, \diamond)$

1. All $p > 0$ and $u > 0$ A sequence $\{w_n\} \rightarrow W$, issue told to Cauchy Sequence

$$\lim_{n \rightarrow \infty} M(A_{n+u}, A_n, A_n, P) = 0 \lim_{n \rightarrow \infty} N(A_{n+u}, A_n, A_n, t) = 1$$

2 if to all to $p > 0$, and $w \in W$ issue told to convergent to sequence $\{w_n\}$ in W it

$$\lim_{n \rightarrow \infty} M(A_n, A, A, p) = 0 \lim_{n \rightarrow \infty} N(A_n, A, A, p) = 1$$

Proposition (2.1): in intuitionistic fuzzy S-metric space in $(W, M, N, *, \diamond)$ be the, to any $p \in [0, 1]$, then said that $W^3 \rightarrow \square^+$ then:

$$\inf \{q > 0 : [M(a_1, a_2, a_3, q) > 1 - p], [N(a_1, a_2, a_3, q) < p]\} = [S_p(a_1, a_2, a_3)] \boxtimes \dots (4)$$

1) A generating space in S-metric space of family $(W, S_p : p \in (0, 1])$?

2) Let $(W, M, N, *, \diamond)$ that topology $T_{(S_p)}$ in $(W, S_p : p \in (0, 1])$ when (M, N) - Topology (then, S_p is a compatible symmetric for $T_{(M, N)}$).

Proof: 1) By introduction on $\{S_p : p \in (0, 1]\}$ issue trivial at $\{S_p : p \in (0, 1]\}$ such that (1) & (2) of definition (2.1), we now such as $\{S_p : p \in (0, 1]\}$ & satisfies that (3) then \diamond & $*$ by lemma (2.3) are continuous, given to any $p \in (0, 1)$, exists then $p' \in (0, p)$ so prove

$$[1 - p] < [(1 - p') * (1 - p') * (1 - p')] \boxtimes \text{ And } [p > p' \diamond p' \diamond p']$$

$$c_1 = S_r(a_1, a_2, a_3) , c_2 = S_r(a_2, a_3, a_1) \text{ and } c_3 = S_r(a_3, a_1, a_2) \text{ in eq. (4)}$$

It follows that for any given $q > 0$

$$1 - p' < [M(a_1, a_2, a_3, a + q)] \boxtimes , p' > [N(a_1, a_2, a_3, a + q)] \text{ And}$$

$$1 - p' < [M(a_2, a_3, a_1, c_2 + p)] \boxtimes , p' > [N(a_2, a_3, a_1, c_2 + p)] \text{ Where}$$

$$1 - p' < [M(a_3, a_1, a_2, c_3 + q)] , p' > [N(a_3, a_1, a_2, c_3 + q)]$$

$$M(a_1, a_2, a_3, c_1 + c_2 + c_3 + 3q) \geq M(a_1, a_2, w, a + q) * M(a_2, a_3, w, c_2 + q) * M(a_3, a_1, w, c_3 + q) \\ \succ [(1 - p') * (1 - p') * (1 - p')] \\ \succ [1 - p]$$

$$[N(a_1, a_2, a_3, c_1 + c_2 + c_3 + 3q)] \leq [N(a_1, a_2, w, c_1 + q) \diamond N(a_2, a_3, w, c_2 + q) \diamond N(a_3, a_1, w, c_3 + q)] < p' \diamond p' \diamond p' < p$$

Then,
have

we

$$[S_p(a_1, a_2, a_3) \leq c_1 + c_2 + c_3 + 3q] = [S_p(a_1, a_2, a_3) + S_p(a_2, a_3, a_1) + S_p(a_3, a_1, a_2) + 3q]$$

We have, to any $q > 0$, then

$$[S_r(a_1, a_2, a_3) + S_r(a_2, a_3, a_1) + S_r(a_3, a_1, a_2) \leq S_r(a_1, a_2, a_3)] \quad \square$$

(2) All $q > 0$ & $p \in (0, 1)$ Prove that condition,

$$[S_p(a_1, a_2, a_3) + S_p(a_2, a_3, a_1) + S_p(a_3, a_1, a_2) \geq S_p(a_1, a_2, a_3)] \quad \square$$

Then it factor $S_p(a_1, a_2, a_3) < q$, & by (1

$$)[M(a_1, a_2, a_3, q)] > 1 - p \& [N(a_1, a_2, a_3, q)] < p$$

Then, when $[M(a_1, a_2, a_3, q)] > 1 - p \& [N(a_1, a_2, a_3, q)] < p$ conversely then M, N are continue work, & exist a $f > 0$ so $M(a_1, a_2, a_3, q - f) > 1 - p, N(a_1, a_2, a_3, q - f) < p$, $S_p(a_1, a_2, a_3) \leq q - f < q$.

Example (2. 1): When (W, S) been an S-metric space.

$[v * h * o] = \min\{v, h, o\}$ Is t-norm and $[v \diamond h \diamond o] = \max\{v, h, o\}$ t- conorm and for all $v, h, o \in W$ & $q > 0$. Let us by

$$[M(v, h, o, q) = \frac{q}{(q + S(v, h, o))}] \quad \& \quad [N(v, h, o, q) = \frac{S(v, h, o)}{(q + S(v, h, o))}]$$

When W issue intuitionistic fuzzy S-metric space in $(W, M, N, *, \diamond)$

3. Schauder fixed point theorem

The notion gives at schauder theory issue intuitionistic S – fuzzy metric – space for fixed point $(W, M, N, *, \diamond)$ & give of intuitionistic S – fuzzy metric – spaces & studied also extend

the theorem about intuitionistic topology of fuzzy (too at S – metric & matric – spaces).

Then study an intuitionistic fuzzy contraction mapping & such in intuitionistic S – fuzzy

metric – space in fixed – point theorem. For the basic notions and concepts,

Definition (3.1): let (W, A) be in intuitionistic, is said to be abounded set in (W, A) to any $p \in (0,1)$ it exist $q > 0$ satisfy

$$[M(a_1, a_2, a_3, q)] > 1-p, [N(a_1, a_2, a_3, q)] < p \text{ to every } a_3, a_1, a_2 \in W$$

Note (3.1): let $A \subset W$ then intuitionistic fuzzy S -metric spaces in $(W, M, N, *, \diamond)$ is induced by a metric S in W . then is intuitionistic fuzzy S -bounded if it is bounded.

Definition (3.2): be intuitionistic S - fuzzy (W, A) metric- space and $B \subseteq W$ is say that a closed set in (W, A) if to any if & only if to each sequence $p \in (0,1)$

$$\{a_n\} \text{ in } B \text{ nearness } \text{ain } W \text{ i.e. } \lim_{n \rightarrow \infty} [M(a_n, a, a, q)] \geq 1 - p$$

$$, \& \lim_{n \rightarrow \infty} [N(a_n, a, a, q)] \leq p \text{ for all } q > 0, a \in B$$

Definition (3.3): Is intuitionistic S -fuzzy (W, A) metric- space being issue told to be compact when any $a_n \rightarrow W$ can it issue a convergent subsequence.

$A = (W, N_1, M_1, *, \diamond)$ & $B = (V, N_1, M_1, *, \diamond')$ will denote two intuitionistic fuzzy S -metric spaces, where W & V are S -metric space.

Definition (3.4): a mapping $T : A \rightarrow C$, A, B & C be three intuitionistic fuzzy S -metric spaces is called to be sectional intuitionistic fuzzy continuous at

$$x_0 = (x_{01}, x_{02}, \dots, x_{0n}) \in X^n \text{ if } \exists r \in (0,1)$$

Such that for each $\epsilon > 0$. There exist $\delta > 0$ such that,

$$N_1(x, x_0, x_0, \delta) \leq r \& M_1(x, x_0, x_0, \delta) \geq 1 - r \text{ then}$$

$$N_2(T(x), T(x_0), T(x_0), \delta) \leq r \& M_2(T(x), T(x_0), T(x_0), \delta) \geq 1 - r \text{ to any } x = (x_1, x_2, \dots, x_n) \in X^n$$

Then $A = \{W, N_1(q, q_0, q_0, \delta), M_1(q, q_0, q_0, \delta) | q, q_0 \in W\}$ and

$$B = \{W, N_2(T(q), T(q_0), T(q_0), \delta), M_2(T(q), T(q_0), T(q_0), \delta) | q, q_0 \in W\}$$

Is continuous sectional intuitionistic fuzzy.

Definition (3.5): at intuitionistic fuzzy $(W, M, N, *, \diamond)$ in S-metric spaces.

Mapping of continuous $B: W^3 \times [0, \infty) \rightarrow W$ issue told about fuzzy S-convex structure on W if for all $a_1, a_2, a_3 \in W$ when $q > 0$ to any $p \in (0, 1)$.

$$[\Phi(u, v(a_1, a_2, a_3, p), q)] \leq [\lambda M(u, a_1, a_2, q) + (1 - \lambda)N(a_3, a_3, a_3, q)]$$

Holds to all $u \in W$ at $(W, M, N, *, \diamond)$ be at intuitionistic fuzzy S-metric spaces together a convex structure is say an intuitionistic fuzzy S – convex metric space.

Note (3.2): if $k \subset W$ & (W, M) is a fuzzy S-metric space and, then \bar{k} is closed in $(W, S_p(a_1, a_2, a_3))$ & $\bar{k}^p \subset \bar{k} \forall p \in (0, 1)$, when \bar{k}^r by the closure of k in $(W, S_p(a_1, a_2, a_3))$.

Theorem (3.1): at fuzzy S-metric space in intuitionistic satisfying (proposition (2.1)) if c be a non- empty convex an intuitionistic fuzzy compact subset of and $E: c \rightarrow c$ be a sectional an intuitionistic fuzzy continuous. Thus fixed point in E .

Proof: satisfies by (proposition (2.1)) then $(W, S_p(a_1, a_2, a_3))$ is an S-metric - space. c is a compact subset of $(W, S_p(a_1, a_2, a_3))$ when c issue intuitionistic S-fuzzy subset of compact subset of W, by detention of (3.3) to any $p \in (0, 1)$.

Where $S_p(a_1, a_2, a_3)$ denotes there-s-metric space of W. first suppose that W is intuitionistic fuzzy bounded then to any $p \in (0, 1), q > 0$ prove it

$$N(a_1, a_2, a_3, q) \leq p \ \& \ M(a_1, a_2, a_3, q) \geq 1 - p \ \square \text{For all } a_1, a_2 \ \& \ a_3 \in W \ \text{---} \ (5)$$

Now from the definition of bounded we have

$$[S_p(a_1, a_2, a_3)] = \inf \{q > 0 : [M(a_1, a_2, a_3, q) > 1 - p], [M(a_1, a_2, a_3, q) < p]\} \ \square \text{by (4)}$$

From (5) we have $S_p(a_1, a_2, a_3) \leq q$ for all $a_1, a_2 \ \& \ a_3 \in W$, W it S- bounded to the $S_p(a_1, a_2, a_3) \leq q$

Contrariwise, if X is bounded to $S_p(a_1, a_2, a_3)$ $0 < r < 1$. Than to any $r \in (0, 1)$ when exist t satisfy

$S_p(a_1, a_2, a_3) \leq q$ To any a_1, a_2 & $a_3 \in W$, that is, $S_p(a_1, a_2, a_3) \leq q \leq q+1$ for all a_1, a_2 & $a_3 \in W$.

$N(a_1, a_2, a_3, q) \leq p$ & $M(a_1, a_2, a_3, q) \geq 1-p$, a_1, a_2 & $a_3 \in W$, W is $(l, -f, -b)$.

Second satisfy there exist subsequence $\{a_{n_k}\}$ & a in B (both depending on p_0)

$\lim_{n \rightarrow \infty} [S_{p_0}(a_{n_k}, a_{n_k}, a)] = 0$ Then to a given $\varepsilon > 0$ there exist apposite integer $N(\varepsilon)$ such that $(a_{n_k}, a_{n_k}, a) < \varepsilon \Rightarrow N(a_{n_k}, a_{n_k}, a, \varepsilon) < p_0$

For all $n \geq N(\varepsilon)$, $\lim_{n \rightarrow \infty} N(a_{n_k}, a_{n_k}, a, \varepsilon) < p_0$ for all $\varepsilon > 0$

Since ε is arbitrary & satisfy by condition (1) definition (2.9)

$\lim_{n \rightarrow \infty} [M(a_{n_k}, a_{n_k}, a, \varepsilon) > 1-p_0] \Rightarrow a \in B$, B is closed with respect to $S_{p_0}(a_{n_k}, a_{n_k}, a)$

$0 < p_0 < 1$, than, it follows that B closed with respect to $S_{p_0}(a_{n_k}, a_{n_k}, a)$, $0 < p_0 < 1$

Convers follows by conation (1), (6) and (12) of definition (2.9) to get $\varepsilon > 0$

With $p_0 - \varepsilon > 0$ and for $q > 0 \exists$ a positive intege $K(\varepsilon, q)$ r such that

$\forall c \geq C(\varepsilon, q) \Rightarrow S_{p_0-\varepsilon}(a_{n_k}, a_{n_k}, a) \leq q, \forall c \geq C(\varepsilon, q) \Rightarrow \lim_{n \rightarrow \infty} S_{p_0-\varepsilon}(a_{n_k}, a_{n_k}, a) = 0$

B is compact with respect to $S_{p_0-\varepsilon}(a_{n_k}, a_{n_k}, a)$ for since $P_0 \in (0, 1)$ and $\varepsilon > 0$ then B is compact with respect to $S_p(a_1, a_2, a_3)$ for each $P_0 \in (0, 1)$.

Again since $E: c \rightarrow c$ at sectional intuitionistic S-fuzzy continuous $\exists P_0 \in (0, 1)$ is

Continuous to $(W, S_{P_0}(a_1, a_2, a_3))$ it follows

$A = (W, N_1, M_1, *, \diamond)$ & $B = (V, N_2, M_2, *, \diamond')$ will denote two intuitionistic fuzzy S-metric spaces, where A & B are S-metric space.

If $E : (A, S_p(a_1, a_2, a_3)^1) \rightarrow (B, S_p(a_1, a_2, a_3)^2)$ At continuous to any $p \in (0, 1)$

One if $T : A \rightarrow B$ at sectional intuitionistic S- fuzzy continuous, to any

$B \in W^n, \exists p_0(0, 1)$ such that for each

$$\varepsilon > 0, \exists \delta > 0, N_1(a_1, a_2, a_3, \delta) \leq p_0 \ \& \ M_1(a_1, a_2, a_3, \delta) \geq 1 - p_0$$

$$\Rightarrow N_2(T(a_1), T(a_2), T(a_3), \varepsilon) \leq p_0 \ \& \ M_2(T(a_1), T(a_2), T(a_3), \varepsilon) \geq 1 - p_0, \forall a \in W^n$$

Choose η_0 such that $\delta_1 = \delta - \eta_0 > 0$, let $[s(a_1, a_2, a_3)]_{p_0}^1 \leq \delta - \eta_0 = \delta_1$ Then

$$[s(a_1, a_2, a_3)]_{p_0}^1 \leq \delta - \eta_0 = \delta_1, N_1(a_1, a_2, a_3, \delta) \leq p_0 \ \& \ M_1(a_1, a_2, a_3, \delta) \geq 1 - p_0$$

$$M_2(T(a_1), T(a_2), T(a_3), \varepsilon) \geq 1 - p_0, [S(T(a_1), T(a_2), T(a_3))]_{p_0}^2 \leq \varepsilon \Rightarrow N_2(T(a_1), T(a_2), T(a_3), \varepsilon) \leq p_0 \ \&$$

Thus T is continuous with respect to the $[s(a_1, a_2, a_3)]_{p_0}^1 \ \& \ [s(a_1, a_2, a_3)]_{p_0}^2$

Next let E be continuous with respect to $[s(a_1, a_2, a_3)]_{p_0}^1 \ \& \ [s(a_1, a_2, a_3)]_{p_0}^2$ thus

$\forall b \in W^n, \varepsilon > 0 \ \& \ \exists \delta > 0$ such

$$\text{that } [s(a_1, a_2, a_3)]_{p_0}^1 \Rightarrow [s(T(a_1), T(a_2), T(a_3))]_{p_0}^2 \leq \frac{\varepsilon}{2}$$

Let $N_1(a_1, a_2, a_3, \delta) \leq P_0$ and $M_1(a_1, a_2, a_3, \delta) \geq 1 - p_0$ Then $[s(a_1, a_2, a_3)]_{p_0}^1 \leq \delta$

Then it follows that compact subset of the S-metric space $(W, S_p(a_1, a_2, a_3))$ K is a non-empty convex & is a continuous mapping in $E : c \rightarrow c$. And by fixed point theorem in schauder (17) it fallows, so we give another version of *fixed point theorem in schauder intuitionistic fuzzy S – metric space* than E t has a fixed point.

Theorem (3.2): Let , $E : c \rightarrow c$, c is

a non – empty, I– f – S – closed, convex subset of an

intuitionistic fuzzy S – metric space satisfying (proposition (2.1)) Then E

has a fixed point in c if sectional intuitionistic S-fuzzy continuous & $\bar{E}(c)$ being intuitionistic S-fuzzy compact.

Proof: since satisfied (proposition (2.1)), then from theorem (3.1) that $(W, S_p(a_1, a_2, a_3))$ is an S-metric space. So then c is I-f-S- closed, c is closed with respect to $S_p(a_1, a_2, a_3)$, for each $p \in (0, 1)$. When $E : c \rightarrow c$ is sectional intuitionistic S-fuzzy continuous? To any $\exists p_0 \in (0, 1)$ so that $E : c \rightarrow c$ is continues with respect to $S_{p_0}(a_1, a_2, a_3)$. Too is $\bar{E}(c)$ is intuitionistic S-fuzzy compact by theorem (3.1 $\bar{E}(c)$) is compact to $S_p(a_1, a_2, a_3)$ for each $\exists p_0 \in (0, 1)$.

In particular $\bar{E}(c)$ is compact an $(W, S_{p_0}(a_1, a_2, a_3))$.

Also from Note (3.2) $\bar{E}(c)$ is closed in $(W, S(a_1, a_2, a_3)_{p_0})$ and $\bar{E}^{p_0}(c) \subset \bar{E}(c)$ where $\bar{E}^{p_0}(c)$ is the closure of $E(c)$ in $(W, S(a_1, a_2, a_3)_{p_0})$.so $\bar{E}^{p_0}(c)$ is compact in $(W, S(a_1, a_2, a_3)_{p_0})$

We have $E : c \rightarrow c$, c are a non-empty, closed convex subset in fuzzy S-metric space $(W, S_p(a_1, a_2, a_3))$ & is continuous with $\bar{E}^{p_0}(c)$ compact.

It follows E that has a fixed point by Schauder fixed point theorem (17).

Example (3.1): let $(W, M, N, *, \diamond)$ be at intuitionistic fuzzy S-metric spaces, $R = O^3$ $q = \{(a_1, a_2, a_3) \in R : a_1, a_2, a_3 \geq 0\}$ $W = O$ where O is real number, $M, N : W^3 \rightarrow [0, \infty)$ define by

$$\left\{ \begin{array}{l} [M(a_1, a_2, a_3, q)] = (|a_1 - a_2 - a_3|, \alpha |a_1 - a_2 - a_3|) \\ [N(a_1, a_2, a_3, q)] = (1 - |a_1 - a_2 - a_3|, 1 - \alpha |a_1 - a_2 - a_3|) \end{array} \right\} \text{ where } \alpha \geq 0 \text{ is constant for all } q \succ 0$$

4.Application in intuitionistic S- fuzzy metric -space

Theorem (4.1): for all open balls $G_w(p, q)$ is an open set.

Note (4.1): $(W, M, N, *, \diamond)$ be intuitionistic fuzzy S-metric spaces. Define $\tau_{(M, N)} = \{A \subset W : \text{for each } w \in A, \exists q \succ 0 \text{ and } p \in (0, 1) \text{ such that } G_w(p, q) \subset A\}$

Satisfy $\tau_{(M,N)}$ is a topology on W

Note (4.2): by theorem (2.1) and note (2.1) make a topology $\tau_{(M,N)}$ on W all intuitionistic fuzzy S-metric spaces (N,M) on W it has a base the family of open sets in the form the topology $\tau_{(M,N)}$ is one

countable. $\{G_w(p,q): w \in W, p \in (0,1), q > 0\}$ since is a local base

$\{G_w(\frac{1}{u}, \frac{1}{u}): u = 1, 2, \dots\}$ is W .

Lemma (4.1): for all intuitionistic fuzzy S – metric space is hausdorff.

Note (4.3): when (W,S) be S-metric spaces.

$$\text{Let } [M(a_1, a_2, a_3, q) = \frac{q}{(q+S(a_1, a_2, a_3))}] , [N(a_1, a_2, a_3, q) = \frac{S(a_1, a_2, a_3)}{(q+S(a_1, a_2, a_3))}]$$

That is the topology τ_s intuitionistic fuzzy S-metric spaces on W .are the same and caused through their S-metric S & the topology $\tau_{(M,N)}$ through their intuitionistic fuzzy S-metric spaces induced (N, M)

Lemma (4.2): if $(W, M, N, *, \diamond)$ intuitionistic fuzzy S-bounded. Then intuitionistic fuzzy S-metric space all compact subset H .

Note (4.4): all compact set is intuitionistic fuzzy S-metric spaces bounded & closed.

Lemma (4.3): let $\tau_{(M,N)}$ is a topology on W induced by fuzzy S- metric. Then to a sequence $\{w_n\}$ in $W, w_n \rightarrow w$ if and only if $(W, M, N, *, \diamond)$ bean intuitionistic fuzzy S-metric spaces and $M(a_u, a_u, a, q) \rightarrow 1$ & $N(a_u, a_u, a, q) \rightarrow 0$ as $u \rightarrow \infty$

Lemma (4.4):

when intuitionistic fuzzy S – metric space if to each nonempty open set in W & an open ball whose closure is disjoint from A . A subset A of $(W, M, N, *, \diamond)$ is nowhere dense if

Theorem (Baire's) (4.2): let intuitionistic fuzzy S-metric spaces complete $(W, M, N, *, \diamond)$ $\{n_u : u \in U\}$ through

a sequence of dense open subsets of W . Then $\bigcap_{u \in U} N_u$ also dense in W

Remark (4.1): when any complete intuitionistic fuzzy S-metric spaces are of the second category so any

complete intuitionistic fuzzy S –

metric spaces can't is represented as \bigcup of a sequence of nowhere dense sets. It isn't of the first category.

Note (4.5): for every S- metric induces at in intuitionistic Fuzzy S –

metric space & intuitionistic fuzzy S – metric space is make of fuzzy S- metric space, (Baires Theory) for complete metric space and Baires of the above theorem to complete fuzzy metric space are particular cases.

Definition(4.1): $(W, M, N, *, \diamond)$ of bean intuitionistic Fuzzy S-metric space , W be

any nonempty set then a sequence $\{T_u\}$ and function in a_1 to a_2 is called be

converge uniformly to a function T in a_1 to a_2 , to any $p > 0$ & $p \in (0, 1)$, there

exist $u_0 \in U$ prove it $M(T_{u_0}(a_1), f_{u_0}(a_1), f_{u_0}(a_2), q) > 1 - p'$,

$M(T_{u_0}(a_1), f_{u_0}(a_1), f_{u_0}(a_2), q) > 1 - p$ to any , $w \in W$.

Theorem (Uniform Limit) (4.2): Let $T_u : a_1 \rightarrow a_2$ be as sequences

of continuous function from a

topological space W intuitionistic fuzzy S – metric space $(W, M, N, *, \diamond)$ if

$\{T_u\}$ converges uniformly to $T : a_1 \rightarrow a_2$ then T be continuous.

References

1. S. Gahler, 2-metric spaces and their topological structure, *Math. Nachr.* 26, 115-148, 1963.
2. B.C. Dhage, Generalized metric spaces mappings with fixed point, *Bull. Calcutta Math. Soc.* 84, 329-336, 1992.
3. Z. Mustafa, B. Sims, Some results concerning D-metric spaces, Proc. Internat. Conf. fixed Point Theory and Applications, pp. 189-198, Valencia, Spain, 2003.

4. S.V.R. Naidu. , K.P.R. Rao, N. Srinivasa Rao, on the topology of D-metric spaces and the generation of D-metric spaces from metric spaces, *Internet. J. Math Sci.* No.51, 2719_2740, 2004.
5. Z. Mustafa, A New Structure for Generalized Metric Spaces with Applications to fixed Point Theory, Ph.D. Thesis, *The University of Newcastle, Callaghan, Australia*, 2005.
6. z. Mustafa, B. Sims, A new approach to generalized metric spaces, *J. Nonlinear Convex Anal.* 7, 289-207, 2006.
7. S. Sedghi, K.P.R.Rao, N. Shobe, Common fixed point theorems for six weakly compatible mappings in D^* -metric spaces, *Internet. J. Math. Sci.* 6 , 225-237, 2007.
8. Z. Mustafa, H. Obredat, F. Awawdah, Some common fixed point theorems for mapping on complete G-metric spaces, *Fixed Point Theory Appl.* vol. *Article ID* 189 870, 2008.
9. R. Chugh, T. Kadian, A. Rani, B.E. Rhoades, Property P in G-metric spaces, *Fixed point Theory Appl.* Vol. *Article ID* 401 684, 2010.
- 10.S. Sedghi, N. shobe, A. Aliouche, A generalization of fixed point theorem in S-metric spaces *Mat. Vesnik* 64, 258-266, 2012.
- 11.S. Sedghi, 1. Altun, N. shobe, M.A.Salahs hour, Some Properties of S-metric Spaces ad Fixed point Results, *Kyung pook Math. J.*, 54, 113-122, 2014.
- 12.J. K. Kim, S. Sedghi, N. Shobkdae, Common fixed Point Theorems for the R-weakly Commuting mappings in S-metric Spaces. *J. Compute, Anal. Appl.*, 19, 751-759, 2015.
- 13.Jong Kyu kim, shaban Sedghi, A. Gholidahuch, M. Mahdi Rezaee, "Fixed point theorems in S-metric space, *East Asian Math. J.*, Vol. 32(5), PP. 677-684, 2016.

- 14.M, Jeyaraman and S. Sowndrarajan, Suzuki-Type of Common Fixed point theorems in S-fuzzy Metric Spaces *EJ. Math.* ISS: 2736-5484, 2021.
- 15.B. Schweizer and A.Sklar Probabilistic metric spaces, North Holland series in probability and Applied mathematics, *North-Holland, Now York*, 16:54-77, 1983.
- 16.Mohamod Ali, A. and Ranjith Kanna, G. Intuitionistic Fuzzy Cone Metric Space and Fixed Point theorems, *J. Math. And it's Appl. Volumes*, Issue 1-A, 25- 36, 2017.
- 17.Schauder, J. Der Fixpunktsatz in Funktionalraumen, *Studia Math.*2, 171-180, 1930.

A Double slot in a single Substrate Integrated Waveguide Antenna

Yasameen F. Azeez ¹, Maryam K. Abboud ²

1 Affiliation 1; dr.yasameen.fawzi@alfarabiuc.edu.iq
maryamkhalifa@alfarabiuc.edu.iq.

* Correspondence: dr.yasameen.fawzi@alfarabiuc.edu.iq

Abstract: A single substrate integrated waveguide antenna is proposed to resonate at dual band frequencies 5.4 GHz and 6.3 GHz. The proposed design is used to resonate at WAS (wireless access system) A low profile and small size is designed using Computer simulation Technology-Microwave Studio software and optimized (CST). The proposed antenna has dual slots with different lengths, the dimension of the antenna is 50×50 (length and width), and the substrate is proposed RT/ Duroid 5580 substrate material with a thickness of 0.787 mm. The parameters of the proposed antenna have been studied, the resonating modes have also been studied. The proposed design achieved gain and directivity at 5.4 GHz 7.24 dB and 7.34 dB respectively with a return loss of -27 dB. At 6.3 GHz the return loss is -15 dB, the gain and directivity 6.37 dB and 6.77 respectively. The proposed design can be rescaled to higher frequencies to resonate at Wi-Fi 5G.

Keywords: Substrate integrated waveguide; dual-band; slotted substrate integrated waveguide; CST simulation.

1. Introduction

The creation of small, low-profile wideband antennas with high performance is required by modern wireless communication systems. Planar technology (microstrip or coplanar waveguides) is used to create microwave devices at lower frequencies, but at higher frequencies (>30 GHz), planar technology is not possible.

High demand to 5G (Fifth generation) millimeter-wave wireless communication due to its high data rate, higher spectral efficiency and number of users. Microstrip components has the advantage of low profile and an easy installation[1-2]. Microstrip antenna has the disadvantage of low loss, narrow bandwidth, and efficiency [3-5]. As a result of high transmission losses the substrate-integrated waveguide (SIW) technology is a possibility to overcome the limitation of this high-frequency constraint. The propagation characteristics of the SIW structure are similar to those of conventional waveguides. SIW structures maintain most of the benefits of classical metallic waveguides. As with traditional waveguides, it has a high Q-factor, greater power handling capacity, and improved electrical shielding [6]. Apart from that, the ability to combine active and passive components on the same substrate is the most significant advantage of SIW technology.

SIW provides various advantages over traditional metallic waveguides, which are bulky and costly to produce. Various losses, such as dielectric loss, copper loss, and radiation loss, are also present in these waveguides. SIWs also have a high

level of immunity to electromagnetic interference. Substrate integrated waveguide become the preferred type due to the combination of planer transmission lines, low loss, high bandwidth leading to millimeter wave applications compared with conventional rectangular waveguide [6].

The growth demand for wireless frequencies need to design a specific antenna to cover different band of frequencies. Multiband antenna becomes more important these days, which plays an important factor in wireless communication systems by providing a good performance over the bands. Dual band and dual polarized leaky wave antenna has been proposed based on slotted SIW [7]. The half-mode (HM) or quartermode (QM) SIW topologies were used to miniaturize traditional SIW slot antennas [8]. The field distribution of the HM/QM SIW cavity is comparable to that of its full-mode counterpart. As a result, the antennas can be lowered to half and quarter their original dimensions [9-10]. HMSIW antennas were proposed in [11-14]. 5G dual-band slotted SIW array antenna proposed in [15].

This paper presents a dual-band SIW that investigates all of the parameters' effects on resonant frequency and analyzes all waveguide modes.

The paper is organized as follows: The theory of a single substrate integrated waveguide antenna is covered in Section 2. The third section focuses on CST simulation and the impact of changing factors on design. The conclusion of the paper is presented in the final part.

2. Antenna description and design procedure

The proposed unit element's geometry and detailed dimensions are shown in Figure 1. Two slots are printed on the broad wall of a SIW. The width of the broad wall of the SIW is a , and the total length is L . The lengths of the slots are L_1, L_2 respectively. The space between the slots is p . The antenna is designed using computer simulation design (CST) on one layer of substrate RT\ Duroid 5580 (dielectric permittivity of 2.2, loss tangent 0.0015) and has thickness of 0.787 mm is utilized. The proposed antenna is a single-layer design, which reduces costs and complexity compared to multilayer PCBs [1113]. *Weirdly, despite the development of a small and low-profile antenna.

To achieve impedance matching and reduce feeding loss, it consists of a microstrip line with port1 that matches 50 and a length equal to a quarter waveguide length. The slots effect the surface current and excite the electromagnetic fields [16]. All the parameters dimensions are shown in table (1)

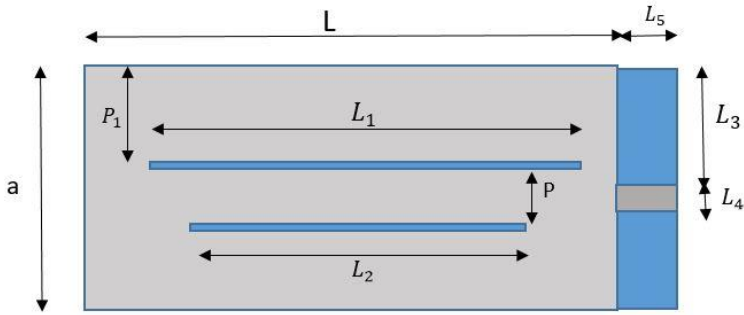


Figure 1. Configuration of the proposed dual slot on one array of SIW

Parameter	Optimizes value (mm)	Description	
L	50	Length of SIW	
a	25	Width of SIW	
L_1	40	Length of slot1	
L_2	30	Length of shorter slot	
L_3	11		
L_4	2	Width of microstrip	
L_5	5	Length of microstrip	
P	6		
P_1	10.5	Space between the two slots	Table (1)
w	0.2	Width of the two slots	

Parameters dimension of single SIW

This antenna is terminated with an open circuit which differs from the conventional waveguide. The reflection coefficient is shown in figure (2), which

has a resonant frequency at 5.4 GHz and 6.3 GHz. The electric field distribution is shown in figure (3).

The proposed antenna can be considered of two regions: the first region is width longest slot with width (p), the second region is with width ($a-P_1 -P$).

By considering the slotted region the waveguides is working a half modes, The cut off frequency can be calculated as

$$f_c = \frac{c}{4(P_n)\sqrt{\epsilon_r}}$$

Where c is the speed of light.

P_n can be considered as P_1 (the region between the sidewall of the waveguide and the longest section of slot L_1)

$a-P_1 - P$ (the region between the sidewall of the waveguide and the shortest section of slot L_2)

ϵ_r is the relative permittivity 2.2

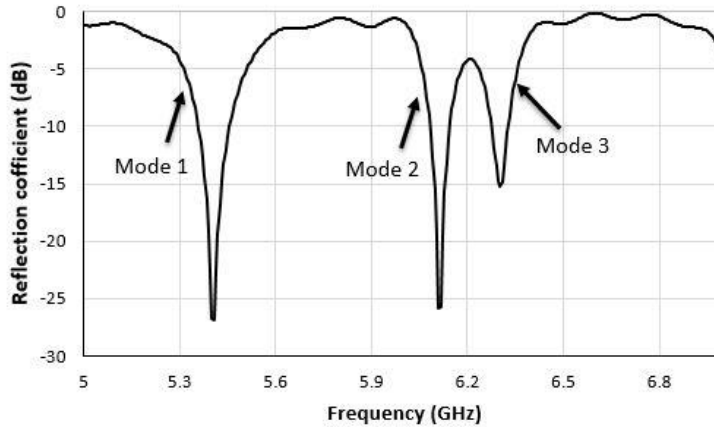


Fig (2) Reflection Coefficient S_{11} against frequency.

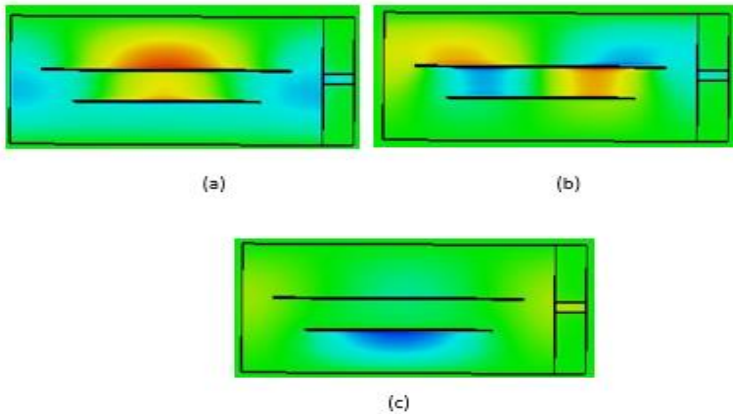


Fig (3) Electric field at (a) 5.4 GHz (b) 6.11 GHz (c) 6.3 GHz.

Mode 1 shows a resonant frequency at 5.4 GHz which is below cutoff frequency at width (P_1), this is because the mode is still excited from the microstrip feed line by the evanescent waves on the SIW due to the short feed sections. The field in the region ($a-P_1 - P$) is therefore evanescent in nature and working in the zero order mode.

Mode 2 has a first order mode at 6.11 GHz which is above cut off frequency at width (P_1), We note that there is no field in the other section since the mode of this region is below cut-off.

Mode 3 has a resonant frequency at 6.3 GHz, it is below the cut off frequency of width ($a-P_1 - P$) due to the short feed sections and the evanescent waves in SIW.

3. Radiation pattern and gain

The 3-D far field radiation pattern at resonant frequencies 5.4 GHz and 6.3 GHz is illustrated in figure (4). By using CST It can be noted that the gain achieved at 5.4 GHz and 6.3 GHz is 7.24 dB and 6.37 dB, respectively. The radiation efficiency at 5.4 GHz and 6.3 GHz is -0.09 and -0.4 respectively. Moreover, the directivity is 7.34 and 6.77 dBi.

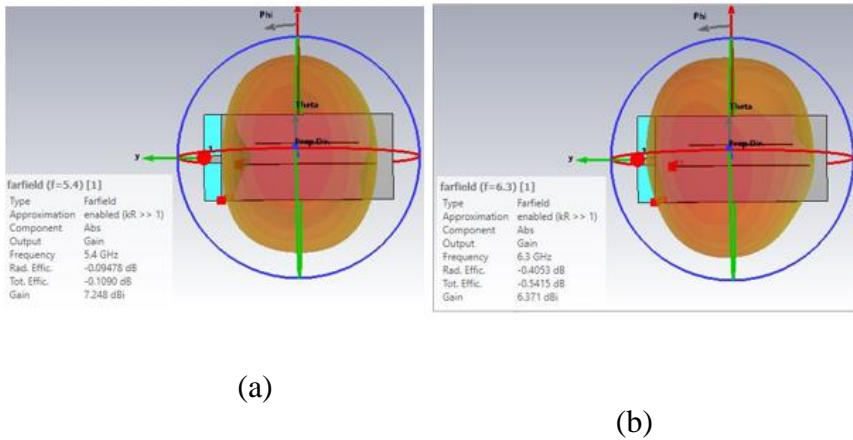


Figure (4) far field radiation pattern

at(a) 5.4 GHz (b) 6.3 GHz

4- Conclusion

A dual beam substrate integrated waveguide antenna has been proposed, a single SIW used with two slots in different length. The resonant frequencies are 5.4 GHz and 6.3 GHz achieved gain 7.24 dB and 6.37 dB, respectively, the reflection coefficient is well matched below 10 dB. The antenna can be rescaled to higher frequency WI-FI 5G applications.

References:

1. Constantine A. Balanis, "antenna theory analysis and design", 4th ed. Wiley 2016.
2. Ramesh Garg, Prakash Bartia, Inder Bahl, Apisak Ittipiboon, "Microstrip Antenna Design Handbook", Artech House Inc 2001.
3. M. Mujumdar and A. Alphones, "Eighth mode substrate integrated waveguide dual band resonator antennas," in *IET Microwaves, Antennas & Propagation*, vol. 11, no. 9, pp. 1262-1266, 7 18.
4. Navneet Kumar, Neeraj Julka, "Star Shaped Multiband Antenna for Wireless Application," *International Journal of Advancement in Engineering Technology, Management and Applied Science (IJAETMAS)*, Vol. 04, pp. 29-33, February.2017.

5. Razin Ahmed and M. Fokhrul Islam, "Slotted Microstrip Patch Antenna for Multiband Application," International Electrical Engineering Journal (IEEj), Vol. 5, No. 3, pp. 1293-1299, 2014.
6. Shalina Garg, Ratish Kumar, "Multiband Microstrip Patch Antenna for Wireless Applications using Metamaterial," International Journal of Advanced Research in Electronics and Communication Engineering (IJARECE), Vol.4, Issue 6, June 2015.
7. Q. Zhang, Q. Zhang, H. Liu and C. H. Chan, "Dual-Band and Dual-Polarized Leaky-Wave Antenna Based on Slotted SIW," in *IEEE Antennas and Wireless Propagation Letters*, vol. 18, no. 3, pp. 507-511, March 2019.
8. Jin, C., Li, R., Alphones, A. and Bao, X.: 'Quartermode substrate integrated waveguide and its application to antennas design', *IEEE Trans. Ant. Propag.*, June 2013, 61, (6), pp. 2921-2928
9. Chaturvedi, D., Raghavan, S.: 'Circular Quarter-Mode SIW Antenna for WBAN Application', *IETE J. Res.*, July 2018, 64, (4), pp. 482-488.
10. Chaturvedi, D., Raghavan, S.: 'A dual-band half-mode substrate integrated waveguide-based antenna for WLAN/WBAN applications', *Int. J. RF Microw. Computer-Aided Eng.*, DOI: 10.1002/mmce.21239
11. Razavi, S. A. , Neshati, M. H.: 'Development of a Low-Profile Circularly Polarized Cavity-Backed Antenna Using HMSIW Technique', *IEEE Trans. Ant. Propag.*, March 2013, 61, (3), pp. 1041-1047
12. Dashti, H., Neshati, M.: 'Development of low-profile patch and semi-circular SIW cavity hybrid antennas', *IEEE Trans. Ant. Propag.*, July 2014, 62, (9), pp. 4481-4488
13. Agneessens, S. and Rogier, H.: 'Compact half diamond dual-band textile HMSIW on-body antenna', *IEEE Trans. Ant. Propag.*, February 2014, 62, (5), pp. 2374- 2381
14. Kaufmann, T., Fumeaux, C.: 'Wearable textile halfmode substrate-integrated cavity antenna using embroidered vias', *IEEE Ant. Wirel. Propag. Lett.*, July 2013, 12, pp. 805-808.
15. Kumawat, Priyanka, and Sunil Joshi. "5G dual-band slotted SIW array antenna." *Journal of Taibah University for Science* 15.1 (2021): 321-328.
16. Marcuvitz, N., Peregrinus, P.: 'Waveguide handbook. On behalf of the Institution of Electrical Engineers', London, UK, 1986

Different Parameters Influence on Electrocoagulation Process

Abbas Salim^a, Tahseen Ali Al-Hattab^b, Huda Saeed Al-Barakat^c

, Eng.Tahseen.Ali@uobabylon.edu.iq, Abbas.Tarfi@student.uobabylon.edu.iq,
hudawww1372@gmail.com

*Chemical Engineering Department, College of Engineering, University of
Babylon*

Abstract. Heavy metals pollution are one of the dangerous environmental problems that produced by the various industries. These pollutants are difficult to remove from wastewater because of their special properties, Electrocoagulation (EC) considers as one of the most important method to purify these pollutant from wastewater. The present study simulate the non-isothermal EC process by using computational fluid dynamic (CFD) model. This mathematical model used partial differential equation to simulate the process. COMSOL multi-physics 5.5 software is used to solve these equations. The heavy metal that used in this study is lead (Pb) with initial concentration (1mol/m^3). The effect of different parameters have been studied on this process, which are the applied voltage (1.5,3,6 and 10 V), rotational anode speed (0,10,50 and 100 rpm) and Hydraulic retention time (HRT) (10,20,30 and 40 min). Then the isothermal process studied to explain the effect of temperature on the process for two situations (isothermal and non-isothermal). The results shows that, the time that needed to remove entire lead (pb) decreases with increase the applied voltages and with increase rotational anode speed till 50 rpm. But for the rotational speed more than 50 rpm the removal Pb efficiency decrease because of the coagulation that produced during the process is dispersed at high rotational speed. The HRT has fewer effect on the process than applied voltage and rotational anode speed.

Keyword: CFD model, EC process ,Wastewater treatment, non- isothermal.

1.Introduction

In the recent decades, the wastewaters that produced by different type of industries are increase into the environment. In many cases the concentration of heavy metals in these wastewaters exceeding the maximum allowable concentration, which causes to important environmental issues. Among these metals, lead (pb) is one of the most dangerous environmental pollutant that leading to serious health problems (**Fogarasi et al, 2016**). There are several technique that used to removal these pollutant such as adsorption, ion exchange, reverse osmosis, chemical coagulation and ect, these methods are not economic and produced secondary sludge that creates environmental hazard. Electrocoagulation (EC) has consider as a good electrochemical method for treating wastewater, because of its versatility and environmental compatibility (**Patidar et al, 2017**). EC is the electrochemical cell which consist of two electrodes (anode and cathode) submerged in the electrolyte and then connected together by the electrical source. Two chemical reactions occurs in the cell that are oxidation and reduction reactions, which happen in the electrode /electrolyte interface. The oxidation reaction occurs at the anode, whereas the reduction reaction occurs at the cathode. The hydrogen gas is releasing at the same time at the cathode. (**Dura, 2013**). The coagulation (sweep floc) that generation from

these reactions has large surface area that is useful for trapping pollutants rapidly and then precipitate in the reactor which are removed by sedimentation. On the other hand the hydrogen gas which are generated at the cathode trapping lighter pollutant and float an the surface of the water, that removed by flotation (**Bazrafshan et al, (2014)** ; **Nwabanne et al, (2017)**). Electrochemical methods are inexpensive, simple, easily operable, fast and eco-friendly in nature. Furthermore, purified water is clear, odorless, potable and colorless with low sludge production. There is no secondary pollution of water in these techniques. The EC system is also influential in removing tannins, suspended solids, dyes and dissolved metals (**Bazrafshan et al,(2015)**).

Fig.1 shows a typical EC configuration. As shown in this figure, the metal ions liberate at the anode (sacrificial electrode) after the electric current is applied on the cell, and electrolysis of the water occurs at the cathode. The hydroxide ions that are generated at the cathode transfer to the metallic ions (at the anode) and react together, then convert to the coagulation. This coagulation adsorb the pollutants that exist in the wastewater. (**Al-Barakat et al,2020**)

The aim of the present work is to study the performance of EC process theoretically by simulate it in the Computational Fluid Dynamic (CFD) model, and then studding the effect of different parameters on it.

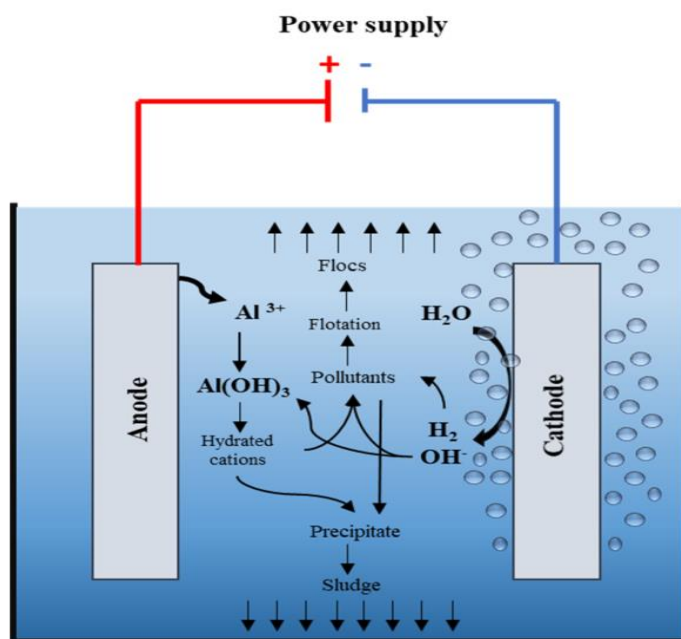
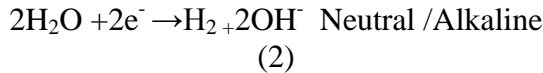
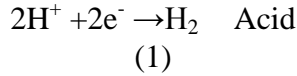


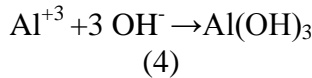
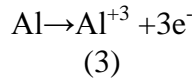
Fig.1.Electrocoagulation process (**Almukdad et al,2021**)

2. Electrochemical Reactions in the Process.

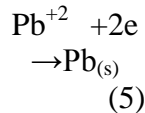
At the cathode the electrolysis of the water occurs. (Al-Barakat et al,2020)



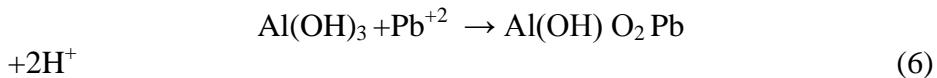
At the Al anode the ions metal liberated and in the bulk solution the coagulation $\text{Al}(\text{OH})_3$ formation.



The electro-deposition of lead can occur as secondary reaction at the cathode.



The following reaction describe the adsorption of lead ions by the coagulation.



The amount of metal that release from the anode can be calculate by Faraday's law .

$$m = \frac{ItW}{nF}$$

Where, m is the mass in g, I is the current in A, t is the time in seconds, W is the gram atomic weight in g mol^{-1} , n is the valence of dissolution and F is Faraday's constant ($96,485 \text{ C mol}^{-1}$).

3. Parameters Affecting on EC process.

Anode and Cathode Martial

The anode and cathode materials are chosen depending on the containment that need to be eliminate and their chemical properties which they responsible to the electrochemical reaction in the EC cell. The most materials are being used are aluminum and iron , aluminum gives the Al^{+3} ions ,while the iron gives either Fe^{+2} or Fe^{+3} .The preferable material in general is the aluminum in efficiency regard in spite of it is cost more than iron.

In case of present the calcium or magnesium ions, it is recommended to use the inert material as cathode such as stainless steel (**Mohammad et al, 2010**).

pH

One of the factors that effects on the electrochemical reaction is the pH. Each pollutant to be removed has optimum pH, which base on that the change from this point (optimum PH) the removal of the pollutant will be decreased. The PH depending on the reaction of the cell and the ions that formation as result of the reaction ,such as OH^- and Al^+ (**Nwabanne et al, 2013**).

Temperature

Naje, et al, 2016 studied the influence of temperature on the EC process using a rotated anode. They found out that the elimination of pollutants that need to be removed and color become better when the temperature increased (95%,96.2% for COD, 93%,94.75% for TSSg, and 95%, 97% for the dye). According to the Stokes- Einstein's, the temperature increase causes to increasing Al^{+3} to $Al(OH)_3$ and increasing in Al^{+3} diffusivity. So the mass transfer is increasing from the electrode surface to the solution bulk. **El-Ashtoukhy et al.(2013)** found that increasing in temperature greater than 40C the solubility of $Al(OH)_3$ increase, that causes to losing of coagulant. Generally, the advantages of the temperature are greater than the disadvantages.

Current

Current density is one of the most important parameters that affecting the efficiency of the EC process, as it causes increasing or decreasing in dissolution of the anode. Which it affecting on the determines of coagulant rate, bubble production rate and size of flocs .The increasing in current density lead to increasing the dissolution of the anode which cause raising in metal hydroxide flocs ,that eventually lead to increasing in the EC efficiency .The increasing in current density above the ideal limits doesn't increasing elimination of the pollutants as a result of available sufficient ions on coagulant (**Nasrullah et al, 2014**).

Voltage

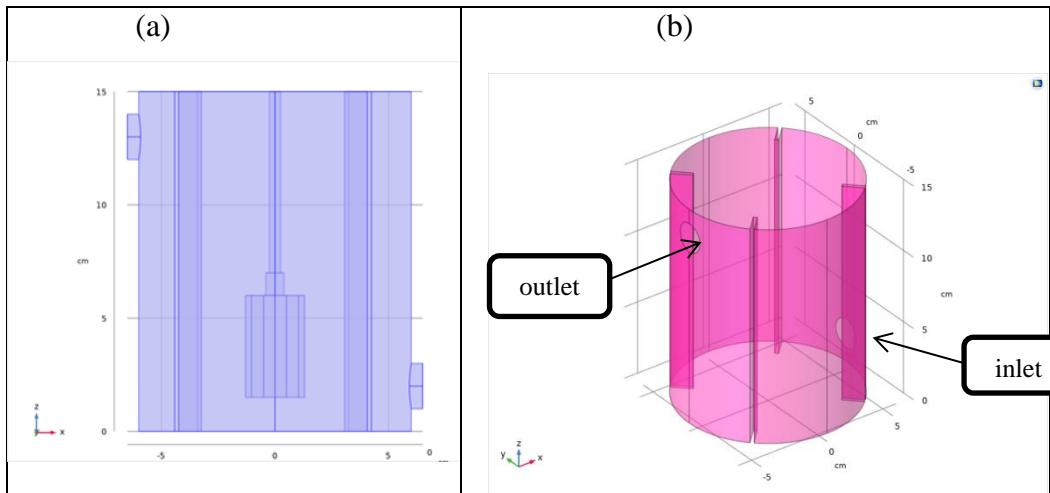
Chavalparit1 et al, 2009 tested the applied voltage between (10 - 30 V) that's equal to the current density range (6.7–20.8 mA/cm²) with regardless the effect of the PH and time, they figure out that significant increasing pollutants elimination by increasing in the applied voltage base on Faraday's law. The increasing in the current density is directly proportional to the coagulant and the anodic ions in certain time .As a result the increasing of the current density or applied voltage ,the aluminum hydroxide ions increase, as aside affect the PH raise.

Mathematical Model

4. EC Configuration

The basic requirements for solving the problem theoretically, is creating the geometry of the EC reactor that will be used in the process. The EC reactor that used in present work consists of two main parts, rotating anode and cathode, which both of them made of Aluminum. The cathode part is a cylinder with radius 5 cm and height 15 cm, it has two holes at its surface which are the inlet and outlet for enter and exit the wastewater. The inlet exist at the bottom and the outlet exist at the top of the cathode.

The anode is a cylinder which have four grooves at its surface. It connected with a shaft for rotating it at the reactor. The water polluted by Pb with different concentrations, which used as electrolyte in the reactor. It feed from the inlet and exit from the outlet of the reactor. Fig.2 shows the EC reactor, the cathode and the anode parts in details.



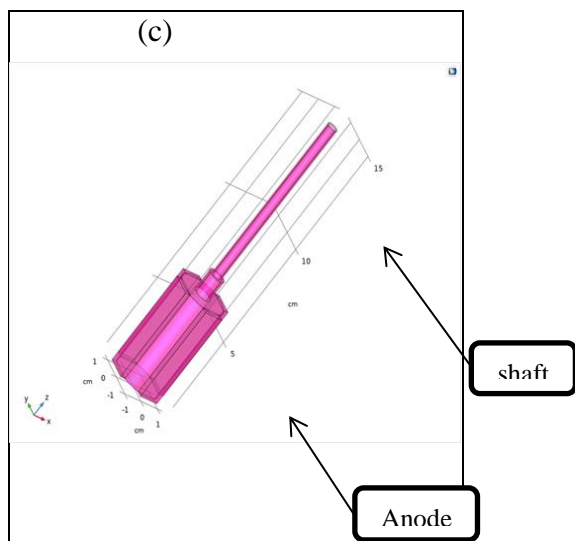


Fig.2. (a) EC reactor configuration (b) the cathode part (c) the anode part.

5. Governing Equation.

After choosing the geometry of the EC reactor we should know the governing equations of the problem. To simulation the motion of the species (mass transfer) uses the Nernst-plank equation. The continuity and Navier-stocks equations use for describe the flow behavior of the species (momentum transfer). And the current distribution equation use for applied voltage on the reactor. After quantified the governing equations on the process use the COMSOL multiphysics to solve these equations.

5.1. Nernst-plank Equation.

$$N_i = -D_i \nabla C_i - Z_i u_{m,i} F C_i \nabla \varphi + C_i u \quad (7)$$

Where N_i is the flux of the chemical species due to convection, D_i is the diffusion coefficient, C_i is the average concentration, Z_i is the charge number, $u_{m,i}$ is mobility of species i, u velocity, F faraday constant and φ is electric potential.

The conservation of charge and species is given by:

$$\frac{\partial C_i}{\partial t} = -\nabla N_i + R_i \quad (8)$$

Where R_i is the reaction rate of species i .

5.2. Continuity and Navier-stocks Equations

-Continuity equation

$$\frac{\partial u}{\partial x} + \frac{\partial u}{\partial y} + \frac{\partial u}{\partial z} = 0 \quad (9)$$

-General momentum equation

$$\rho \frac{\partial u}{\partial t} + \rho(u \cdot \nabla)u = \nabla \cdot [-pI + \mu(\nabla u + (\nabla u)^T)] + F \quad (10)$$

Where p is the pressure (pa), ρ is density (kg/m³), F is the volume force vector (N/m³), μ is dynamic viscosity (pa.s), u is the mean velocity (m/s) and I is the current (A).

5.3. Secondary Current Distribution Equation

$$\nabla \cdot i_l = Q_l \quad , \quad i_l = -\sigma_l \nabla \phi_l \quad (11)$$

$$\frac{\partial i}{\partial x} + \frac{\partial i}{\partial y} + \frac{\partial i}{\partial z} = Q_l \quad , \quad i_l = -\sigma_l \left(\frac{\partial \phi}{\partial x} + \frac{\partial \phi}{\partial y} + \frac{\partial \phi}{\partial z} \right) \quad (12)$$

5.4. Heat transfer equation

This study uses the isotherm EC reactor, so should be use the heat transfer equation to describe the heat transfer in the reactor (the reaction is endothermic).

Heat transfer in liquid

$$\rho C_p \frac{\partial T}{\partial t} + \rho C_p U \nabla T + \nabla \cdot q = Q + Q_p + Q_{vd} \quad (13)$$

Heat transfer in solid

$$\rho C_p \frac{\partial T}{\partial t} + \rho C_p U \nabla T + \nabla \cdot q = Q + Q_{ted} \quad (14)$$

$$q = -K \nabla T \quad (15)$$

where K is thermal conductivity ($W/(m \cdot K)$), C_p is specific heat capacity ($J/(kg \cdot K)$), ρ is density (kg/m^3).

Q_p is the work done by the pressure change and Q_{vd} Viscose dissipation in the fluid.

6. Adsorption Isotherm Model

The adsorption isotherm model use for describe the adsorption phenomenon in the process. There are several adsorption isotherm model such as Langmuir isotherm , Frenlich isotherm ,Langmuir-Frenlich isotherm and ect. The isotherm that use in this study to simulate the adsorption phenomenon is Langmuir isotherm.(**Hakizaman et al.(2017)**)

Langmuir isotherm:

$$q_e = q_{max} \frac{K_L C_e}{1 + K_L C_e} \quad (16)$$

And for removal pollutant use the following kinetic law:

$$-\frac{dC_t}{dt} = \varepsilon_M \cdot \varepsilon \frac{I}{Z F V} q_{max} \frac{K_L C_e}{1 + K_L C_e} \quad (17)$$

Where q_e is the amount of adsorbed molecules per amount of adsorbent at equilibrium, C_e is the equilibrium adsorbate concentration in water, q_{max} is the adsorption capacity of adsorbed molecules per amount of metal cations, K_L is the Langmuir constant. And ε_M is the efficiency of hydro-pollutant-aluminum formation, ε is the current efficiency, I is the applied current, Z is the valence of the electrode metal, F is the faradays constant, V is the volume of solution.

7.Application of COMSOL Multiphysics.

After creating the geometry of the model , adding all equations that need to solve the problem in COMSOL software. COMSOL solves these equations by numerical solution. After solving the problem by COMSOL software, the results will extract. These results show all phenomenon that happen in the process and how the variables distribute in the reactor. The following Fig. show the extracted results from the COMSOL after applied the model on it.

Fig.3 shows the mesh that used in the model. The mesh choosing is based on the accuracy of the result that want to reach ,where the finer mesh could give more accurate result. However some time not the finest mesh is the better choice

depending on the solutions of the equations that deal with equipment. The mesh that use here contains of 86324 elemnts,1240 edges,8652 triangles.

Fig.(4,5,6,7,8,9, and 10) show the distribute of the velocity, pressure ,electrolyte potential , current density, coagulants concentration, lead concentration and temperature respectively.

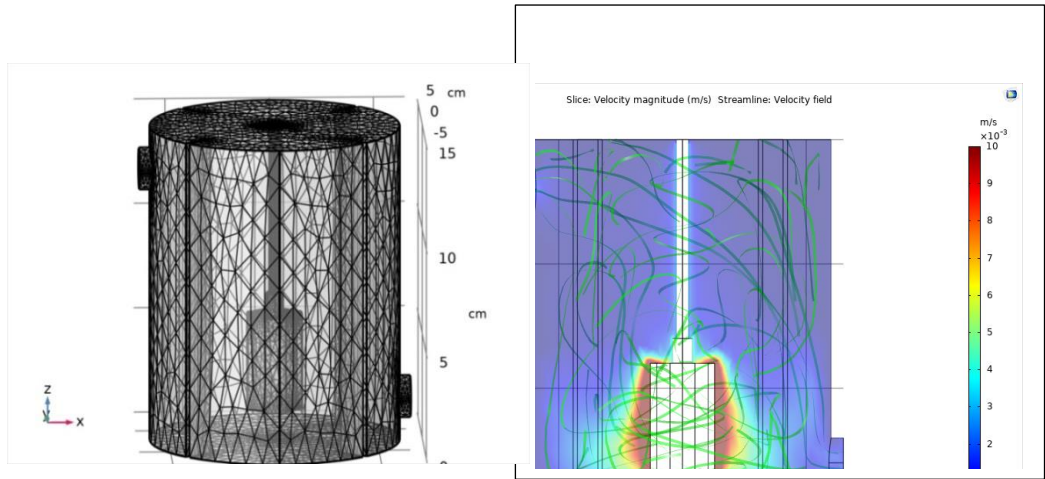


Fig.3. Mesh in the in EC reactor
Fig.4. Velocity distribution

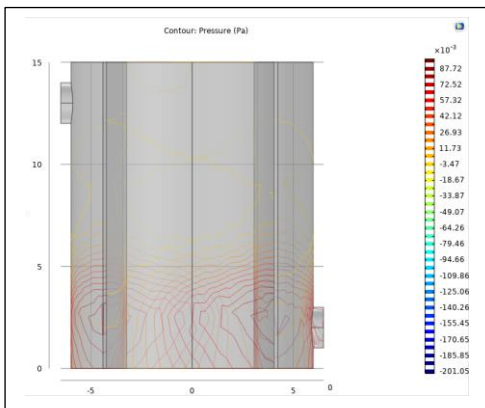


Fig.5. Pressure distribution

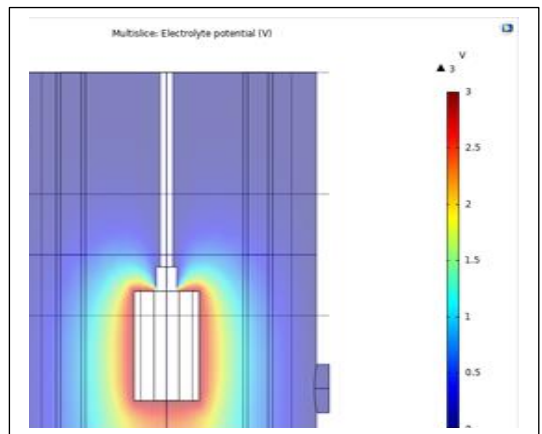


Fig.6. Electrolyte potential distribution

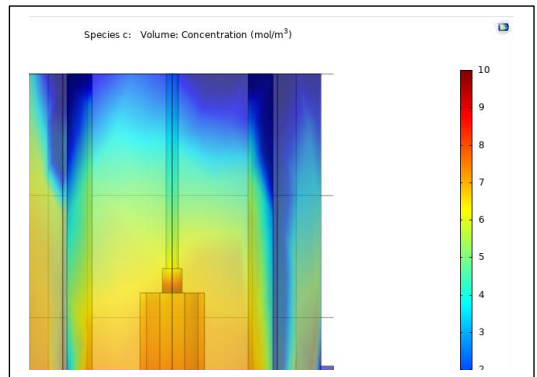
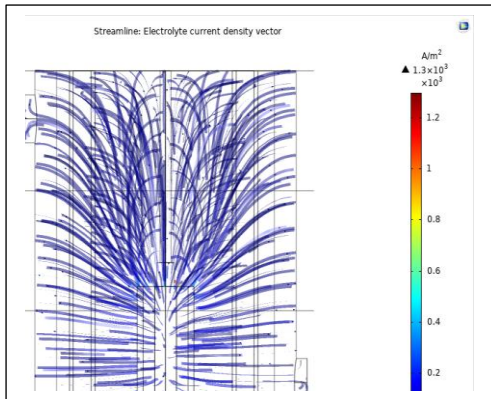


Fig.7.Current density distribution

Fig.8.Coagulants concentration distribution

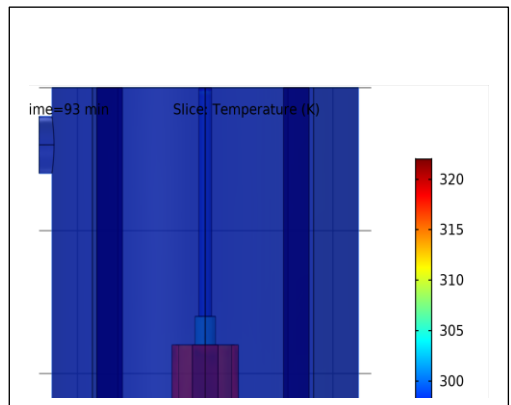
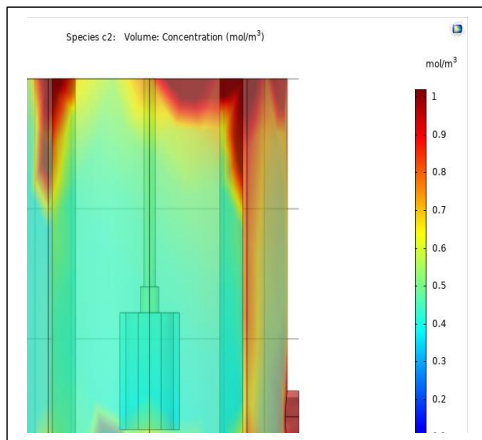


Fig.9. Lead concentration distribution

Fig. 10. Temperature distribution

8 .Result and Discussion.

8.1. Applied Voltage Effect on the EC Process

Fig.11 shows the voltage distributions in the EC reactor. The different voltages are applied at the Anode which are (1.5, 3, 6 and 10V) and the voltage is zero at cathode. As shown in this Fig. the voltage starts to increase from the anode to the cathode and reaches zero at the cathode. Fig.12. shows the current density distribution in the reactor. As shown in this Fig. the current goes from the anode to the cathode where the source of the voltage applied on it.

Table.1. shows the amount current densities at different applied voltages. As shown in this table, by increasing applied voltage the current density increase.

Fig.13 shows the amount of coagulant production at the outlet of the EC reactor for different applied voltage, which it increase by increasing applied voltage. The coagulant reach to around 41mol/m^3 for the applied voltage 10V , 28mol/m^3 for 6V , 15mol/m^3 for 3V and 8mol/m^3 for 1.5V .

Fig.14 shows the removal of lead concentration at the EC outlet, which it increase by increasing applied voltage with time. As shown in this Fig. the lead concentration reach to 0 after 44 min when the applied voltage is 10V , it reach to 0 after 52min for voltage 6V and for 3V it reach to 0 after 80 min and for 1.5V after 100 min the lead concentration reach to around 0.2mol/m^3 .

Fig.15 shows the degree of the temperature of the water at the outlet of the EC reactor. As shown in this Fig. the temperature increase by increasing applied voltage with time. The temperature after 100min reach to 311K at voltage 10V and reach to (299, 295, 294 K) when the applied voltage are (6, 3 and 1.5V) respectively.

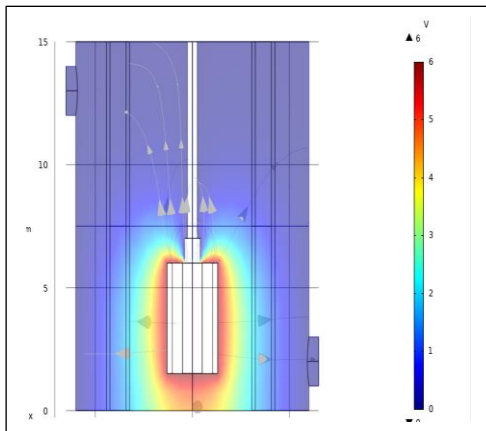


Fig.11. Voltage Distribution in the EC Reactor when the Applied

Voltage is (6V)

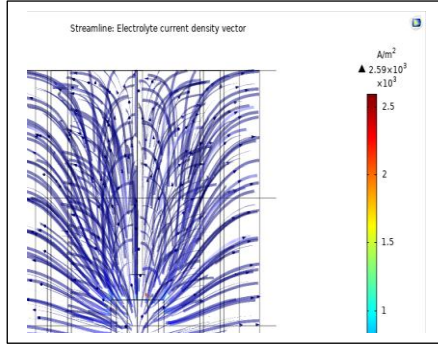


Fig.12. Current Distribution in the EC Reactor when the Applied Voltage is (6V)

Table.1. Current densities at different applied voltages.

No.	Applied Voltage (V)	Current Density (A/M ³)
1	1.5	694
2	3	1300
3	6	2590
4	10	4320

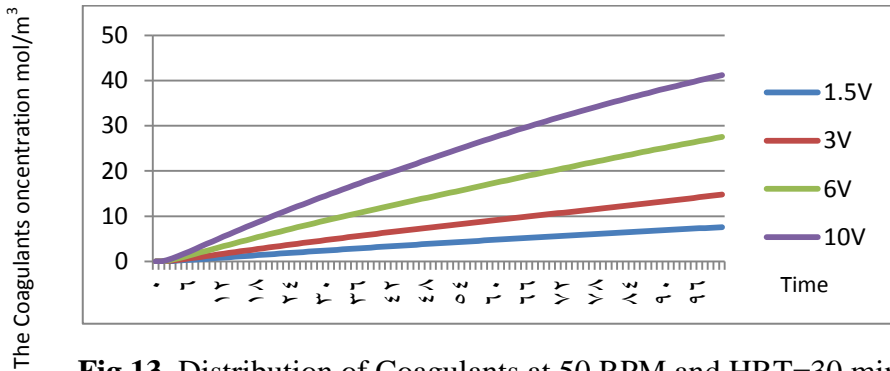


Fig.13. Distribution of Coagulants at 50 RPM and HRT=30 min.

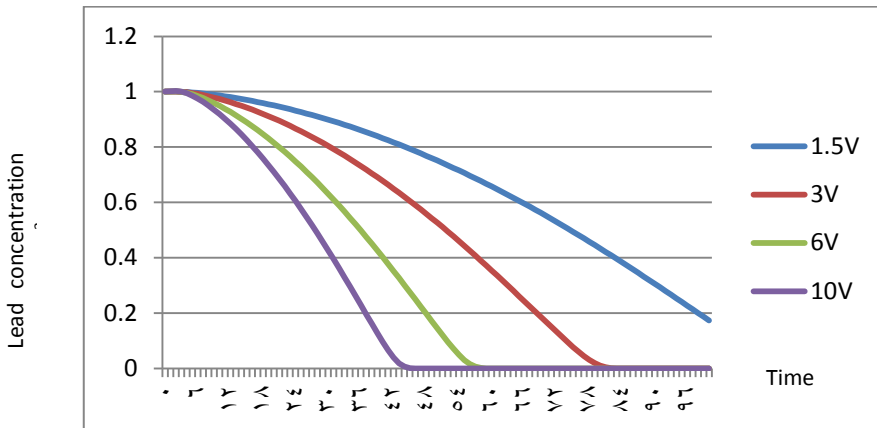


Fig. 14. Lead distribution at HRT=30 min and 50 RPM .

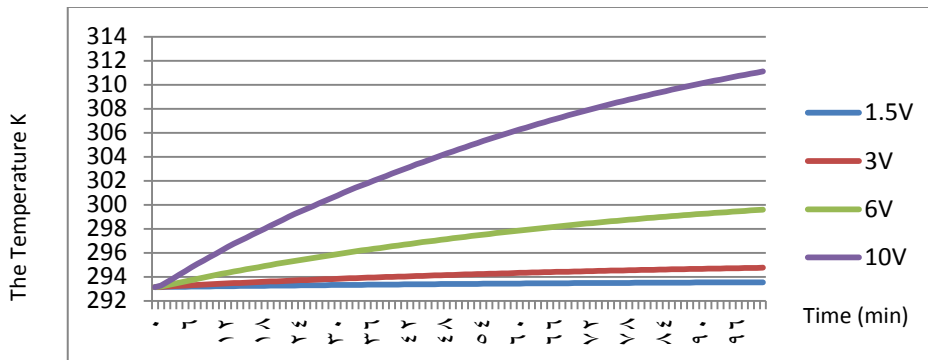


Fig. 15. Distribution of temperature in the EC reactor at HRT=30 min and 50rpm.

8.2. Rotating speed effect on the EC process

Fig.16 shows the velocity distribution on the reactor with different anode rotational speed which are (0,10,50 and 100 rpm). In the case 0 rpm, the anode does not move in the reactor, so as shown in this case the speed of the water is zero in the reactor, however there are some speed in the inlet and outlet of the reactor because of continuously feed of water in the reactor. As shown in this Fig. when the anode begin to rotate, the speed of the wastewater changes, where the maximum speed exist near the anode and increases with increase rotating of the anode.

Table.2 explains the relationship between the rotating anode and the velocity of wastewater, where the speed of the solution are (0.002,0.01, 0.07 and 0.14 m/s) when the rotating of the anode speed are (0, 10, 50 and 100 rpm) respectively.

Fig.17 shows the amount of coagulants production with the time, which it increase by increasing the rotating speed of anode until reach to 50 rpm then the increasing in speed of the anode become not effected. Fig.18 shows the amount of lead concentration which remove from the water, as shown in the Fig. the amount of lead concentration begin to decreasing with time by increasing the anode speed until reach to 50 rpm beyond this value the increasing in speed become useless because the coagulants concentration doesn't increase beyond 50rpm.

Fig.19 shows the degree of the temperature of water with time for different anode rotating speed. As shown in this Fig. the temperature increases with time by increasing rotating anode speed. When the anode does not rotate in the reactor the temperature is low, and it increase for anode speed more than 0, then become stable even when increasing in the anode speed.

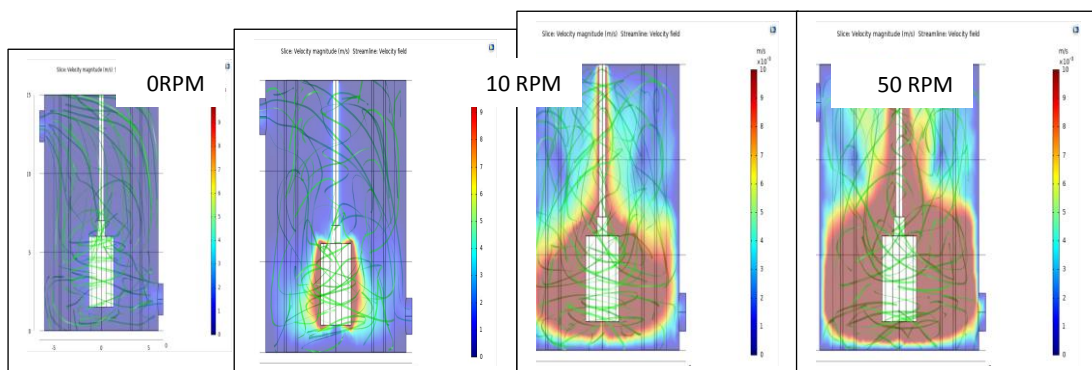


Table.2. The rotational

Fig.16. Velocity Distribution in the EC Reactor when using different rotating anode speed (0,10,50 And 100 rpm)

Table.2. the Rotational speed (rpm) VS velocity (m/s)

No.	Rotational Speed (rpm)	Velocity m /s
1	0	0.002
2	10	0.01
3	50	0.07
4	100	0.14

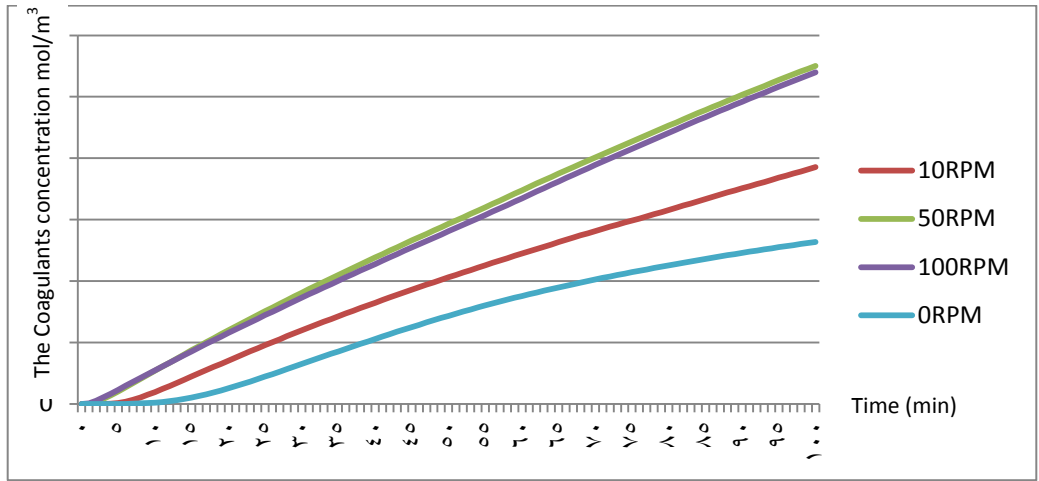


Fig.17. Distribution of Coagulants in the EC reactor at HRT=30 min ,V=6V.

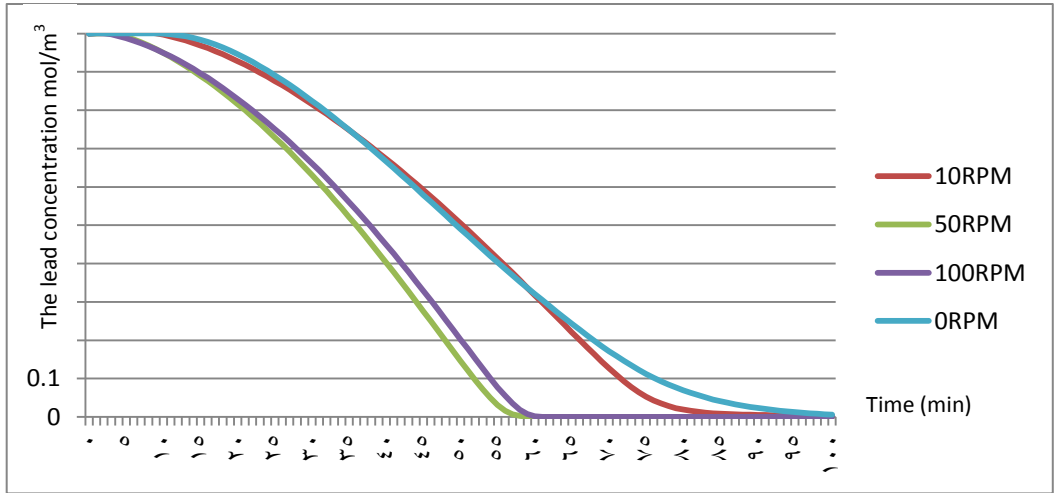


Fig.18. Lead distribution at voltage 6V and HRT=30 min.

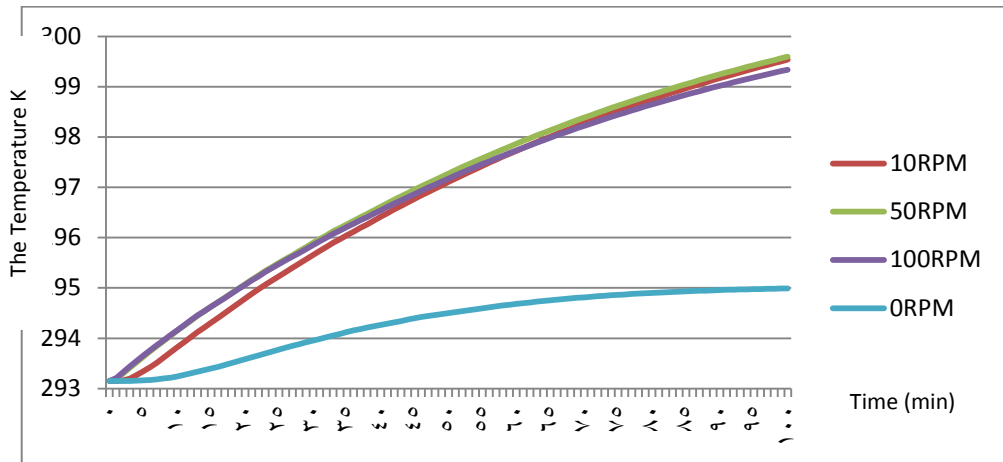


Fig.19. Distribution of temperature in the EC reactor at HRT=30 min ,V=6V .

8.3. Temperature effect on the EC process

The source of the temperature in the solution is the resistance of the material to the current, which is bigger in the metal (anode). The temperature has two effects: one is positive and the other one is negative. The positive one is increasing the diffusivity (Naje, et al (2016) which helps to minimize the time and eventually the cost. And the negative one is that the solubility of ions becomes bigger at higher temperature which is minimize the removal efficiency of the pollutant (El-Ashtoukhy et al.(2013).

Fig.20. shows the temperature distribution in the reactor for different time when HRT is 30 min, applied voltage is 6V and when anode speed is 50 rpm. As shown in this Fig. the temperature starts increasing around the anode because of the applied voltage. The temperature become higher when the reaction between the coagulants and pollutants has only take place for the first time, and then transfer to the rest of the reactor by the movement of the wastewater inside the reactor. As show in this Fig. the temperature increases with increasing the applied voltage. The distribution of the temperature to the bulk of the reactor becomes homogenous with increasing the anode speed.

Fig.(21 and 22) show the temperature distribution on the reactor in both isothermal and non-isothermal case respectively. As shown in these Fig. the temperature in non-isotherm change more than isotherm case and in isotherm case the temperature is more stable than in non-isotherm.

Fig.(23 and 24) show the coagulants production in the isothermal and non-isothermal cases respectively. In this Fig. the maximum coagulant concentration

for the two cases after 100 min is about 28 mol/m^3 when the anode speed is 50rpm, applied voltage is 5V and HRT is 30min. The production starts increasing around the anode and moves to the rest of the reactor. The speed of anode helps to transfer the coagulants concentration to the rest of the reactor and at same time making the coagulants concentration production higher ,which helps to remove the pollutants in shorter time.

Fig. (25and 26) show the lead removal from wastewater for the isothermal and non-isothermal cases respectively. As shown in this Fig. the lead is completely removed after almost 56 min for two cases. The lead concentration starts to disappear at first around the anode which has higher coagulants concentration than the rest of the reactor. Then the anode speed helps in making the lead removal homogenous in the entire reactor in both the isothermal and non-isothermal cases.

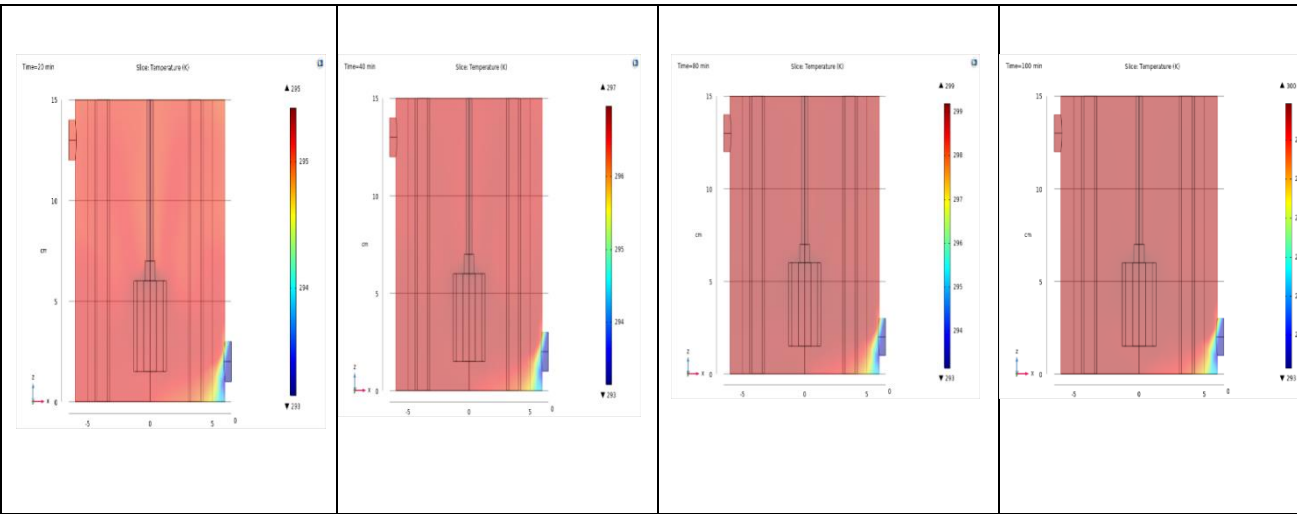


Fig.20. Temperature distribution at (V=6V, HRT=30 min and RPM=50)

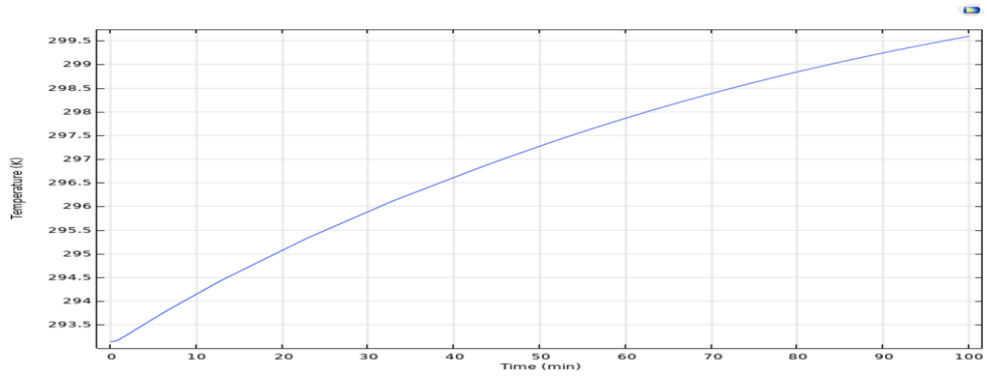


Fig.21. Temperature distribution at (V=6V, HRT=30 min and RPM=50) for Non-isothermal.

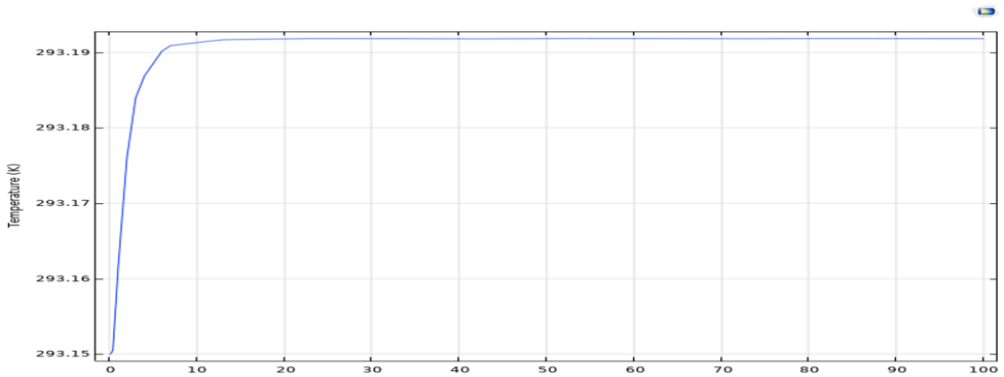


Fig.22. Temperature distribution of isothermal process at (V=6V, HRT=30 min and RPM=50)

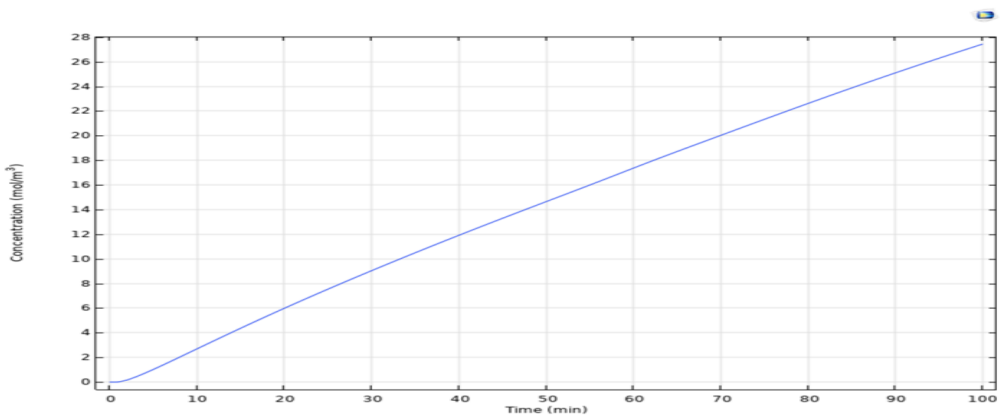


Fig.23. Coagulants concentration in the EC reactor when (HRT=30 min ,V=6V and RPM=50) for Isothermal.

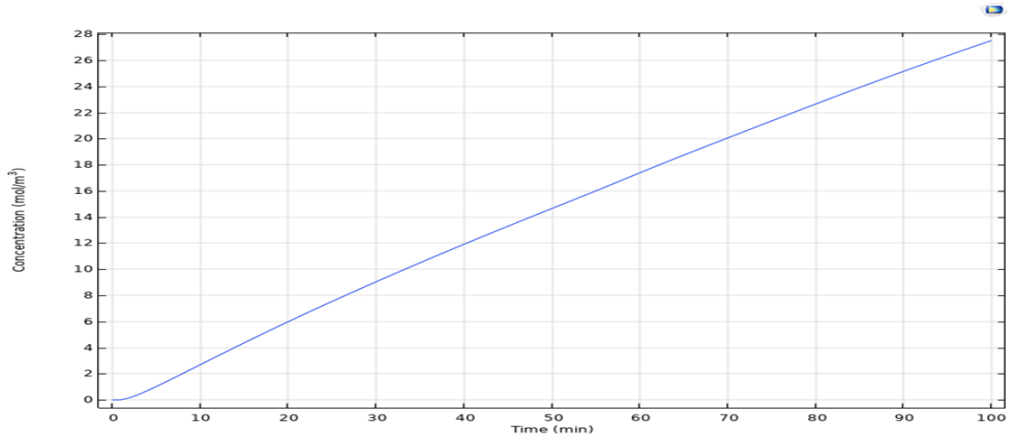


Fig.24. Coagulants concentration in the EC reactor when (V=6V, HRT=30 min and RPM=50) for Non isothermal.

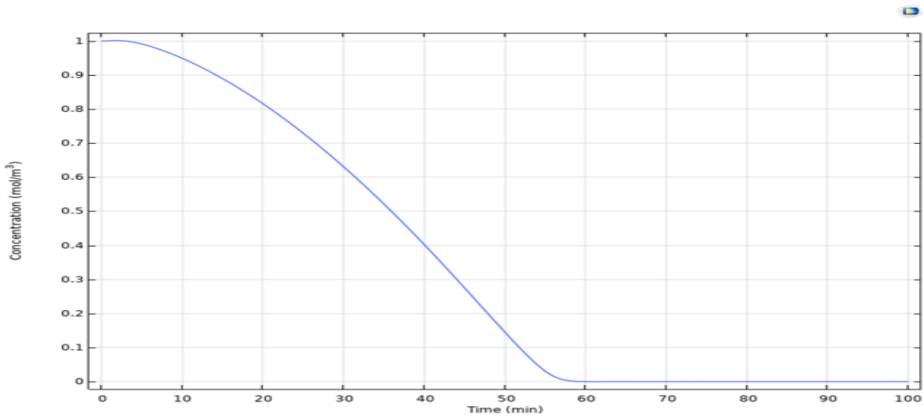


Fig.25. Concentration of lead (V=6V, HRT=30 min. and RPM=50) for Isothermal

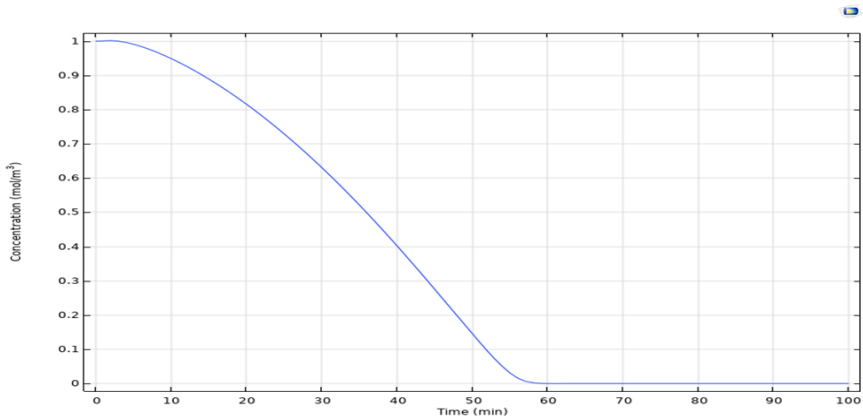


Fig.26. Concentration of lead when (V=6V, HRT=30 min and RPM=50) for Nonisothermal

8.4. HRT Effect on EC Process

The HRT effect on the coagulants production and lead removal is very slight as shown in Fig.(27 and 28). The amount of lead removal and coagulant production is nearly same for different HRT.

Fig.29 shows the effect of HRT on the temperature with time, which the temperature increases by increasing the HRT.

HRT is the hydraulic retention time which define in the below equation:

$$HRT = V_r / Q_i$$

Where V_r is reactor volume (800 Cm^3) and Q_i is the volumetric flow rate (m^3 / s).

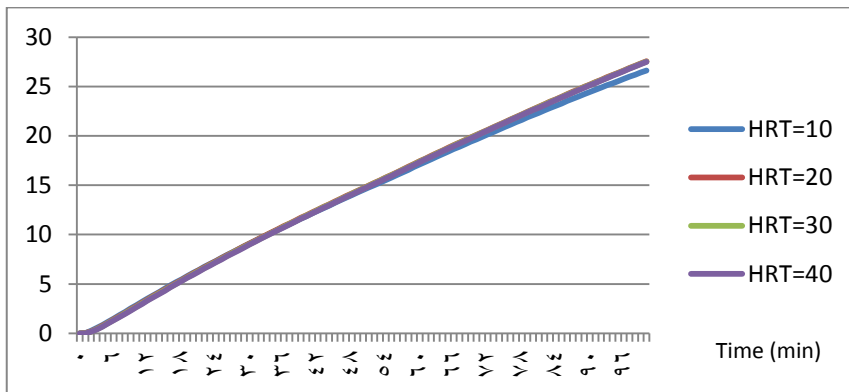
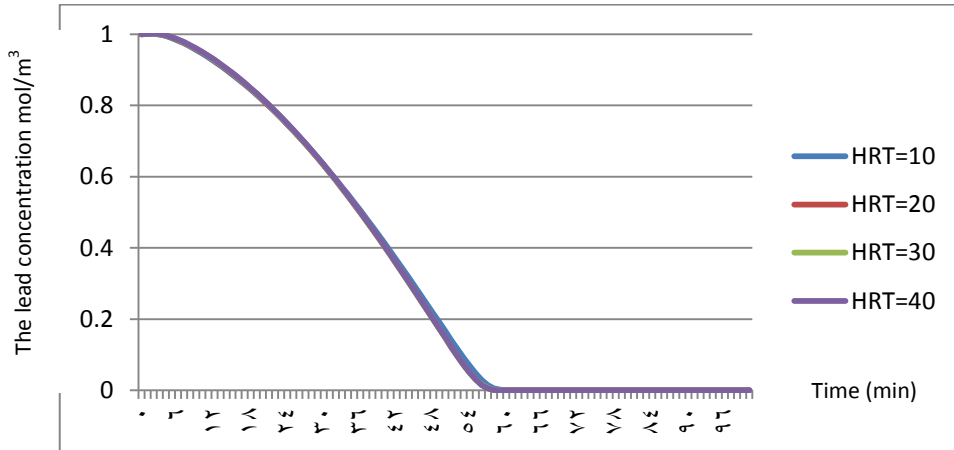
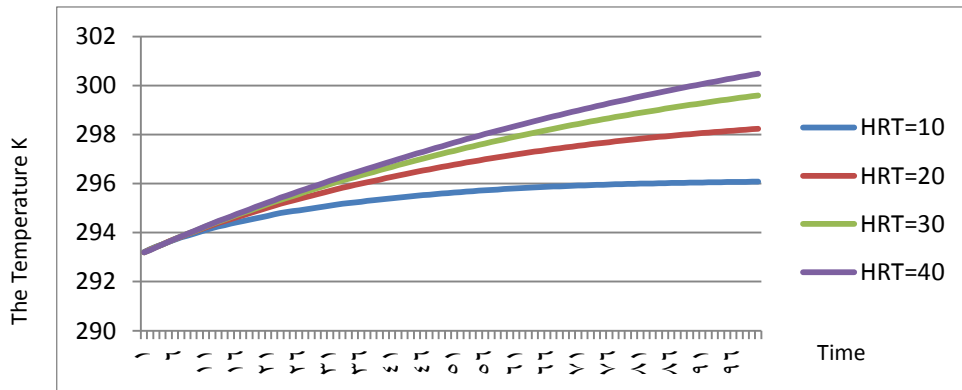


Fig.27. Distribution of Coagulants in the EC reactor at 6V and 50 rpm.**Fig.28.** Lead distribution at 6V and 50 rpm.**Fig.29.** Distribution of Temperature in the EC reactor at 6V and 50 rpm

9. Conclusion

The mathematical model is a good method to understand the all phenomenon occur on the process. In present work used the CFD model to simulate the EC reactor to know the effect of different parameters on the process and to show how the different variables distribute in the EC reactor. the following points can be conclude from present study.

- The distribution of the voltage, current, potential, pressure, temperature, coagulant production and lead removal are good simulated by this model.

- The extracted results from this model show that the coagulants production and lead removal increase with increasing applied voltage, current density and rotating anode speed. Which has the same results with experimental works.
- The lead and coagulants concentration don't effected by temperature changing .
- HRT doesn't effect on the EC very much.
- Main effecting parameters is applied voltage .

References

Al-Barakat, H. S., Matloub, F. K., Ajjam, S. K., & Al-Hattab, T. A. (2020, June). Modeling and Simulation of Wastewater Electrocoagulation Reactor. In *IOP Conference Series: Materials Science and Engineering* (Vol. 871, No. 1, p. 012002). IOP Publishing.

Almukdad, A., Hawari, A. H., & Hafiz, M. (2021). An Enhanced Electrocoagulation Process for the Removal of Fe and Mn from Municipal Wastewater Using Dielectrophoresis (DEP). *Water*, 13(4), 485. Chavalparit, O., & Ongwandee, M. (2009). Optimizing electrocoagulation process for the treatment of biodiesel wastewater using response surface methodology. *Journal of Environmental Sciences*, 21(11), pp. 1491-1496.

Bazrafshan, E., & Mahvi, A. H. (2014). Textile wastewater treatment by electrocoagulation process using aluminum electrodes. *Iranian journal of health sciences*, 2(1), pp. 16-29.

Bazrafshan, E., Mohammadi, L., Ansari-Moghaddam, A., & Mahvi, A. H. (2015). Heavy metals removal from aqueous environments by electrocoagulation process—a systematic review. *Journal of environmental health science and engineering*, 13(1), pp. 1-16.

Dura, A. (2013). Electrocoagulation for Water Treatment: the Removal of Pollutants using Aluminium Alloys, Stainless Steels and Iron Anodes (Doctoral dissertation, National University of Ireland Maynooth).

El-Ashtoukhy, E. S. Z., El-Taweel, Y. A., Abdelwahab, O., & Nassef, E. M. (2013). Treatment of petrochemical wastewater containing phenolic compounds by electrocoagulation using a fixed bed electrochemical reactor. *Int. J. Electrochem. Sci*, 8(1), 1534-1550.

Fogarasi, S., Imre-Lucaci, F., GHIRIŞAN, A., MIŞCA, H., RADU, B., & IMRE-LUCACI, Á. R. P. Á. D. (2016). Removal of lead from industrial wastewater by

electrocoagulation using sacrificial aluminium electrodes. *Studia Universitatis Babes-Bolyai, Chemia*, 61, pp. 145-154

Gheraout, D., Alghamdi, A., & Gheraout, B. (2019). Electrocoagulation process: A mechanistic review at the dawn of its modeling. *Journal of Environmental Science and Allied Research*, 2(1), 23-31.

Hakizimana, J. N., Gourich, B., Chafi, M., Stiriba, Y., Vial, C., Drogui, P., & Naja, J. (2017). Electrocoagulation process in water treatment: A review of electrocoagulation modeling approaches. *Desalination*, 404, pp. 1-21.

Mohammed, A. A., & Al-Mureeb, M. D. (2010). Removal of lead from simulated wastewater by electrocoagulation method. *J Engineering*, 16(4), 5811-21.

Naje, A. S., Chelliapan, S., Zakaria, Z., & Abbas, S. A. (2016). Electrocoagulation using a rotated anode: A novel reactor design for textile wastewater treatment. *Journal of environmental management*, 176, pp. 34-44.

Nasrullah, M., Siddique, M. N. I., & Zularisam, A. W. (2014). Effect of high current density in electrocoagulation process for sewage treatment. *Asian Journal of Chemistry*, 26(14), pp. 4281-4285.

Nwabanne, J. T., & Obi, C. C. (2017). Abattoir Wastewater Treatment by Electrocoagulation Using Iron Electrodes. *Der Chemica Sinica*, 8(2), pp. 254-260.

Nwabanne, J. T., & Okoye, A. C. (2013). Treatment of synthetic and battery industry wastewater by electrocoagulation. *Der Chemica Sinica*, 4(6), pp. 32-39.

Patidar, K., Chouhan, A., & Thakur, L. S. (2017). Removal of heavy metals from water and waste water by electrocoagulation process—a review. *Int Res J Eng Technol*, 4(11), pp. 16-25.

Safonyk, A., & Prysiazniuk, O. (2019). Modeling and simulation in engineering modeling of the electrocoagulation processes in nonisothermal conditions. *Modelling and Simulation in Engineering*, 2019.

Implementation of Digital Twin in Industrial 4.0 Technology

Omer W.Taha ¹, Prof.Dr. Salim A. Abbas¹,Issraa J.Kazim ¹

ALMustafa University College; ¹
omer.cet@almustafauniversity.edu.iq

*Correspondence:
omer.cet@almustafauniversity.edu.iq; Tel.:
009647706817811

Abstract: Industry 4.0 is a recent technology revolution that has significantly altered the industrial landscape. It requires introducing Internet of Things technology and principles, like higher connection, integration, and collaboration across numerous parts, to the work place. Advanced methodologies for industrial applications, monitoring, and improvement have been made conceivable because of smart device innovation, software program expansion, and the advent of new communication technologies. Digital Twins are a technique for linking real systems to virtual counterparts that emulate the processes of actual equipment and instruments in a virtual world. The most difficult issues in this setting are constructing reliable models with real-time communication, reasonable computational costs, and deep analytical methodologies. The construction of a Digital Twins application methodology is described in this work. For modeling and 3D visualization, the architecture depends on an open-source application that provides compact protocols, diverse instruments, and process improvement. On the Digital Twin structure, methods were selected to enable for the presentation and modeling of productive systems and varied devices.

Keywords: Digital Twin, industrial 4.0, manufacturing.

1. Introduction

Industry 4.0 is a revolution in the industrial environment whose proposal and implementation will transform traditional productive plants into smart factories [1], in order to meet the demands for faster, more efficient, and flexible production. This revolution is marked by the strong integration of the ground floor and superior manufacturing management via the Internet, allowing the implementation of new business models and operating concepts that focus on individual needs of customers, as opposed to the model of production lines in bulk [2]. To remain competitive in the market, companies must deal with factors such as the short cycle of product life, demand fluctuations, and expectations in terms of delivery time and quality [3]. The digitization of manufacturing has been incorporated into industrial practice through various techniques, such as Cyber-physical systems, systems engineering based on models, and the use of big data in industrial systems, among others [4], since the great advances in the technology of information have made possible the development of more complex and powerful computational tools for simulation, emulation, and data processing. In general, the aim is to integrate the physical production systems with the software apparatus that serves as support for decision-making, various evaluations, and the implementation of strategic optimization. In this context, Digital Twins (DTs) play an important role in Industry 4.0. The idea of building a DT consists of the creation of a virtual replica (twin) of a given mechatronic system in a simulation environment. A virtual system must reflect the behavior of the real system and provide useful information for a variety of purposes, such as failure prediction,

performance metrics, and optimization [5]. Although the research and application of DGs has grown in recent years.

The concept itself is of DT still lacks a unified definition, since definitions in the literature that present the DTs as objects, but also other definitions that consider it as a technology or medium [6]. Other question still open and the definition of a framework complete application and a reference solution [6], [4]. According to recent studies, some typical challenges regarding the implementation of DTs. In the real part, you have a large number of devices without intelligence, or they cannot be integrated by themselves. Being thus, appropriate techniques are needed to extract data from the ground floor in an intelligent way without being it is necessary to replace all old equipment with smart devices, which would generate high levels of implementation costs [1]. In the virtual part, the modeling of complex systems and machines is not a trivial and requires appropriate labor [6]. Another challenge is to get one adequate balance between the complexity of the model and its computational cost. As for data transmission, keep the timing between the real plant and its virtual counterpart a critical task, which requires methods, interfaces and protocols appropriate [7]. There are several proposals for frameworks in the literature and conceptual architectures of DTs [8], that is, without the development of the apparatus for practical implementation. considering the architectures that contemplate the implementation practice of DTs, most make use of closed solutions and landlords [9]. These solutions do not provide flexibility in relation to the use and integration of tools to carry out necessary activities. In this context, the objective of this work and develop a distributed, modular and flexible for the implementation of DTs, based on the tool process control OpenPLC [10], code software open for process control. The developed architecture does not depend on industrial solutions proprietary and enables the creation of process DTs automated with the use of remote Input hardware and Output (I / O), without the need to insert new instruments or smart devices. The flexibility of the architecture allows modules can be developed in different tools (modeling and visualization) and provides scalability for that new module with different functionalities can be incorporated into the architecture. Unlike the architectures in the literature, the proposal of this work allows the virtual part of the DT is composed of separate applications, promoting better management of the computational cost of the tool's software. The modular layout reduces the interdependence between the modules and increases the generalizability, so that various types of systems can be described and represented in the proposed architecture. Additionally, communication in architecture network standardizes the exchange of information between real and virtual parts of DT.

2. LITERATURE REVIEW

A. Concept of Digital Twins

DTs are a concept initially presented [11], however there are currently several explanations and definitions proposed for the term [12]. One typical definition presents DT as an object, which includes a set of information, models and data in the environment virtual. On the other hand, some authors list GDT as technologies or methods, such as a simulation method [6]. In general, you can define a DG as a system capable of simulating, monitoring, calculating, regulating and control the states and processes of a system. The DT and de- developed through data acquisition, use of technology of virtual manufacturing and is based on control units, communication and computing [6]. A more general definition used so far says that GDT are a simulation integrated probability of a complex product, using the best physical models available to mirror the life of his corresponding twin [13]. A stricter definition presents the DT as a set of virtual information that is completely describes a real or potential physical production from the micro atomic level to the geometrical macro level, presenting the characteristics of virtualization, dynamism, multi-scale, integration, computation and ultra-realism [6]. In a nutshell, it can be said that DT is a solution to the problem of “how to simulate physical products in a Realistic.

B. Basic Elements of Digital Twin

The conceptual model of a digital twin is composed of three parts, being:

- (1) physical products in Real Space.
- (2) virtual products in the Virtual Space.
- (3) data connections and information that interconnect the two spaces [11].

The space Real and a complex, dynamic and diverse environment, in which people, machines and materials interact. Its members different characteristics of performance and behavior, which may vary over time due to the wear and aging. You must prepare the physical space for integration with the DG, that is, using devices so that it is possible to collect field data for use with the virtual counterpart [6], [14]. The Virtual Space, on the other hand, and where the replication operations of the operation of the Real Space. The representation of physical products and carried out especially using computer-aided design (CAD) technologies (Computer-Aided Design) and modeling 3D [6], both of which are commonly used in step of industrial products design. The modeling of virtual products includes three aspects, which are the elements, behaviors and rules. The elements are characteristic physical and geometrical characteristics of the products, refer both to the behavior of the product itself and to the interaction of the product with the user. As for the rules, in general include evolution, optimization and forecasting models that are established according to the product operating rule physical [14]. As for computational complexity and cost of the

virtual implementation, it is possible to create lightweight versions of virtual model, in such a way that only the most relevant aspects of the product, which reduces complexity and increases processing speed. The goal of such simplification and to make possible the simulation of systems complex and systems-of-systems in real time and with cost acceptable computing power, also reducing the time and cost the communication of the information generated [11]. The element of integration between the Real and Virtual spaces and the communication layer, which allows for mapping bidirectional and interoperability between them [6]. The connection can be established through various technologies, such as networks communication, cloud computing, among others.

3.Proposed Architecture

Based on the analysis of the literature, an architecture is proposed for the implementation of DGs with a focus on techniques and tools typical tools of Industry 4.0, shown in Figure 1. Control of the Manufacturing Process The control of the manufacturing process is carried out by 'OpenPLC [10], which is a code platform that incorporates the features of a PLC and allows the use of different types of hardware such as I / O interfaces in automation processes. Through the OpenPLC Editor, it is possible to develop programming logic in the five languages defined by the IEC 61131-3 standard. An app server and runs on Windows, Linux or Raspberry Pi and performs communication with the interface hardware. Through the use of auxiliary software, and it is possible to communicate with the server through the UDP communication protocol, which is a light standard [13-17].

OpenPLC is responsible for controlling the system of manufacturing according to the programming logic. It is necessary that the signals from real sensors and actuators are reflected to the virtual I / O space so that they are then transmitted to the simulation modules. This operation is performed through a simple logic of express replication on the Ladder diagram. To avoid confusion between the I / O addresses used in real and virtual applications, the space is divided addressing OpenPLC in two parts, one being destined to the real part and another to the virtual part.

According to the schematic, we have that:

- The actual automation process is governed by ladder logic defined in the PLC.
- The logical model receives the signals from the real sensors reflected in the virtual I / O space and returns to the PLC the states of the virtual actuators computed.

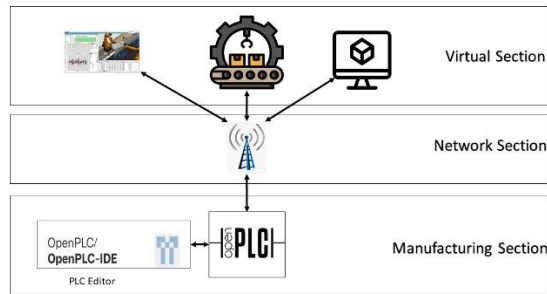


Figure 1. Modular architecture for the implementation of Digital Twin proposed.

4. Manufacturing Process

Physical space and a production environment are usually complex, diverse and dynamic, in which they are inserted by various types of equipment. Machines and materials are arranged in the working space in order to allow the sequencing and execution of the tasks of the production process. All of these final elements (sensors and actuators) must be connected to the process control system, in order to allow the collection of data for processing in the PLC and in other virtualization tools. The equipment group must be connected to OpenPLC through I / O hardware appropriate, in such a way that the server can govern the operation of the plant.

5. Process Model

To make the creation of the automation system DG possible, it is necessary to replicate it in a virtual environment. In this context, only simulation applications are used with the aim of creating a logical model that describes the behavior of the system, of such that software can imitate in a virtual environment the operating characteristics of a real process. Based in a reliable model, and it is still possible to carry out operations of evaluation, study and optimization on the system by means of analysis and reconfiguration. Briefly, modeling automation systems can be performed through three:

steps: (1) obtain a set of measurable variables of input, (2) obtain a set of output variables that vary according to the input variables and (3) define mathematical functions that list inputs and outputs measured in order to obtain a model of the functioning of the system [14]. Modeling Discrete Event Systems (SEDs) can be accomplished through specific approaches, such as state machines, finite automata, networks of Petri and others. The modeling tool used in this work is Table of States and Transitions (TST) State-Transition Table, which is part of the block library Simulink simulation application, part of the software for MATLAB engineering. This feature allows description of the logical behavior of a system

through conditional relations (if-else), allowing the definition of the states of output variables, transition conditions and action implementation of timing. This block has compatibility with the available UDP communication interfaces Simulink, which in turn allow for the exchange of information with the OpenPLC server. In this way, it is possible to carry out the feeding TET continuously with PLC data. The first step to create a TET and observe the system automation, analyzing which are their states and which are phenomena bring about a change of state. In general, states concern the condition of the actuators, while transitions are most often associated with reading sensor elements. After the identification of states and transitions, the measurement of transition times when the system is has timed transitions. The TET tool has own command to insert delay delays in the evolution of the logical model. Finally, it is necessary to transcribe the states and conditions of transition in the tool table.

6.Experimental Work

The proposed architecture was implemented in a laboratory automation system in order to have its functionality verified. Functional modules have been implemented and integrated. It is section presents the details of DG implementation.

A. Manufacturing Process

The manufacturing process used in the experimental arrangement. It is station receives pieces of three different colors and performs separation of the pieces by color, through the reading of sensors. It has four presence sensors and four actuators, being a displacement conveyor, two diverters and one passage blocker associated with the treadmill. Control was realized through OpenPLC. For control to be executed, and a microcontroller compatible with OpenPLC, which functions as a remote I / O interface. This one microcontroller has been integrated into the industrial process of a signal conditioning plate. Then it was Ladder diagram for process control was developed. the Figure 2 shows the workstation.



Figure 2. Sporting workstation.

B. Process Model

Once the actual automation process has been defined, step and the creation of its virtual counterpart. From mapping of states and system transition variables, and it is possible to generate the ETT that corresponds to the behavior station.

7. RESULTS AND DISCUSSIONS

The group composed of the physical station, the model of simulation of discrete events (TET) and module 3D visualization is the implemented DT, whose physical parts and virtual are integrated through network infrastructure. In the experimental work, it was possible to visualize the replication states of the physical plant on the virtual side, as well as the convergence and interaction between the real and virtual sides. So, the architecture fulfills the requirements of a DT as described in the literature. To visualize the operation of the physical plant and the replication of states in the virtual environment.

During the implementation phase of the project, it was possible verify the main functional aspects of the architecture. OpenPLC was able to provide all the functionality of Industrial PLC, including the five programming languages IEC 61131-3, industrial communication protocols trial and the various I / O hardware options to establish control of physical processes. OpenPLC also makes it possible examined the implementation of UDP communication between the functional modules. TET provided adequate modeling for the system discrete events used in the experimental work. It is based on an approach of state machines, allowing programming in the form of if-else conditionals and conditions user-defined transition periods, which can be based on input signals or timing. Since the TET blocks are part of the Simulink simulation environment, tables can be used in conjunction with blocks of native UDP communication, available in the library of blocks. Thus, TET that describes the logical behavior of the manufacturing plant can be fed in tempo time execution with PLC data, the default UDP messages forwarded through OpenPLC and auxiliary interface software. Using a template Animated CAD, it was possible to provide a realization experience virtual capacity with acceptable computational cost. Considering the use of the system on the local network, the delay between the occurrence of an event in the real plant and the corresponding display in the ambience between 3D and imperceptible by observation. In the implemented DT architecture, communication between OpenPLC and the Manufacturing Process is carried out through the Modbus TCP / IP protocol (Wi-Fi wireless network) and the communication between OpenPLC and the model modules Process and 3D visualization are through the protocol UDP / IP. Considering the processing capacity computational structure of the OpenPLC server (and architecture) and that communication between OpenPLC and modules are very fast (low number of messages), it is possible to obtain the synchronism in the execution of the DT. Latency network communication

between modules exists, however has very little variability and could be neglected, as it has no significant impact on the operation of DT when compared to the dynamics of execution of the manufacturing process. For comparison purposes, in [6] and [9] the authors note a latency of less than 1s between execution real and the virtual model. In the DT architecture of this work, latency is directly related to UDP communication, the that allows latency inferior to the examples of the literature. In accordance with the concepts of Industry 4.0, Wireless communication was prioritized in this architecture. All the devices were integrated through a network without implemented on a local router. Each virtual module can be implemented on a separate machine, as long as control of the IP address is made to avoid errors of Communication. As the tests were performed on a network restricted with little traffic, there were no problems regarding loss of packets or abnormal communication delays.

References

- [1] M. A. Pessoa, M. A. Pisching, L. Yao, F. Junqueira, P. E. Miyagi, and B. Benatallah, "Industry 4.0, how to integrate legacy devices: A cloud iot approach," in IECON 2018-44th Annual Conference of the IEEE Industrial Electronics Society. IEEE, 2018, pp. 2902–2907.
- [2] N. Jazdi, "Cyber physical systems in the context of industry 4.0," in Automation, Quality and Testing, Robotics, 2014 IEEE International Conference on. IEEE, 2014, pp. 1–4.
- [3] R. A. Diogo, C. A. Vicari, E. de FR Loures, M. A. Busetti, and E. A. Santos, "An implementation environment for automated manufacturing systems," IFAC Proceedings Volumes, vol. 41, no. 2, pp. 10 552–10 557,2008.
- [4] B. Schleich, N. Anwer, L. Mathieu, and S. Wartzack, "Shaping the digital twin for design and production engineering," CIRP Annals, vol. 66, no. 1, pp. 141–144, 2017.
- [5] F. Tao and M. Zhang, "Digital twin shop-floor: a new shop-floor paradigm towards smart manufacturing," Ieee Access, vol. 5, pp. 20 418– 20 427, 2017.
- [6] Y. Zheng, S. Yang, and H. Cheng, "An application framework of digital twin and its case study," Journal of Ambient Intelligence and Humanized Computing, pp. 1–13, 2018.
- [7] H. Zipper, F. Auris, A. Strahilov, and M. Paul, "Keeping the digital twin up-to-date — process monitoring to identify changes in a plant," in 2018 IEEE International Conference on Industrial Technology (ICIT),Feb 2018, pp. 1592–1597.

- [8] W. Kritzinger, M. Karner, G. Traar, J. Henjes, and W. Sihn, "Digital twin in manufacturing: A categorical literature review and classification," IFAC-PapersOnLine, vol. 51, no. 11, pp. 1016–1022, 2018.
- [9] J. Vach'alek, L. Bartalsk'y, O. Rovn'y, D. ˇ Si'smi'sov'a, M. Morh'a'c, and M. Lok's'ik, "The digital twin of an industrial production line within the industry 4.0 concept," in Process Control (PC), 2017 21st International Conference on. IEEE, 2017, pp. 258–262.
- [10] T. R. Alves, M. Buratto, F. M. de Souza, and T. V. Rodrigues, "Openplc: An open source alternative to automation," in Global Humanitarian Technology Conference (GHTC), 2014 IEEE. IEEE, 2014, pp. 585–589.
- [11] M. Grieves, "Digital twin: manufacturing excellence through virtual factory replication," White paper, 2014.
- [12] F. Tao, J. Cheng, Q. Qi, M. Zhang, H. Zhang, and F. Sui, "Digital twindriven product design, manufacturing and service with big data," The International Journal of Advanced Manufacturing Technology, vol. 94, no. 9-12, pp. 3563–3576, 2018.
- [13] E. Glaessgen and D. Stargel, "The digital twin paradigm for future nasa and us air force vehicles," in 53rd AIAA/ASME/ASCE/AHS/ASC Structures, Structural Dynamics and Materials Conference 20th AIAA/ASME/AHS Adaptive Structures Conference 14th AIAA, 2012, p. 1818.
- [14] F. Tao, F. Sui, A. Liu, Q. Qi, M. Zhang, B. Song, Z. Guo, S. C.-Y. Lu, and A. Nee, "Digital twin-driven product design framework," International Journal of Production Research, pp. 1–19, 2018.

Enhancing the electrical conductivity and mechanical properties of the PVA electrospun polymeric film by adding a Silver nanoparticles

Shafaq Y. Abd 1.a

a Al-mustafa University collage_ Dept. of Building and Cons. Engineering .¹
Technique

1.a Shafaq.abd@almustafauniversity.edu.iq

Abstract

PVA/with (0, 2, 4, 6, 8 and 10) wt. % Ag nanoparticles films conductive polymers were prepared by electrospinning technique. Prepared films morphology test by SEM and the average fibres diameters measure statically was (75 nm) for PVA/ 10 wt. % Ag NPs film. The nano-fiber films show enhancing the direct current electrical conductivity by increasing Silver nanoparticles concentration, from (3.7×10^{-7} S/ cm) for pure PVA film to (1.08×10^{-2} S/cm) for 10wt.% Ag NPs, also enhance the alternative current electrical conductivity by increasing Silver nanoparticles concentration, from (1.17×10^{-6} S/ cm) for pure PVA film to (1.80 S/cm) for 10wt. % Ag nanoparticles. The activation energy and S factor decreased with increasing the Ag nanoparticles concentration. The mechanical properties of PVA film are enhanced with adding Ag nanoparticles by enhancing the modulus of elasticity from (12.87) MPa for pure PVA to (110) MPa for PVA/ 8wt. % Ag film.

Keywords: Conductive Polymer, Electrospinning, Nano-fibers, PVA, Ag nanoparticles.

1. Introduction

Conductive polymers are firstly characterised via controllable conductivity and have unique electric and optical residences comparable to the ones of metals and inorganic semiconductors. The particular electronic structure is accountable for their high electron affinity [1], so it no wonder that conductive polymers are called the materials of the 21's century. Recently, the electrically conductive polymers have been called synthetic metals [2] to signify their organic characteristic and metal-like properties. The use of conductive polymers has become commonplace. The earth contains versatile materials, and each of these materials has characteristics that distinguish them from others; they've electric residences like that of metals and semiconductors in addition to the benefits of traditional polymers like operability, resilience, operation capacity, ecological balance, lower cost, etc. [3]. Few of the essential applications of conductive polymers are rechargeable and lightweight batteries, thermal and chemical sensors, supercapacitors, light-emitting diodes, organic solar cells [4] and many other applications like dental resin composite reinforcement [5], television screens, cheap, thin, flexible laptops and robots artificial skin possible [6 , 7]. There many methods are used to produce conductive polymers like chemical, electrochemical, Hydrogels, composites and electrospinning processes [8]. This article will be a focus on the Ag nanoparticles effect on the electrical and mechanical properties of Polyvinyl alcohol (PVA) nano-films produced by the electrospinning technique and study the physical properties of PVA solutions in

addition to the (DC and AC) electrical conductivity, activation energy and tensile strength of different wt. % Ag NPs films at different temperatures and frequencies.

Conductive polymers formation by adding metallic nanoparticles to the host polymer attracted considerable importance resulting from structural characteristics such as high aspect ratio, surface area, and electrical, thermal, and mechanical properties [9]. Metal nanoparticle-based nanocomposites are now one of the main focus points of research because of their technological applications, including the conceptual understanding of involved physics and chemistry. It is properly hooked up that polymers, as dielectric materials, are excellent host matrices for encapsulation of metallic nanoparticles like silver, copper, gold, and so on. as they act each as reducing in addition to capping retailers and additionally provide environmental and chemical balance [10]. The conductive Silver nanoparticles have been used as conductive fillers in a polymeric matrix to enhance conductivity). Ag nanoparticles will form a conduction pathway that allows the electrons to move through the composite structure of the fibres. The uniform dispersion is essential for allowing the formation of an interconnecting filler network of Ag NPs. Small concentration of Ag nanoparticles would be needed to obtain relatively high electrical conductions, which is helpful in many of industrial applications [11].

Polyvinyl alcohol (PVA) polymer is especially giving a high deal of-attention. This polymer is useful in high applications due to its excellent chemical resistance, physical properties, and biodegradability [12]. Polyvinyl alcohol (PVA) has excellent film-forming, emulsifying, and adhesive properties, also have resistant to oils, greases and solvents. PVA is odorless and nontoxic, as well as has high oxygen(O₂) and aroma barrier properties[13]. The electrical conductivity of pure PVA (which is very low) can be modified by doping with appropriate (dopant material) in different quantities and forms like (Silver ion, Nickel ion, Copper ion, Carbon and Ferric ion), where it will be incorporated within the polymeric system, and It will enhance the conductivity as expected [14].

Electrospinning is a versatile process used to produce a wide range of polymers in Nano and micrometer-scale fibres. It is one of the most straightforward techniques for obtaining polymer nanofibers characterised by a large surface area to volume ratio [15]. The principle of electrospinning operation is using a high-voltage electrostatic field to draw a jet from a polymer solution. When this jet travels toward the collector electrode, the solvent evaporates, and a polymer fibre will be formed. Electrospinning is used to produce conductive polymers by combining

additives with a spinnable polymer [16]. The nanofiber is the extremely-satisfactory solid fibers fantastic for owing a tiny diameter which is lower than a hundred nm, nanofibres have a large surface area per unit mass as well as small pore size.

There are many solution parameters affecting the electrospinning process such as polymeric molecular weight, viscosity, conductivity and surface tension of the polymeric solution [17]. The effects of the solution parameters may be difficult to isolate because varying one parameter will generally affect other solution parameters; for example, changing the conductivity of the solution is a result in increasing the addition of the Ag solution to the polymeric solution resulting in reducing the viscosity and also decrease the surface tension [18]. Solution parameters are molecular weight, viscosity, electrical conductivity, and surface tension affects directly the fibre dimensions and morphology. Increasing the polymeric molecular weight cause increasing the density of chain entanglements (in solution) at the same polymeric concentration. Consequently, the minimum concentration to produce polymeric nanofibers was lower for the highest molecular weight PVA [19]. Viscosity is one of the most critical solution parameters. Nanofibers can be obtained without beads when the polymer solution develops a minimum polymeric chain network in other words, minimal entanglement concentration, in fact, both solution viscosity and solution concentration are carefully associated [20]. Increasing the solution conductivity or charge density can be used to produce more uniform fibres with fewer beads and smaller fibre diameters. Increasing the polymeric solution conductivity cause more electric charges carried by the electrospinning jet resulting in higher elongation forces imposing on the jet under the electrical field. The overall tension will be depended on the self-repulsion of the excess charges on the jet [21,22]. Surface tension is the function of solvent compositions in the solution. It is an influential factor in electrospinning. It is found that different solvents cause different surface tensions. If the concentration of solution is fixed, reducing the surface tension of the solution, leads to the formation of smooth fibres [23]. It is essential to say that the surface tension controls the formation of beads and the beaded fibres. The surface tension role is trying to make the surface area per unit mass smaller by changing the jets into spherical shapes [24].

2. Experimental part

2.1 Preparations of solutions: PVA was purchased from (Gerhard Buchmann KG Tuttlingen / Germany). The molecular weight for the repeat unit is equal to 80,000 g/mol. Seven wt.% PVA solution was prepared by dissolving in (93ml) Distilled water (DW) for (5-8 hours) at (80-120 °C). Ag NPs were purchased from

Hongwu International Group Ltd, spherical particles of diameter of 20nm. Silver nanoparticles were dispersed directly in a PVA solution of concentration Seven wt.% by using an Ultra-sonic homogenizer device to get good dispersion. PVA / (2, 4, 6, 8 and 10) wt. % (Ag NPs) solutions were prepared.

2.2.1 The Electrical Conductivity of Solutions: The prepared solution's electrical conductivity was measured via the instrument of electrical conductivity type (C & 7110 inolab). The device probe was steeped in the polymeric solution, and the conductivity values were appeared and read quickly. The solution's conductivity was measured in mS/cm.

2.2.2 The Viscosity of Prepared Solutions: The solutions viscosity were measured via the instrument of Viscometer type (DV – II – Pro.) Brook field. The top plate was rounded with a controlled rotational rate in order to produce a shearing force over the solution. The solution viscosity values were measured by (cp).

2.2.3 The Surface Tension of the Prepared Solutions: The Surface Tensiometer Model (JYW –200A LARYEE TECHNOLOGY CO,) has been used to perform surface tension measurements of the solution. A polymeric solution was poured into a standard petri dish that was then placed on the stage. The lever with a loosely hanging platinum ring was lowered until was submerged into the solution. The lever has been then raised gradually till the ring simply separated free from the solution. The value of the surface tension within the (mN/cm) unit is measured from the display at this point.

2.3 Electrospinning process: after cooling to room temperature, the solution was electrospun using the electrospun device of type (Bio-electrospinning / Electropray system ESB-200), provided by Nano (NC), South of Korea. The solution was applied through a (5 ml syringe needle with an internal diameter of 0.7 mm) using a syringe pump of type (Bio-electrospinning / Electropray system ESB-200) at a flow rate of five ml/h. The electric field was generated using a high voltage supply of about 25 kV. The positive end was connected to the syringe needle and the collector plate was grounded. The needle-collector distance was 15 cm, and the process performed at room temperature. Films obtained from sterile solution and solutions of (0, 2, 4, 6, 8 and 10) wt. % Ag NPs.

2.4 Electrospun Films Characterization

2.4.1 Scanning Electron Microscopy (SEM): SEM is a powerful technique for analyzing the structure of the prepared samples used for determining and characterizing the morphology of fibres. SEM was performed by (VEGA3 LM – TESCAN). A Small pieces (1×1) cm were cut from the created electrospun films to prepare them for SEM inspecting. Firstly, the films have to be coated with gold using Fine Coating Ion Sputtering Device (GSL-1100X-SPC-12 COMPACT PLASMA SPUTTERING COATER). Coating was performed for two minutes to obtain (100 Å) thickness.

2.4.2 Energy Dispersive X. Ray Spectroscopy (EDX): This inspection has been done in an identical test as in the SEM testing for getting full information about the chemical composition of the electrospun film, in addition, confirm getting the ions of the additives to the structure of pure polyvinyl alcohol (PVA) film.

2.4.3 Thickness measuring test: The electrospun thickness was inspected by the instrument of (COATING THICKNESS METER CM 8829S) Solar Energy Research Center. A thickness test would be essential for films, because of the enormous role of film thickness in the electric conductivities estimations and the bandgap estimation. The electrospun films were put on an overhead paper as a substrate, in addition via standing the instrument probe vertically and somewhat touch the film, the test readings will show up on the screen of the instrument in units (nm and μm).

2.4.4 The electrical conductivity measurements:

The electrical measurements included direct current (DC) conductivity and alternative current (AC) conductivity for the electrospun films. The electrodes utilized in (DC and AC) estimation were self-made by drawing two circles of Silver paste by the aiding of foil mask. Figure 1, represents the silver paste electrodes and foil template used in this work.

The resistivity of the films can be calculated from an equation:

$$\rho = R. W.t / L \quad \text{Eq. (1)}$$

Then the electrical conductivity can be calculated from equation:

$$\sigma = 1/\rho \quad \text{Eq. (2)}$$

Where ρ : the resistivity of the films, R: the resistance, σ : the electrical conductivity, t: the thickness, W and L are dimensions of the electrodes.

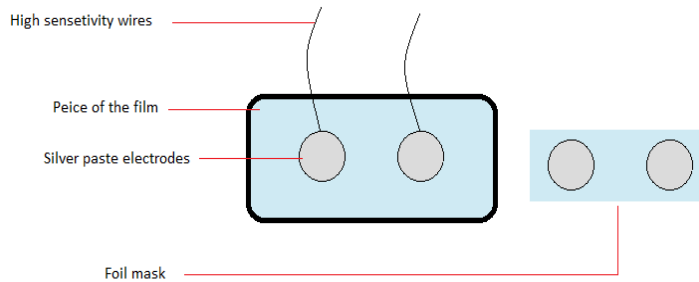


Figure 1: The foil template and the silver paste electrodes.

2.4.4.1 D.C Electrical Conductivity Measurement: The electrospun film's electrical resistance was measured as a temperature function in the range (30 - 100 °C) via the electrical circuit. The measurements were done using a sensitive digital electrometer / high resistance meter type (KEITHLY 6517B) and electrical oven type BINDER Solar Energy Research Center.

2.4.4.2 AC Electrical Conductivity: (LCR) meter model (GW INSTRON LCR-A21) multi-frequency was utilized to measure AC conductivity in Renewable Energies Research and Environment Center. The electrospun film electrical resistance was measured as a function of frequency in the range (10^3 - 10^5) KHz.

3. Results and discussion

3.1 Solution properties

3.1.1 The electric conductivity: increase embedding the wt. % of Silver nanoparticles leads to increasing the electrical conductivity of PVA solutions because of the formation of a charge-transfer complex inside the polymer chain network, and this will increase the concentrations of charge transporters in the solution. The electrical conductivity of pure PVA solution was 1.047 mS/cm and increased to 2.6 mS/cm for PVA /10 wt.% Ag NPs as represented in figure 2.

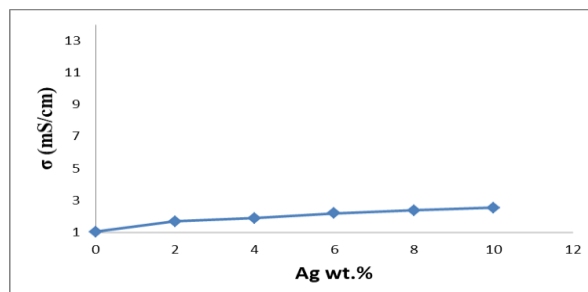


Figure 2: The effect of Ag NPs addition on the electrical conductivity of PVA / Ag solution.

The slight increase in electrical conductivity for PVA/ Ag NPs solutions may be due to the fact that the silver metallic nanoparticles are added directly as a metallic powder without any treatment, thus the solution will contain polymer and metal without any bonding or adhesion between them, but in PVA/ Ag electrospun film, this metallic nanoparticles will enter into nano-fiber and cause a high increases in films electrical conductivity, as will see in SEM, EDX and electrical conductivity results.

3.1.2 The surface tension: Surface tension of PVA/Ag NPs solutions increase with increasing the percentage of Ag NPs. The increase in the surface tension for Ag nanoparticles solutions is due to the addition of these nanoparticles directly as a nanopowder within the polymer solution without any prior dispersing in any other solvents, as represented in figure 3.

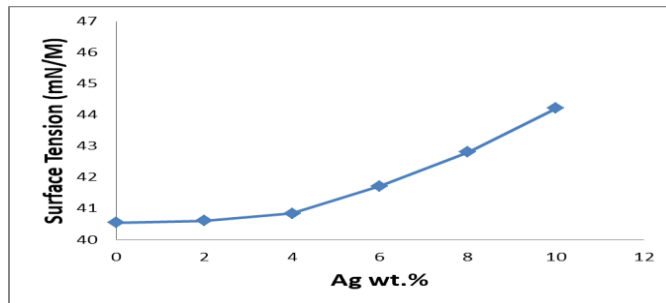


Figure 3: The effect of Ag NPs addition on the surface tension of PVA/Ag solution.

3.1.3 The viscosity: solution viscosity increase with increasing the addition ratio of Ag NPs because of the increasing of Ag nanoparticles in PVA solution, as represented in figure 4.

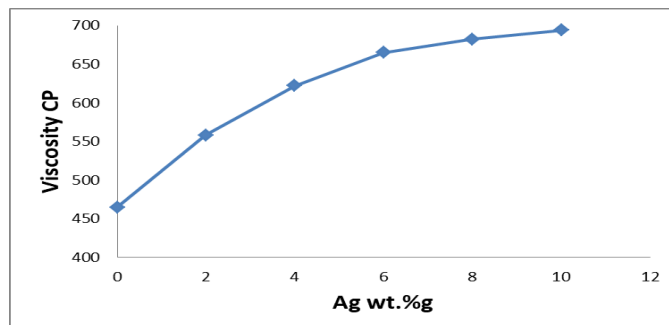


Figure 4: The effect of the addition of Ag NPs on the viscosity of PVA / Ag solution.

3.2 SEM and EDX results:

The SEM image for the pure PVA electrospun film represents in Figure 5-A, which appears fine smooth nanofibers. The produced nanofiber average diameter of the pure PVA film is 170 nm with a few microfibers of about (1-2) μm in the background of the nano-fibers film due to fast solution feeding at the starting of the electrospun process, as shown in figure (5-B). The energy dispersive x-ray (EDX) spectrum analysis for a pure PVA membrane is shown in Figure 5-C. The (EDX) spectra was gathered with SEM zoomed into the nano-fibre only. The (EDX) spectra of pure PVA electrospun film recommend the chemical composition consists of mainly C (Carbon), O (Oxygen) and Au (Gold) crests showed up because of the process of coating required for electric conductivity for an inspected specimen of SEM-test.

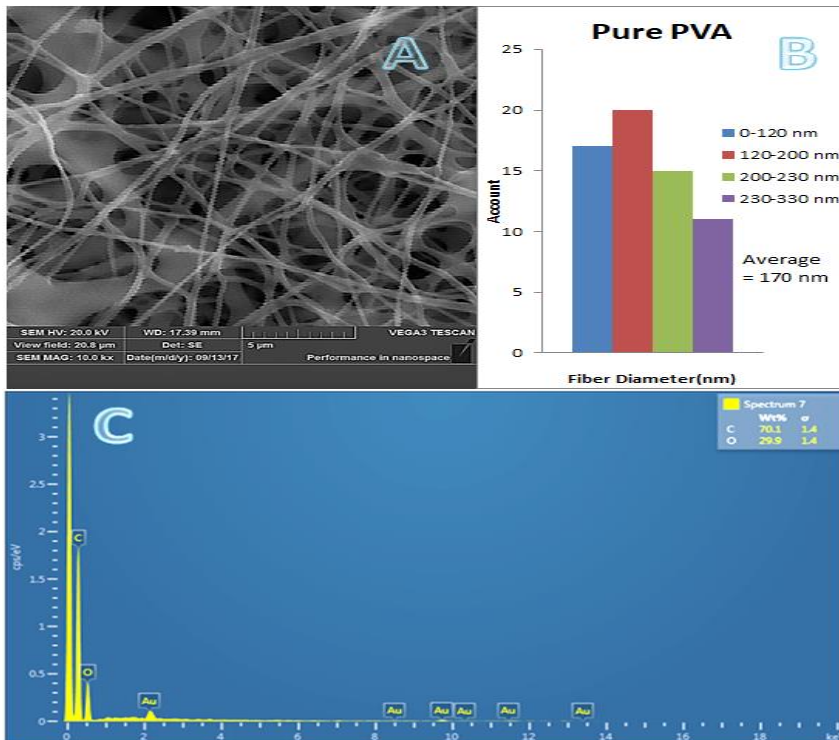


Figure 5: Pure PVA Electrospun film (A): SEM image (B): Fibers diameter distribution (C): EDX spectrum.

Figure 6-A represents the SEM image for the PVA / 10 wt.% Ag film, and the slight swelling that appear into the fibres clarify the presence of Ag nanoparticles inside the fibres. So higher amount of Ag ratio could produce a thinner fibre diameter due to increasing the number of charge carriers in PVA/ Ag wt.% solutions, and thus, more charges were produced during the electrospinning process. The average fibre diameter for the PVA / 10 wt. % Ag film is (75 nm), has appears in Figure 6-B. Figure 6-C acts the PVA / 10 wt.% Ag film's (EDX) spectrum analysis suggests that the chemical composition consists of C (Carbon),O (Oxygen), Ag (Silver) and Au (Gold) as a result of coating process of a specimen by Gold for SEM and (EDX).

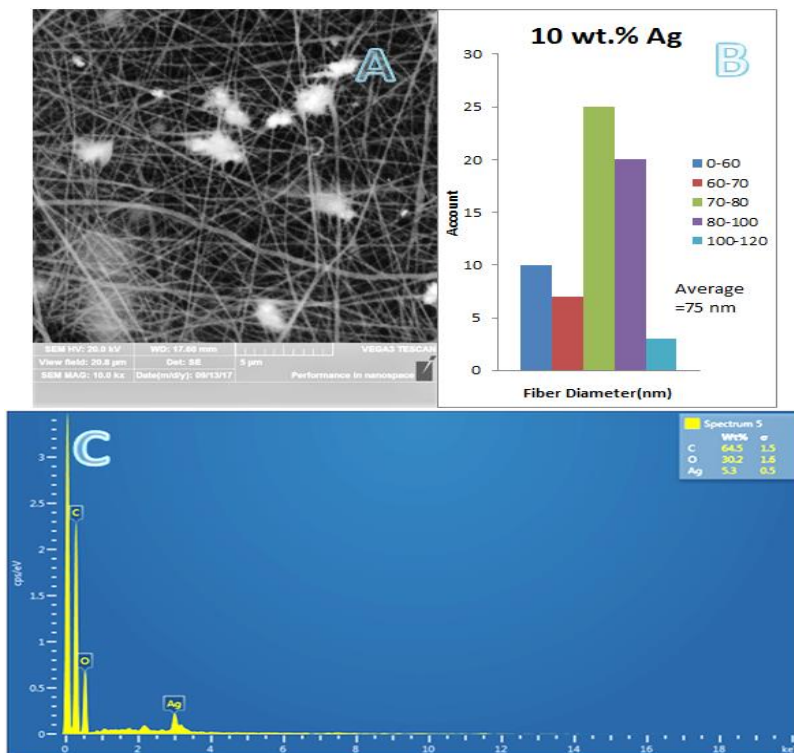


Figure 6: PVA / 10 wt.% Ag Electrospun film (A): SEM image (B): Fibers diameter distribution (C): EDX spectrum.

3.3 Thickness measuring test results:

It has been observed that on at the constant conditions of the electrospinning process, the thickness of PVA/ Ag electrospun films decreases with increment the Ag NPs ratio. This is due to the fact that PVA / Ag solution electrical conductivity might be incremented with incrementing the Ag NPs wt. %. When the high voltage of the electrospinning is applied to the solutions of more significant

electrical conductive (these solutions have greater concentration additives and greater solvent liquid in the polymeric solutions), this may reduce the size and quantity of the collected fibres on the collectors due to volatile the dissolving solution during electrospinning process, as represents in Figure 8.

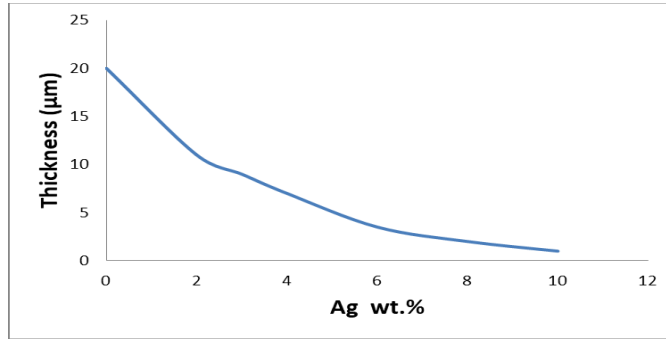


Figure 7: The effect of addition Ag on the thickness of PVA /Ag films.

3.4 Results of electrical conductivity measurements

3.4.1 Results of DC Conductivity Measurements of prepared films:

Polyvinyl alcohol is one of the recognized insulating materials. The electrical conductivity of bulk pure PVA is 10^{-11} S/cm [25], while a pure PVA electrospun film has electrical conductivity equivalent to 3.7×10^{-7} S/cm (due to DC conductivity results). In general, making use of the electrospinning process to get ready pure Poly vinyl alcohol films increases the electrical conductivity four orders over the bulk pure PVA; this means, that the process and dimension of the readied specimens are vital in expanding the electric conductivity. The mechanism of heating the polymer film above room temperature is thermally induced; the resistance versus temperature behaviour may be understood by the activation energy values of the nanocomposites fibres according to the Arrhenius equation:

$$\sigma = \sigma_0 \exp (Ea / K_B T) \quad Eq. (4)$$

Ea = activation energy in eV (corresponding to $E_g / 2$ for intrinsic conduction)

T =the absolute temperature in $0^\circ K$

k_B =Boltzmann constant= 1.38×10^{-23} J/K,

and dividing by the electron charge, $k_B = 8.62 \times 10^{-5}$ eV.

σ_0 =the minimum electrical conductivity at $0^\circ K$ [23-25].

The electric conductivity (σ_{dc}) and the activation energy were measured for PVA films with different concentrations of Ag NPs at different temperatures (303 - 383) $^\circ K$ are representing in Table 1. Figure 8, represents $(\ln \sigma_{dc})$ vs $(1000/T)$ for different compositions of PVA / Ag films.

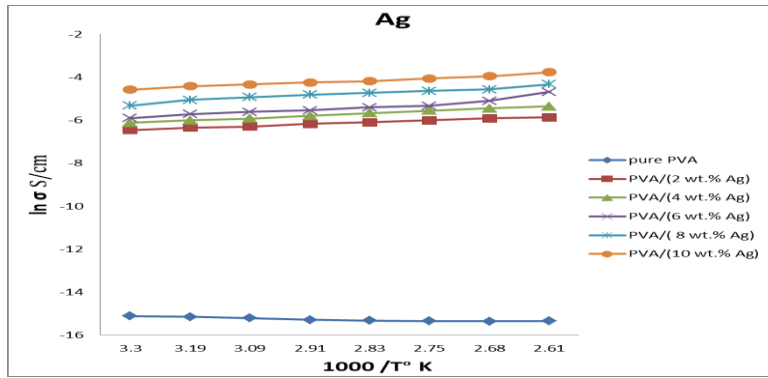


Figure 8: $(\ln \sigma)$ vs $(1000/T)$ for different compositions of PVA / Ag electrospun films.

Table 1: The activation energy and electrical conductivity ($\sigma_{d.c}$) of different compositions of PVA / Ag films.

Electrospun composition films	The activation energy (eV)	$\sigma_{d.c}$ conductivity (S/cm) of films at 303°K
Pure PVA	0.188	3.7×10^{-7}
PVA/ 2wt.% Ag	0.1292	3.80×10^{-3}
PVA/ 4wt.% Ag	0.1092	4.73×10^{-3}
PVA/ 6wt.% Ag	0.0883	5.59×10^{-3}
PVA/ 8wt.% Ag	0.0613	8.52×10^{-3}
PVA/ 10wt.% Ag	0.0347	1.08×10^{-2}

As shown from the results, the DC electrical conductivity increased from (3.7×10^{-7}) S/cm for a pure PVA to (3.80×10^{-3}) S/cm for PVA/ 2 wt.% Ag and (1.08×10^{-2}) S/cm for PVA/ 10wt.% Ag at 303°K, that means the electrical conductivity (σ_{dc}) increases by four orders with PVA/ 2wt.% Ag and five orders with PVA/ 10 wt.% Ag with the increasing of Ag NPs concentration. These increases are attributed to the fact that the Ag NPs nanoparticles act as conductive dopants fillers in the polymer matrix, the conductivity of any material is the product of carrier mobility and a number of charge carriers, and if we dope the materials, conductivity rise will result in a simultaneous increase of carrier concentration and carrier mobility with increasing temperature, Also activation energy decrease with increasing amounts of Cu nanoparticles concentrations. This explanation agrees with *Majeed H. et al.*[26], who clarifies that the DC electrical conductivity increments with incrementing of a temperature; this implies that this fabric has negative thermal coefficient resistance (i.E. with temperature increase, that resistance decreases). The clarification of this behaviour is that the PVA polymeric chains, and impurity metallic ions go about as traps to make charge transporters move by the process of hopping. While the activation energy has high

values at low titanium nanoparticles concentration, at high concentration, the activation energy has low values, because of increment in the local levels in the distance between the valence band and conduction band, as represented in Figure 9.

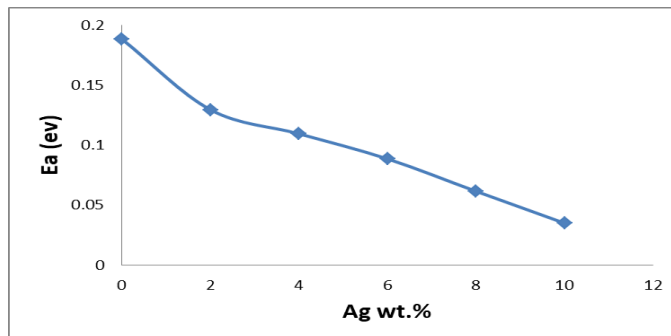


Figure 9: The adding effect of different percentages of Ag on the activation energy.

3.4.2 Results of AC Conductivity Measurements:

Alternating Current Conductivity or (AC) electrical conductivity measurement lies in its ability for providing information about the electrical conductivity which is measured as a function of the angular frequency (ω), where $[\omega = 2\pi f]$ where f is the frequency.

The AC electrical conductivity σ_{ac} at a particular frequency and temperature is defined as:

$$\sigma_{ac}(\omega) = A \omega^S \quad Eq. (3)$$

Where A is a constant parameter, S is an exponential factor and its value is $0 < s < 1$, ω is the frequency.

Electrospun film of pure PVA has AC electrical conductivity equal to (1.17×10^{-6}) S/cm (due to results of AC conductivity in a table (2)). In general, utilizing the process of electrospinning to prepare pure Polyvinyl alcohol films increases the electrical conductivity by four orders more than bulk pure PVA.

Different PVA film concentrations were tested by frequencies (0.1, 10, 100, 200, 300) KHz, respectively. It was observed that the alternative electric conductivity (σ_{ac}) Improved with increasing frequency. The dependence of the measured σ_{ac} on the angular frequency (ω) for different PVA/ Ag ratio films is shown in Figure 10, which indicates that σ_{ac} is proportion to ω^s . It also indicates that the values of exponent (S) were estimated from the slope of the curves plotted between $(\ln \sigma_{ac})$ versus $(\ln \omega)$, for PVA/ Ag films and the calculated value of (S) factor changed into less than unity for all tested films. The estimated values of the (S) factor and (σ_{ac}) for PVA/ Ag are illustrated in the Table 2.

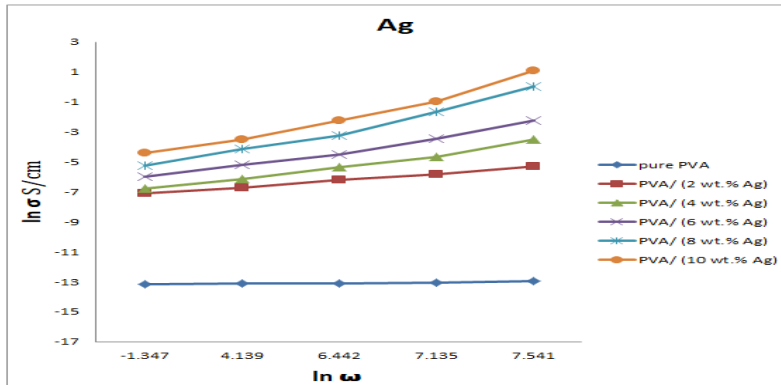


Figure 10: Variation of (AC) conductivity with angular frequency for PVA/ Ag films.

Table 2: The AC conductivity and (S) factor for different composition PVA/ Ag films.

The film composition	(S) factor	σ_{ac} (S/cm) at 300 KHz
Pure PVA	0.0125	1.17×10^{-6}
PVA/ 2 wt.% Ag	0.390	1.96×10^{-2}
PVA/ 4 wt.% Ag	0.351	2.75×10^{-2}
PVA/ 6 wt.% Ag	0.337	3.27×10^{-2}
PVA/ 8 wt.% Ag	0.268	4.42×10^{-1}
PVA/ 10 wt.% Ag	0.245	1.80

As shown from the results for PVA / Ag films, the AC electrical conductivity increased by six orders for (PVA/ 10wt.% Ag) also S factor decrease, and this increase is attributed to that the Ag nanoparticles act as conductive dopants metallic fillers in the polymer matrix, conductivity rise will result in a simultaneous increase of carrier concentration and carrier mobility with increasing Ag nano-contents in addition to increase frequency. This observation is has the same opinion with *M. Ali Habeeb et al* [26], who observed that the dielectric constant is reduced (i.E. electrical conductivity increases) with an increasing frequency which attributed to a decrease in the distance rate polarization. Also, AC electrical conductivity is increased with an increase of titanium nanoparticles concentration which because of the growth in the charge carries numbers in the PVA matrix.

3.5 Tensile Test:

The results of (stress-strain) curves for (pure PVA and PVA /8 wt. % Ag) are shown in Figure 11. The maximum stress for pure PVA was (1.360) MPa and enhanced to (2.305) with adding of 8wt. % Ag NPs. The modulus of elasticity were (12.87 MPa) and also enhanced to (110 MPa) by adding 8wt.% Ag NPs, but the maximum strain decreased from (38.98)% for the pure PVA to (2.245)% for PVA/8wt.% Ag NPs. This means that adding Ag NPs to the PVA polymer matrix will make the polymer stiffer, due to the restriction of Ag NPs nanoparticles to polymer chain mobility and thus make the electrospun film less flexible against stress.

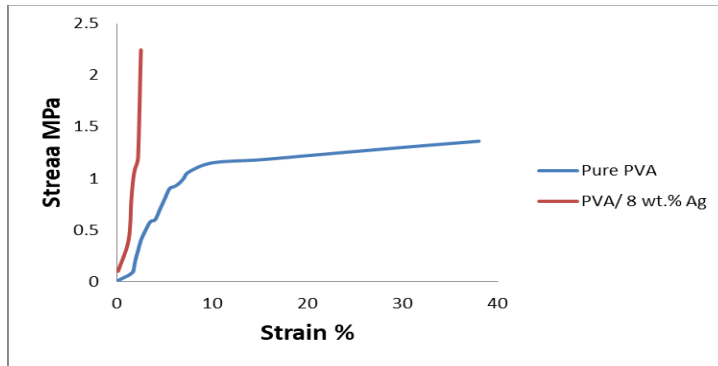


Figure 11: Stress-Strain curve for pure PVA and PVA/ 8 wt.% Ag films.

4. Conclusion

Ag nanoparticles have an excellent effect on the electrical properties of PVA solution and electrospun films. The electrical conductivity of the resulted polymeric solution increases with increasing the Ag wt. % in the solution, while viscosity and surface tension reduces. The resistance of the electrospun films decreases (the electrical conductivity increases) with increasing temperature and frequency, so the PVA electrospun films exhibit semiconductor behaviour. The electrical conductivity increases four orders between the bulk PVA and the electrospun films while increases five to six orders between pure and doped electrospun films. The mechanical properties; thus, the modules of elasticity increase with adding Ag nanoparticles content.

Reference:

- [١] A. MacDiarmid, " Synthetic Metals°: A Novel Role for Organic Polymers (Nobel Lecture)" , Angew. Chem. Int. Ed. Engl. , Vol.40, No. 14, pp.2581- 2590, (2001.(
- [٢] F. Yilmaz, "Polyaniline synthesis: Characterization Solution Properties and Composites", Ph.D Thesis, Middle East Technical University, Ankara (Turkish), (2007.(
- [٣] S. Gul, A.Shah and S. Bilal, "Calculation of Activation Energy of Degradation of Polyaniline-Dodecylbenzene Sulfonic Acid Salts via TGA" , Journal of Scientific and Innovative Research, Vol. 2, No.3, pp. 673-684, (2013.(
- [٤] A. R. Jabur , F. A. Chyad and N. M. Jalal , " Fabrication and Characterization of Nylon 6/ MWCNTs Conductive Polymer by Electrospinning Technique " , Int. J. Thin. Fil. Sci. Tec. 5, No. 2, 1-9 (2016.(
- [٥] A.L. Borges, E.A. Mu'nchow, A.C. de Oliveira Souza, T. Yoshida, P.K. Vallittu, M.C. Bottino, Effect of random/ aligned nylon-6/MWCNT fibers on dental resin composite reinforcement, J. Mech. Behav. Biomed. Mater 48 (2015 Aug) 134e144, <http://dx.doi.org/10.1016/j.jmbbm.2015.03.019>. Epub 2015 Apr 1.
- [٦] R. Parajuli, " Developing Conducting Polymer Nanocomposites with Carbon Nanomaterials for Molecular Detection and Fuel Cell Applications", Ph.D Thesis, Rutgers University, New Jersey (US),(2011(
- [٧] P. KAR, "Doping in Conjugated Polymers", Wiley, India, pp. 31-50, (2013.(
- [٨] F. A. Chyad, A. R. Jabur and N. M . Jalal, " Effect of NaCl Solution Addition on Improving Some of the Physical Properties of Nylon 6 Solutions used for Electro Spinning Purpose" Eng. &Tech.Journal, Vol.34,Part (A), No.7,2016.

- [٩] W.S.
Khan, R. Asmatulu, M.M. Eltabey, Electrical and Thermal characterization of electrospun PVP nanocomposite fibers, Hindawi Publishing Corporation, J. Nanomater. (2013) 9, [http:// dx.doi.org/10.1155/2013/160931013](http://dx.doi.org/10.1155/2013/160931013). Article ID 160931.
- [١٠] S.
Mahendiaa, A.K. Tomara, S. Kumara, " Electrical conductivity and dielectric spectroscopic studies of PVA–Ag nanocomposite films " Journal of Alloys and Compounds 508 (2010) 406–411.
- [١١] L.
Bokobza, Multiwall carbon nanotubes-filled natural rubber: electrical and mechanical properties, Express Polym. Lett. 6 (3) (2012) 213e223.
- [١٢] M. F. M.
Ahmad Zamri, S. H. Sharif Zein, A. Z. Abdullah and Nor I. Basir, " Improved electrical conductivity of polyvinyl alcohol/ multiwalled carbon nanotube nanofibre composite films with MnO₂ as filler synthesised using the electrospinning process " International Journal of Engineering & Technology IJET-IJENS Vol:11 No: 06,(2011.(
- [١٣] S. A.
Salman, N. A. Bakr , M. H. Mahmood, " Preparation and Study of Some Electrical Properties of PVA-Ni(NO₃)₂ Composites" International Letters of Chemistry, Physics and Astronomy 136-42(2015(
- [١٤] İ.
Yücedağ, A. Kaya, Ş. Altındal, and I. Uslu, "Frequency and voltage-dependent electrical and dielectric properties of Al/Co-doped PVA/p-Si structures at room temperature" ,Chin. Phys. B, vol. 23, no. 4, p. 47304, 2014.
- [١٥] J. B.
Veluru, Satheesh K. K., Trivedi D.C., Murthy V. Ramakrishna, Natarajan T. Srinivasan, "Electrical properties of Electrospun Fibers of PANIPMMA Composites", J. Eng. Fibers Fabr. ,Volume 2, Issue 2, pp. (25e31(

- [١٦] W.
Nuansing, Electrospinning of Biomolecules, Department of Physics, University of Pais Vasco, Donostia, Spain, 2014, pp. 90e92 [PhD thesis.]
- [١٧] Akram
R. Jabur, " Effect of polyaniline on the electrical conductivity and activation energy of electrospun nylon films" Department of Materials Engineering, University of Technology, Baghdad, Iraq, international journal of hydrogen energy xxx (2017) 1 e7 .
- [١٨] T. Lin,
Nanofibers Production, Properties and Functional Applications, 2011, pp. 132e135. InTech.
- [١٩] S.S.
Ojha, M. Afshari, R. Kotek, R.E. Gorga, Morphology of electrospun Nylon-6 nanofibers as a function of molecular weight and processing parameters, J. Appl. Polym. Sci. 108 (2008) 308e319.
- [٢٠] A.R.
Jabur, L.K. Abbas, S.M. Muhi Aldain, The effects of operating parameters on the morphology of electrospun polyvinyl alcohol nanofibres, in: The International 3rd. Scientific Conference of the College of Science, Journal of University of Kerbala, 2015, pp. 35e46.
- [٢١] X.
Kima, D. Fangb, S. Rana, B. Hsiaoa, B. Chua, Structure and process relationship of electrospun bioabsorbable nanofiber membranes, Elsevier Polym. 43 (2002) 4403e4412.
- [٢٢] A. R.
Jabur , F. A. Chyad and N. M. Jalal , " Fabrication and Characterization of Nylon 6/ MWCNTs Conductive Polymer by Electrospinning Technique ", Int. J. Thin. Fil. Sci. Tec. 5, No. 2, 1-9 (2016).(
- [٢٣] N.
Norkhairunnisa, A. Azizan, M. Mariatti, H. Ismail, L.C. Sim, Thermal stability

and electrical behavior of polydimethylsiloxane nanocomposites with carbon nanotubes and carbon black fillers, J. Compos. Mater. 46 (8) (2011) 903e910.

[٢٤]

A.R.

Blythe, Electrical Properties of Polymers, first ed., United States of America by Cambridge University Press, New York, 1977, pp. 90e93.

[٢٥]

M.

Aghelinejad and Siu N. Leung, " Electrical conductivity and humidity sensing properties of PVA/CNT nanocomposites" York University, Toronto, ON, Canada, SPE ANTEC™ Indianapolis 2016/596.

[26]

M. A.

Habeeb and W. K. Kadhim, "Study of the Electrical Properties of (PVA-PVAC-Ti) Nanocomposites" Australian Journal of Basic and Applied Sciences, 8(10) July \ (2014), Pages: 316-3

Software for teaching sign language based on image processing and machine learning

Khlood Ibraheem Abbas¹, Muna Abdul Hussain Radhi², Nadia Mahmood Hussien³, Yasmin Makki Mohialden⁴

^{1,2,3,4}Computer Science Department, Collage of Science, Mustansiriyah University, Baghdad-Iraq

¹ a.khlood@uomustansiriyah.edu.iq

² muna.ali@uomustansiriyah.edu.iq

³ nadia.cs89@uomustansiriyah.edu.iq

⁴ ymmiraq2009@uomustansiriyah.edu.iq

abstract

When integrating image processing with machine learning techniques, the result was certainly amazing. In this research, a method was devised to help people with hearing and speech problems (deaf and mute) communicate using sign language. It is a simulated process of the hand movements of the images captured by the camera by a trainer and teacher, and the translation of sign language for the deaf and mute. In Arabic, each sign of the hand has a distinct meaning. The system has been designed in a way that makes it easy to understand and use. It is considered an alternative application for teaching sign language to the deaf and dumb. Or mute, as in a three-dimensional model. This program was implemented using image processing techniques and machine learning techniques in Python, which were developed based on the MediaPipe library.

Keywords : pipeline ML, Image processing , palm detection, detect gesture, knuckles, machine learning .

1. Introduction

Sign language is a term that refers to a non-audio means of communication, used by people with special needs such as the audio-dumb and the audio-deaf. Hand movements as a means of communication and the fingers of the hands in reference to numbers, as well as expressions drawn on the face to convey tendencies and feelings accompanied by some movements in the hands, can construct many meanings, in addition to following the movements of the lips, which is the most advanced stage for the power of observation, where the deaf can read words through lip movements. In addition, there are some movements in the body, like putting some signs on either side of the head, or above or on the shoulder, chest, or abdomen, as a kind of suggestion to help people understand what they want to say or express themselves. These languages and signs vary from country to country.

Hand sign language has existed as a language since the sixteenth century AD, and it consists of a collection of traditional signs such as hand signs, or spelling and counting using the fingers of the hand to represent the letters of the alphabet. It is worth noting that signs are typically complete sentences, not just words, and that the majority of these languages are sign languages. Many natural languages are used by deaf people to communicate with each other and with other people [4].

The system's purpose is to facilitate communication with deaf and hard-of-hearing individuals. To aid in the acquisition of sign language for the deaf and dumb, it aids in the expression of the deaf and dumb's diverse requirements. It focuses on the mental, verbal, and expressive development of deaf and hard-of-hearing individuals with particular abilities. easing the emotional and psychological strains created by a lack of communication and hearing. It assists deaf and dumb individuals in overcoming fear, melancholy, and frustration. There is no better approach to teaching sign language than through the use of a three-dimensional model.

The remainder of this paper is divided into five sections: Section two is about related work, Section three is about sign language basics, and Section four is about the proposed system. Section five is devoted to the results and discussions, and Section six is devoted to the conclusion

1. Related Work

[Nashwa, Hossam, Mahmoud Aboul Ella, and Kazumi, 2011] In this work, an Arabic sign language alphabet gesture translation system is presented. Rather than relying on gloves or visual marks to perform recognition, the Arabic Sign Language Alphabets Translator (ArSLAT) technology is proposed. Alternatively, it uses images of bare hands so the user can interact with the device in a more natural way. In the proposed ArSLAT system, preprocessing, best-frame identification, category detection, feature extraction, and classification are all part of the five primary stages that make up the system. In order to increase the system's adaptability, translation, scaling, and rotation invariant extracted features were utilised. At 91.3 percent and 83.7 percent of the time, the ArSLAT system that was suggested was found to be very good at recognizing Arabic alphabets when it used the MDC and MLP classifiers [5].

[Elbourhamy and Hosnia, 2016] In this study, a new method for translating Arabic Sign Language (ArSL) is proposed. To begin with, there are two parts to this system: the first is a speech-to-ArSL translation subsystem. A large portion of this subsystem relies on the speech-recognition engine. An ArSL to speech translation subsystem uses the GTTS library in order to translate sign images into spoken words. With the use of this technology, there will be increased interaction between those who are deaf and those who are able-bodied and want to learn ASL. Adding new signs to the database and using the system online (at

<https://sr.gravita-demo.com/>) are two of the system's many benefits. Several ways of evaluating the proposed system were employed. The results show that the algorithm can translate ArSL with a 95% accuracy rate. Experimentation was done to test the suggested system's effectiveness. According to the study's findings, the academic performance of Arab deaf kids improved dramatically as a direct result of the system's implementation. In a survey, users said they liked this method better than ArSL's learning and teaching and learned new things, which shows that this system has a bright future in academic settings [6].

[Bala, Song, 2020] This study describes an application called SSLATA, which enables people to learn and master sign language. The newly developed program can translate from sign language to English or Hausa, as well as from text to speech to sign and back again. Interacting with one another in spoken or sign language will be possible thanks to the SSLATA's user-friendliness. The study used a flexible research paradigm and a collaborative strategy to gather data. Developers utilize Android Studio, SQLite, and Java to build their apps. The app operates on Android-based mobile devices [7].

[Abdallaha, Fayyoubi, 2016] It is the goal of this article to present a novel application that allows for seamless communication between users with disabilities and those who do not. An important thing about this software is that it uses Arabic to teach sign language. The application's power comes in two forms: Firstly, it enables the ability of normal individuals to communicate with the targeted population without prior knowledge of sign language. This can be done either by voice recognition or by entering the words in the Arabic language. The application then shows the proper sign language images. Secondly, and more importantly, people with special needs connect with the general population by selecting the sign images on their phones from a wide variety of categories that reflect their thoughts and ideas. As a result of this, a collection of photos is turned into a paragraph of text. Real deaf and dumb users were used to test our program. They used well-crafted scenarios based on real-world circumstances. The preliminary results are encouraging, as the proposed technology was used by everyone who was deaf. Ninety percent of them said they'd utilize it on a regular basis [8].

2. Sign Language Basics

Like any language, there are basics that must be learned and understood before starting to use and practice this language. Among these basics, we mention the following:

1) **hand movements**

Every movement denotes a specific thing or the meaning of what you want to convey. For example, the hand is clenched and facing upwards, or it is flat and facing upwards, or it is facing downward with curved fingers.

Placing the fingers with the palm of the hand at a right angle is also one of these methods.

2) **Letters** It is in two ways:

a) **Alphabet signs**

The alphabet varies by country and in turn, the sign language and the gestures that express each letter differ.

b) **Finger spelling**

As we have already mentioned, there are certain movements corresponding to the letters of the alphabet, and through them we can formulate complete sentences with finger movements.

c) **Facial movements**

To convey the full meaning and appropriate expressions, facial movements are linked with finger and hand gestures. For instance, the brow movement provides message.

3. Proposed system

System that is proposed the ability to comprehend and regulate the shape and feelings of the hands can serve as a foundation for sign language instruction and hand gesture control. The advancement of technology, as well as the experience of programmers, particularly in real-time intelligent systems, aided in the development of this subject. For example, robust real-time hand perception is a particularly difficult computer vision problem due to the fact that hands frequently occlude themselves or one another (e.g., finger/palm occlusions and handshakes) and lack high contrast patterns. The system was built using the MediaPipe framework, which enables academics and developers to rapidly design world-class machine learning solutions and apps for mobile, edge, cloud, and the web. It provides cross-platform, tailor-made machine learning solutions for live and streaming media. It is developing pipelines for the processing of perceptual input from a variety of modalities. To implement the system,

we employed a pipeline machine learning methodology. The pipeline machine learning module is divided into three sections:

1. BlazePalm (which is used to determine the location of the hand)
Our proposed method uses SSD approbation for a single-shot detector model. The output of this part is the orientation of the
2. Hand Landmark Design
The input of this step is the output of palm detection step of the input image. It is used to detect and determine the key point location of the 3D knuckle coordinates for the hand. This knuckle is a 21 point in the hand.
3. Gesture Recognition: In this step, you understand the emotion of the gesture and convert it into a meaningful sign. The coach learns the sign language by presenting the emotion of his hand with its meaningful

Figure 1 shows the block diagram of the system.

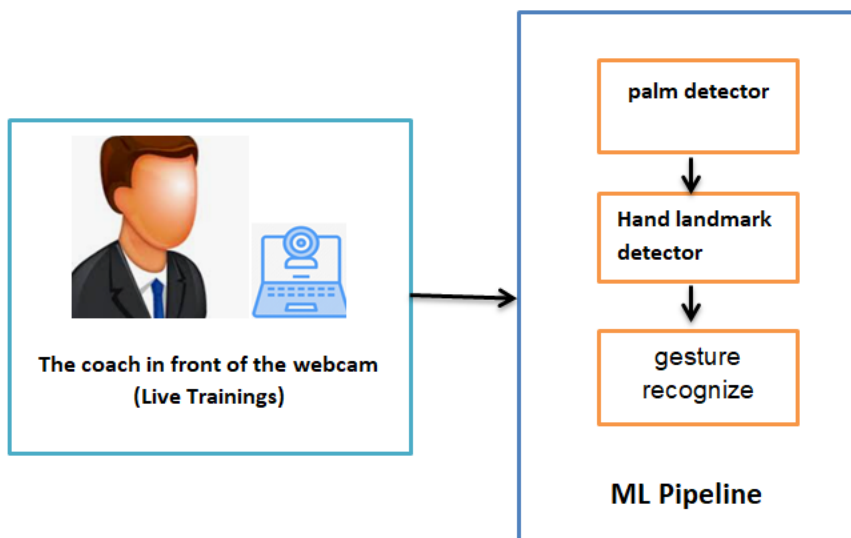


Figure 1: Block diagram of the system

Figure 2 shows the use case diagram of the system, which is composed of actors and use cases. The use case diagram represents the functionality of the system, meaning: what are the system's functions? In our proposed system, it contains two actors and four basic use cases with generalization relations.

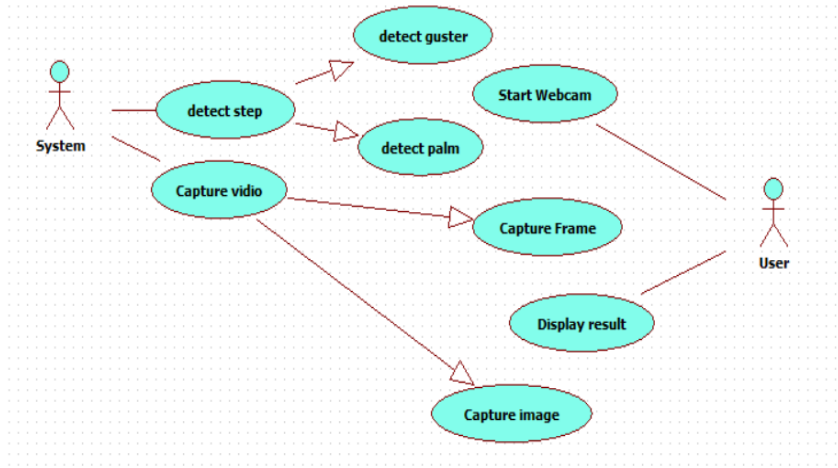


Figure 2 : use case diagram of the system.

4. Result and discussions

The system used to learn the sign language by emotion of the hand.

Figure 3 represents some examples of the execution system as a system testing . each sign is given represents the meaning word or leter in the sign language. The system worked 90% of the time when it was tested by people of different ages and scientific background.

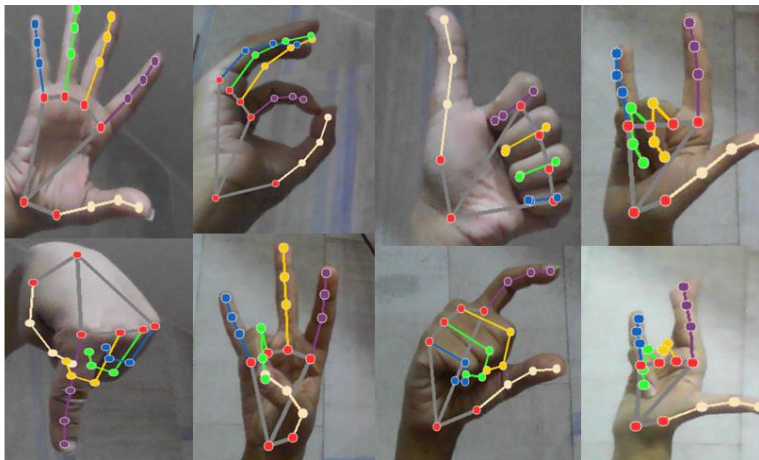


Figure 3: System testing

5. Conclusions

Nowadays, the development of technologies is making life better. Our proposed method is designed and implemented based on image processing and machine learning techniques. The system can be used to teach the sign language with high accuracy, good results, and a more attractive view. The user starts the webcam, and the system executes the detection and recognition processes. Our methodology used a pipeline ML to implement the system.

Acknowledgements: the Authors would like to thank Mustansiriyah University(<https://uomustansiriyah.edu.iq/>) Baghdad -Iraq for its support in the present work.

references

- [1]Haseeb, A. A., & Ilyas, A. (2012). Speech Translation into Pakistan Sign Language.
- [2] Bhatti, Z., Muhammad, F., Malik, H. A. M., Hussain, M., Chandio, H., Channa, S., & Mahar, Z. (2021). Text to Animation for Sign Language of Urdu and Sindhi. IKSP Journal of Emerging Trends in Basic and Applied Sciences, 1(1).
- [3]Y. Bajaj and P. Malhotra, "American sign language identification using hand trackpoint analysis", 2021.
- [4] Mercanoglu Sincan, Ozge ;Yalim Keles, Hacer," Using Motion History Images with 3D Convolutional Networks in Isolated Sign Language Recognition", IEEE Access, 2022.**
- [5] N. El-Bendary, H. M. Zawbaa, M. S. Daoud, K. Nakamatsu et al. , "Arslat: Arabic sign language alphabets translator," in Computer Information Systems and Industrial Management Applications (CISIM), 2010 International Conference on. IEEE, 2010, pp. 590–595.
- [6] Hosnia,Mohammdia and Doaa ,Elbourhamy. An intelligent system to help deaf students learn Arabic Sign Language" Department of Computer Science, Faculty of Computers and Informatics, Suez Canal University, Ismailia, Egypt,2016.
- [7] Bulus P. Bala & Laminu Aminu SongAndroid App for Improvising Sign Language Communication in English and Hausa" Department of Computer Science, Federal College of Education, Yola Nigeria,2020.
- [8] Emad E. Abdallaha,, Ebaa Fayyoubi Assistive Technology for Deaf People Based on Android Platform' The 11th International Conference on Future Networks and Communications (FNC 2016),2016.

The Role of Machine Learning Methods in Dealing with DDoS Attacks and Data Poisoning Cyberattacks

**Mustafa Al-Alani¹, Ahmed Alshaibi ¹, Abeer Al-Azzawi ¹, Ayman Al-Ani ²,
Waleed Hammood ², Evgeny Kost-yuchenko ¹, Anton Konev ¹ and
Alexander Shelupanov ^{1*}**

¹ Department of Complex Information Security of Computer Systems, Faculty of Security, Tomsk State University of Control Systems And Radioelectronics, 634000 Tomsk, Russia; alshaibi@fb.tusur.ru; al-azzawi@fb.tusur.ru; key@fb.tusur.ru; saa@tusur.ru * Correspondence: al-ani@fb.tusur.ru

² Department of Computer Science, Faculty of Computer Science, Al-Mustansiriya University, Baghdad, Iraq; aymanmajid@uomustansiriyah.edu.iq; engwaleed54@yahoo.com

Abstract: New technological advancements have resulted in a massive volume of data being generated, referred to as "big data". To construct an intelligent system, we need to use this data with the help of machine learning. This means that big data and machine learning might be considered complementary. The Internet of Things (IoT) technology has led to an exponential increase in the amount of data being generated. It is imperative that we utilize this information effectively. This paper investigates the role of Machine Learning (ML) and the countermeasures based on machine learning techniques to deal with DoS and unknown attacks. This paper is a review of a study formulation of a new hybrid machine learning-based model to deal with DDoS attacks and data poisoning cyberattacks. The purpose of this paper to study formulation of a new hybrid machine learning-based model to deal with DDoS attacks and and unknown attacks.

Keywords: Cybersecurity; machine learning; cyberattacks; datasets; deep learning

1. Introduction

The application of artificial intelligence (AI) in various industries has undoubtedly led to significant improvements in the digital age. With the ability to interpret and make complex decisions based on data, (AI) technologies enable tasks or processes to function alongside human intelligence, making business operations faster and more innovative, and adding valuable user experience. Modern cyber threats are the potential source of the most costly losses that an organization, industry, government or even a global market can face [1].

The cybersecurity industry is one of the many sectors that have benefited greatly from the development of artificial intelligence. Faster and more accurate malware detection can be achieved with intelligent machine learning. However,

most deep learning applications are usually focused on areas such as marketing, sales, finance, etc. There is very little material on deep learning in cybersecurity that is used to protect IT products and businesses from malware and hacker attacks [2].

Existing machine learning methods face great difficulty in detecting cyber-attacks in large distributed environments, and the scalability of these methods in a large network is not great. One disadvantage of traditional machine learning algorithms is that they use hand-crafted features for the recognition task. But it is desirable that the machine itself find and structure functions for detecting attacks [3,4].

Currently, machine learning is one of the most intensive areas of research in the field of artificial intelligence and offers great opportunities to overcome the limitations of traditional machine learning methods. In traditional machine learning algorithms, features are extracted by humans. But when processing big data, deep learning is much better.[5, 6]. This research focuses on the practical application of deep ML methods in providing maximum cyber security against cyber-attacks in IoT devices.

2. Taxonomy of Machine Learning Methods

Data can be turned into decisions and actions more quickly and precisely with ML. ML techniques use data for descriptive, diagnostic, predictive, and prescriptive purposes (which include decision support and automation). When the system learns from a collection of training data rather than being explicitly designed, it is considered ML. When fresh data is available, ML can create predictions (which can change) based on that data [7].

New technological advancements have generated a massive volume of data. This is what we refer to as "big data". To construct an intelligent system, we need to use this data with the help of ML. This means that big data and ML might be considered complementary [8]. IoT technology has exponentially increased the amount of data being generated. It is imperative that we utilise this information effectively [9].

The future can be predicted using ML. ML techniques can be applied in a variety of ways, including:

2.1. Rationale

Data can be turned into decisions and actions more quickly and precisely with ML. ML techniques use data for descriptive, diagnostic, predictive, and prescriptive purposes (which include decision support and automation). When the system learns from a collection of training data rather than being explicitly designed, it is considered ML. When fresh data is available, ML can create predictions (which can change) based on that data [7].

New technological advancements have generated a massive volume of data. This is what we refer to as "big data". To construct an intelligent system, we need to use this data with the help of ML. This means that big data and ML might be considered complementary [8]. IoT technology has exponentially increased the amount of data being generated. It is imperative that we utilise this information effectively [9].

The future can be predicted using ML. ML techniques can be applied in a variety of ways, including:

2.1.1. Supervised Learning

In this type of learning, the data is labelled, and the decisions are based on that data. Using multiple simple models, ensemble learning is an extension of supervised learning [9-11].

2.1.2. Unsupervised Learning

In the absence of labelled data, unsupervised learning is used. The quality of data is used to make decisions [9-11].

2.1.3. Semi-Supervised Learning

When a combination of labelled and unlabelled data is available, semi-supervised learning is used. It exploits both supervised and unsupervised techniques. The goal of cyber security may be to reduce the number of assaults, but it must be understood that attacks can never be completely averted. Fewer people are likely to resist the attacks in the defence system than those who plan to attack [11]. The cyber machine must be able to solve problems in a well-reasoned way based on learning [12]. It should incorporate existing tools and architecture. To detect and verify fraud, a classification technique might be used. Dimensional reduction can also be utilised for face detection [9].

CPS is one of the most widely utilized cyber infrastructures, and it is used by governments and other businesses to address the issues of everyday cyber life. Our greatest challenge is to quickly and accurately decide in a massive data world [4, 13]. The Internet of things (IoT) and CPS integration could be useful in transforming production to the next level. Furthermore, we confront a wide range of problems in our daily lives, including the lack of smart analytical tools that directly impact industries, whereas some instruments and equipment are extremely reliable for the improvement of CPS [10].

The ability to analyse the infrastructure of a system is not enough to handle these devices. The vulnerabilities are more likely to occur on IoT devices that are often interconnected. Hence, cybersecurity and ML must be integrated into CPS to achieve the mandated standards [14]. ICS used to be segregated from the rest of the world so that it might be shielded from possibly dangerous risks that might

come its way. Considering recent technological breakthroughs, increased network connectivity, and faster internet communications, cyberattacks on these systems are viable now [15, 16]. Since the information is so sensitive, security must be taken very seriously in this industrial application. The high level of security concern in IoT applications necessitates detection of intrusion in IoT [17, 18].

Table 1. Taxonomy of Existing Machine Learning Methods

Source	Topic	Context	Outcome
[21]	Cyber-attacks in smart grid—dynam impacts, analyses, and recommendations	The study was based on primary data. The author selected a smart grid as a domain and discussed fo types of cyber-attacks concerning the IEEE benchma model of the Western System Coordinating Coun system	The study concluded that an effective detection ai prevention mechanism w needed to deal with the fo mentioned attacks. I discussion of ML / DL dealing with these fo attack
[15]	Smart Intrusion Detection with Expert systems. In Advances on P2P, Parallel, Grid, Cloud and Internet Computing	On the KDD99 dataset, the authors proposed using an MLP classifier.	The proposed model, according to the authors, an identify new types of security attacks without requiring the entire network to be retrained. No experimental or theoretical analysis was done
23]	Performance Comparison of Supp Vector Machine, Rando Forest, and Extern Learning Machine f Intrusion Detectic	To solve the efficiency issue of using ML algorithms to handle large datasets in training intrusion detectic classifiers, SVM, random forest (RF), and extren learning machine (ELM) were utilized. The metho were tested on the NSL-KDD dataset by the autho	Their findings revealed that ELM performs bett when dealing with hu data, while SVM excels wh dealing with tiny data. Us ML methods only; No DL w use
[9]	Spider Monkey Optimisation and Deep Neural Network hybrid Classifier Model for Intrusion Detection. Electronics''	To minimize dataset dimensionality, the authors proposed a hybrid model that combines a deep neur network (DNN) classifier with the spider monkim optimisation (SMO) techniqu	Using the KDD99 dataset, the suggested moc improved the F1-score by 3 percent over a single DN model with significant reduced training tim There was only one DL method employed; i

			additional DL methods we evaluate
[24]	A Hybrid Intrusion Detection System Based on the Stacking Ensemble Classifier and One-Class Support Vector Machi	Using the KDD99 dataset, they proposed a hybrid two-layer technique for detecting known and unknown threats that combines signature-based IDS with anomaly-based IDS.	<ul style="list-style-type: none"> Only one DL method was used; no evaluation was done with other DL methods <p>An obsolete and additional KDD99 dataset was used.</p>
[2]	A reference model for IoT middleware	They also created a recurrent neural network and provided an intelligent mechanism model to identify intrusion based on a decision-making technique (RN	Obsolete and traditional KDD99 dataset was used

Table 2. Studies Scenario on DL and their Approach

Source Type	Practical Application	Approach
[25] Supervised DL	Detect routing attacks	Artificial neural networks
[26] Supervised DL	Suspicious behaviour detection	Recurrent neural network
[27] Unsupervised DL	Malicious attack detection	Deep belief network
[25] Supervised DL	Detect routing attacks	Artificial neural networks
[26] Supervised DL	Suspicious behaviour detection	Recurrent neural network
[27] Unsupervised DL	Malicious attack detection	Deep belief network
[28] Unsupervised DL	Isolation of network anomaly	Restricted Boltzmann machines
[29] Supervised DL	Cyberattack detection	Artificial neural networks
[30] Supervised DL	Detection of tampered data	Artificial neural networks

[31]	Unsupervised DL	Malware detection	Encoders of deep auto
[32]	Supervised DL	Malware detection	Neural networks convolutional
[33]	Supervised DL	Authentication	Artificial neural networks
[34]	Supervised DL	Access control	Artificial neural networks

3. Discussion.

Cybercriminals have utilized malevolent AI to aid assaults, either to avoid intrusion detection systems in IoT or to target beneficial AI in such a manner that it acts against its own system [34,35]. ML can be used to find vulnerabilities in a system. While this technology can help those who want to safeguard a system by intelligently searching for vulnerabilities that need to be fixed, it can also be used by attackers to find and exploit weaknesses in their target system [36]. The amount of vulnerabilities that attackers may exploit, including zero-day faults, has risen as technology becomes more widely utilized, particularly lax security technologies like IoT devices. AI is commonly used by attackers to discover and exploit flaws significantly faster than developers can repair them [22].

Developers can use these detection techniques as well; however, developers are at a disadvantage because they must find and fix every single vulnerability, but attackers only need to find one, making automated detection a valuable tool for attackers. Security risks are getting more targeted and less general as attack complexity grows exponentially. To circumvent detection by typical IDS, attackers are increasingly depending on unknown attack strategies that resemble normal traffic and are fragmented, encrypted, or obfuscated [37, 38]. When it comes to IDS types based on detection processes and their ability to handle unknown threats, signature-based IDS is generally incapable of recognizing either whole new attacks or new variants of existing attacks. This is owing to its design, which matches an assault to a well-known signature to identify it [17, 39].

Data poisoning and input attacks are extremely similar, but data poisoning modifies inputs over a long enough period that the AI that analyzes data shifts and becomes intrinsically defective; as a consequence, data poisoning is generally done when the AI is still being trained before it is deployed. In many cases, AI learns to fail on the attacker's specified inputs; for example, if a military uses AI to identify aircraft, the opposing military may poison the AI to prevent it from detecting particular types of aircraft, such as drones. Data, algorithm, and model poisoning are three key approaches that attackers can use to poison an AI [40].

Poisoning an AI's dataset is the most direct form of data poisoning, because AI learn everything from the training datasets they're given, and any defects in those

datasets harm the AI's knowledge. The target dataset is polluted when it contains erroneous or mislabeled data. Because AI learns by detecting patterns in datasets, poisoned datasets can cause patterns to be disrupted or introduce new incorrect patterns, causing AI to misidentify or incorrectly identify inputs. Because many databases are big, locating poisoned data within them can be difficult. Using traffic patterns as an example, an attacker may modify dataset labels so that the AI no longer recognizes stop signs, or add data and labels so that the AI incorrectly classifies a red light as green [40].

The efficiency of an IDS is determined by a number of factors, including whether the model is supervised, unsupervised, binary classification, or multi-classification. The false alarm rate (FAR) and true alarm rate (TAR) are two metrics commonly used to evaluate an IDS's capacity to identify security threats. The former refers to the proportion of harmless events that are misclassified as malicious, whereas the latter refers to the percentage of harmful events that are correctly classified as threats. A perfect IDS has a FAR of 0 and a TAR of 100%, meaning that it correctly identifies all anomalous and usual activities. But achieving this aim is difficult, if not impossible [15].

4. Security Challenges in IoT Devices

Malicious attacks are deployed into the wild before anti-virus signatures are made available. If anti-virus (AV) signatures are applied to a vulnerable and weak system and at the same time the malware is launched, then eventually the malware will infect the system. AV does not consistently defeat typical malware. It takes time for a vendor to generate them and for end-users to install and apply security updates. Until then they do not reliably block attacks of known vulnerabilities. During this time, systems are susceptible, and security updates are occasionally incorrect. They are ineffective in addressing the known vulnerability that they were created to eliminate when they are erroneous. Detection and monitoring systems are commonly recommended by cyber-security and intrusion detection systems (IDS), and security monitoring systems are also deterrents rather than preventative measures. They ensure that network activity is not abnormal, and that no suspicious activity is detected. In case of any trigger incident response, actions are taken by these systems. Despite their importance, when a system is under malware attack by a remote attacker or automatically by autonomous malware, IDS and monitoring systems take much time detecting intrusions and responding to incidents, and because of this, they do not always prevent attacks.

Network intrusion detection (NID) systems are designed to spot malicious network activity that jeopardizes a network's confidentiality, integrity, or availability. [41, 42] conceived and developed neural networks (NNs) and support vector machines (SVMs). This warning categorization method aids in the

prevention of distributed denial of service attacks (DDoS). According to the researchers, the average accuracy of neural network alert categorization is 83 percent, compared to 99 percent for SVM.

For preventing unauthorised use and abuse of the system, communications, and other data, and for electronic information recovery, IDS takes all necessary technical, regulatory, or administrative precautions. IDS enhances the protection, confidentiality, and privacy of personal data by doing so. It ensures that they are available, and that the continuity of the information systems is maintained.

Cybersecurity, usually referred to as information technology security, is a way of safeguarding computers, servers, mobile devices, electronic systems, networks, and data from malicious attacks. In network incursions, packets approaching the network system conduct operations such as DOS assaults resulting in system denial or system division.

Land attacks, ping of death (POD), and flood attacks are all possible. and any other DoS attack seek to render intended customers' PC assets unreachable. Depending on the charges of different clients, moderate system execution, as well as sudden system crashes and modifications in sections of information structures are indicators of intrusions that result in abnormal outcomes.

To transfer information from one device to another, a smart grid structure known as an IoT environment is used. It uses sensor devices to attack unknown vulnerabilities and protect known signatures. As IoT has grown in popularity, attackers are more successful in attaining their goals. To detect weaknesses in sensor devices, AI based on DL algorithms can be used.

The information-driven approach that AI requires takes some necessary steps. The primary key is to understand what the data is. Network traffic, and other various forms of data can represent some sort of specific attack. Attacks vary in form, each with its own pattern. For example, network traffic reflects network behaviours, while server logs describe host behaviours. Choosing appropriate data sources to detect diverse attacks based on the threat's characteristics is important.

Flow data is perfect for detecting DoS attacks because of the rapid transmission of multiple packets of DOS attacks in such short times. Thus, certain network behaviours can be detected through the advancement of DL algorithms. For session data detection, two separate IP addresses having a hidden channel that contains a data-leaking activity are ideally suited.

5. Machine Learning Vs Deep Learning

Experts in machine learning and deep learning have yet to agree on these concepts in this context, and fresh ideas are proposed on a daily basis. Deep Learning is a more recent concept, although Machine Learning is older. Deep learning is a kind of machine learning.

The distinctions are as follows:

5.1 An excessive amount of data is required in deep learning, to achieve the perfect algorithm structure. Because the human provides precise attributes to the algorithm, the problem can be solved with considerably less data in machine learning.

5.2 Deep learning algorithms attempt to extract data features. The expert determines the features in machine learning.

5.3 Machine Learning algorithms can run on our regular CPUs; however Deep Learning algorithms require high-performance machines to run.

5.4 In machine learning, each of the problem is solved separately after dividing it into pieces before the solutions are assembled. The problem is solved in deep learning altogether in a single attempt.

Table 3. Possible Attacks and Datasets for Narrowing down Research Direction

Type of Attack	Dataset	Dataset Description
Denial of Service (DoS) Attack	USNSW NB-15	The collection includes examples of typical activity as well as recent attacks. After capturing 100 GB of network traffic cap files and converting them to a csv file, the dataset was created.
Phishing Attack	Phishing attacks Kummur (Available at Kaggle.com)	The dataset includes URLs having different characteristics such as length and sub-domain, etc.
Backdoor Attack	CIFAR10 Dataset (Available at http://www.cs.toronto.edu/kriz/cifar.html)	The dataset includes 100,000 images of 32×32 dimensions.
Malware Attack	Dataset of malware attack in Microsoft endpoint system	The dataset was created to suit particular business requirements for privacy and the duration of the machine's operation. The information includes machine infections created by merging a threat report from Microsoft Endpoint Protection Solution and Windows Defender.
Cyber Physical Systems Attack	Dataset of attacks (self-generated)	The simulator was used to create a variety of datasets, including normal,

attack, and evaluation datasets. There are four distinct sorts of assaults to consider: Scaling assault, ramp attack, step attack, and random attack.

6. Types of Basic Network Attacks

Fundamental network attacks are described in this section:

6.1 Malicious attacks infiltrate a network and spread malware from compromised devices to other devices on the network. A botnet is a malicious attack in which a group of infected devices connects to the Internet and collaborates to carry out illicit operations [41].

6.2 Insider assaults, also known as insider threats, are hostile threats that originate from within a company. User to root (U2R) attacks on systems occur when an attacker gains access to a user's account and then exploits a vulnerability to get root access. Attackers may also attempt to shut down a service by flooding it with requests. Another insider attack is port scanning, in which unsecured ports are discovered and targeted for future assaults [1].

6.3 Password assaults include a malevolent party acquiring access to someone's password using a variety of methods, such utilizing a dictionary to decrypt an encrypted password or brute force, which involves repeatedly trying multiple usernames and passwords until one of them succeeds [21].

6.4 Distributed assaults target not only a single server or user, but also the network's infrastructure. A backdoor attack, for example, is when an attacker obtains access to a website via a weak entry point, or "back door" [21, 24].

6.5 DDoS (distributed denial of service) or denial of service (DoS) attacks flood a network with requests, preventing other users from accessing network resources such as servers [24].

6.6 Spam attacks use messaging systems to send out large batches of communications that may include phishing techniques [21, 35].

7. Types of DoS attacks

7.1 HTTP flood: This attack is similar to refreshing a web browser on numerous machines at once—a large number of HTTP requests flood the server, resulting in a denial-of-service issue. This is a type of attack that can be simple or complex. To reach the same URL, simpler implementations may use the same range of attacking IP addresses, referrers, and user agents. Complex versions may target random URLs with a large number of attacking IP addresses and random referrers and user agents [43].

7.2 Protocol assaults, also known as state-exhaustion attacks, disrupt service by consuming excessive server resources and/or network equipment resources such firewalls and load balancers [19, 43].

7.3 SYN Flood functions similarly to a supply room employee who takes orders from the front of the store. The employee receives a request, travels to the location, finds the package, and awaits confirmation before delivering it to the consumer. The worker then receives countless further shipping requests without confirmation until they are unable to carry any more parcels, become overburdened, and requests go unanswered. This attack exploits the TCP handshake, the chain of exchanges by which two computers establish a network connection, by sending a large number of TCP "Initial Connection Request" SYN packets to a target with faked source IP addresses. The target computer responds to each connection request and then waits for the final step of the handshake, which never arrives, sapping the resources of the target [1].

7.4 Volumetric attacks try Use all available bandwidth between the target and the rest of the Internet to try to create congestion. Huge volumes of data are sent to a target using amplification or another way of producing large traffic, such as requests from a botnet [32].

8. Conclusions and Future Research

It is concluded that integrating cybersecurity and ML has become crucial to dealing with cyber-attacks and providing maximum security to Internet users. It has become crucial for companies to install high levels of IDS to detect the threat before they penetrate the system, which would jeopardise the whole ICPS of industries. It is concluded that companies need to protect themselves as much as they can by using the maximum effective cyber solutions, which include intrusion detection systems and antivirus. Cyber attackers change their attacks with time, and it is irrational to depend on the installed system permanently. The installed intrusion system must be checked from time to time and updated, as well as advanced security systems considered. Companies need intelligent IDS, based on effective ML to discover the attacks on the system by finding the vulnerable patches as well. IoT devices themselves are vulnerable to cyber-attacks. As we discussed above, attackers also use AI in the attacks to assess the security flaws in a company's system. Signature-based intrusion systems have failed to deal with advanced attacks that intensify the need for an efficient IDS based on ML.

Moreover, we cannot ignore the role of datasets in developing an efficient intrusion system. The datasets to test the algorithms must be selected carefully. The dataset quality plays a vital role in developing the algorithm, as without checking the quality of the algorithm through the datasets, executing the algorithm in real situations would be risky. The quality of the datasets itself depends on several aspects that must be considered while selecting the datasets. They must be updated ones. Therefore, to develop an effective as well as efficient intrusion detection algorithm, the datasets must be selected carefully in terms of their quality.

For future research, if we use public datasets for the evaluation of the model, we can't guarantee that it will work in a real-world setting. As a result, the suggested methodology's greatest difficulty is to be as effective as it was in the lab experiments. After being evaluated in the lab, the suggested approach should be validated in a real-time setting to ensure its suitability for current networks. Private datasets might be utilized as a substitute for the actual world. Because the models were not trained with adequate attack kinds and patterns, the majority of the proposed approaches were unable to identify zero-day assaults. An effective IDS model should be tested and confirmed on a dataset that includes both older and current assaults.

Including as many attack definitions as possible in a dataset, the machine learning model will be able to learn more patterns and, as a result, protect against a greater number of various types of invasions. Dataset construction, on the other hand, is an expensive operation that necessitates a large number of resources and a high level of competence. As a result, one of the IDS research difficulties is the systematic creation of an up-to-date dataset with sufficient examples of practically all attack types. The dataset should be updated on a regular basis to cover the most recent intrusion cases, and it should be made accessible to aid the research community. Furthermore, it is necessary to critically review different public datasets used in testing anomaly detection algorithms. To develop two new anomaly detection algorithms, based on the selected two ML learning methods can be used in a real environment to deal with DoS attacks and cyberattacks.

References

1. Jiang, H., et al., Network intrusion detection based on PSO-XGBoost model. *IEEE Access*, 2020. 8: p. 58392-58401.
2. da Cruz, M.A., et al., A reference model for internet of things middleware. *IEEE Internet of Things Journal*, 2018. 5(2): p. 871-883.
3. Bhattar, P.L., N.M. Pindoriya, and A. Sharma, A combined survey on distribution system state estimation and false data injection in cyber-physical power distribution networks. *IET Cyber-Physical Systems: Theory & Applications*, 2021. 6(2): p. 41-62.
4. Bolomsky, A., et al., Preclinical validation studies support causal machine learning based identification of novel drug targets for high-risk multiple myeloma. *Blood*, 2018. 132: p. 3210.
5. Hua, H., et al., Review of distributed control and optimization in energy internet: From traditional methods to artificial intelligence-based methods. 2021.
6. Hammood, W.A., et al. User Authentication Model based on Mobile Phone IMEI Number: A Proposed Method Application for Online Banking System. in 2021 International Conference on Software Engineering & Computer Systems and 4th International Conference on Computational Science and Information Management (ICSECS-ICOCSIM). 2021. IEEE.

7. Santikellur, P., et al. Optimized multi-layer hierarchical network intrusion detection system with genetic algorithms. in 2019 2nd International Conference on new Trends in Computing Sciences (ICTCS). 2019. IEEE.
8. Ali, A., et al. Network intrusion detection leveraging machine learning and feature selection. in 2020 IEEE 17th International Conference on Smart Communities: Improving Quality of Life Using ICT, IoT and AI (HONET). 2020. IEEE.
9. Khare, N., et al., SMO-DNN: spider monkey optimization and deep neural network hybrid classifier model for intrusion detection. *Electronics*, 2020. 9(4): p. 692.
10. Tang, T.A., et al., DeepIDS: deep learning approach for intrusion detection in software defined networking. *Electronics*, 2020. 9(9): p. 1533.
11. Kim, J., et al., CNN-based network intrusion detection against denial-of-service attacks. *Electronics*, 2020. 9(6): p. 916.
12. Hasan, A.M., et al. A Combined Weighting for the Feature-Based Method on Topological Parameters in Semantic Taxonomy Using Social Media. in IOP Conference Series: Materials Science and Engineering. 2020. IOP Publishing.
13. Hammood, W.A., et al. A Review of User Authentication Model for Online Banking System based on Mobile IMEI Number. in IOP Conference Series: Materials Science and Engineering. 2020. IOP Publishing.
14. Hammood, O.A., et al., The VANET-Solution Approach for Data Packet Forwarding Improvement. *Advanced Science Letters*, 2018. 24(10): p. 7423-7427.
15. Amato, F., et al. Smart intrusion detection with expert systems. in International Conference on P2P, Parallel, Grid, Cloud and Internet Computing. 2018. Springer.
16. Hammood, O.A., et al., RESP: Relay Suitability-based Routing Protocol for Video Streaming in Vehicular Ad Hoc Networks. *International Journal of Computers, Communications & Control*, 2019. 14(1).
17. Meira, J., et al. Comparative results with unsupervised techniques in cyber attack novelty detection. in International Symposium on Ambient Intelligence. 2018. Springer.
18. Hammood, O.A., et al., An effective transmit packet coding with trust-based relay nodes in VANETs. *Bulletin of Electrical Engineering and Informatics*, 2020. 9(2): p. 685-697.
19. Okolie, S., S. Kuyoro, and O. Ohwo, Emerging Cyber-Physical Systems: An Overview. *International Journal of Scientific Research in Computer Science, Engineering and Information Technology*, 2018. 3(8): p. 306-316.
20. Monostori, L., et al., Cyber-physical systems in manufacturing. *Cirp Annals*, 2016. 65(2): p. 621-641.
21. Amin, B.R., et al., Cyber attacks in smart grid—dynamic impacts, analyses and recommendations. *IET Cyber-Physical Systems: Theory & Applications*, 2020. 5(4): p. 321-329.

22. Kukielka, P. and Z. Kotulski, Adaptation of the neural network-based IDS to new attacks detection. arXiv preprint arXiv:1009.2406, 2010.
23. Ahmad, I., et al., Performance comparison of support vector machine, random forest, and extreme learning machine for intrusion detection. IEEE access, 2018. 6: p. 33789-33795.
24. Khraisat, A., et al., Hybrid intrusion detection system based on the stacking ensemble of c5 decision tree classifier and one class support vector machine. Electronics, 2020. 9(1): p. 173.
25. Yavuz, F.Y., Deep learning in cyber security for internet of things. 2018, Fen Bilimleri Enstitüsü.
26. Torres, P., et al. An analysis of recurrent neural networks for botnet detection behavior. in 2016 IEEE biennial congress of Argentina (ARGENCON). 2016. IEEE.
27. Chen, Y., Y. Zhang, and S. Maharjan, Deep learning for secure mobile edge computing. arXiv preprint arXiv:1709.08025, 2017.
28. Fiore, U., et al., Network anomaly detection with the restricted Boltzmann machine. Neurocomputing, 2013. 122: p. 13-23.
29. Diro, A.A. and N. Chilamkurti, Distributed attack detection scheme using deep learning approach for Internet of Things. Future Generation Computer Systems, 2018. 82: p. 761-768.
30. Canedo, J. and A. Skjellum. Using machine learning to secure IoT systems. in 2016 14th annual conference on privacy, security and trust (PST). 2016. IEEE.
31. Yousefi-Azar, M., et al. Autoencoder-based feature learning for cyber security applications. in 2017 International joint conference on neural networks (IJCNN). 2017. IEEE.
32. McLaughlin, N., et al. Deep android malware detection. in Proceedings of the seventh ACM on conference on data and application security and privacy. 2017.
33. Shi, C., et al. Smart user authentication through actuation of daily activities leveraging WiFi-enabled IoT. in Proceedings of the 18th ACM International Symposium on Mobile Ad Hoc Networking and Computing. 2017.
34. Nguyen, D.C., et al., Secure computation offloading in blockchain based IoT networks with deep reinforcement learning. IEEE Transactions on Network Science and Engineering, 2021. 8(4): p. 3192-3208.
35. Karatas, G. and O.K. Sahingoz. Neural network based intrusion detection systems with different training functions. in 2018 6th International Symposium on Digital Forensic and Security (ISDFS). 2018. IEEE.
36. Dong, B. and X. Wang. Comparison deep learning method to traditional methods using for network intrusion detection. in 2016 8th IEEE international conference on communication software and networks (ICCSN). 2016. IEEE.

37. Garcia, S., et al., An empirical comparison of botnet detection methods. *computers & security*, 2014. 45: p. 100-123.
38. Hammood, W.A., K.Z. Zamil, and A.M. Ali, A Review of Bio-inspired Algorithm.
39. Arshah, R.A., W.A. Hammood, and A. Kamaludin, An Integrated Flood Warning and Response Model for Effective Flood Disaster Mitigation Management. *Advanced Science Letters*, 2018. 24(10): p. 7819-7823.
40. Kuzlu, M., C. Fair, and O. Guler, Role of artificial intelligence in the Internet of Things (IoT) cybersecurity. *Discover Internet of things*, 2021. 1(1): p. 1-14.
41. Vimal, S., et al., Deep learning-based decision-making with wot for smart city development, in *Smart Innovation of Web of Things*. 2020, CRC Press. p. 51-62.
42. A Hammood, W., et al., A systematic review on flood early warning and response system (FEWRS): a deep review and analysis. *Sustainability*, 2021. 13(1): p. 440.
43. Tchakoucht, T.A. and M. Ezziyyani, Building a fast intrusion detection system for high-speed-networks: Probe and dos attacks detection. *Procedia Computer Science*, 2018. 127: p. 521-530.

**STUDY AND OPTIMIZATION OF ELECTRO-FENTON TECHNOLOGY TO
REDUCE COD IN REFINERY WASTEWATER USING MODIFIED
ELECTRODES WITH PbO_2 AND GRAPHENE BY THE TAGUCHI
APPROACH**

Rowaida N. Abbas ^a and Ammar S. Abbas ^b

*Chemical Engineering Department, College of Engineering, University of
Baghdad, Baghdad, Iraq*

- a) rowida.abbas1307d@coeng.uobaghdad.edu.iq
b) Corresponding author: ammarabbas@coeng.uobaghdad.edu.iq

Abstract

This study investigates organic pollutants degradation by electrochemical advance oxidation technique in a batch reactor cell consisting of graphite anode modified by electrodeposition of PbO_2 and carbon fiber cathode modified by graphene. The experiment was designed by the Taguchi design approach with an orthogonal array of L_{18} runs to study and optimize the degradation of chemical oxygen demand (COD) by the electro-Fenton oxidation process. Four process parameters (current density (CD), temperature (T), Fe^{2+} concentration (Fe^{2+}), and time (t)) at different levels were measured for this design. The impact of each factor on the process performance was analyzed by Analysis of variance (ANOVA). Furthermore, a linear model analysis was applied for the signal to noise (S/N) ratios with "larger the better" and means. The optimum condition is obtained from the S/N ratio and means. The most significant parameter of the COD removal efficiency was time, and the least one was temperature.

Keywords: Organic pollutants; Taguchi; electro-Fenton; COD removal

Introduction

Wastewater from the oil industry will frequently be produced and discharged into the world's main water bodies, causing serious environmental issues. The amount and characteristics of pollutants in refinery wastewater depend on the type of oil being processed, the plant configuration, operation procedures, and the processing unit type in the petroleum refinery [1].

Pollutants in refinery wastewater often consist of free hydrocarbons, suspended solids, and inorganic, with a high concentration of salts, sulphides, ammonia, organic carbon, phenol, benzene, heavy metal, and nutrient grease and chemical additives [2], [3]. Among them, phenol is the most produced contaminant in the refinery industry. It is the worst pollutant of surface and ground waters that causes harmful effects on modern health-quality standards and restricts the environmental rules [4]–[7]. Phenol and its derivatives are highly soluble in water, so they can be present in a wide range of water concentrations from a few milligrams per liter to high concentrations that reach 7000 mg/L; refineries contribute about (6–500 mg/l). The phenolic compounds persist in water or transform various reactions like chlorination and methylation into more harmful and toxic material than phenol itself, like chlorophenols and cresols [8].

Phenol is classified as one of the most harmful pollutants identified by the Environmental Protection Agency (EPA) and the European Agency (EU) that causes noxiousness to humans and the environment [9]. Phenol can cause

poisonousness to humans by skin contact, inhalation, or ingestion. Phenol vapors cause severe irritation to the eyes and mucous. Other serve symptoms caused by exposure to phenol include fatigue, headache, loss of consciousness, nausea and vomiting. Exposure to phenol for long time can change blood pressure, leads to liver and kidney damage and cause a bad effect on the nervous system [10].

Phenol and phenolic compound can be treated by several methods such as adsorption [11], biological treatments [12], coagulation/flocculation [13], chemical oxidation [14], ion exchange [15], and electrochemical oxidation processes [16]. Adsorption is limited by adsorber, and adsorber cannot be renewable easily, need regeneration after a period of use, and the pollutant is not converted to less hazardous materials. Still, it is concentrated and transferred to a vapor or an organic phase [17]. Biological treatment related with many problems that concern the operation condition, which contains providing suitable environment for the microorganisms, the low settleability of the sludge because of the low ratio of food to microorganism, making polymers consisting of lipids, proteins and carbohydrates that affected negatively on the sludge settling, poisoning the microorganisms due to the toxic compounds which needs very long times to acclimatization and start up [18], [19].

Coagulation needs the junction of non-reusable chemicals (coagulants, flocculants, aid chemicals); they require physical and chemical monitoring of the effluent (pH), and the volume of the sludge generated is increased, and the needed management and cost for treated contaminates [13], [20].

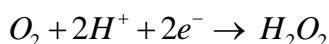
Chemical oxidation like simple oxidation, ozonation, and hypochlorite treatment considers completed physical and chemical treatments. Still, these process chemicals are needed, and thereby, they require production, transportation, and managing with the necessary oxidants for the pre-treatment step; the type of oxidant directly affects the efficiency of the process. The creation of intermediates that may be toxic more than the treated substance has a limited effect on chemical oxygen demand, aromatic compounds, and volatile substances, especially when using hypochlorite, and the formation of sludge [14], [21]. Ion exchange technology needs high initial cost of the selective resin, maintenance costs, regeneration time-consuming, needed large equipment if there is a large volume of wastewater to be treated, beads easily fouled by organic matter that requires a physicochemical pre-treatment to remove these pollutants, not effective for organic target pollutants [15].

At this time, electrochemical treatment is one of the cleaners and eco-friendly methods used as an alternative to other treatment processes for environmental protection. Electrochemical technology is one of the promising

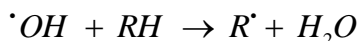
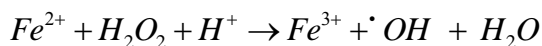
technologies for treating organic pollutants in refinery wastewater. These technologies include electrocoagulation-electroflotation, anodic oxidation, electrochemical reduction, and electrochemical advanced oxidation processes [22], [23]. Electrochemical methods are not needed to add a lot of chemical reagents because the leading reagent used is the electron, and it is considered a clean reagent. These processes can also remove contaminants from even a massive quantity of different phases of polluted streams and require lower temperature and pressure than other non-electrochemical processes. Many electrochemical processes are of high selectivity, which prevents the formation of unwanted by-products because the potential that is applied can be controlled, which helps to attack specific bonds. The chemical substances that are added in electrochemical processes are small and safe. Electrochemical processes flexibly operate and control process, and the equipment used in it is simple and inexpensive[16], [23], [24].

Electrochemical oxidation processes are popular electrochemical processes for treating organic pollutants in refinery wastewater, and it is classified as direct and indirect oxidation processes. Direct oxidation occurs on the anode electrode surface, and indirect oxidation uses an oxidizing mediator that contributes to force the organic matter to contribute to the oxidation reaction, such as hypochlorite [25], chlorine [26], and hydrogen peroxide (H_2O_2) [27].

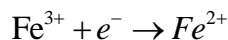
The electro-Fenton oxidation process is one of the indirect advanced oxidation processes that use the electro-generated hydroxyl radical ($\bullet OH$) on the surface of the electrodes, which has a high oxidation capability in the oxidation of organic substances [28]. In the electro-Fenton oxidation process, ferrous ion (Fe^{2+}) is added externally, and H_2O_2 is generated electrochemically in-situ on specific electrodes that have appropriate cathodic potential by a two-electron reduction of oxygen (Eq. 1) [29].



The electricity used in electro-Fenton oxidation processes is clean and contaminated-free, so these processes are eco-friendly and do not generate secondary pollutants. ($\bullet OH$) generated in the solution by using (Fe^{2+}) as a catalyst (Eq. 2), and this attacks the organic contaminants (Eq. 3) [29].



Fe^{3+} ion that produced in (Eq. 2) can be transform to Fe^{2+} by one-electron reduction reaction (Eq. 4) [29].



The electrode material is a leading factor affecting the electro-Fenton oxidation performance as it affects the selectivity, efficiency, mechanism, and the products of the oxidation process [2], [30]. So, when choosing the electrode, material-specific properties must consider its; electrical conductivity, selectivity, catalytic activity, cost, lifetime, and oxygen overvoltage [30]. The effect of the cathodic reaction on the efficiency of the overall oxidation process is also taken into account [30], [31].

Carbon electrodes are widely used as anodes and cathodes in electro-Fenton processes. It has a high surface, high porosity, resists corrosion, and offers low-pressure drops compared with other materials as it has high space. Examples of these electrodes are graphite[32]–[34], reticulated vitreous carbon[35], activated carbon fiber[36], carbon nanotube[37].

This study investigates the electro-Fenton oxidation process of Phenol and its derivatives in refinery wastewater by using the Taguchi approach. The process was carried out in a batch reactor cell consisting of graphite anode modified by electrodeposition of PbO_2 film on its surface and carbon fiber cathode modified by graphene. Different operating conditions were used in the oxidation process, and the effect of each of these parameters on the COD removal was also studied.

Experimental Work

Design of Experiment

Taguchi experimental design was used to examine the effect of several factors on the response characteristic with a minimum number of experiments by using the technique of orthogonal array. The studied parameters were three operating temperatures (15, 25, 35 °C), three current density (2, 5, 8 mA/cm²) and three concentrations of Fe^{2+} (0.1, 0.2, 0.4 mM) and 6 hours of electrolysis. Three levels were investigated for each current density, temperature, and (Fe^{2+}) concentration, and six levels for time and their interaction, as shown in Table (1).

Table 1 Control parameters and levels

Control parameters	Levels
Temperature (°C)	15, 25, 35

Current density (mA/cm ²)	2, 5, 8
Fe ²⁺ concentration(mM)	0.1, 0.2, 0.4
Time (h)	1, 2, 3, 4, 5,6

The orthogonal array layout of L₁₈ (3³×6¹) used in this study is presented in Table 2. The notation 3³ denotes 3 parameters studied on 3 different levels, and the notation of 6¹ represents one of the parameters investigated on 6 levels. Later, the Taguchi parameter design identifies the best-operating levels that lead to a high performance of COD removal. Investigate which factor has the most increased significant effects on the efficiency of the process and which one has the smallest impact. A mathematical relation between the process parameters and the output is also employed by using regression analysis.

Table 2 Layout of L₁₈ (3³×6¹) experimental design

No	Time, h	CD, mA/cm ²	T, °C	Fe ²⁺ , mM
1	1	2	15	0.1
2	1	5	25	0.2
3	1	8	35	0.4
4	2	2	15	0.2
5	2	5	25	0.4
6	2	8	35	0.1
7	3	2	25	0.1
8	3	5	35	0.2
9	3	8	15	0.4
10	4	2	35	0.4
11	4	5	15	0.1
12	4	8	25	0.2
13	5	2	25	0.4
14	5	5	35	0.1
15	5	8	15	0.2
16	6	2	35	0.2
17	6	5	15	0.4
18	6	8	25	0.1

Electro-Fenton Oxidation Process

The aqueous solution was prepared to simulate the organic pollutants in al-Dora refinery wastewater (150 ppm). Electro-Fenton oxidation process used to treat phenolic compound and carried out in an open undivided cell equipped with anode and cathode with 3 cm distance between them. The volume of the treated solution was 0.4 L. PbO₂ deposit on graphite was used as anode in the process, and carbon fiber was modified by graphene as a cathode. A rotation of 200 rpm was achieved in the treated solution using a magnetic stirrer with a heating plate (LABINCO, model L-81). Compressed air was bubbled into the treated solution at a 1 L/ min flow rate using an electromagnetic air pump (ACO-001). The electrolysis process for the treated solution was carried out at three different operating temperatures (15, 25, 35 °C ± 1 °C). The pH of the treated solution was adjusted to 3 by adding 1M H₂SO₄ to maximize the production of H₂O₂. The experiments were carried out by applying different CD 2, 5, and 8 mA/cm² by using a DC power supply (KORAD KA3005D). FeSO₄·7H₂O was added externally as a catalyst with different concentrations of 0.1, 0.2, and 0.4 mM. Sodium sulfate (Na₂SO₄) was used as a supporting electrolyte with a concentration of 0.05 M to enhance the solution conductivity. The electrolysis was carried out for up to 6 h, and samples were collected after each 1 h to check the degradation efficiency by COD analysis. COD removal (%) was calculated using Eq. (5).

$$\text{COD removal, \%} = \frac{\text{COD}_o - \text{COD}_t}{\text{COD}_o} \times 100$$

COD_o and COD_t were the initial COD and the COD concentration at time t in (mg/L), respectively.

Results and Discussion

Taguchi Design Analysis for COD Removal

The effect of the most influencing parameters on the organic pollutants removal was investigated by applying Taguchi experimental design (TED). The process operating parameters obtained from this design in the L18 (33×61) orthogonal array has been carried out. The phenol and COD removal by electro-Fenton oxidation process calculated from (Eq. 5) are listed in Table 3 .

Table 3 Taguchi experimental design of L18 (33×61) standard orthogonal array, phenol and COD removal and S/N ratios corresponding to each parameters sets

No	Time, h	CD, mA/cm ²	Temp., °C	Fe, mM	Phenol removal, %	S/N	COD removal, %	S/N
1	1	2	15	0.1	37.27	31.43	33.52	30.51
2	1	5	25	0.2	47.34	33.50	43.62	32.79
3	1	8	35	0.4	54.87	34.79	51.78	34.28
4	2	2	15	0.2	51.31	34.20	48.32	33.68
5	2	5	25	0.4	57.34	35.17	57.32	35.17
6	2	8	35	0.1	60.11	35.58	52.34	34.38
7	3	2	25	0.1	58.74	35.38	50.87	34.13
8	3	5	35	0.2	67.83	36.63	67.81	36.63
9	3	8	15	0.4	73.54	37.33	68.75	36.75
10	4	2	35	0.4	79.32	37.99	73.64	37.34
11	4	5	15	0.1	75.47	37.56	60.87	35.69
12	4	8	25	0.2	78.74	37.92	69.78	36.87
13	5	2	25	0.4	80.37	38.10	75.41	37.55
14	5	5	35	0.1	79.43	38.00	73.65	37.34
15	5	8	15	0.2	83.47	38.43	79.36	38.00
16	6	2	35	0.2	86.47	38.74	82.32	38.31
17	6	5	15	0.4	89.34	39.02	82.89	38.37
18	6	8	25	0.1	93.43	39.41	84.72	38.56

The experimental data were analyzed using MINITAB 19 software to analyze the data obtained from the experiment. Taguchi method uses a signal-to-noise ratio S/N to evaluate the optimum removal conditions and determine the response variation about the mean value that causes experimental noise. It uses it to recognize the levels of controlling factors that minimize the response variance from noise factors. The quantitative measure S/N ratio refers to the mean of the output value (desired value) to the standard deviation of the output value (undesired value) [38]. S/N ratio can be divided into three categories: smaller the better characteristics (STB), nominal the better characteristic (NTB), and larger the better characteristics (LTB). Depending on the experimental process goal and the empathetic of the process quality characteristic looked for, the type of the S/N ratio has been chosen. For example, the (LTB) characteristic signal-to-noise ratio has been selected to maximize the efficiency of the phenol and COD removal. The (LTB) response can be evaluated by the standard formula for this type of characteristic Eq. (6)[39], [40].

$$\left(\frac{S}{N}\right)_i = -10 \log \frac{1}{n} \sum_{j=1}^n \frac{1}{Y_{ij}^2}$$

Where i is trail number, Y_{ij} represents the response of the measured value for ith trial and jth run, and n is the number of replications for the experimental combination. Generally, the highest value of S/N ratio is preferable. Table 3 shows Taguchi's experimental design with the obtained responses (COD reduction) and S/N ratio.

Figure (1) represents a plot of S/N ratio against CD, T, Fe^{2+} , and t. The main effects plot (Figure 2) for means represents the relationship between the operating parameter under study and the obtained response.

The results that are plotted in Figures (1) and (2), represented in tables (4) and (5), respectively, showed the effect of each operating parameter on COD removals. Ranks in these tables are based on delta statistics. Delta statistics equal the difference between the highest and lowest average for each factor. The highest delta value assigned by Rank 1 followed by Rank 2 is the second-highest delta value and so on [41].

The values of delta in tables (4) and (5) indicate that the time of experiment has the most significant effect on the COD removals. The second parameter influences the COD removal is Fe^{2+} concentration, followed by current density, and the temperature has the lowest impact on COD removals.

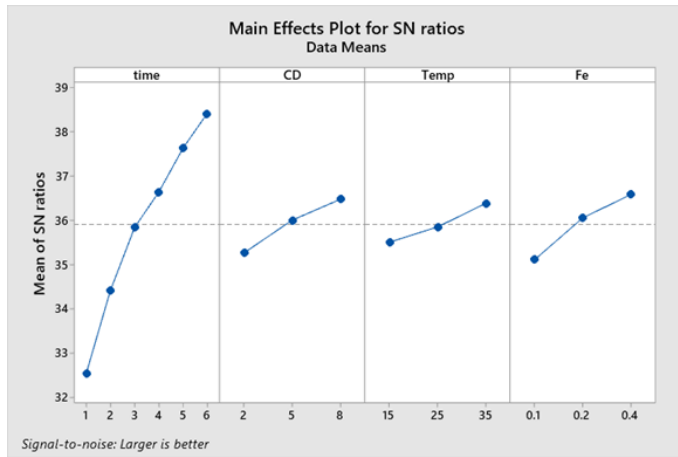


Fig. 1. Main effects plot for S/N ratios

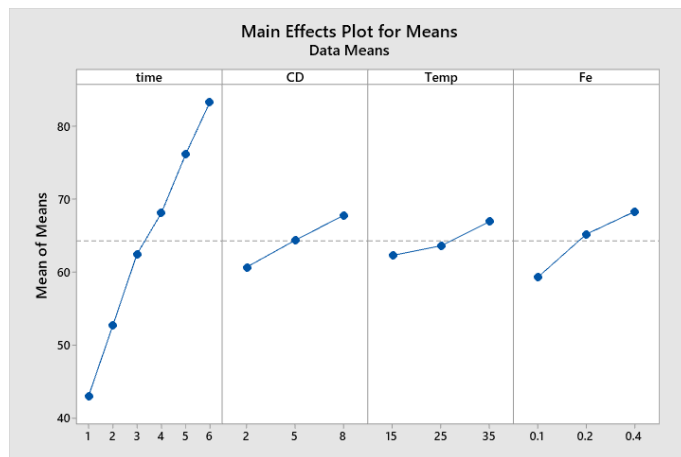


Fig. 2. Main effects plot for means

Table 4 Response Table for Signal to Noise Ratios for COD removal (Larger is better)

Level	Time, h	CD, mA/cm ²	Temp., °C	Fe, mM
1	32.53	35.25	35.50	35.10
2	34.41	36.00	35.85	36.05
3	35.83	36.47	36.38	36.58
4	36.63	-	-	-
5	37.63	-	-	-
6	38.41	-	-	-
Delta	5.89	1.22	0.88	1.48

Rank	1	3	4	2
------	---	---	---	---

Table 5 Response Table for Means for COD removal

Level	Time, h	CD, mA/cm ²	Temp., °C	Fe, mM
1	42.97	60.68	62.28	59.33
2	52.66	64.36	63.62	65.20
3	62.48	67.79	66.92	68.30
4	68.10	-	-	-
5	76.14	-	-	-
6	83.31	-	-	-
Delta	40.34	7.11	4.64	8.97
Rank	1	3	4	2

Analysis of Variance for Means and S/N Ratio (ANOVA)

The orthogonal array in Taguchi experiments contributes to each process parameter on the process response. ANOVA is used to show which parameters have the most significant effect on the process and to find out the percentage contribution of each parameter to changing the value of the dependent parameter [42]. The order of significance of the process variables is identified easily by using ANOVA because it is accomplished to calculate the source of the variation during the process [43].

The ANOVA table involves the degree of freedom (DF), The sequential sum of squares (Seq SS), the adjusted sum of squares (Adj SS), the adjusted mean of squares (Adj MS), F-value, and P-value.

These terms are defined in many handbooks as statistical expressions and studied and analyzed with experimental design. These factors showed the importance of each parameter on the process performance [44]. A small variation in any process variable with an excellent contribution percent will greatly influence the process performance. A portion of the total variance detected in the experiment for each effecting parameter is the percent contribution. So, the factor of the greater value of percentage contribution contributes more than other factors to the process's final results [45].

Each element in the ANOVA table is explained below [46].

- Source: The source of the variance can be factors, interactions, and errors. The total refers to the sum of all variance sources.
- DF: The degree of freedom for each source refers to the parameter number-1 (No. of levels -1).
- SS: The squares sum between groups or factors, and the sum of the squares within groups or errors.
- MS: The mean square of each source is equal to the sum of squares divided by the degree of freedom.
- F: This value is evaluated by dividing the mean square variance between groups by the mean square variance within-group ((**MS**)/ (error **MS**)). The statistical significance of each source in the ANOVA table can be evaluated by comparing the F value with a critical one in the same Table. P-value also can be used for the same purpose.
- P: This value is used to determine the significance of each factor statistically.

Tables 6 and 7 showed that the highest sum of square (SS) value went to time 't', which has the most significant effect on the COD removal. These tables also showed that the statistical significance of the mentioned factors is as follows, Fe²⁺, CD, and T based on p-values. The variable time has the most significant factor in the phenol and COD removal, and its degree of freedom is 5. The least important factor on the processes is T, and the degree of freedom for the variables CD, T, and Fe²⁺ is 2, so the total degrees of freedom for all sets of variables is 17. Generally, when F value is greater than 4, this indicates that the change in the studied parameter significantly affects the process performance [38]. It is clear from the results of F value represented in all tables that all the factors (time, current density, ferrous ion concentration, and temperature) significantly affect COD removal by the electro-Fenton oxidation process since F values are > 4.

Also, the significance of process factors by using a p-value indicates that when the p-value is less than 0.05, the process parameter significantly affects the quality characteristic [38]. So, from the p-value results in the Table, the time has the most significant parameter on the removals, followed by Fe²⁺ concentration, current density, and temperature is the minor important parameters on the phenol and COD removals.

Table 6 Analysis of Variance for S/N ratios of COD removal

Source	DF	Seq SS	Adj SS	Adj MS	F	P
Time	5	70.3327	70.3327	14.0665	104.65	0.000

CD	2	4.5298	4.5298	2.2649	16.85	0.003
Temp	2	2.3735	2.3735	1.1868	8.83	0.016
Fe ²⁺	2	6.7040	6.7040	3.3520	24.94	0.001
Residual Error	6	0.8065	0.8065	0.1344	---	---
Total	17	84.7465	---	---	---	---

Table 7 Analysis of Variance for Means of COD removal

Source	DF	Seq SS	Adj SS	Adj MS	F	P
Time	5	3328.85	3328.85	665.771	84.30	0.000
CD	2	151.65	151.65	75.824	9.60	0.013
Temp	2	68.42	68.42	34.208	4.33	0.069
Fe ²⁺	2	249.09	249.09	124.546	15.77	0.004
Residual Error	6	47.38	47.38	7.897	---	---
Total	17	47.38	----	----	----	---

The adequacy of the results from the model and meeting the assumption of the analysis can be evaluated by using residual plots that are random and normally distributed. The various residual plots are 'histogram of residuals', 'normal probability plot', 'residual fit', and 'residual order'. Figure 3 shows the residual plot for COD removals in a four-in-one block layout; it shows the following.

- Histograms showed that the data are not skewed, and there are no outliers.
- Normal probability plots showed that the data are distributed normally, the factors are employing the response, and there are no outliers in the data.
- Residuals versus order showed that there are methodical influences in the data because of the time or the order of collection data.
- Residuals versus fitted data showed that there is constant variance, and the relationships are non-linear. In the ideal case, the data points should drop around the zero line randomly.

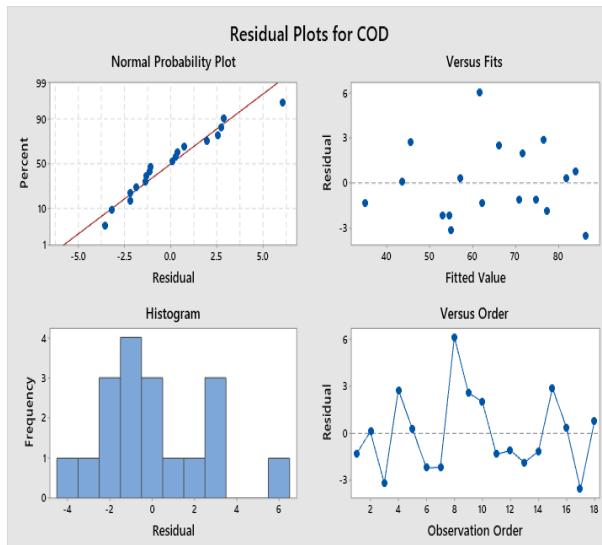


Fig.3. Residual plots of COD removal

Multiple Regression Model and Optimization

The equations that describe the multiple regression model for COD removals that examine the effect of process variables on the process response was as Eq. (7).

$$COD_{removal}, \% = 11.08 + 7.936X_1 + 1.185X_2 + 0.2319X_3 + 102.0X_4 - 144.2X_4^2 \quad (7)$$

Where X_1 is time of experiment (h), X_2 is CD (mA/cm^2) X_3 is Temp. ($^{\circ}\text{C}$) and X_4 is Fe^{2+} (mM).

The squared value of the correlation coefficient (R^2) for the predicted equation was 98.07 %.

Figure (4) shows the optimum conditions for these experimental designs. Obviously, from this figure, the optimum conditions approve with the optimums obtained from the analysis of S/N ratio previously.

All four factors are affected COD removals efficiency. The most influential parameter is time, followed by ferrous ion concentrations and current density, and the least effective parameter on the process efficiency is temperature.

The optimization for COD removal is shown in the optimization plot (Figure 5). The obtained result confirms those obtained from S/N ratio and means analysis results. All these results indicate that the combination of the parameters (Temperature = 35 °C, Fe²⁺ = 0.4 mM, CD= 8 mA/cm² and t= 6 hr.) give the highest response.

Finally, the regression equations obtained from experimental design and analysis were utilized to observe the effect of the process variables on COD removal by the electro-Fenton oxidation process.

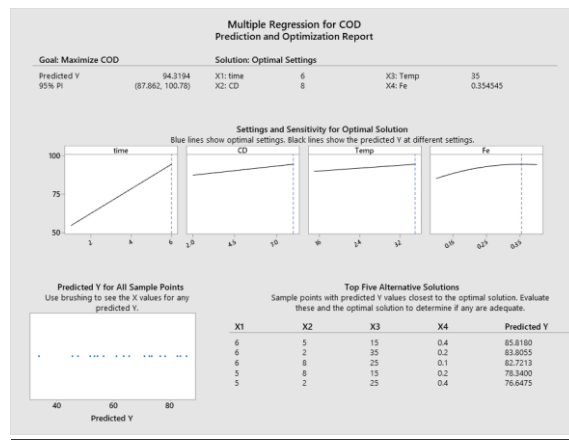


Fig.4. Prediction and optimization report for COD removal

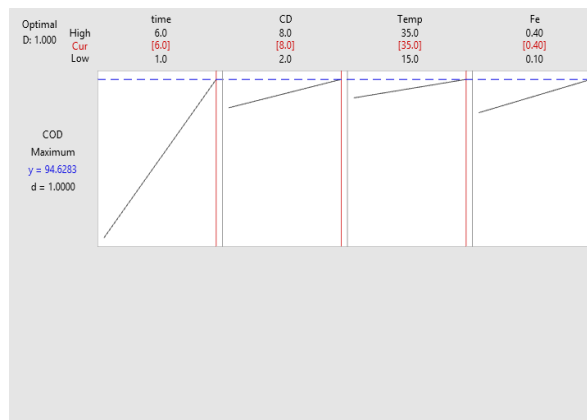


Fig.5. Response optimization plots for COD removal

The Impact of Operating Parameters on COD Removal

The Effect of CD

The effect of current density on COD removal from simulated wastewater studied by electro-Fenton oxidation process at a temperature of 35 °C, ferrous ion concentration ($\text{Fe}^{2+} = 0.4 \text{ mM}$), supporting electrolyte consisted of sodium sulfate ($\text{Na}_2\text{SO}_3 = 50 \text{ mM}$), solution pH at 3 and applied CD ranging from 2 to 8 mA/cm^2 . Figure (6) represents the effect of current density on COD removal, and it presents that the COD removals were 86.9, 89.28, 91.65, and 94.02% at 2, 4, 6, and 8 mA/cm^2 respectively, after 6 hours of electrolysis. Increasing CD from 2 to 8 mA/cm^2 improves the rate of organic pollutants degradation.

Increase in organic degradation with current density due to an increase in H_2O_2 amount that was generated electrochemically through the electrolysis. When the amount of hydrogen peroxide increases, $\bullet\text{OH}$ increases enough to react with the organics pollutants that existed in the treated solution, leading to minimizing the COD values [47], [48]. Our results agree with the results of other researchers of previous works [49] [2], where they treated organic wastewater by electro-Fenton oxidation process and removed about 87.35% of COD after 6 h and 95% of TOC after 8 h of electrolysis, respectively.

The Effect of Fe^{2+} Concentration

The effect of the concentration of Fe^{2+} on the performance of the electro-Fenton oxidation process of COD removal from simulated wastewater studied at a Temperature of 35 °C, 8 mA/cm^2 CD, 50 mM of Na_2SO_3 , and the pH of the solution was 3. Fe^{2+} added to the system was externally considered an important parameter influencing the performance of the electro-Fenton oxidation process. The reaction rate increases with increasing the concentration of Fe^{2+} up to a limiting value, and increasing the concentration over this value will decrease the organic degradation because of the scavenging reactions [50], [51]. Figure (7) showed that the COD removal were 81.03, 85.05, 90.92 and 94.02 % at 0.05, 0.1, 0.2 and 0.4 mM of Fe^{2+} respectively. Increasing Fe^{2+} leads to increased organic degradation because of the increased amount of $\bullet\text{OH}$ radicals produced [52]. The results showed that ferrous ion concentration greatly affects the removals, especially on COD, proved that the Electro-Fenton oxidation process was largely influenced by reaction conditions in the bulk solution between Fe^{2+} and H_2O_2 , not upon the electrochemical reactions on the electrode surface [53].

Our results agree with other researchers [53], who reach a COD removal efficiency of 95.9% by using 0.7 mM FeSO₄ concentration and 25 mA/cm² CD.

The Effect of Temperature

The effect of operating temperature on COD removals from simulated wastewater was investigated at 8 mA/cm² current density, 0.4 mM of Fe²⁺, and 50 mM of Na₂SO₃ as supporting electrolyte, and the solution pH was adjusted initially at 3. Sometimes increasing temperature will lead to an increase in the degradation performance.

Choosing an optimum temperature is essential because a further increase in temperature is not needed and depends on the system.

Figures (8) present the effect of temperature on the COD removal and show that the removals were 89.38, 91.70, and 94.02 % at 15, 25, and 35 °C. Increasing the process temperature leads to a slight increase in organic pollutants degradation by the electro-Fenton oxidation process because raising the temperature promotes the generation of ferrous ion Fe²⁺ [54]. Our results agree with the temperature behavior reported so far by many researchers found that temperature increase in improving the organic degradation by the electro-Fenton oxidation process is relatively low compared with other factors [55], [56].

Also, many researchers found that the best range of operating temperature is (25-35 °C) because temperatures lower or higher than the range are of negative impact on the removal efficiency. Lower temperature causes slower process initial kinetic and reduces the degradation performance and reaction rate.

Higher temperatures were also of unfavorable influence on COD removals because the floccule may be damaged at high temperatures [55], [56].

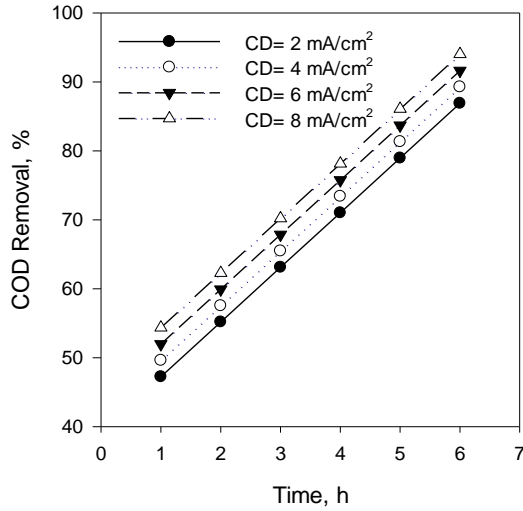


Fig.6. The effect of applied current density on COD removal from phenolic wastewater, Temperature = 35 °C, $Fe^{2+} = 0.4 \text{ mM}$, $Na_2SO_3 = 50 \text{ mM}$, pH = 3

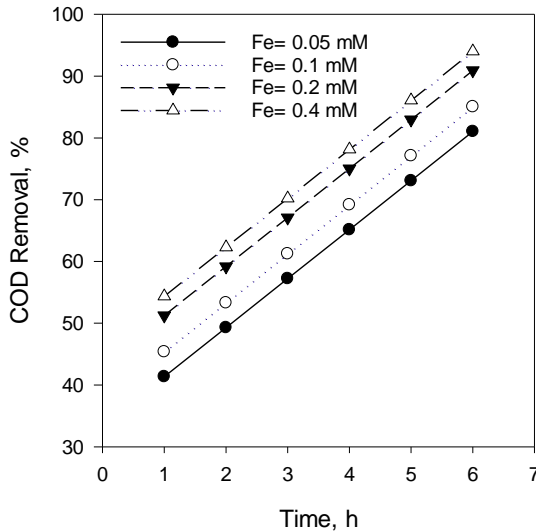


Fig.7. The effect of Fe^{2+} concentration on the COD removal from phenolic wastewater, Temperature = 35 °C, current density = 8 mA/cm², $Na_2SO_3 = 50 \text{ mM}$, pH = 3

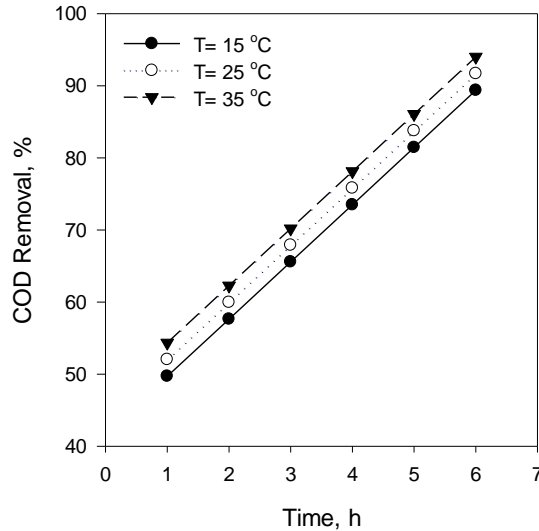


Fig.8. The effect of operating temperature on COD removal from phenolic wastewater, current density = 8 mA/cm^2 , $\text{Fe}^{2+} = 0.4 \text{ mM}$, $\text{Na}_2\text{SO}_3 = 50 \text{ mM}$, $\text{pH} = 3$

Conclusions

The impact of the process parameters on the COD degradation process by the electro-Fenton oxidation technique was studied by using Taguchi experimental design method. This experimental design was achieved by using the L_{18} orthogonal array technique. The effect of the variable parameters on the COD removal was studied by choosing four factors: CD, T, Fe^{2+} , and t. From linear model analysis for S/N ratios and means, the optimum condition was obtained. The optimum operating condition for the reduced COD was a temperature of $35 \text{ }^\circ\text{C}$, the current density of 8 mA/cm^2 , Fe^{2+} concentration of 0.4 mM , and 6 h of electrolysis. COD removal at the optimum operating condition is 94.02% . The time of process variables has the most significant effect on COD reduction efficiency, and the temperature has the lowest impact. The highest removal of COD by electro-Fenton oxidation technique obtained at the optimum condition was 98.07% . Electro-Fenton oxidation process of Organic pollutants largely influenced by the bulk conditions like Fe^{2+} concentration as electro-Fenton process occur in the bulk between Fe^{2+} and H_2O_2 not at the electrode surface. Increasing in optimum operating temperature is important because it will improve the generation of Fe^{2+} but further increase is not important.

References

- [1] B. H. Diya'Uddeen, W. M. A. W. Daud, and A. R. Abdul Aziz, "Treatment technologies for petroleum refinery effluents: A review," *Process Saf. Environ. Prot.*, vol. 89, no. 2, pp. 95–105, 2011, doi: 10.1016/j.psep.2010.11.003.
- [2] Y. Yavuz, A. S. Koparal, and Ü. B. Ögütveren, "Treatment of petroleum refinery wastewater by electrochemical methods," *Desalination*, vol. 258, no. 1–3, pp. 201–205, 2010, doi: 10.1016/j.desal.2010.03.013.
- [3] D. S. Ibrahim, "Electrochemical Oxidation Treatment of Petroleum Refinery Effluent," *Int. J. Sci. &Engineering Res.*, vol. 4, no. 8, pp. 0–5, 2013, doi: 10.14299/00000.
- [4] C. B. Molina, J. A. Casas, J. A. Zazo, and J. J. Rodr, "A comparison of Al-Fe and Zr-Fe pillared clays for catalytic wet peroxide oxidation," vol. 118, pp. 29–35, 2006, doi: 10.1016/j.cej.2006.01.007.
- [5] A. S. Abbas, M. H. Hafiz, and R. H. Salman, "Indirect Electrochemical Oxidation of Phenol Using Rotating Cylinder Reactor," *Iraqi J. Chem. Pet. Eng.*, vol. 17, no. 4, pp. 43–55, 2016.
- [6] H. Wake, "Oil refineries: A review of their ecological impacts on the aquatic environment," *Estuar. Coast. Shelf Sci.*, vol. 62, no. 1–2, pp. 131–140, 2005, doi: 10.1016/j.ecss.2004.08.013.
- [7] S. Uzoekwe and F. Oghosanine, "The Effect of Refinery and Petrochemical Effluent on Water Quality of Ubeji Creek Warri, Southern Nigeria.," *Ethiop. J. Environ. Stud. Manag.*, vol. 4, no. 2, 2011, doi: 10.4314/ejesm.v4i2.12.
- [8] M. J. González-Muñoz, S. Luque, J. R. Álvarez, and J. Coca, "Recovery of phenol from aqueous solutions using hollow fibre contactors," *J. Memb. Sci.*, vol. 213, no. 1–2, pp. 181–193, 2003, doi: 10.1016/S0376-7388(02)00526-4.
- [9] A. Medel, E. Bustos, K. Esquivel, L. A. Godínez, and Y. Meas, "Electrochemical incineration of phenolic compounds from the hydrocarbon industry using boron-doped diamond electrodes," *Int. J. Photoenergy*, vol. 2012, 2012, doi: 10.1155/2012/681875.
- [10] L. N. Bujanović, M. Čekerevac, M. Zdravković, and M. S. Č. Đoković, "Application of electrochemically synthesized ferrate (VI) in the treatment

- of phenol contaminated wastewater from food industry,” *ACTA Tech. CORVINIENSIS– Bull. Eng.*, vol. 10, no. 1, pp. 39–42, 2017.
- [11] I. Polaert, A. M. Wilhelm, and H. Delmas, “Phenol wastewater treatment by a two-step adsorption-oxidation process on activated carbon,” *Chemie-Ingenieur-Technik*, vol. 73, no. 6, p. 764, 2001, doi: 10.1016/S0009-2509(02)00034-9.
- [12] R. D. Tyagi, F. T. Tran, and A. K. M. M. Chowdhury, “Performance of RBC coupled to a polyurethane foam to biodegrade petroleum refinery wastewater,” *Environ. Pollut.*, vol. 76, no. 1, pp. 61–70, 1992, doi: 10.1016/0269-7491(92)90117-S.
- [13] F. Renault, B. Sancey, P. M. Badot, and G. Crini, “Chitosan for coagulation/flocculation processes - An eco-friendly approach,” *Eur. Polym. J.*, vol. 45, no. 5, pp. 1337–1348, 2009, doi: 10.1016/j.eurpolymj.2008.12.027.
- [14] E. Forgacs, T. Cserháti, and G. Oros, “Removal of synthetic dyes from wastewaters: A review,” *Environ. Int.*, vol. 30, no. 7, pp. 953–971, 2004, doi: 10.1016/j.envint.2004.02.001.
- [15] S. D. Alexandratos, “Ion-Exchange resins: A retrospective from industrial and engineering chemistry research,” *Ind. Eng. Chem. Res.*, vol. 48, no. 1, pp. 388–398, 2009, doi: 10.1021/ie801242v.
- [16] Z. Tasic, V. K. Gupta, and M. M. Antonijevic, “The mechanism and kinetics of degradation of phenolics in wastewaters using electrochemical oxidation,” *Int. J. Electrochem. Sci.*, vol. 9, no. 7, pp. 3473–3490, 2014.
- [17] A. Mojiri, “Wastewater Engineering: Advanced Wastewater Treatment Systems,” *Wastewater Eng. Adv. Wastewater Treat. Syst.*, no. September, 2014, doi: 10.12983/1-2014-03-01.
- [18] M. Singh and J. D. Desai, “Settling behavior of activated sludge from an effluent treatment plant of a petrochemical industry: Involvement of biofactor in sludge bulking,” *J. Ferment. Technol.*, vol. 65, no. 6, pp. 731–733, 1987, doi: 10.1016/0385-6380(87)90019-7.
- [19] A. H. Abbar, R. H. Salman, and A. S. Abbas, “Electrochemical Incineration of Oxalic Acid at Manganese Dioxide Rotating Cylinder Anode: Role of Operative Parameters in the Presence of NaCl,” *J. Electrochem. Soc.*, vol. 163, no. 13, pp. E333–E340, 2016, doi: 10.1149/2.0551613jes.

- [20] *Coagulation and Flocculation in Water and Wastewater Treatment*, Second Edi. LONDON: IWA Publishing, Alliance House, 12 Caxton Street, London SW1H 0QS, UK.
- [21] F. I. Hai, K. Yamamoto, and K. Fukushi, "Hybrid treatment systems for dye wastewater," *Crit. Rev. Environ. Sci. Technol.*, vol. 37, no. 4, pp. 315–377, 2007, doi: 10.1080/10643380601174723.
- [22] A. Ali, M. Hewehy, X. Chen, G. Huang, and J. Wang, "Electrochemical Reduction / Oxidation in the Treatment of Heavy Metal Wastewater Related papers Electrochemical Reduction / Oxidation in the Treatment of Heavy Metal Wastewater."
- [23] K. Rajeshwar, J. G. Ibanez, and G. M. Swain, "Electrochemistry and the environment," *J. Appl. Electrochem.*, vol. 24, no. 11, pp. 1077–1091, 1994, doi: 10.1007/BF00241305.
- [24] F. Zhang *et al.*, "Degradation of phenol by a combined independent photocatalytic and electrochemical process," *Chem. Eng. J.*, vol. 175, no. 1, pp. 349–355, 2011, doi: 10.1016/j.cej.2011.09.122.
- [25] L. Szyrkowicz, C. Juzzolino, and S. N. Kaul, "A comparative study on oxidation of disperse dyes by electrochemical process, ozone, hypochlorite and fenton reagent," *Water Res.*, vol. 35, no. 9, pp. 2129–2136, 2001, doi: 10.1016/S0043-1354(00)00487-5.
- [26] A. H. Abbar and A. S. Abbas, "A kinetic study of oxalic acid electrochemical oxidation on a manganese dioxide rotating cylinder anode," *Port. Electrochim. Acta*, vol. 36, no. 5, pp. 325–337, 2018, doi: 10.4152/pea.201805325.
- [27] B. Neppolian, H. Jung, H. Choi, J. H. Lee, and J. W. Kang, "Sonolytic degradation of methyl tert-butyl ether: The role of coupled fenton process and persulphate ion," *Water Res.*, vol. 36, no. 19, pp. 4699–4708, 2002, doi: 10.1016/S0043-1354(02)00211-7.
- [28] J. Krýsa, D. Mantzavinos, P. Pichat, and I. Poulios, "Advanced oxidation processes for water/wastewater treatment," *Environ. Sci. Pollut. Res.*, vol. 25, no. 35, pp. 34799–34800, 2018, doi: 10.1007/s11356-018-3411-2.
- [29] M. Zhou, Q. Yu, L. Lei, and G. Barton, "Electro-Fenton method for the removal of methyl red in an efficient electrochemical system," *Sep. Purif. Technol.*, vol. 57, pp. 380–387, 2007, doi: 10.1016/j.seppur.2007.04.021.

- [30] A. Urriaga, I. Ortiz, Á. Anglada, A. Urriaga, and I. Ortiz, "Contributions of electrochemical oxidation to wastewater treatment: Fundamentals and review of applications," *J. Chem. Technol. Biotechnol.*, vol. 84, no. 12, pp. 1747–1755, 2009, doi: 10.1002/jctb.2214.
- [31] F. King, *Environmental Electrochemistry: Fundamentals and Applications in Pollution Abatement*, vol. 27, no. 6. 1998.
- [32] H. Hammani *et al.*, "Electro-catalytic effect of Al₂O₃ supported onto activated carbon in oxidizing phenol at graphite electrode," *Mater. Today Chem.*, vol. 3, pp. 27–36, 2017, doi: 10.1016/j.mtchem.2017.01.002.
- [33] Z. I. Abbas and A. S. Abbas, "Oxidative degradation of phenolic wastewater by electro-fenton process using MnO₂-graphite electrode," *J. Environ. Chem. Eng.*, vol. 7, no. 3, p. 103108, 2019, doi: 10.1016/j.jece.2019.103108.
- [34] R. H. Salman, M. H. Hafiz, and A. S. Abbas, "Preparation and Characterization of Graphite Substrate Manganese Dioxide Electrode for Indirect Electrochemical Removal of Phenol," *Russ. J. Electrochem.*, vol. 55, no. 5, pp. 407–418, 2019, doi: 10.1134/S1023193519050124.
- [35] R. M. Farinos, R. L. Zornitta, and L. A. M. M. Ruotolo, "Development of three-dimensional electrodes of PbO₂ electrodeposited on reticulated vitreous carbon for organic electrooxidation," *J. Braz. Chem. Soc.*, vol. 28, no. 1, pp. 187–196, 2017, doi: 10.5935/0103-5053.20160162.
- [36] F. Yi, S. Chen, and C. Yuan, "Effect of activated carbon fiber anode structure and electrolysis conditions on electrochemical degradation of dye wastewater," *J. Hazard. Mater.*, vol. 157, no. 1, pp. 79–87, 2008, doi: 10.1016/j.jhazmat.2007.12.093.
- [37] Y. X. Liu, Z. Y. Liao, X. Y. Wu, C. J. Zhao, Y. X. Lei, and D. Bin Ji, "Electrochemical degradation of methylene blue using electrodes of stainless steel net coated with single-walled carbon nanotubes," *Desalin. Water Treat.*, vol. 54, no. 10, pp. 2757–2764, 2015, doi: 10.1080/19443994.2014.903524.
- [38] G. Barman, A. Kumar, and P. Khare, "Removal of congo red by carbonized low-cost adsorbents: Process parameter optimization using a Taguchi experimental design," *J. Chem. Eng. Data*, vol. 56, no. 11, pp. 4102–4108, 2011, doi: 10.1021/je200554z.
- [39] M. Nandhini, B. Suchithra, R. Saravanathamizhan, and D. G. Prakash,

- “Optimization of parameters for dye removal by electro-oxidation using taguchi design,” *J. Electrochem. Sci. Eng.*, vol. 4, no. 4, pp. 227–234, 2014, doi: 10.5599/jese.2014.0056.
- [40] P. K. Chaulia and R. Das, “Process parameter optimization for fly ash brick by Taguchi method,” *Mater. Res.*, vol. 11, no. 2, pp. 159–164, 2008, doi: 10.1590/S1516-14392008000200008.
- [41] H. Ashassi-Sorkhabi and R. Bagheri, “Sonochemical synthesis, optimized by Taguchi method, and corrosion behavior of polypyrrole-silicon nitride nanocomposite on St-12 steel,” *Synth. Met.*, vol. 195, pp. 1–8, 2014, doi: 10.1016/j.synthmet.2014.05.008.
- [42] Y. G. Adewuyi and B. A. Oyekan, “Optimization of a sonochemical process using a novel reactor and Taguchi statistical experimental design methodology,” *Ind. Eng. Chem. Res.*, vol. 46, no. 2, pp. 411–420, 2007, doi: 10.1021/ie060844c.
- [43] A. Habrioux, S. Hebié, T. W. Napporn, J. Rousseau, K. Servat, and K. B. Kokoh, “One-Step Synthesis of Clean and Size-Controlled Gold Electrocatalysts: Modeling by Taguchi Design of Experiments,” *Electrocatalysis*, vol. 2, no. 4, pp. 279–284, 2011, doi: 10.1007/s12678-011-0064-z.
- [44] T. P. Ryan, “Taguchi’s Quality Engineering Handbook,” *J. Qual. Technol.*, vol. 37, no. 3, pp. 249–251, 2005, doi: 10.1080/00224065.2005.11980326.
- [45] A. Zirehpour, A. Rahimpour, M. Jahanshahi, and M. Peyravi, “Mixed matrix membrane application for olive oil wastewater treatment: Process optimization based on Taguchi design method,” *J. Environ. Manage.*, vol. 132, pp. 113–120, 2014, doi: 10.1016/j.jenvman.2013.10.028.
- [46] M. Mtb, S. C. Qref, H. O. W. T. O. Use, M. Mtb, S. C. Qref, and H. O. W. T. O. Use, *User ’s Guide 2 : Data Analysis*. 2000.
- [47] N. Beqqal, M. S. Yahya, M. El Karbane, A. Guessous, and K. El Kacemi, “Kinetic study of the degradation/mineralization of aqueous solutions contaminated with Rosuvastatin drug by Electro-Fenton: Influence of experimental parameters,” *J. Mater. Environ. Sci.*, vol. 8, no. 12, pp. 4399–4407, 2017, doi: 10.26872/jmes.2017.8.12.464.
- [48] Gökkuş, N. Yıldız, A. S. Kopalal, and Y. Yıldız, “Evaluation of the effect of oxygen on electro-Fenton treatment performance for real textile

- wastewater using the Taguchi approach,” *Int. J. Environ. Sci. Technol.*, vol. 15, no. 2, pp. 449–460, 2018, doi: 10.1007/s13762-017-1404-1.
- [49] Z. I. Abbas and A. S. Abbas, “Optimization of the electro-fenton process for cod reduction from refinery wastewater,” *Environ. Eng. Manag. J.*, vol. 19, no. 11, pp. 2029–2037, 2021, doi: 10.30638/eemj.2020.192.
- [50] M. Pushpalatha and M. B. Krishna, “Electro-Fenton Process for Waste Water Treatment A Review,” *Int. J. Adv. Res.*, vol. 3, no. 1, pp. 439–451, 2017.
- [51] C. S. D. Rodrigues, L. M. Madeira, and R. A. R. Boaventura, “Optimization of the azo dye Procion Red H-EXL degradation by Fenton’s reagent using experimental design,” *J. Hazard. Mater.*, vol. 164, no. 2–3, pp. 987–994, 2009, doi: 10.1016/j.jhazmat.2008.08.109.
- [52] C. T. Wang, W. L. Chou, M. H. Chung, and Y. M. Kuo, “COD removal from real dyeing wastewater by electro-Fenton technology using an activated carbon fiber cathode,” *Desalination*, vol. 253, no. 1–3, pp. 129–134, 2010, doi: 10.1016/j.desal.2009.11.020.
- [53] A. S. Fahem and A. H. Abbar, “Treatment of petroleum refinery wastewater by electro- Fenton process using porous graphite electrodes,” vol. 63, no. 12, pp. 4805–4819, 2020, doi: 10.21608/EJCHEM.2020.28148.2592.
- [54] E. Fockedey and A. Van Lierde, “Coupling of anodic and cathodic reactions for phenol electro-oxidation using three-dimensional electrodes,” *Water Res.*, vol. 36, no. 16, pp. 4169–4175, 2002, doi: 10.1016/S0043-1354(02)00103-3.
- [55] M. Umar, H. A. Aziz, and M. S. Yusoff, “Trends in the use of Fenton, electro-Fenton and photo-Fenton for the treatment of landfill leachate,” *Waste Manag.*, vol. 30, no. 11, pp. 2113–2121, 2010, doi: 10.1016/j.wasman.2010.07.003.
- [56] F. C. Moreira, R. A. R. Boaventura, E. Brillas, and V. J. P. Vilar, “Electrochemical advanced oxidation processes: A review on their application to synthetic and real wastewaters,” *Appl. Catal. B Environ.*, vol. 202, pp. 217–261, 2017, doi: 10.1016/j.apcatb.2016.08.037.

smart attendance student system using IoT RFID

Safa Ihsan ¹, Lubna a-alnabi ², Dr.Hussam Dheaa Kamel ^{2*} Prof. Dr Alaa kadhim farhan³

Affiliation 1; safaihsan@almustafauniversity.edu.iq ¹

Affiliation 2; lubna.cet@almustafauniversity.edu.iq, ²
hussam.cet@almustafauniversity.edu.iq,

Affiliation 3; Alaa.k.farhan@uotechnology.edu.iq ³

Correspondence: safaihsan@almustafauniversity.edu.iq;

^{1,2} Department of Computer Technique Engineering - Al-Mustafa University College

³ Department of Computer sciences - University of technology

Abstract: Radio Frequency Identification (RFID) technology is used in numerous applications, and among these applications is to determine the entry to rooms in different departments and hotels, RFID is used in technical process with programming Arduino to control of access to rooms and buildings according references it's been connect the LCD screen, in addition to a large animated LED display to display any phrase or statement using the Arduino, use Bluetooth instead of an RFID card to open the door with text or voice.

Keywords: Radio frequency Identification (RFID), A light-emitting diode (LED), Internet of Thing (IoT), Attendance system, Sensors , Tags, open source Arduino software (IDE) .

1. Introduction

Not so long ago, working on electronic circuits to do a particular job meant building an electronic design for complex components like resistors, transistors, capacitors...etc.

The Static Circuit Design, Re-change or Modify a part which means a lot of complicated process like soldering, cutting wires, rethinking electronic schematics and a lot of annoying things which led to a limited job of developing electronic products for a group of professional engineers only. Technological development in the field of semiconductors and the invention of integrated circuits (IC) made it possible to develop a complete electronic circuit on a small chip size , Figure (1) show the integrated circuit [1].

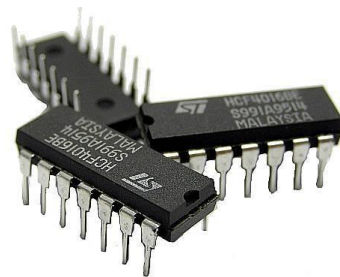
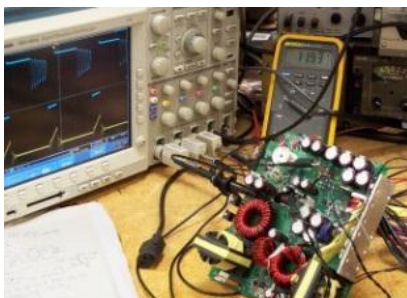


Figure 1. integrated circuit

Successful schools start with the participation of students and the assurance that they come to school regularly, so attendance becomes critical. To keep track of student attendance, attendance system should be used and can be applied in schools, industries, universities or workplaces [1].

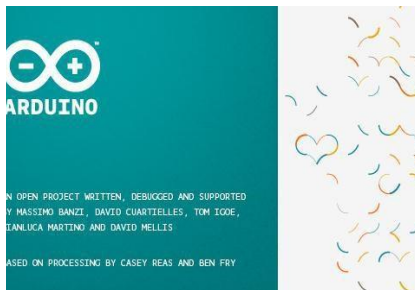
The RFID technology based attendance system that consists of RFID tag, RFID radar, LCD, display and microcontroller unit [2].

RFID can be linked to a microcontroller through the Universal Asynchronous Synchronous Transmitter (USART). The data is transmitted from the RFID cards to the reader and from there to the microcontroller. These attendance systems are important for large sized organizations so that they can quickly process a large number of worker attendance. It makes work more efficient and gives accurate results [2,3].

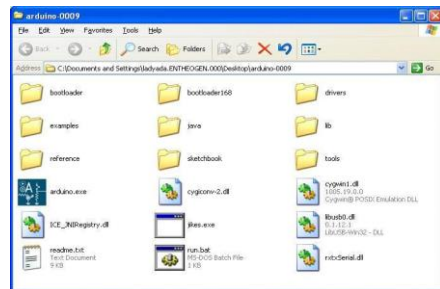
2. Materials and Methods

The Arduino (IDE) is a tool used to write programming codes using the Arduino-C language and then convert them into an executable format that can be placed on a micro-controller on the board.

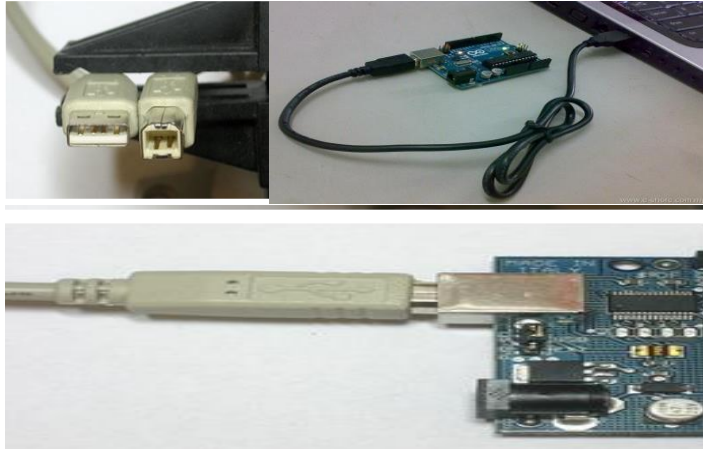
The Arduino (IDE) is easy and simple to handle. It is virtually devoid of any complexity in its general appearance and contains only what a programmer needs to start developing programs in the Arduino-C language, which is used at the same time to upload the program directly to the microcontroller, figure (2) shown the Arduino IDE [3,4].



a) Arduino IDE



b) files of Arduino IDE



c) Interface of Arduino

Figure 2. Arduino

Arduino IDE consists of a simple interface is divided into four main parts :

- First: the menu bar.
- Second: Fast-orders bar.
- Third: area of writing-codes.
- Fourth: the portion of display alerts and programming errors.

The implemented system includes 3 main subsystems that are integrated and worked together to Smart Attendance System. These subsystems are:

1. RFID
2. ARDUINO
3. DATA BASE

The paper work flow chart is shown in Figure (3).

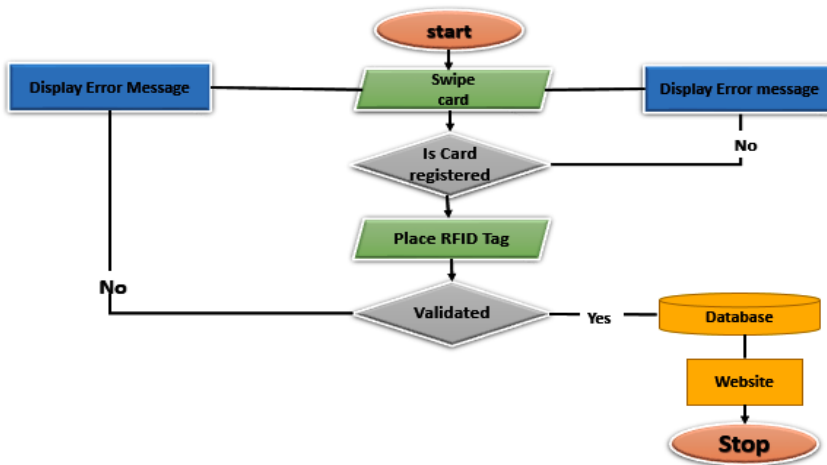


Figure 3. work flow chart

3. Results

There are many features of this paper can determine as following[5,6]:

1. Access from any places: After store all information on server, information are passes on website that have access everywhere and anytime.
2. Information database: Students information are stored in database such as Students profile, their details, their entry/out all information are store in Google database.
3. Wireless communication: website used as a wireless communication. Anyone can access it. This website can use in mobile also used by mobile apps.
4. Fast data transfer: Central server stores all information and it transfers all information in website. Where it is too fast. That is a reason for transfers data fastly.
5. Authentication Valid students to entry classroom: Design and development of a wireless smart attendance system is website that have high authentication. This website only authenticates valid students to entry classroom. RFID is the only way that tries to identify all students.

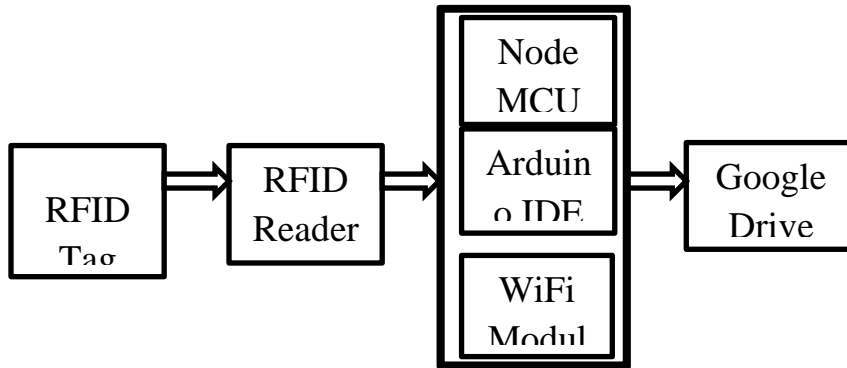


Figure 4. Block diagram of Proposed system

3.1 Hardware components

hardware system is a simple design and need five components with low cost system. This system provides wireless communication that is main hardware system transfer data into the server using Wi-Fi [7].

- **RFID Tag :** is composed of a silicon microchip connected to a small antenna, mounted on a substrate, and encapsulated in various types of materials in the manner of plastic or glass veil and with a sticky on the backside to connect to objects .
- **RFID reader** is composed of a scanner with antennas to transmit and receive signals and is carrying the load for connection with the tag and receives the information from the tag .
- **NodeMCU:** is a free origin IoT platform. It comprehends firmware , which escape on the ESP8266 Wi-Fi Sock from Express, and hardware that is establish on the ESP-12 module. The term "NodeMCU" by default, assign to the firmware rather than the development kits. The Lau scripting language used by the firmware. It is established on the Eula system, and configuration on the Express if Non-OS SDK for ESP8266. It causes many free origin systems, such as Lua-cjson, and spiffs”.
- **Servo Motor:** a servo motor is a type of motor that can rotate with great precision. Normally this type of motor consists of a control circuit that provides feedback on the current position of the motor shaft, this feedback allows the servo motors to rotate with great precision .
- **A jump wire:** is an electrical wire and group of them in a cable, with a pin at individual edge, which normally used to interconnect the components of a breadboard. Internally or with other equipment or components, without soldering .

- 16×2 LCD: it has 16 Columns and 2 Rows which a common screen that used.

3.2 Software components

The Arduino IDE is Integrated Development Environment. Where it is a cross platform application (for Windows, macOS, Linux) that deals with programming language Java. It originated from the IDE for the languages Processing and Wiring. There are different type of development environments that used to program the ESP8266. The ESP8266 section created an add-on for the Arduino IDE that permit to program the ESP8266 using the Arduino IDE and its programming language [8].

3.3 System Implementation

Abase configuration in Figure 5 show the circuit's diagram where the hardware components are connected and shown in the diagram

Figure 5. System proposed circuit diagram

Maintaining the attendance of the students in an institution is a hefty task. Always there is a difficulty in handling attendance manually. This paper aims at designing a smart attendance system that automatically monitors and manages attendance of the students in an institution efficiently. The whole system is developed with an ESP8266 Arduino microcontroller and RFID reader MFRC522 Module. Unique RFID tags can be deployed in students id card. In this paper, the entry and exit of students to and from the university is controlled, and the project can also be used to take attendance of students during lectures, in the Student Affairs Unit and in all administrative departments at the university. Thus, students' information is fully known, and it is easy to control and manage it.

This paper aims at designing a smart attendance system that automatically monitors and manages attendance of the students in an institution efficiently. Also, Wi-Fi communication modules are used to make convenient communication depend on the availability of the network. Database of students created. This system will reduce a lot of manual work of teachers and administrators of any institution. The proposed work comprises of two most popular trend in technology research; IoT and RFID [9].



Figure 6. Practical design

4. Discussion

Attendance system means that keep records of all students are genuinely enter in their institute. When students enter in their institute security guard ask them please to show their id card, after showing that then they get permission to enter. This system is continuing day by day. When teachers take attendance in the class they start roll call then give attendance as attendance system.

First, it is a waste of time. When teacher came at their class they, start roll call so time is resume and it also affect teacher's lecture. Teacher cannot complete their lecture properly. Sometimes teachers give this attendance sheet to students, so anyone can give proxy, sometime attendance sheet may get misplaced. 5% or 10% marks are including in our attendance, but this calculation is so hard. This system has no authentication, anyone can show others IDcard, or anyone can proxy. Therefore, it is impact on our security.

5. Conclusions

Design and development of a wireless smart system using is one of best way to take attendance of the student. New Technology's modern invention in the monitoring system that provides more advantageous way and will be a massive success in improving the current traditional way of monitoring students.

The Institution Management faces many challenges like student missing, student bunking class, faculty marking fake attendance, faculty spending 30% time on Error manual Attendance, lack or no communication among students, faculty, parents, and Admin staffs. So all these things solved by Smart Attendance System using RFID. These RFID can detect student entry mark their attendance within 1 minute and sent notification to the parent and student whole information will kept in database server.as a suggestion for future work would provide more security by using finger identity, face identity, eye identity and voice.

Author Contributions: “Conceptualization, Dr.Hussam Dheaa. and M.Sc Safa Ihsan; methodology M.Sc Lubna a-alnabi.; software, M.Sc Safa Ihsan.; validation, M.Sc Lubna a-alnabi and M.Sc Safa Ihsan.; formal analysis, M.Sc Safa Ihsan.; investigation, M.Sc Safa Ihsan.; resources, M.Sc Lubna a-alnabi.; data curation, M.Sc Lubna a-alnabi.; writing—original draft preparation, M.Sc Safa Ihsan.; writing—review and editing, Dr.Hussam Dheaa.; visualization, Dr.Hussam Dheaa; supervision, Dr.Hussam Dheaa.; project administration, Dr.Hussam Dheaa.; funding acquisition, M.Sc Lubna a-alnabi.

Acknowledgments: Authors are thankful to our students (**Ali Ahmed Hussien, Yasser Wasef Abd algine, Mohamed Ali Aboud, Dheyaa Qasim Saeid**) in Department of Computer Technique Engineering for their support to providing the main requirements and implementing the station.

Conflicts of Interest: “The authors declare no conflict of interest.”

Reference

1. Cheah B.Chew, Manmeet M.Singh, Kam C.Wei, Tan W. Sheng, Mohd H. Husin, Nurul H.Ahamed H.Malim, "The Society of Digital Information and Wireless Communications" ,The Society of Digital Information and Wireless Communications, School of Computer Sciences, University Sains Malaysia, 2015.
2. T.S.Lim, S.C. Sim, M.M. Mansor, “RFID Based Attendance System”, IEEE Symposium on Industrial Electronics and Applications (ISIEA 2009), Kuala Lumpur, Malaysia, 2009.
3. S. K. Jain, U. Joshi, B. K. Sharma, “Attendance Management System,” Masters Project Report, Rajasthan Technical University, Kota.
4. Nguyen, H. K., & Chew, M. T. (). RFID-based attendance management system, *Recent Trends in Telecommunications Research (RTTR)*, 2017, February ,pp. 1-6, IEEE.
5. Sabri, M. Y., Aziz, M. A., Shah, M. M., & Abd Kadir, M. F. (2007, December). Smart Attendance System by using RFID. *Asia-Pacific Conference on Applied Electromagnetics* (pp. 1-4). 2007, IEEE.
6. Sarker, D. K., Hossain, N. I., & Jamil, Design and implementation of smart attendance management system using multiple step authentication. *International Workshop on Computational Intelligence (IWCI)* (pp. 91-95), 2016, IEEE.
7. http://en.wikipedia.org/wiki/Microsoft_SQL_Server.
8. <http://en.wikipedia.org/wiki/rfid>.
9. <https://en.wikipedia.org/wiki/E5P8266>

face recognition¹ with A security system based on a neural network

Rasha jamal 1 , Salim Ali Abas 2 , *

1 Affiliation 1; Rasha.cta@almustafauniversity.edu.iq

2 Affiliation 2; salim.Ali.Abas.cet@almustafauniversity.edu.iq

* Correspondence: Rasha.cta@almustafauniversity.edu.iq

* Department of Computer Science- Al-Mustafa University College

Abstract: Home door security is a same important matter becomes A foundation for the simplest coupled with the easiest safety and enough to provide a sense of security for home owners alongside with developments, technological especially in the field of the Internet of Things, Making technological advances in the lock home doors¹ have remained It has been developed a lot like locking house doors with faces and others. facial recognition systems have also been implemented and developed for home door lock² systems and it is a very simple, easy to use and completely accurate option in recognizing the face of homeowners². CNN method development for facial² Recognition has become one the easy-to-implement facial recognition systems with good face Recognition accuracy¹ It is used in object recognition systems² and others. In this second study, using CNN Alex net for Facial recognition is implemented in the door lock system, data is collected² by collecting 1,048 Facial data on the owner of the house Face with a system that is then used to train learning machine where the results . Quite accurate as the result was 97.5% which is very good compared to some other studies³. The conclusion is that CNN Alexnet¹ method can perform facial recognition which is quite accurate and can be implemented on Iota device, Raspberry² Pi.

Keywords: home door security: CNN Alexandre facial recognition raspberry² pie .

1. Introduction

One the past few years², 3 have remained several options in traditional technology¹ and technology biometric to chance the security requests of homes or offices². Certain traditional security systems¹, such as the use of Keys, passcodes, ID cards, and/or RFID cards can be unreliable if accessible objects are stolen or lost. [1]. These security systems¹ have drawbacks when admission is stolen by publics who don't have² access authority, and daily activities¹ sometimes force someone to leave the house empty¹, example during work or school hours². This makes the home vulnerable to break-ins¹ and theft, even when the home² is securely locked or locked². Currently, the development of information¹ and communication technology provides convenience to users¹ in various lifestyles. One technology that is currently trending is the keen home or what is commonly¹ known as the smart home. A smart home is a term used to define a dwelling¹ that contains equipment, lighting, heating, air conditioning, television, computer, audio system², video entertainment, security, and camera systems¹ that can communicate with each other and can be controlled¹ remotely. Timetable. Online or by phone³ [2]. Biometrics systems are developing¹ rapidly, especially for home security technology² because it can fulfill two functions¹, Namely, identification

and verification, biometrics¹ have properties that cannot² be lost, forgotten and cannot be forgotten¹. their inherent False as existence in humans will differ¹ between humans and other humans so that there is guaranteed uniqueness [3]. In Journal [4], facial recognition¹ as authentication is good because the face is a physiological feature that facilitates¹ discrimination between individuals, so facial recognition¹ is one of the biometric technologies¹ often studied and developed.

2- Method

In this propose study, face recognition process for the home¹ door opening process that can replace² home security process using an electronic¹ key or RFID, where the search stages are divided¹ into 3 parts which are the stages of home owner data, the data training process, as well as the face recognition¹ process using Pi. In this journal, implement a CNN method of facial recognition [14] which you will install on a microcompute²r, a raspberry pi which will act as a Face-controlled¹ automatic door locking and unlocking¹. From the owner of house¹ [15].

a. Homeowner's facial¹ collection data steps of data collection the performed manually, i.e. using software designed¹ to collect facial data from all homeowner¹ consisting of 5 people where the total data is 1100 data which will then¹ divided into 1040 training data and 60 data is used¹ for validation during Training by doing the face augmentation¹ process that starts from shifting from 10 to 15 degrees with different expressions [16]. The results of data collection¹ can seen in (Figure 2 and 3).

b. Training model by the point, the exercise process is no performed¹ on raspberry pi due to raspberry¹ pi micro computation training process are carried¹ out on a separate computer with Intel¹ Core i5 8400 processor specification and 10GB DDR4 RAM¹ as this will , constitute the training process¹ A model that will be used¹ to detect face [17]. The stages of training process¹ use CNN Alexnet method¹ with convolution, aggregation and¹ softmax operations with several 20 iterations with the¹ parameters (shown in Figure 4).

c. System Operation This prototype¹ will complete by connecting a modified¹ Pi camera as home¹ owner face identification camera¹ module connected to a Raspberry Pi 4 Model B+ Raspberry¹ Pi will be connected WLAN as a home owner identification process¹ [18] as shown in Figure 5.

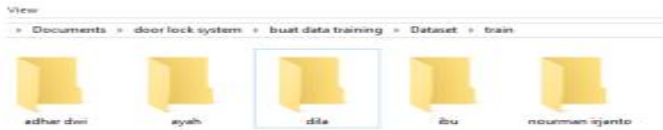


Fig. 2. Dataset of Homeowners Faces.



Fig. 3. Dataset of Face.

```

===
Parameters
===
img_width, img_height = 224, 224
batch_size = 32
samples_per_epoch = 1000
validation_steps = 300
nb_filters1 = 32
nb_filters2 = 64
conv1_size = 3
conv2_size = 2
pool_size = 2
classes_num = 5
lr = 0.0004
    
```

Fig. 4. Parameter Training Method.

➤ Flowchart system¹: workflow in the system is separated into 2 parts, which are recording stage², where this stage the resulting² data used as training data² [19]. At this point there will process of recording² face data of¹ the homeowner who be trained² on the computer to produce² a training model that will be stored in the database on the Raspberry² Pi and will be backed up if the device is already in standby mode and ready to use as in (Figure 6). An installation² process is performed The system is at the front door of the house² which is the only entrance² to existing house as shown popular (Figure 7 and Figure 8).

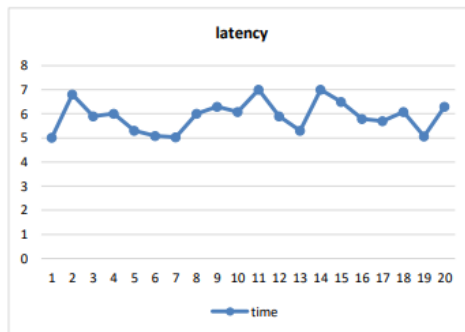


Fig. 9. Latency Testing.

TABLE I. HOMEOWNER TESTING SAMPLES

People	Face
	
	
	
	
	

3. Result

After¹ the above-mentioned tests were carried out, it resulted² at a significant development terms of increased image reading accuracy and faster processing¹. The full data can be seen in the fourth table and the fifth² table. After testing 4 times at 3 different times and based on the fourth table and the fifth table¹, it can concluded² that this¹ system works well and has test results in the morning², afternoon, evening and night with 3 conditions¹ and can be concluded in sixth table¹.

TABLE IV. HOMEOWNER TEST RESULTS

Time	Face	Distance					
		1.5 m		1 m		0.5 m	
		Success	Fail	Success	Fail	Success	Fail
Morning	5	4	1	5	0	5	0
Afternoon	5	4	1	5	0	5	0
Evening	5	4	1	5	0	5	0
Night	5	5	0	5	0	5	0

TABLE V. TEST RESULTS ARE NOT HOMEOWNERS

Time	Face	Distance					
		1.5 m		1 m		0.5 m	
		Success	Fail	Success	Fail	Success	Fail
Morning	5	0	5	0	5	0	5
Afternoon	5	0	5	0	5	0	5
Evening	5	0	5	0	5	0	5
Night	5	0	5	0	5	0	5

3- Conclusion

Fifth: The search was conducted¹ at 3 distances of 1.4 meters, 1 meter and 0.4 meters. It was searched¹ 4 times, morning, afternoon¹, evening and evening, where a mistake occurred three times, namely from a distance¹. 1.5m as it was very light against the background of the parking space. This research has resulted¹ in blurry images, The method was used to increase the accuracy of facial recognition up to 97.5% accuracy¹. after comparisons with the Open CV proprietary method [11] using same data set and test stages¹, this search was slightly better, yielding an accuracy of 97.83% as 95% accuracy was obtained in the previous search. Additional research includes optimizing the process for augmenting¹ the face data used as a dataset¹, camera resolution better, using the latest Raspberry Pi to improve computing capabilities¹.

4- Reference

- 1- Y. D. S. V. D, A. Rakhmansyah, and N. A. Suwastika, "Implementasi Sistem Kunci Pintu Otomatis Untuk Smart Home Menggunakan SMS Gateway," e-Proceeding Eng., vol. 2, no. 2, pp. 6395–6407, 2015. [2]
- 2- A. Siswanto, A. Efendi, and A. Yulianti, "Alat Kontrol Akses Pintu Rumah Dengan Teknologi Sidik Jari Di Lingkungan Rumah Pintar Dengan Data Yang Di Enkripsi," J. Penelit. Pos dan Inform., vol. 8, no. 2, p. 97, 2019. [3]
- 3- A. Yudhana, "Perancangan pengaman pintu rumah berbasis sidik jari menggunakan metode uml," (Jurnal Teknol. Informasi) Sist. PENGGAJIAN KARYAWAN PADA LKP GRACE Educ. Cent., vol. Vol.1, No., no. 2, p. 12, 2018. [4]
- 4- B. Septian, A. Wijayanto, F. Utaminingrum, and I. Arwani, "Face Recognition Untuk Sistem Pengaman Rumah Menggunakan Metode HOG dan KNN Berbasis Embedded," Pengemb. Teknol. Inf. dan Ilmu Komput., vol. 3, no. 3, pp. 2774–2781, 2019. [5]
- 5- M. Yan, M. Zhao, Z. Xu, Q. Zhang, G. Wang, and Z. Su, "VarGFaceNet: An Efficient Variable Group Convolutional Neural Network for Lightweight Face Recognition," Iccvw 2019, pp. 2647– 2654, 2019. [6]
- 6- A. Krizhevsky, I. Sutskever, and G. E. Hinton, "ImageNet classification with deep convolutional neural networks," Adv. Neural Inf. Process. Syst., vol. 2, pp. 1097–1105, 2012. [7]
- 7- A. Najmurokhman, K. Kusnandar, A. B. Krama, E. C. Djamal, and R. Rahim, "Development of a secured room access system based on face recognition using Raspberry Pi and Android based smartphone," MATEC Web Conf., vol. 197, pp. 1–6, 2018. [8]

- 8- R. A. Isaac, A. Agarwal, and P. Singh, "Face Recognition Security Module using Deep Learning," J. Netw. Commun. Emerg. Technol., vol. 8, no. 10, pp. 10–13, 2018. [9]
- 9- J. Nasir and A. A. Ramli, "Design of Door Security System Based on Face Recognition with Arduino," vol. 3, no. 1, pp. 127–131, 2019. [10]
- 10- B. M. Susanto, F. E. Purnomo, and M. F. I. Fahmi, "Sistem Keamanan Pintu Berbasis Pengenalan Wajah Menggunakan Metode Fisherface Security System Based On Face Recognition Using Fisherface Method," J. Ilm. Inov., vol. 17, no. 1, p. 10, 2017. [11]
- 11- F. Faisal and S. A. Hossain, "Smart security system using face recognition on raspberry Pi," 2019 13th Int. Conf. Software, Knowledge, Inf. Manag. Appl. Ski. 2019, no. August, 2019. [12]
- 12- R. Singh, M. Singh, and L. Ragha, "Real-time Face Recognition Under Different Environment," SSRN Electron. J., 2019. [13]
- 13- M. F. A. Hassan, A. Hussain, M. H. Muhamad, and Y. Yusof, "Convolution neural network-based action recognition for fall event detection," Int. J. Adv. Trends Comput. Sci. Eng., vol. 8, no. 1.6 Special Issue, 2019. [14]
- 14- R. Ranjan, S. Sankaranarayanan, C. D. Castillo, and R. Chellappa, "An All-In-One Convolutional Neural Network for Face Analysis," Proc. - 12th IEEE Int. Conf. Autom. Face Gesture Recognition, FG 2017 - 1st Int. Work. Adapt. Shot Learn. Gesture Underst. Prod. ASL4GUP 2017, Biometrics Wild, Bwild 2017, Heteroge, pp. 17–24, 2017. [15]
- 15- Soe Sandar | Saw Aung Nyein Oo, "Development of a Secured Door Lock System Based on Face Recognition using Raspberry Pi and GSM Module," Int. J. Trend Sci. Res. Dev., vol. 3, no. 5, pp. 357–361, 2019. [16]
- 16- N. A. Al-Johania and L. A. Elrefaei, "Dorsal hand vein recognition by convolutional neural networks: Feature learning and transfer learning approaches," Int. J. Intell. Eng. Syst., vol. 12, no. 3, 2019.

Prediction on the Conduction to Heat Transfer for Plane-Channel of Complex Geometry

R.SHAKIER ,*

University of Thi-qar- College of engineering-Department of Petroleum and Gas engineering; raed-sh@utq.edu.iq; shraed904@gmail.com

*Correspondence: raed-sh@utq.edu.iq; shraed904@gmail.com; Tel.: 07811646919

Abstract: Guess study has been used to investigate the heat transfer capabilities of heat sinks in the plane-channel under heat flux circumstances. The Guesses are implemented for the Reynolds number (524–2099.97) and heat applied (5–30) Watts, respectively. A wire electrical discharge machine finished the heat sink's plane-channel by channel height (10 mm) and channel width (50 mm). The effects of various for geometrical configurations, plane-channel characteristics, and heat flow on heat transfer qualities are considered. A possible heat transfer mechanism for a plane-channel heat sink has been revealed. The geometric configuration of the plane-channel has a significant impact on the augmentation of heat transfer characteristics. The findings of this inquiry are expected to lead to recommendations that will allow the design of a plane-channel heat exchanger based on the studied heat transfer behavior of electronic and electronic equipment. Finally, because I had no empirical data from the empirical set-up, the air data from the guess analysis was only used to anticipate the set-up, which was extremely comparable to genuine lab testing under steady-state circumstances.

Keywords: Plane-channel; Fluid temperature; Characteristics of heat transfer.

1. Introduction

The increasing need for improved performance of electronic devices, as well as the level of dependability of heat rejection, is a major requirement for these devices. Heat sink by diverse to geometrical configuration has been employed in numerous sectors on a traditional size. So, investigations as well as applications of heat-transfer devices on a plane-channel are currently restricted. Lately Wang et al. [1] Numerically studied the gas flow and heat transfer on a mini-channel had employed to uniform heat flux for boundary conditions. Lee and Son [2] reported to nucleate and heat transfer of flow boiling on a mini-channel. Lie [3] studied the heat transfer on flow boiling of FC-72 as a working fluid on a heated to micro-pin-fins for silicon chip. Yu [4] reported to the thermal performance of at the plate-pin fins of a heat sink. Also, R.SHAKIR [5] reported mathematically to R113 stream and heat flow on inline-pin-fins of complex geometry by employing the iteration method by uniform heat flux on the boundary situations. In addition to R.SHAKIR [6] was recorded to guess (Dp) and heat transmission of a geometry-scale on heat sink as well as R.SHAKIR [7] was reported to predict of boiling-phase on heat transmission for geometry-scale of heat sink. As indicated above, numerous investigations had been reported concerning the heat transfer of heat sink by a lot of mini-channel, so, there are still continuous fields to discuss the properties of heat transfer on the plane-channel of a heat sink. In the present

article, the major concern is to investigate the conduction heat transfer properties on the plane-channel of heat sinks (the temperature of wall; the temperature of fluid as well as fluid characteristics). Due to influences of various suitable parameters on the heat transfer properties are as well as considered.

2. Materials and Methods

Evaluations of heat transfer from parameters to flow are represented as temperature points relied on the wall of air temperature at system pressure; as viewed in Fig.1, the specification cases that only a distribution of single heat flux can be subsisted at the solid-air interface. As viewed in the 2-D layout, the major influence on the wall line; the first-D array was perpendicular to the airflow, the second-D array was parallel to the airflow, and the thermal conductivity was as steps below. [8]&[9].

$$\delta^2 T / \delta y^2 + \delta^2 T / \delta z^2 = 0 \tag{1}$$

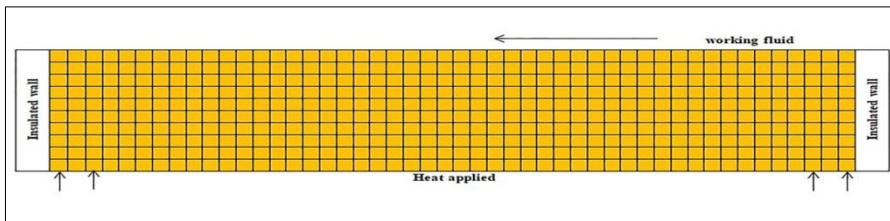


Figure.1 Wall Conduction of copper test Piece[8]&[9]

Where (y) is perpendicular to the flow axis; (T) is the temperature in the copper wall. The heat transfer for equation (1) has been determined by dividing by the square element of cell area (1mm).The energy balances for each cell must attain are seen in Fig.1. [8]&[9].

$$= \delta y^2 (T_{i+1,j} + T_{i-1,j}) + \delta z^2 (T_{i,j+1} + T_{i,j-1}) / 2 (\delta y^2 + \delta z^2) T_{i,j} \tag{2}$$

Where (δz) and (δy) are cell areas So the eq.(2) Deviating via the boundary conditions of the iterative solution until the point where each element has the same temperature as the previous, the guessed error of the iterative method was (0.005) also the number of iterative was (1000) on each guess test.The value for (T_w) at mini and micro-pin-fins of heat sink can be getting by . [10]

$$= T_{th} - \frac{q_h L_{th}}{K_C} \quad T_w \quad (3)$$

The value of (T_a) at mini and pin-fins-heat sink can be obtained by. [10]

$$= T_{in} + \frac{q_h W Z}{M_a C_{pa}} \quad T_a \quad (4)$$

The Nussle number can be gained by [10]:-

$$= NU_{x,4} \frac{NU_{fd,3}}{NU_{fd,4}} \quad NU_{x,3} \quad (5)$$

In where ($NU_{x,4}$), ($NU_{fd,3}$), "and ($NU_{fd,4}$), " are given to be gained by liquid properties respectively.[10]

The prandtls number can be obtained by[10]

P_r

The Reynolds number can be obtained by [10]

$$= \rho_a V D_h / \mu_a \quad R_e \quad (7)$$

In where (D_h), can be seen by. [10]

$$= A_h / P_h \quad D_h \quad (8)$$

The equation on the coefficient of heat transfer for plane-channel can be obtained by employing the below[10]

$$\begin{aligned} q_h \\ &= Y(T_w \\ &- T_a) \end{aligned} \quad (9)$$

3. The Perdition of setup

The Perdition of set-up is consisting of the set-up loop, the plane of the test section, and the conditions of the method.

3.1. The setup loop

A graph of the prediction set-up is seen in Fig.2. The test loop is consisting of a test loop, a cooling air loop and a data acquisition system. Air has employed as the working liquid. So; the loop of wind tunnel has a rectangular air duct invented to acrylic with a size of (25 x 25 cm) and a length of (200 cm). The duct has insulated by Aero-flex compliant (20 mm) thick on sheet metal. The air on the wind tunnel was discharged via the air compressor to the wind tunnel, directed to the test section, and to then discharge to the atmosphere. The rate of air flow was measured to a flow meter by an accuracy of fully scale (0.4%). The pressure drop on the metering section was measured by a differential on pressure sensor with an accuracy of (0.04%) of fully scale. There are (2) pressure taps on each wall downstream and upstream of the test section. So; type K-copper constantan of thermocouples, accurate to (0.4%) of fully scale, for measuring air temperature So the inlet and outlet temperatures of the air was measured by (2) thermocouples via probes (1.5 mm), the diameter of the probes respectively extending into the channel via which the air flows. All thermocouple probes are pre-calibrated with a dry box temperature for calibrator by (0.04°C).

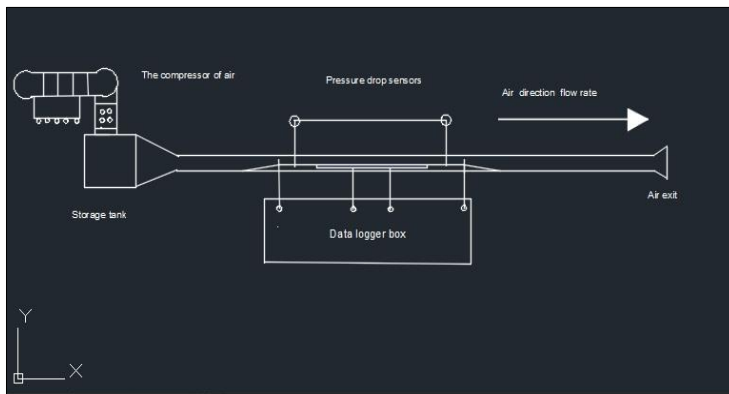


Figure.2. Prediction Rig

3.2. The plane of test section

The schematic diagram of the test section has seen on Fig.2. The width of heat sink and length of heat sink are (50 mm and 50 mm respectively). The plane-channel of the heat sink has accomplished by a wire of electric discharge machine. As Seen on Fig.2. For details of the plate-channel of heat sink. As well (AC) power has the power supply for the plate type. The Rear face of the test section was insulated by standard (20 mm) thick heat-resistant of mica board, standard (8 mm) of Aero-flex board, and standard (8 mm) thick of acrylic board. (2) T-type copper constantan thermocouple with a diameter of (1.5 mm) was employed to measure of wall temperature of the plane channel of heat sink. The thermocouple was installed by mounting on the wall drilled holes via the rear face and fixed by special adhesive employed to the wall of rear face.

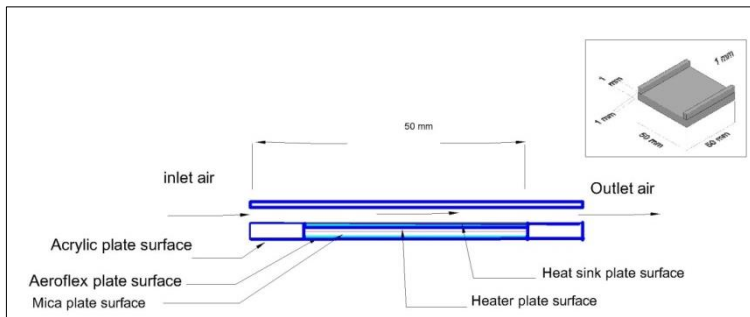


Figure.3. Test section & Plane piece

3.3. The conditions of method

Guesses had conducted via various heat fluxes and via various flow rates of air entering to test section. On the guesses, the airflow rate was increased on little increases so the heat input at the plane channel of the heat sink was preserved constantly. The heat input to the plane channel of walls on the heat sink was adjusted to reach the required level by utilizing an electric heater. The supplied power was found employing the measured voltage and current supplied to the heaters. The supplied voltage and current to the heaters had measured via the meter of a digital clamp. The sensible of steady-state heat obtained via the airflow can be found by energy balance. In the present study, only the data that accept the energy balance conditions via utilizing to process an iteration method for all guess tests.

4. The Results and Discussion

By the short review of the above, key findings are grown by using iteration method to obtain the main parameters of heat transfer for the plane-channel of the heat sink.

Fig.4.has be seen to the variation of the temperature of inlet and outlet air with to air Reynolds number for square channel so air mass flow rate increases due to bigger heat transfer rate had applied So the increase of the rate of heat transfer has less than that of the rate of air mass flow. So, the temperature of outlet air tends to decrease as the Reynolds number increases. Reynolds number had laminar and developing flow on all guess tests. It is significant to note, that the present study has relied on equations of heat transfer to guess all data during steady-state guess method. Therefore; outlet data is higher than inlet data also can be seen all data are staying on the same line which means the results confirm that this is a good selection for any guess tests. At last, the results of the guess established clearly supported the iteration method.

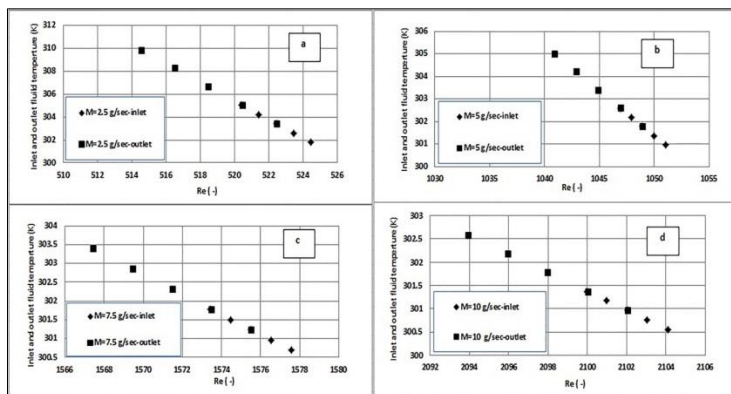


Figure.4. Alteration to temperature of fluid versus (Re) for air (a) $M=2.5$ "g/sec" (b) $M=5$ "g/sec"(c) $M=7.5$ "g/sec" (d) $M=10$ "g/sec

Fig.5.the variation of the temperature of the heat wall with the Reynolds number of air has been seen for (50mm) channel on width and (10mm) channel on height.As predicted, the heat transfer rate depends on the cooling capacity rate of the air. Therefore, the temperature of the heat sink decreases as the air Reynolds number increases. As shown in Fig.5. Because of the larger surface of the heat transfer area, the smaller mass flow heat sink gives to heat sink temperature higher than that smaller one. Continue; reporting and estimating wall temperature is highly recommended.

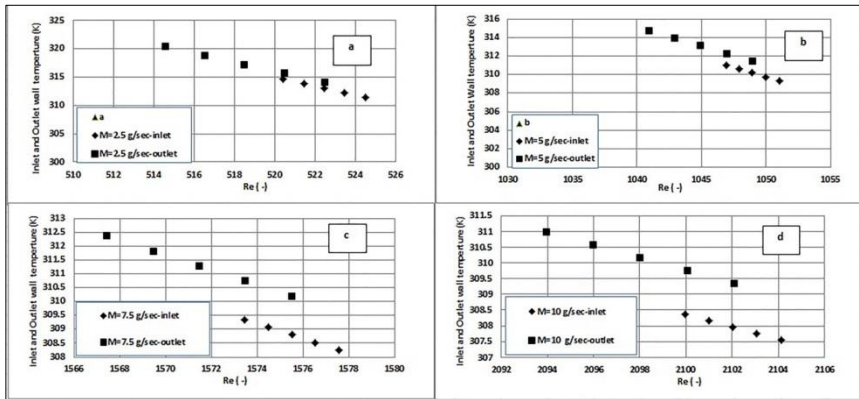


Figure.5. Alteration to temperature of wall versus (Re) for air (a) M=2.5 "g/sec" (b) M=5 "g/sec" (c) M=7.5 "g/sec" (d) M=10 "g/sec"

Fig.6. is presented to be the variation of the temperature of a wall against to temperature of liquid for a square channel. The temperature of the wall tends to increases as the temperature of liquid increases due to the temperature of a wall depending on the temperature of a liquid which means the relationship was proportional between each other. So, this parameter has a slight influence on the heat sink temperature with (M=2.5 g/sec) being higher than those of (M=5, 7.5 and 10 g/sec). It is significant to note, that the present study has relied on heat flow as well as mass flow to guess all data on the prediction process. Further research; needs to predict more closely the links between (T_w) and (T_f). At last; there are a number of important steps which need to be made.

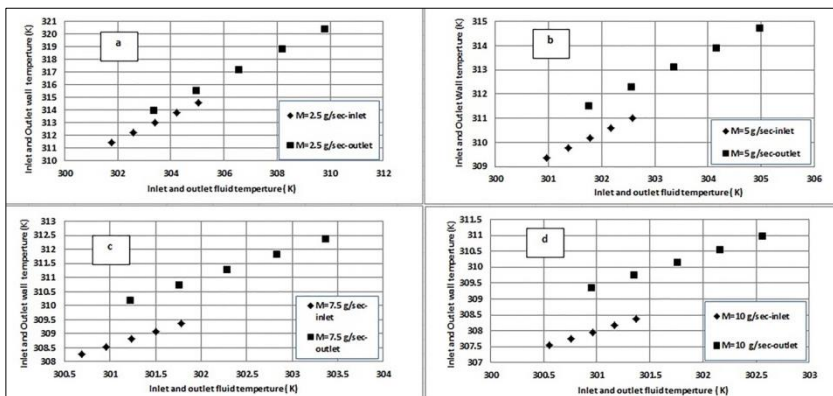


Figure.6. Alteration to temperature of wall versus temperature of liquid (a) M=2.5 "g/sec" (b) M=5 "g/sec" (c) M=7.5 "g/sec" (d) M=10 "g/sec"

As shown in Fig.7.the prediction data on (Re) versus heat applied (ha) so there was a significant positive correlation on between each other so the (ha) tends to decreases as the (Re) increases due to the (T_w) depended on the (Re) which means the relationship was polynomial between each other.When (ha) was stimulated with (Re), no significant difference in the number of (Re) was detected, So the overall response to the study was good.

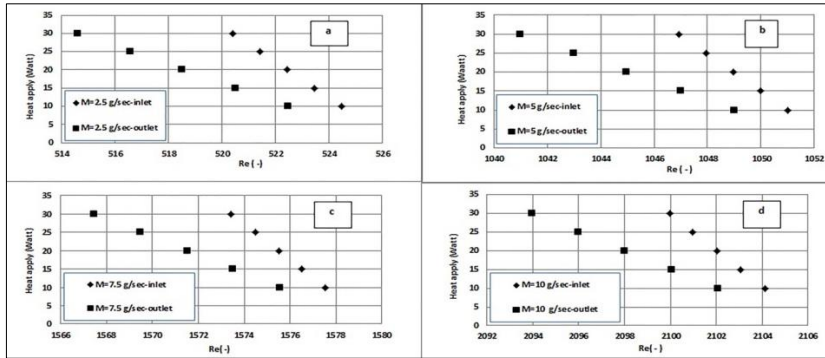


Figure.7. Alteration to heat applied versus (Re) for air (a) M=2.5 "g/sec" (b) M=5 "g/sec"(c) M=7.5 "g/sec" (d) M=10 "g/sec"

Conclusions

In this work, the heat transfer characteristics in the plane-channel of the heat sink are only considered as predictions so that the conclusion depends on the iterative method of the transfer and the heat transfer equations so the main conclusions can be drawn by the following points.

- The airflow was laminar and was developing for all estimation tests.
- The data inlet higher than the data outlet, the data inlet was not big different with to the data outlet.
- The objective of this present work was to get a (T_w) and (T_f) on a flat-channel of heat sink has employed air as coolant liquid.
- In order to achieve this, phenomenon; appropriate predictable facilities; a suitable prediction device was designed and engineered for a copper plate on the heat sink, and all tested conduction heat transfer conditions.
- Estimation investigation can be explained better or similar than classical tests for a plane- channel of a heat sink.

References

- [1] Wang Q-W, Zhao C-L, Zeng M, Wu Y-N. Numerical investigation of rarefied diatomic gas flow and heat transfer in a microchannel using DSMC with uniform heat flux boundary condition—part II: applications. *Numer Heat Transf Part B Fundam* 2007;53:174–87.
- [2] Lee W, Son G. Bubble dynamics and heat transfer during nucleate boiling in a microchannel. *Numer Heat Transf Part A Appl* 2008;53:1074–90.
- [3] Lie YM, Ke JH, Chang WR, Cheng TC, Lin TF. Saturated flow boiling heat transfer and associated bubble characteristics of FC-72 on a heated micro-pin-finned silicon chip. *Int J Heat Mass Transf* 2007;50:3862–76.
- [4] Yu X, Feng J, Feng Q, Wang Q. Development of a plate-pin fin heat sink and its performance comparisons with a plate fin heat sink. *Appl Therm Eng* 2005;25:173–82.
- [5] Shakir R. INVESTIGATION OF SINGLE-PHASE FLOW CHARACTERISTICS IN A STAGGER PIN-FINS COMPLEX GEOMETRY. *J Eng Sustain Dev* 2021;25:74–81.
- [6] Shakir R. Pressure Drop Effect on Mini-Scale Heat Sink by Multi-phase: Review & Prediction. *Univ Thi-Qar J Eng Sci* 2022;vol.1:50–5.
- [7] Shakir R. Investigate the Flow of Boiling Heat Transfer in a Complex Geometry Flat Channel. *Univ Thi-Qar J Eng Sci* 2022;Vol.1:56–61.
- [8] Shakir R. Boiling Heat Transfer in a Micro-Channel Complex Geometry. *IOP Conf. Ser. Mater. Sci. Eng.*, vol. 928, IOP Publishing; 2020, p. 22129.
- [9] Shakir R. Investigation of Single-Phase Flow Characteristics in an Inline Pin-Fins Complex Geometry. *J. Phys. Conf. Ser.*, vol. 1879, IOP Publishing; 2021, p. 32118.
- [10] Holman JP. *Heat Transfer (Si Units)* Sie. Tata McGraw-Hill Education; 2008.

Estimation of Heat Flow Properties on Inline-Channel Heat Sink

R.SHAKIER *

University of Thi-qar- College of engineering-Department of Petroleum and Gas engineering; raed-sh@utq.edu.iq; shraed904@gmail.com

Correspondence: raed-sh@utq.edu.iq; shraed904@gmail.com; Tel.: *
07811646919

Abstract: The rapid growth of technology has shrunk electronic devices and improved their efficiency. So the miniaturization of electronic devices and the thickening of electronic devices are decreasing the Space obtainable for cooling and for raised heat dissipation. This investigation concerns air flow heat transfer in array of in-line square micro-pin-fins having a $(1 \times 1 \text{ mm}^2)$ cross-section by a (1mm) on height. One inlet temperatures of (299.15 K), (2) mass airflow for inlet temperature, ranging by (2.5 and 5 g/ s), and Heat applies had ranged from (20 to 100 Watts). The guesses had performed for the Reynolds number; pressure drop and the temperature of heater on the ranges of (2660. 68– 5329. 99) and (2.53–5. 19) mbar, (309.71 - 369.92 K) respectively. Therefore, an important product design trouble has effectively prevented Instability and damage by overheating electronic as well as electrical equipment on products that had the goal of this study.

Keywords: Heat estimation; Inlinepin-fins heat sink; Heat properties.

1. Introduction

The recent progression of micro-scale on manufacture techniques, So, permitted extra complex mini-heat geometries to be invented, to the higher thermal conductivity rigid substrate at a low charge, which created it possible to discover one more grown structures that may be extra succeeded than the mentioned parallel mini-channels of a heat sink. A favorable configuration had arrays of inline or staggered mini-scale pin-fins such as. [1];[2];[3];[4];[5];[6];[7];[8];[9];[10] and [11].[12] reported numerically to R113 stream and heat transmission in an inline-pin-fins of heat sink by employing the iteration method by uniform heat flux on the boundary situations. [13] was recorded to study (Dp) and heat transmission of a mini-scale on heat sink in addition to [14] was reported to investigate of boiling-phase on heat transmission for micro-scale of heat sink.

The goals of the present investigation are: (1) to estimate new heat transfer data for airflow in an inline-pin-fin array, (2) to appear in substantial parametric ways and discover the possibility of mechanisms of heat transfer, (3) to guess the accuracy of past experimental for inline-pin-fin correlations with for guessing the new data and (4) to disclose a new correlation of heat transfer for airflow in the inline-pin-fin array.

2. Materials and Methods

The guessing software are employed over than (500) equations of heat transfer then pushed them on Excel software by Iteration method; as seen in Fig.1, the

creation states that only a single to position of heat flux can exist to solid-air interface. So that 2-D array had employed on, So the main effect on the wall line; the 1- D array had perpendicular to the air-flow, the 2-D array had parallel to the airflow, and the thermal conductivity should be followed steps as seen to Fig.1, [15]; [16].

$$\delta^2 T / \delta y^2 + \delta^2 T / \delta z^2 = 0 \tag{1}$$

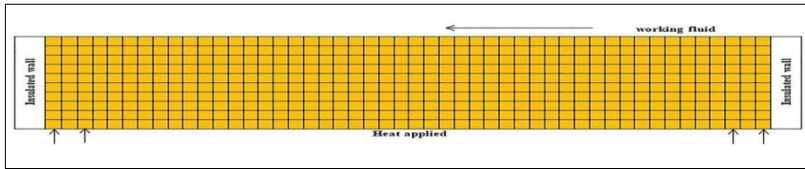


Figure.1. Wall Conduction of copper test Piece [15]; [16].

On which (T) is the temperature on the wall of copper and (y) was perpendicular on airflow axis so that heat transfer on eq. (1) had found by dividing via the square of the square cell area (1mm).[15]; [16].

$$= \delta y^2 (T_{i+1,j} + T_{i-1,j}) + \delta z^2 (T_{i,j+1} + T_{i,j-1}) / 2 (\delta y^2 + \delta z^2) T_{i,j} \tag{2}$$

The formula on the coefficient of heat transfer for pin-fins can be got by employing the equation below[17].

$$q_h B_{cell} = \psi (T_w - T_f) [(B_{cell} - B_c) + \eta_{fin} B_{fin}] \tag{3}$$

The side on the right has a heat dispersion to unit cell airflow by employing a formula

$$B_{cell} = S_l S_t \tag{4}$$

Where

S_l= a distance from of central cell to another center-cell in a length direction.

S_t= a distance form of central cell to another center-cell in a width direction.

B_{fin}= a wetted surface an area of single pin-fins.

$$B_{fin} = P_{fin}H_{fin} \quad (5)$$

And (η_{fin}) shows fin efficiency, [17].

$$\eta_{fin} = \tanh(m_{fin}H_{fin})/m_{fin}H_{fin} \quad (6)$$

Bfin factor is

$$m_{fin} = \sqrt{\psi P_{fin}/K_c B_c} \quad (7)$$

In which (B_c) is a cross-sectional area of a single in-line-pin-fins.

$$B_c = W_{fin}L_{fin} \quad (8)$$

A (P_{fin}) is a cross-section perimeter of a single inline-pin-fins, while (W_{fin}) is an inline pin-fin width in (mm); (L_{fin}) is an inline pin-fins length in (mm) and (H_{fin}) is an inline pin-fins height in (mm).

$$P_{fin} = 2(W_{fin} + L_{fin}) \quad (9)$$

Which (Pr) based on hydraulic diameter of channel as follows[17].

$$Pr = \frac{C_p \mu_f}{k_f} \quad (10)$$

The Reynolds number can be got by formula below[17].

$$Re = \rho_f V D_h / \mu_f \quad (11)$$

where a hydraulic diameter can be seen via formula[17].

$$D_h = \frac{4 \cdot A_h}{P} \quad (12)$$

To guess the (NU) in flow based on the results on the literatures that apple it all (4) sides of the pin-fins being heated can get via formula [17]:

$$NU_{x,3} = NU_{x,4} \frac{NU_{fd,3}}{NU_{fd,4}} \quad (13)$$

where $NU_{x,4}$; $NU_{fd,3}$; and $NU_{fd,4}$; were obtained to be acquired respectively, for the geometry and boundary conditions considered. Friction factor can be got by Ref.[17].

$$f_{laminar} Re = 24(1 - 1.3553 + 1.946\Gamma^2 - 1.7012\Gamma^3 + 0.95641\Gamma^4 - 0.2537\Gamma^5) \quad (14)$$

For the pin-fins-channel had boundary conditions on theorized ($f_{turbulent} Re$) has been got,[17].

$$f_{turbulent} = 0.0791 Re^{-0.025} \quad (15)$$

In which (Γ) is the aspect ratio of square channel, and laminar is the Fanning friction factor. The pressure drop can be got according to the method of Liu and Garimella.[17]

$$\Delta P = 2 f_{laminar} Re \rho_f V^2 \frac{L}{D_h} \quad (16)$$

The value for (T_w) at mini and pin-fins-scale can be got as, [17]

$$T_w = T_{th} - \frac{q_h L_{th}}{K_C} \quad (17)$$

The value of (T_f) at mini and pin-fins-scale is got by, [17]

$$T_f = T_{in} + \frac{q_h W Z}{M_f C_{pf}} \quad (18)$$

3. The guess setup

The guess set-up consists of (3) important parts; the loop, the pin-fins channel as well the conditions of the technique.

3.1. The Loop

The prediction set-up diagram is shown in Fig.2. The loop consists of a test loop, a cooling airflow loop, and a data acquisition system, air was employed for liquid cooling; so; the air wind tunnel was a rectangular "acrylic" air duct measuring (20 x 20) cm by (150) cm long, the "duct" was isolated by Aero-Flex compliant (10 mm) thick via a metal plate. The air inside the wind tunnel was released to the wind tunnel by the air compressor, released for the test section movement, and to the ambience. As well as airflow values are "measured" with a "flow meter" with fully-scale accuracy (0.5%).The pressure drop across the meter section was measured by a differential pressure sensor with an accuracy of (0.05%) of fully scale. Identify (2) pressure taps for each wall, located downstream and upstream of the test section. So, type K -copper "constantan" from "thermocouple", accurate (0.5%) fully scale, was employed to measure air temperature. So that, the inlet and

outlet temperatures of the air are measured by (2) thermocouples via probes (1mm), each extending of diameter to duct through the air flows. As well as; all thermocouple probes are pre-calibrated using the calibrator's dry box temperature (0.05 °C).

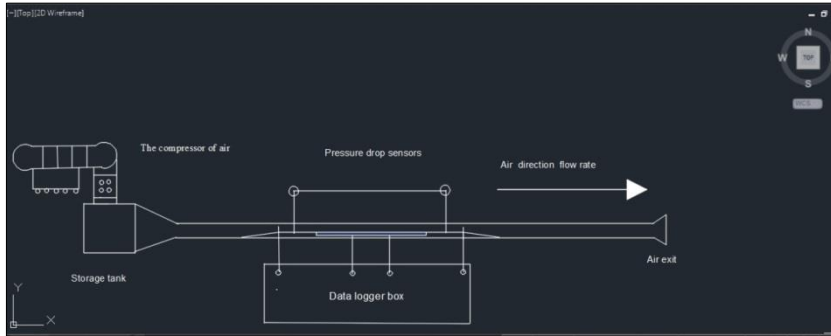


Figure.2. Prediction Rig

3.2. The pin-fins channel

The planning scheme of test piece has seen on Figs.3&4. Are seen test section and pin-fins details that the width" of heat sink as well as heat sink length is (50 mm by 50 mm) "respectively". The pin-fins-channel of heat sinks had supplemented via a wire of electric "evacuation machine". As Seen on Fig.3.pin-fins-scale of complex geometry "has" (25) solid fins each fin has (1mm x1mm) cross-section by a (1mm) on height.AC power has the power supply on plate kind so the rear surface on test segment was isolated by standard (15 "mm") solid resistant heat of "mica board, criterion (10 "mm") of Aero-flex board, and standard (10 mm) thick of acrylic board. (2) T-type copper constantan thermocouple has a diameter of (1mm) was employed to obtain of temperature of wall for pin fins-scale. By supporting of wall drilled by thermocouple has been an inserted hole on rear face as well fixed via distinct gluey employed on wall of rear face for the pin-fins of heat sink.

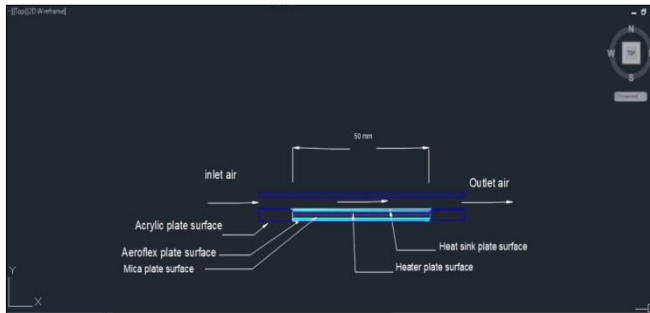


Figure.3.Test section

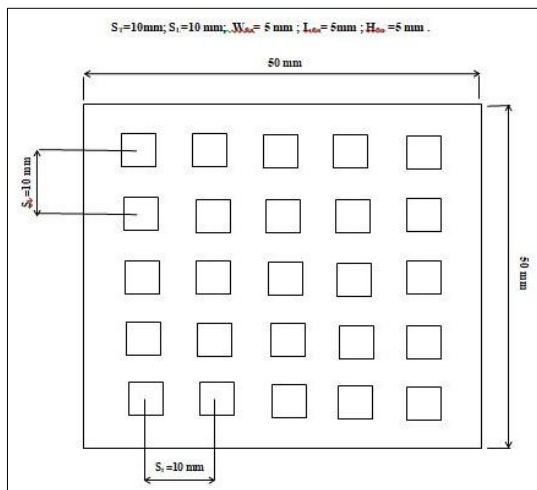


Figure.4.Test piece

3.3. The conditions of the technique

Predictions had conducted via different heat flows and different flow rates of air entering to test section. On the predictions, the airflow was increased with a slight increase so that the small-scale heat input was stably protected on a heat sink, so that the small-scale heat input of walls to complex geometries, was achieved by using an "electric" heating needs to be of the size required, as the well-supplied power supply has stopped supplying current and voltage to the heater on a large scale. The supplied voltage and heater's current are scaled using a "digital clamp" measurement device. As well a sensible of heat on Steady-state data was obtained from the airflow could be got by the energy balance method. Only data for energy balance conditions had been accepted for this study by using an iterative procedure for all estimation tests. Additionally, at each temperature point (Dp) a number of "times" are listed compared to the test segment. So; Values data was collection as well executed by employing a system had acquisition data so the

uncertainty of the prediction should be liked an airflow meter (± 0.05); the temperature of the thermocouple (± 0.02); and the difference of the pressure sensor (± 0.05).....etc.

4. Results and Discussion

Through the brief review of the above analysis key results are grown by employing the iterative method to get the major parameters of heat transfer for the pin-fins of the heat sink.

Figure.5.presents to the results obtained from the expected analysis of (Re) that can be seen the difference of the temperature of heater for inlet and for outlet locations versus it (Re) for pin-fins of heat sink with (50 mm) on width and (50 mm) on height. so the heater temperature of heat sink with (M= 2.5 g/sec) was higher than (M=5 g/sec) as well as the temperature of heater on the inlet as well as "outlet locations on pin fins of heat sink are seen to decreases with increasing (Re) with an outlet data substantially smaller than an inlet data for all guess data tests. Issues related to the temperature of heater had particularly prominent on the results data.

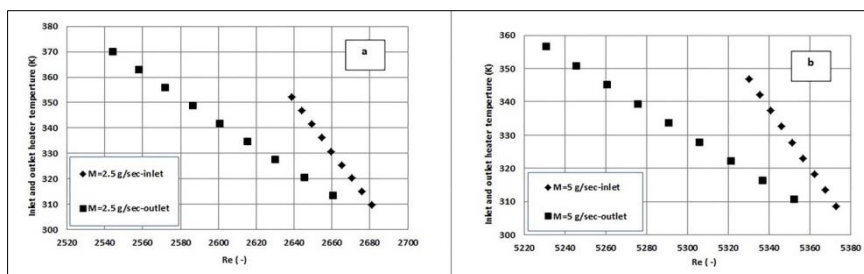


Figure.5. Alteration to temperature of heater versus (Re) for air (a) M=2.5 "g/sec" (b) M= 5 "g/sec

The results of the temperature of heater had correlational analysis are had showed Fig.6.the temperature of heater was variation at inlet and at outlet locations versus of inlet and of outlet air temperature. The temperature of heater at outlet tends to increases as the temperature of fluid increases as well as temperature of heater at inlet tends to increases as the temperature of fluid increases due to the temperature of a wall depending on the temperature of a heater which means the relationship was power among each other; Finally the process was guessed for all data tests.

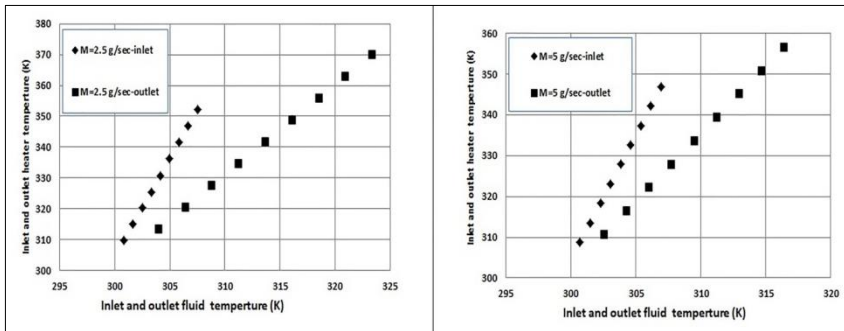


Figure.6. Alteration to temperature of heater versus inlet and of outlet air temperature for air (a) $M=2.5$ "g/sec" (b) $M=5$ "g/sec"

Fig.7.shows that the difference of temperature of heater against to (D_p) on inlet and on outlet locations for pin-fins-scale of heat sink.It can be seen from the data in "Fig.7.that the data inlet reported significantly more than data outlet .The increasing of (T_h) according to increasing (D_p) .Generally, the surface area of this heat sink has extra heat area due to has pin-fins that will add more activity area to remove unwanted heat come from electrical devices So that the pin-fins heat sink was studied and reported in this paper, so these data still demand can be investigated.

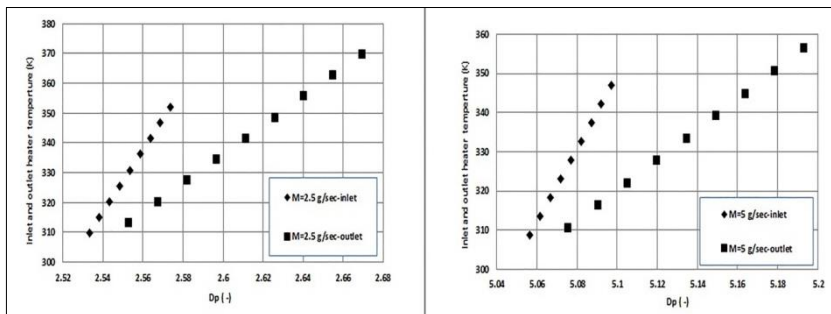


Figure.7. Alteration to temperature of heater versus pressure drop (a) $M=2.5$ "g/sec" (b) $M= 5$ "g/sec"

Fig.8.presents to the predictable data on (D_p) between an inlet and outlet locations so it can contributions to obtain (D_p) guess. Due to the air of the pin fins heat sink also an inlet loss and an exit loss. So, the (D_p) at inlet and at outlet positions was decreased as the (Re) increases as well as (D_p) at outlet data greater than at inlet data that due to the temperatures at outlet positions higher that at inlet positions. In summary these results see that good to be closed to actual results.

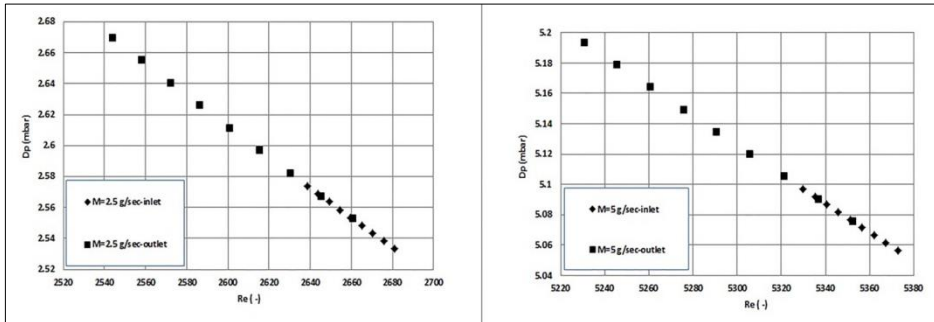


Figure.8. Alteration to (D_p) versus (Re) (a) $M=2.5$ "g/sec" (b) $M= 5$ "g/sec

5. Conclusions

The main goal of the current study was to determine the properties of heat transfer on pin fins heat sink. In general, these findings had significant implications for the understanding of how to get the best heat sink so more information on pin-fins heat sink would help us to establish a greater degree of accuracy on this matter. The findings of this investigation have a number of practical implications so the following conclusions can be drawn from the present article.

- Air flow was laminar and turbulent for all guess data tests.
- Air flow was developing for all guess data tests.
- The scope of this investigation was limited in terms of one shape of heat sink
- In spite of its limitations, the study certainly adds to our understanding of the pin-fins heat sink better than another one.

6. References

- [1] J. Lee and I. Mudawar, "Two-phase flow in high-heat-flux micro-channel heat sink for refrigeration cooling applications: Part II—heat transfer characteristics," *Int. J. Heat Mass Transf.*, vol. 48, no. 5, pp. 941–955, 2005.
- [2] P.-S. Lee and S. V Garimella, "Saturated flow boiling heat transfer and pressure drop in silicon microchannel arrays," *Int. J. Heat Mass Transf.*, vol. 51, no. 3–4, pp. 789–806, 2008.
- [3] J. R. Thome, R. Groll, and R. Mertz, "Microscale Heat transfer: boiling

and evaporation,” 2003.

[4] A. Koşar and Y. Peles, “Convective flow of refrigerant (R-123) across a bank of micro pin fins,” *Int. J. Heat Mass Transf.*, vol. 49, no. 17–18, pp. 3142–3155, 2006.

[5] R. S. Prasher *et al.*, “Nusselt number and friction factor of staggered arrays of low aspect ratio micropin-fins under cross flow for water as fluid,” 2007.

[6] A. Siu-Ho, W. Qu, and F. Pfefferkorn, “Experimental study of pressure drop and heat transfer in a single-phase micropin-fin heat sink,” 2007.

[7] W. Qu and A. Siu-Ho, “Liquid single-phase flow in an array of micro-pin-fins—Part I: Heat transfer characteristics,” *J. Heat Transfer*, vol. 130, no. 12, 2008.

[8] A. Koşar and Y. Peles, “Boiling heat transfer in a hydrofoil-based micro pin fin heat sink,” *Int. J. Heat Mass Transf.*, vol. 50, no. 5–6, pp. 1018–1034, 2007.

[9] S. Krishnamurthy and Y. Peles, “Flow boiling of water in a circular staggered micro-pin fin heat sink,” *Int. J. Heat Mass Transf.*, vol. 51, no. 5–6, pp. 1349–1364, 2008.

[10] T. H. Hwang and S. C. Yao, “Forced convective boiling in horizontal tube bundles,” *Int. J. Heat Mass Transf.*, vol. 29, no. 5, pp. 785–795, 1986.

[11] M. K. Jensen and J.-T. Hsu, “A parametric study of boiling heat transfer in a horizontal tube bundle,” 1988.

[12] R. Shakir, “INVESTIGATION OF SINGLE-PHASE FLOW CHARACTERISTICS IN A STAGGER PIN-FINS COMPLEX GEOMETRY,” *J. Eng. Sustain. Dev.*, vol. 25, no. 6, pp. 74–81, 2021.

[13] R. Shakir, “Pressure Drop Effect on Mini-Scale Heat Sink by Multi-phase: Review & Prediction,” *Univ Thi-Qar J Eng Sci*, vol. vol.1, no. No.12, pp. 50–55, 2022.

[14] R. Shakir, “Investigate the Flow of Boiling Heat Transfer in a Complex

Geometry Flat Channel,” *Univ Thi-Qar J Eng Sci*, vol. Vol.1, no. No.12, pp. 56–61, 2022.

[15] R. Shakir, “Boiling Heat Transfer in a Micro-Channel Complex Geometry,” in *IOP Conference Series: Materials Science and Engineering*, 2020, vol. 928, no. 2, p. 22129.

[16] R. Shakir, “Investigation of Single-Phase Flow Characteristics in an Inline Pin-Fins Complex Geometry,” in *Journal of Physics: Conference Series*, 2021, vol. 1879, no. 3, p. 32118.

[17] J. P. Holman, *Heat Transfer (Si Units) Sie*. Tata McGraw-Hill Education, 2008.

Exploration of the General Algorithms and Standard Methods in TSP

¹Shaymaa Taha Ahmed

University of Diyala, Diyala, Iraq
mrs.sh.ta.ah@gmail.com

²Qusay Kanaan Kadhim

Department of Computer Techniques Engineering
Middle Technical University, Baghdad, Iraq
Bilad Alrafidain University College Diyala, Iraq
qusaykn@gmail.com qusaykn@bauc14.edu.iq

³Hamid Sadeq Mahdi

University of Diyala, Diyala, Iraq

⁴Rana M.Zake

Computer Science Department, University of Technology, Baghdad, Iraq
Rana.M.Zaki@uotechnology.edu.iq

Abstract - The traveling salesman problem (TSP) is investigated using some polynomial time algorithms to find "excellent," but not essentially ideal, tours. The percentage of the measured tour length to the shortest tour length is used to determine a tour's proximity. When using the method of the closest neighbour. It appears to be more logical to investigate any TSP by first learning about its historical context to grasp the principles of the task typically required in such exercises. TSP challenges are briefly summarized as an easy model to grasp but a difficult problem to solve. Simply recognize that TSP falls within the category of [issues that are more difficult to solve]; in most cases, these are non-polynomial-based issues (i.e., no polynomial-time techniques are available). In reality, TSP did not include math principles at first (1800-1832). Despite the lack of direct methods for TSP situations, there are still ways to fix the problem, but not to the exact solutions that are necessary, to the permissible (nearest/most) level This problem-solving procedure entails locating certain approximation approaches as well as the optimization solution series, both of which are more susceptible to human comprehension than the machines', as a result, heuristic decisions are required in both routine and difficult issues. As a result, the focus of this article's paper review is on analysing via TSP investigation, the conventional methods or general algorithms, then, primarily based on study literature, aiming to categorize each uses with TSP domains of use.

1 -INTRODUCTION

TSP stands for traveling salesman problem and is a computational technique with several applications, including truck routing, logistics, planning, and scheduling. The TSP's basic problem is to discover a tour of a given number (n) of cities that covers the shortest distance and visits each city exactly once before returning to the beginning location [1]. Given a collection of n cities, named $\{c_1, \dots, c_n\}$ and permutations $\sigma_1, \dots, \sigma_n!$, the goal is to select σ_i so that the summing of all Euclidean distances between cities in a tour is minimal. In domains of computer science and mathematics TSPs (The Traveling salesperson problems) are well-known for their important applications in real-life problems (e.g. Transport/traffic management). They are said to be easier to understand than to solve[2].

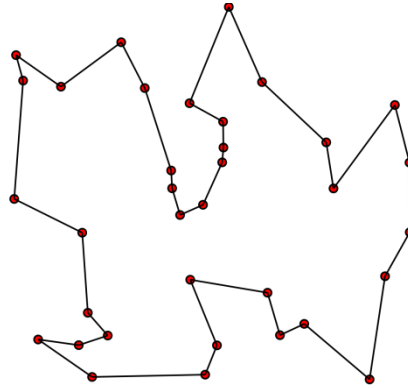


Figure 1. Traveling Salesman Problem

The Traveling Salesman Problem (TSP) is a classical and well-studied combinatorial optimization problem[3]. Since the 1950s, it has been studied extensively in both Operations Research and Computer Science, resulting in the development of a wide variety of solutions to handle this problem. TSP research isn't always motivated via direct applications; rather, it is distinguished by the fact that it provides an excellent platform for the study of general approaches that can be utilized in a wide range of separate optimization problems. Several direct applications of TSP, in fact, breathe new life into the study field and aid in the direction of future work. The goal of the problem is to identify the quickest salesman route starting from a specific city, only visiting n cities once before returning to the origin city. TSP is described by an edge-weighted graph $G=(V,E)$, where V represents a collection of $n=|V|$ nodes or vertices indicating cities and E represents a set of directed edges or arcs. Every arc $(i,j) \in E$ has a length d_{ij} assigned to it, which equals the distance between cities i and j with $i, j \in V$. In nature, TSP can be asymmetric or symmetric. If the TSP is asymmetric, The distance between two nodes i and j is determined by the direction of the traverse edge or arc, i.e. $d_{ij} \neq d_{ji}$ exists for at least one arc (i,j) . For any arcs in E , $d_{ij}=d_{ji}$ holds in symmetric TSP. TSP's purpose is to find a graph with the shortest Hamiltonian Circuit [2], The Hamiltonian Circuit is a closed path that visits each of G 's n nodes once. Permutation of node indices $\{1, \dots, n\}$ such that length $f(\pi)$ is minimal, where $f(\pi)$ is given by, is an optimal solution to TSP.

$$f(\pi) = \sum_{i=1}^{n-1} d_{\pi(i)\pi(i+1)} + d_{\pi(n)\pi(1)}$$

Despite the hardness of their solutions procedure, some various methods are defined for some such situations by application some mathematical techniques and specific algorithms. But, most extreme cases need human particular understanding and interpretation (i.e. Heuristic analysis) to get to better acceptable solutions[4]. Up to recent decades, many businesses and industries people got rocked by the economic crisis before getting to know how important a good transport management could greatly help the situation[5].

2- Review of TSP

Chauhan C. et al. [6] explains the numerous methods/techniques for solving the traveling salesman problem and analyzing them in order to make a critical assessment of their time difficulties. Exact and non-exact TSP solvers are the two types of TSP solvers. Exact solvers are divided into two categories. Solving flexibilities of the TSP Linear Programming formulations, for example, using methods such as Cutting Plane, Branch-and-Cut, Interior Point, and Branch-and-Bound. Dynamic Programming is used by a smaller group. At least three groups independently identified branch and bound. Using calculations when the integer restrictions of the issues are relaxed, the Branch and Bound approach indirectly enumerates all conceivable solutions. To put it another way, the branch and bound technique separates a problem into several sub-problems. Approximation Algorithms and Heuristic Algorithms are used in non-exact solvers.

Dominique Feillet et al. [7] describe Traveling salesman problems using profits (TSPs with profits), a generalization of the traveling salesman problem (TSP), in which all vertices do not have to be visited. Each vertex has a profit linked with it. The overall goal is to optimize both the obtained profit and the trip expenditures at the same time. These two optimization requirements exist as a constraint or as an objective function. Various application classifications, modelling methodologies, and exact or heuristic optimization algorithms are identified and contrasted. Conclusions highlight the importance of this class of problems in terms of both applications and simulated results.

Exnar Filip et al. [8] explained the TSP so that it can be used in the logistics industry. For a 15 node problem four matrix were obtained viz. two for distance and time matrix of shortest route and two for distance and time matrix of fastest route. The shortest route was discovered to take the most time, whereas the fastest route was the longest in terms of the distance. As a result, the nodes were split into two groups; one part transporting the imports by owns vehicle and other by subcontracting. The main aim was to economically benefit the company.

Mohammad Asim et al. [9] proposed traveling salesman problem. The authors of this paper demonstrate how the heuristic method of genetic algorithms is used to solve the traveling salesman problem. The goal is to identify the closest solution that results in the shortest distance, where is the quickest route for travelling the cities in the data collection such that each city is only visited once and the traveling salesperson returns to the starting city. The authors achieve this by implementing the algorithm by developing a fitness formula and using genetic operators such as selection, crossover, and mutation.

Sumanta Basu [10] explain The Traveling Salesman Problem (TSP) and related issues such as the Vehicle Routing Problem (VRP) are two of the most well-known combinatorial optimization challenges. It's been known for a long time that it's NP-hard, hence research into building algorithms for the TSP has focused on approximation methods rather than accurate methods. One of the most often used met heuristics for solving the TSP is tabu search.

Younis Elhaddad et al. [11] proposed an algorithm, a hybrid of Genetic algorithm (GA) and Simulated Annealing (SA) which uses TSPLIB instances to obtain good results. This hybrid method helps the GA to take a jump as it gets stuck after 20 consecutive iterations. Using a CPU having Matlab 7.0 the results obtained indicated that the Hybrid Genetic and Simulated Annealing Algorithm (HGSAA) In comparison to the Local Search Heuristics Genetic Algorithm(LSHGA), delivered more optimal solutions.

1.2. TSP Brief Presentation

1.2.1 What about TSP? What Problem in TSP

A TSP issue is about finding on a region (or travel system) routes' map the location of a service requesters along with the proper order of possibly visiting all of them. And that is all as the basic problem of TSP[12] .

1.2.2 TSP Concerns

Finding out a shorter path for all above-mentioned visits but, the entirely visited distance bearing minimum costs is the main objective in TSP. In addition to searching for a solution with the cheapest of costs, any of each location must be visited only once (with the start and the ending point being the same)[12]. Obtaining optimal solutions is often not enough especially in the case of a hard-NP or difficult problem with respect to required solution quality.

Therefore, the expected effective and efficient solution here will be ensured through heuristic methods[13] .

1.2.3 TSP Basic Elements

Though much information enters into consideration throughout problem and solution formulation, these are at the bottom line. These are for instance: location/city/site to visit or a host of services; customer-location or visit point; beginning-point (**visit orientation**) and ending-point (**Visits distance**). Based on either solving method, additional details will be added to these for better understanding and interpretation of the solution in the preparation process.

1.3 Heuristics Importance in TSP Solving Process

The heuristic approach or technique is one that aids in learning and exploration, rather of solving an issue naively or by simply applying equations or algorithms (where computing is necessary). The heuristic method is based on the mathematics science idea of solving issues by discovering new solutions rather than relying on pre-existing rules or equations. Therefore, in computer science, this will include the use of a basic rule in problem-solving, but in a different way, not always using all of the suggested algorithms [14]. All of these are things to consider when designing an intelligent system using a heuristic method; otherwise, the human tremendous sense of reasoning survives and dominates in real-time decision-making.

Here are some data on the significance of heuristics in solving TSPs. Many efforts have been made by researchers to facilitate the current new approaches for discovering TSP solutions. Because mathematical and computational tools for modelling have indisputable potential, it's only natural that these tools have had some difficulty reacting properly to TSP that falls into the realm of non-deterministic instances (i.e. very difficult problems), It was a problem a few generations earlier. For example, the authors of [8] built a multiple TSP (as a network model that demonstrates) about such limitations in traditional methods, demonstrating that the issue could not be solved if remained in the framework of the original problem, and their allegation is only one of several [15] . The availability of various polynomial-time methods known to be good yet limited in providing optimum solutions in TSP is discussed in [9]. In any case, it is critical that heuristics principles are followed, problem-solving judgments and options must aim to satisfy the user's specific needs while taking into account the case's numerous factors and restrictions [16]; meanwhile, heuristic approaches are considered as part of the non-exact techniques category [4] . It simply means that, unlike computers, they are prone to human error. Human experience, on the other hand, is far superior to that of any man-made intelligent system in terms of choosing, using, and regulating knowledge in the solution of complex issues[16] .

- Heuristics overlook the interdependencies of pieces of a system. It can occasionally have a significant impact on the overall system's solution to the issue.

2 TSP GENERAL SOLVING METHODS

2.1 algorithms or standard methods

Thanks to [17] for one of the recent surveys produced on some common TSP solving methods. Their review focused mainly on screening out cases for which heuristics have failed to stand for the best as much believed in some other studies. This article under this subsection attempts to briefly discuss TSP standard or commonly used algorithms, with a biased view on heuristics. Moreover, in the next section, some related TSP solving methods are also introduced, to further verify the position of heuristics and the role played in handling difficult TSP.

2.2 Difficult Problem in TSP Research

The theory of complexity showing TSP as being under the called NP-complete problems or simply difficult problems' group is mentioned in [18]. It also conducted a study on symmetric TSP that ended with an optimal solution but that could not be improved merely with some changes in K-edge—a situation's view supported in related works in the same article. Otherwise, another truth regarding local search algorithms with polynomial time complexity per iteration is that they have a polynomial time difficulty per iteration, bringing about approximation impossibility for such TSP solving progress (Unless $P=NP$) [3][4][5].

A summary for a general definition of difficult TSP is in [18] as follows.

1. Consider an example with a large number of local optima for a neighborhood structure N and a single global optimum. This is a challenging case in which N is used for local search.
2. Another case: For high values of k (e.g., k equivalent to n), TSP with the k -change search is a tough case for local search algorithms in general.
3. Due to its applicability in other study fields made possible by researchers, TSP gets harder to solve than its mere formulation. Some of the obvious reasons are the problem inputs difference, their interpretation of the TSP standard, and the solution model. Hence, the heuristic approach is important in providing the appropriate alternative to get ahead of a given problem.

2.3 TSP Common Algorithms Standards

2.3.1 Brief Review on TSP Solving using Heuristic Method

Many important studies have discussed heuristic algorithms applicable in TSP, which can produce TSP solutions nearer to optimal in distance and costs expectation [19]. From past decades to nowadays, TSP helped to model and solving various management-based problems such as routing, facility location, tasks scheduling, travel/shipment, network design issues, and many more in different science fields. And according to [19], Bellmore and Nemhauser (1968), Bodin (1975), Golden et al. (1975), Gillett and Miller (1974), and Turner et al. (1974) are examples of articles. (1974) are among the great examples which provide useful literature reviews for TSP.

2.3.2 Example of Algorithms for TSP Solving

2.3.2.1 Hamiltonian Cycle into TSP Solving Method

Based on principle similarity, circuit Imagine a Hamiltonian cycle around a dodecahedron's edges finding process can be seen as the original/basic algorithm of TSP, and it is originated from Icosian game—i.e. a game invented (1859) by Sir William Hamilton (Figures '1' & '2'). And that game required solution is today's TSP basic solution —i.e. obtaining a Hamiltonian circuit or a path with every vertex visited only once, no edge can be revisited, and the ending and the starting points are the same[4] .



Figure 1 Icosian Game

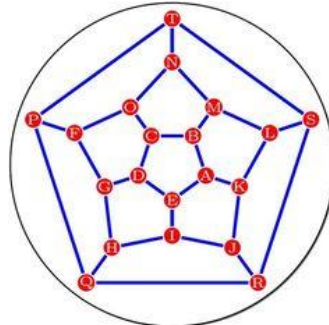


Figure 2 Dodecahedron

A clearer form for TSP was developed by 1930 by the mathematician Karl Menger, the father of brute-force algorithm and nearest neighbour heuristic. And based on this source, many people have contributed in improving TSP solving fundamental algorithm. However, almost each new improvement algorithm received its contributor name(s) and an illustrative phrase (e.g. Richard M. Karp (1972) with NP-Complete for Hamiltonian cycle; Lin and Kernighan (1973) with “Lin-Kernighan” algorithm; Bentley (1990) with the k-D tree; Lin-Kernighan heuristic algorithm (1998), called (LKH), etc. ;). Overall, the pluralism of TSP solving algorithms has occurred as a reason of many attempts with different concepts even under same problems category. These are few dire about TSP solving algorithm by contributors, which in turn make up another source of TSP solving complexity. Therefore, there is a permanent need for consensus on divergent views with respect to especially difficult problems whenever alternative method is available.

3 ANALYSIS OF TSP SOLVING METHODS STANDARD

3.1 At Beginning

TSP (since 1950) is as old as other applied math than computers problems under the Combinatorial Optimization model [20]. Its various solving techniques/methods have remained theoretical but, they have rendered its concept background interesting and applicable to other problems with a general principle and acceptable for Discrete Optimization Problems[20] .

3.2 Problem Solving Basic Modelling (Formulation)

The TSP basis model consists of number (n) of cities (V) geometrically represented by a given E edge-weighted graph G, whose vertices are (V) such as,

- $G = (V, E)$ and V is a set of $n=|V|$ cities to visit;
- $E \subseteq (V * V)$ is a set of directed edges linking each couple of cities at $(i, j) \in E$, with endpoints $(i \neq j)$, $i \in V_1$ and $j \in V_2$ such as the two cites have d_{ij} distance parameter,

Then, for each $V(i, j)$ in the graph: TSP is either asymmetric or symmetric, meaning:

- TSP Symmetric $\leftrightarrow d_{ij}=d_{ji}$ –i.e. any direction from which to visiting either (i) or (j) does not matter (but, yes in opposite case)
- Else, TSP Asymmetric $\leftrightarrow d_{ij} \neq d_{ji}$ –i.e. direction does matter in starting point of visits

Hence, once these conditions hold together, TSP solution can be determined using either credible method. Thus, for [4] an optimal solution can be obtained in finding $f(\pi)$ minimum distance through permutation π of nodes (i.e. $n=|V|$ nodes or vertices/point referring to as cities).

Therefore, for node indices $\{1, \dots, n\}$ the path distance $f(\pi)$ minimal is derived from:

$$f(\pi) = \sum_{i=1}^{n-1} d_{\pi(i)\pi(i+1)} + d_{\pi(n)\pi(1)}$$

3.2.1 TSP Solution Main Concern

In TSP solving process, the following three principles are very important. The first is to determine the called Hamiltonian minimum length [19]-- i.e. the trip closed shortest-road going only once through n nodes /cities, with fewer costs. Next is to find a TSP optimal solution by permutation π of node indices (n). And finally, the heuristic algorithm is the alternative for more difficult problems in general.

3.3 TSP Common Solving Methods

They are categorized as exact and non-exact solving techniques[19] ; many being used like a standard method for similar problems over time.

The first group -- comprises basically of:

1. Linear Programming based techniques Cutting Plane, Interior Point, Branch-and-Bound, and Branch-and-Cut are only some examples.
 2. Branch and Bound method: -lists down every possible solution and breaks TSP into small sets, proven efficient for the network of about 60 nodes
 3. Cutting Plane: - applicable to all problems; uses linear programming relaxation at iterations start.
 4. Branch and Cut: - useful for TSP with huge of instances
- **Dynamic Programming based techniques**—method involving efficiently recurrences computations whose results are utilizing the results and repurposing them if appropriate
 - Brute-force technique—a turbo solver, as it can fit for any problem and produce the two basic required answers elements.

Whereas the second category consists of a group of three namely: approximation, heuristics and a group of algorithms combining both approximate solutions and large running-times cases.

4 HEURISTIC METHOD BASED TSP SOLVING

4.1 Travel Based TSP Study and Analysis

In a typical TSP that is based on trip design, the basic aspects of the travel network designer are getting to know the participants' desires and the fascinating sites/locations/cities they would want to visit. Such travel-related considerations, on the other hand, are about determining the aforementioned inputs in such a manner that they may closely satisfy the visitors' preferences at reduced costs and with maximum pleasure[21]. Every potential roadblocks and problems (e.g. spatial, climatic, environmental, and social), other key concerns include finances, time, logistics, gastronomy, health, and security, which all contribute to the total cost of a tour and therefore its practicality [21] .

4.2 TSP Solving Techniques Category

Heuristic algorithms, based on [4], fall under the category called “non-exact solvers”. The other techniques group mates are “approximation algorithms” – i.e. TSP Solving Traditional Methods (MST-based algorithm, mixed MST, and Minimum Matching Problem/MMP); and a collection of "interesting algorithms" (e.g. Simulated Annealing, Genetic Algorithms, Ant-Colony Algorithms, and some machine learning algorithms (e.g. Neural Networks)).

However, heuristic algorithms produce only feasible solutions (i.e. free from too many theoretical outcomes). Two kinds to distinguish simple tour-construction-based algorithm (e.g., Nearest Neighbour, Clarke-Wright, and Multiple Fragment1), as well as complex tour-improving algorithms based approaches (e.g., Nearest Neighbour, Clarke-Wright, and Multiple Fragment1) (e.g. Tabu Search and Lin-Kernighan).

4.3 Issues in TSP Solving

4.3.1 TSP Iteration & Solution Particular Principle

Based on the literature general rules and regardless of TSP's two main categories (i.e. regular or hard-NP /difficult cases), any TSP requires visiting each of the v -cities only once with the last trip returning to the origin city (V_1). And under this condition, with the shortest-distance and lowest-costs travel, the ideal option is satisfied. As a result, these two criteria are the most important in the TSP solution procedure. Moreover, no (unique) method exists to solve all TSP instances, the best of reasoning references will almost always be heuristics notions [1] when and when all other tried-and-true tactics have failed. As far as prejudice is concerned, this is owing to the fact that humans have a better level of decision-making (appreciation) than machines (computer systems in general).

4.3.2 Optimal versus Heuristics Solutions/Method

There are many valuable reasons [2][3] to choose specific techniques.

- a) The suitability with the type of problems including the frequency in practice can be the general rule of thumb. But what justification beyond this?
- b) The numerous existing optimal-based algorithm as presented in [3] and discussed here in “ 2.2.2” required a good knowledge of existing algorithms and a good understanding of TSP in hand to pick up the right solving method.
- c) Another inherent cause is the extension of the TSP concept for application with other problems of general principle. For, it arguable to agree on a reasonable number of visiting locations in an ordinary travel system problem. But, under real-life application (e.g. mail distribution. Product distribution, assembling managements, etc.), the number (n) theoretically grows too high up and turns down the efficiency of well-known algorithms learned from a similar problem. Therefore, the heuristic can allow drawn a fair conclusion when facing such cases.
- d) As a particular remark, heuristically referring to TSP solving main principles, distance (or shortest-path) may not the best of consideration if only in terms of its cost (though the direct path is known a minimizing cost), but instead for significant shipment (i.e. true sign of service effectiveness) involved [16][22] .

5- Application of TSP and connections to other challenges

i. Drilling of printed circuit boards

The TSP is directly applied to the problem of drilling printed circuit boards (PCBs) [17]. To connect conductors over one layer to conductors on another layer, holes must be bored through the board, or to locate integrated circuit pins. Different sized holes are possible. To drill two holes of different diameters in a row, the machine's head must walk to a tool box and replace the drilling equipment. It will take a long time to complete this task. As a result, it's obvious that one must select a diameter, Change the drill, drill holes of the next diameter, and so on. As a result, this drilling issue can be thought of as a succession of TSPs, one for each diameter size, with 'cities' referring to the starting point and a selection of all holes which can be drilled with the same drill. The time it takes to move the drilling head from one location to the next determines the "distance" between two cities. The goal is to keep the machine head moving as quickly as possible.

ii. Gas turbine engine overhauling

This application was described by [23] and occurs when aircraft gas turbine engines need to be overhauled. To maintain a uniform gas flow through the turbines, nozzle-guide vane assemblies are positioned at each turbine stage. The number of nozzle guiding vanes is mounted around the periphery of such an arrangement. Each one of these vanes has its own characteristics, and the precise

placement of the vanes can result in substantial advantages (reducing vibration, increasing uniformity of flow, reducing fuel consumption). The problem of optimum vanes location can be modelled as a TSP with a specific target function.

i. X-ray crystallographic

The TSP is used to investigate the structure of crystals [24]. In this scenario, an X-ray diffractometer is utilized to determine the structure of the crystalline substance. A detector is used to measure the intensity of the crystal's X-ray reflections from various angles. While the measurement itself can be done quickly, there is a significant overhead in positioning time because some studies require hundreds of thousands of locations to be realized. The location in the two instances we've given entails shifting four motors. The amount of time it takes to travel from one position to another can be calculated extremely precisely. The order in which the measurements at the various sites are taken has no bearing on the outcome of the experiment. The overall time required for the experiment, however, is determined by the sequence. As a result, the challenge is to develop a sequence that minimizes total positioning time. As a result, a traveling salesman dilemma arises.

ii. Computer wiring

A unique case of linking components on a computer board was reported by [25]. Modules are positioned on a computer board and must be attached to a certain subset of pins. Unlike in most cases when a Steiner tree connection is sought, here no more than two wires are allowed to be joined to each pin. As a result, the task at hand is to identify the smallest Hamiltonian path with no defined beginning and ending point. The so-called test bus wiring is in a similar condition. To test the made board, create a connection that enters the board at a specific place, passes through all of the modules, and exits at a different point. For this test wiring, we have a specific entrance and exit location for each module. This problem is similar to a Hamiltonian route problem, the distances, however, are not uniform, and the starting and finishing positions are supplied.

iii. The order-picking problem in warehouses

Material handling in a warehouse is the source of this issue [26]. Assume a certain order for a subset of the items on the list hand arrives at warehouse. To ship all of the things in this order to the consumer, some vehicle must collect them all. The connection to the TSP is obvious right away. The graph's nodes correspond to the locations where items are stored. The distance between two nodes is determined by the time it takes to convey a vehicle from one location to another. The difficulty of selecting the fastest route for a vehicle while

using the least amount of fuel a TSP can now be used to tackle the problem of pickup time. This difficulty can be readily remedied in some circumstances, for a detailed discussion and references.

5 –Conclusion

This review attempted initially to go through some selected articles for TSP general rules and especially those about problems solving methods. The lessons from those sources have provided some good insights in understanding and differentiating between optimal and heuristics methods. In concluding points, here is some consideration for motivation to learners and researchers interested in TSP-based studies in general and in particular on intelligent systems design for a tour activity management using heuristic methods. And for TSP solving, few recalls about heuristics usefulness were reported in the introduction of this review. Simple adjustments of the distance matrix can address a number of difficulties related to the fundamental traveling-salesman problem. We can, for example, push a set of cities to be together in a tour by arbitrarily reducing the distance between them; similarly, we can force them apart with artificially increasing the distance between them. As a result, we can solve problems involving the shortest Hamiltonian path by connecting the two end locations with a short distance. They were more a reminder; the other sections have also proved that one must develop an interest in heuristic-based algorithms and their development for better handling of TSP difficult problems.

REFERENCES

- [1] Q. Liu, S. Du, B. J. van Wyk, and Y. Sun, “Niching particle swarm optimization based on Euclidean distance and hierarchical clustering for multimodal optimization,” *Nonlinear Dyn.*, vol. 99, no. 3, pp. 2459–2477, 2020, doi: 10.1007/s11071-019-05414-7.
- [2] E. Nechita, G. C. Crisan, L. B. Iantovics, and Y. Huang, “On the resilience of ant algorithms. Experiment with adapted MMAS on TSP,” *Mathematics*, vol. 8, no. 5, 2020, doi: 10.3390/MATH8050752.
- [3] P. Jedrzejowicz and I. Wierzbowska, “Parallelized swarm intelligence approach for solving TSP and JSSP problems,” *Algorithms*, vol. 13, no. 6, 2020, doi: 10.3390/a13060142.
- [4] Ł. Kowalik, S. Li, W. Nadara, M. Smulewicz, and M. Wahlström, “Many-visits TSP revisited,” *J. Comput. Syst. Sci.*, vol. 124, no. 677651, pp. 112–128, 2021, doi: 10.1016/j.jcss.2021.09.007.
- [5] M. M. Krishna, N. Panda, and S. K. Majhi, “Solving traveling salesman problem using hybridization of rider optimization and spotted hyena optimization algorithm,” *Expert Syst. Appl.*, vol. 183, no. May 2020, p. 115353, 2021, doi:

10.1016/j.eswa.2021.115353.

[6] D. L. Hershman *et al.*, "Prevention and management of chemotherapy-induced peripheral neuropathy in survivors of adult cancers: American society of clinical oncology clinical practice guideline," *J. Clin. Oncol.*, vol. 32, no. 18, pp. 1941–1967, 2014, doi: 10.1200/JCO.2013.54.0914.

[7] D. Cattaruzza, N. Absi, D. Feillet, and J. González-Feliu, "Vehicle routing problems for city logistics," *EURO J. Transp. Logist.*, vol. 6, no. 1, pp. 51–79, 2017, doi: 10.1007/s13676-014-0074-0.

[8] F. Exnar, O. Machač, and J. Svědík, "The Travelling Salesman Problem and its application in logistics," *Proc. World Multiconference Appl. Econ. Bus. Dev.*, vol. 8, no. 4, pp. 60–64, 2011.

[9] M. Asim *et al.*, "A review on pineapple leaves fibre and its composites," *Int. J. Polym. Sci.*, vol. 2015, 2015, doi: 10.1155/2015/950567.

[10] S. Basu and G. Michailidis, *Regularized estimation in sparse high-dimensional time series models*, vol. 43, no. 4. 2015.

[11] Y. R. Elhaddad, "Combined Simulated Annealing and Genetic Algorithm to Solve Optimization Problems," *World Acad. Sci. Eng. Technol.* 68, vol. 6, no. 8, pp. 1508–1510, 2012.

[12] M. Lehenauer, S. Wintersteller, M. Uray, and S. Huber, "Industrial Application of Artificial Intelligence to the Traveling Salesperson Problem," pp. 1–6, 2021, [Online]. Available: <http://arxiv.org/abs/2109.14392>.

[13] E. Baş and E. Ülker, "Discrete social spider algorithm for the traveling salesman problem," *Artif. Intell. Rev.*, vol. 54, no. 2, pp. 1063–1085, 2021, doi: 10.1007/s10462-020-09869-8.

[14] M. Abbasi and M. Rafiee, "Efficient parallelization of a genetic algorithm solution on the traveling salesman problem with multi-core and many-core systems," *Int. J. Eng. Trans. A Basics*, vol. 33, no. 7, pp. 1257–1265, 2020, doi: 10.5829/ije.2020.33.07a.12.

[15] Z. A. Ali, S. A. Rasheed, and N. No'man Ali, "An enhanced hybrid genetic algorithm for solving traveling salesman problem," *Indones. J. Electr. Eng. Comput. Sci.*, vol. 18, no. 2, pp. 1035–1039, 2020, doi: 10.11591/ijeecs.v18.i2.pp1035-1039.

[16] M. F. Demiral, "A parameters analysis of sine cosine algorithm on travelling salesman problem," *El-Cezeri J. Sci. Eng.*, vol. 7, no. 2, pp. 526–535, 2020, doi: 10.31202/ecjse.662864.

[17] J. Triana, V. Bucheli, and A. Garcia, "Traveling salesman problem solving using evolutionary algorithms guided by complex networks," *Int. J. Artif. Intell.*, vol. 18, no. 2, pp. 101–112, 2020.

[18] S. Bouzbita, A. El El Afia, and R. Faizi, "The behaviour of ACS-TSP algorithm when adapting both pheromone parameters using fuzzy logic controller," *Int. J. Electr. Comput. Eng.*, vol. 10, no. 5, pp. 5436–5444, 2020, doi:

10.11591/IJECE.V10I5.PP5436-5444.

- [19] A. Seyyedabbasi, R. Aliyev, F. Kiani, M. U. Gulle, H. Basyildiz, and M. A. Shah, "Hybrid algorithms based on combining reinforcement learning and metaheuristic methods to solve global optimization problems," *Knowledge-Based Syst.*, vol. 223, no. July, 2021, doi: 10.1016/j.knosys.2021.107044.
- [20] S. K. R. Kanna, K. Sivakumar, and N. Lingaraj, "Development of Deer Hunting linked Earthworm Optimization Algorithm for solving large scale Traveling Salesman Problem," *Knowledge-Based Syst.*, vol. 227, p. 107199, 2021, doi: 10.1016/j.knosys.2021.107199.
- [21] Y. Cui, J. Zhong, F. Yang, S. Li, and P. Li, "Multi-subdomain Grouping-based Particle Swarm Optimization for the Traveling Salesman Problem," *IEEE Access*, pp. 227497–227510, 2020, doi: 10.1109/ACCESS.2020.3045765.
- [22] M. E. B. Menai and M. Batouche, "An effective heuristic algorithm for the maximum satisfiability problem," *Appl. Intell.*, vol. 24, no. 3, pp. 227–239, 2006, doi: 10.1007/s10489-006-8514-7.
- [23] F. Krampah, N. Amegbey, S. Ndur, Y. Y. Ziggah, and P. K. Hopke, "Fractal Analysis and Interpretation of Temporal Patterns of TSP and PM10 Mass Concentration over Tarkwa, Ghana," *Earth Syst. Environ.*, vol. 5, no. 3, pp. 635–654, 2021, doi: 10.1007/s41748-021-00237-2.
- [24] R. Matai, S. Singh, and M. Lal, "Traveling Salesman Problem: an Overview of Applications, Formulations, and Solution Approaches," *Travel. Salesm. Probl. Theory Appl.*, 2010, doi: 10.5772/12909.
- [25] J. K. Lenstra, A. H. G. Rinnooy Kan, and P. Brucker, "Complexity of machine scheduling problems," *Ann. Discret. Math.*, vol. 1, no. C, pp. 343–362, 1977, doi: 10.1016/S0167-5060(08)70743-X.
- [26] P. Guo, M. Hou, and L. Ye, "MEATSP: A Membrane Evolutionary Algorithm for Solving TSP," *IEEE Access*, vol. 8, pp. 199081–199096, 2020, doi: 10.1109/ACCESS.2020.3035058.

Administrative creativity and its impact on improving employee performance
(An exploratory study of the opinions of a sample of workers in the prefab factory / Kirkuk)

Mueyyed Akram Omar arslan¹, Sawsan Ibrahim Rajab²
Sivadass Thiruchelvam³, Gasim Hayder³,

¹ College of Graduate Studies, University Tenaga Nasional (UNITEN), 43000 Kajang, Malaysia

² Northern Technical University, Kirkuk Technical Institute, Iraq

³ Department of Civil Engineering, College of Engineering, University Tenaga Nasional (UNITEN), 43000 Kajang, Malaysia
Alparslan1961.ma@gmail.com

ABSTRACT

The research sought to identify the role played by the prefabricated building factory for the issue of administrative creativity in terms of (sensitivity to problems, an abundance of ideas, flexibility, originality, ability to analyze, risk) and its relationship to improving the performance level of employees, because of its impact on the possibility of achieving competition for the company to obtain It has a distinguished position in the prefabricated building market. To achieve the goal of the research, which was built on its problem, and to achieve this, a questionnaire was designed as a tool for data collection to achieve the objectives of the research, as it was distributed to a sample of (40) employees and engineers, and (39) questionnaires valid for analysis were recovered, i.e. a response rate of (98%) was completed. Reliance on the program (SPSS VER 12) in data analysis. The research reached some conclusions, most notably the presence of an effect of (sensitivity to problems, abundance of ideas, flexibility, originality, ability to analyze, risk) in improving the performance of employees in the company in question. Accordingly, some suggestions were presented that the respondents' suggestions should be taken into consideration to reach accurate problem identification and continuous improvement. As well as re-examining work procedures and overcoming the problems related to the rigidity of the systems by requesting periodic reports from the heads of departments and other departments.

Keywords: administrative creativity, employee performance, prefabricated building factory.

1. Introduction

Creativity has become a distinctive feature in contemporary companies as it offers the optimal solutions in a world teeming with the challenges imposed by the new globalization system. The intense competition between companies and technical change in addition to the information revolution and the abolition of trade and service barriers put companies to the test, which necessitated the provision of capable creative capabilities. In this case, creativity has become an essential function in modern organizations. Therefore, the completion of work in the company requires that the administrative creativity is at a high degree of efficiency and effectiveness, the need for an effective organization and proper planning for the performance of employees, in addition to a real follow-up to the aspects of improvement. A catalyst for improving the performance of employees and the organization as a whole.

2. The research problem

For the company to be at the top, it must keep pace with development and improve the performance of employees, because the work, no matter how

technically developed or possessed of capabilities, remains dependent on the minds that manage it and manage its affairs. Evolution is not dependent on machines and technology, but rather dependent on human development, growth, advancement, and improving performance. The hands of managers intervene in laying the real building blocks of this approach, just as leaders and decision-makers interfere in improving their performance. Hence, this research transforms access to specific transformative results for the impact of administrative creativity in improving the performance of employees. This is done by answering the following questions:

- 2.1 What is the level of managerial creativity in the company under study?
- 2.2 What is the level of improvement in the performance of employees in the company under study?
- 2.3 Is there a relationship between administrative creativity and improving the performance of employees in the company under study?
- 2.4 What is the effect of administrative creativity on improving the performance of employees in the company under study?

3. The importance of research

The importance of the research lies in three main axes:

- 3.1 Academic, which is represented in the presentation and theoretical definition of the research variables that different organizations need to deal with.
- 3.2 Field, and lies in the statement of the relationship and the impact between administrative creativity and improving the performance of employees.
- 3.3 Submit proposals that address problems.

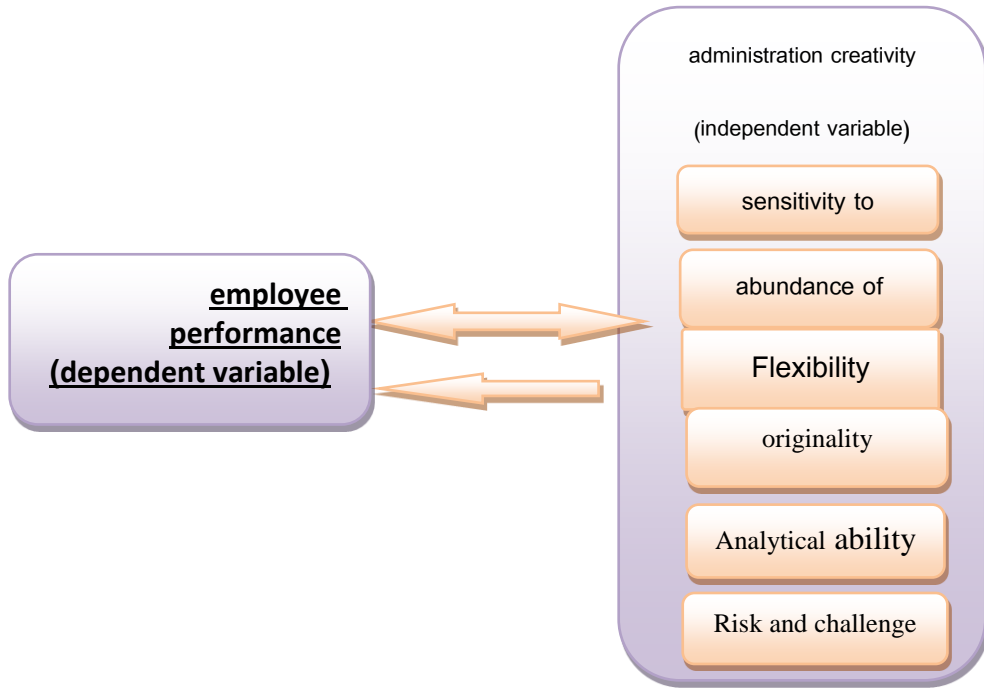
4. Research objectives

The research aims to achieve the following:

- 4.1 Identifying the level of administrative creativity in the company under study.
- 4.2 Indicating the level of importance of improving the performance of employees in the company under study.
- 4.3 Identifying the relationship and the impact between administrative creativity and improving the performance of employees in the company under study.

4. The research hypothesis model

Research model: To achieve the purpose of the research and reach its specific objectives, the variables represented by the variable administrative creativity and the variable improving the performance of employees were identified. As a prelude to presenting the research hypotheses and testing the extent to which there is an effect among the investigated variables, as shown in Figure (1).



Source: Prepared by the researchers

Figure (1) Hypothesis Research Model

5. Research hypotheses:

In line with the objectives of the research and its proposed problem, the following guesses were adopted as research hypotheses, which are:

The first main hypothesis: There is a statistically significant correlation between administrative creativity and employee performance, and the following sub-hypotheses are branched from it:

5.1 There is a statistically significant relationship between the sensitivity dimension to problems and the performance of employees in the company under study.

5.2 There is a statistically significant relationship between the abundance of ideas and the performance of the employees in the company under study.

5.3 There is a statistically significant relationship between the dimension of originality and the performance of the employees of the company under study.

5.4 There is a statistically significant relationship between the flexibility dimension and the performance of employees in the company under study.

5.5 There is a statistically significant relationship between the risk and challenge dimension and the performance of the employees of the company under study.

5.6 There is a statistically significant relationship between the ability dimension of analysis and the performance of employees in the company under study.

The second main hypothesis: There is a statistically significant effect of administrative innovation in improving the performance of employees. The following sub-hypotheses are derived from it:

5.7 There is a statistically significant effect of the sensitivity dimension to the problems in the performance of the employees of the company under study.

5.8 There is a statistically significant effect of the abundance of ideas on the performance of the employees of the company under study.

5.9 There is a statistically significant effect of the dimension of originality on the performance of the employees of the company under study.

5.10 There is a statistically significant effect of the flexibility dimension on the performance of employees in the company under study.

5.11 There is a statistically significant effect of the risk and challenge dimension on the performance of the employees of the company under study.

5.12 There is a statistically significant effect on the dimension of the ability to analyze the performance of employees in the company under study.

6. study limits

6.1 the spatial boundaries of the study

The Prefabricated Building Factory in Kirkuk was chosen, which is one of the construction companies in the public sector. Some reason called the researchers to choose this company as a field for research as it is one of the important companies that provide its services in Iraq in general and Kirkuk in particular.

6.2 temporal limits of research

The temporal limits of the research took from the period 1/9/2021 until 15/1/2022, and it was interspersed with repeated visits to the prefabricated construction plant in Kirkuk.

7. Data collection methods

In completing their research, the researchers relied on the following methods:

7.1 Theoretical aspect: the two researchers employed what foreign scientific references were available to them related to the subject of the research.

7.2 The practical aspect: a questionnaire prepared for this research was adopted and prepared by the researchers.

8. the statistical methods used

To reach the results of the study and verify the validity of the hypotheses put forward, the researchers used the ready-made software (SPSS), and based on that, we used a set of statistical tools represented in the following:

Frequencies, percentage, arithmetic means, and standard deviations to display and analyze the results of the answers of the sample members, and then indicate the degree of dispersion of the values from their arithmetic mean.

The Simple Correlation Coefficient was used to determine the nature of the relationship between two variables and to determine the internal communication of the questionnaire items on strategic intelligence and organizational creativity.

-Multiple regression was used to measure the significant effect of the independent variables on the dependent variable.

The coefficient of determination (R^2) shows the amount of change in the dependent variable, which can be explained by the independent variable.

-Test (f test) Use this test to find out whether there is an effect of the independent variables on the dependent variable.

The t-test was used to measure the significance of the correlation between the two variables.

The second topic: the theoretical framework

The first aspect: is administrative creativity

1. The concept of administrative creativity

From a scientific point of view, there are many definitions of administrative creativity, some of which can be referred to as follows:

It is defined (Arafa, 2011, 83) as “a mental ability that appears at the level of the individual, group or organization, and it is a multi-stage process that results in a new idea or action that is characterized by the greatest degree of fluency, flexibility, originality, sensitivity to problems, retention, and continuity of direction, and is characterized by the ability to focus for long periods in the field of interest, and the ability to form new connections, discoveries and relationships, and this creative ability can be developed and developed according to the capabilities and capabilities of individuals, groups and organizations.

2. The importance of administrative creativity

Administrative creativity is considered one of the basic ingredients in the process of change. The developments surrounding us resulting from the information revolution and the technological explosion, the increase in competition between companies, the diversity of individuals' needs, the lack of resources, the increase in the ambition of individuals, the increase in the effectiveness of communications, the large size of business organizations, and the change in values and principles, may It has created and created many problems, so organizations must respond to these developments by making changes and modifications that go along with these developments. This can only be achieved by the presence of new ideas and modern methods that respond to these continuous changes. (Al-Azzawi, 2011, 31).

3. Types of administrative creativity

The researchers differed in determining the types of creativity, and despite their differences, they did not depart from the following types that are:

Taylor identified five types of creativity, which are: (Al-Azzawi, 2011, 37).

3.1 Expressive creativity, is the automatic method by which a particular person is distinguished in doing something, practicing a profession, or practicing an art.

3.2 Technical creativity represents the aesthetic aspect that is added to the goods and services, such as the appearance of the commodity, the functions it performs, and the needs that satisfy it.

3.3 Invention, which is the creation of something new for the first time, except that its elements and the parts that compose it exist before, but a modification has been made to it, making it take a new form and perform a distinct task.

3.4 Complex creativity, represents an unusual combination of things, such as taking different ideas and putting them in one model to arrive at new information.

3.5 Creation, which is the use of something that already exists but is applied in a new field.

4. The dimensions of administrative creativity

The researchers agreed on the existence of the following dimensions of administrative creativity:

4.1 A sense of the problem: which is considered the most important element of creative thinking, and a sense of the problem means seeing it, defining it precisely, and recognizing its size, aspects, dimensions, and effects (Agha, 2011, 44).

4.2. The abundance of ideas: Creativity needs an abundance of ideas, and most of them may not be suitable for implementation, but the important thing is that the innovator or creator does not reject an idea that comes to his mind, but rather has the task of collecting the largest amount of ideas, then starts examining, evaluating and categorizing them, so the lesson here is at a rate The production of ideas during a certain period (Aga, 2011, 44).

4.3 Flexibility: It means the ability to change the state of mind by changing the situation. Flexibility is the diversity or difference of ideas that the creative individual brings, and therefore it refers to the degree of ease with which the individual changes a position or point of view. Or a specific approach, but rather can adapt to the renewed circumstances, changes and situations. (Al-Shammari: 2001: 72).

4.4 Authenticity: by which we mean that a person moves away from traditional ways of thinking as he explores original ideas. Authenticity is the result of imagination in the sense of dissatisfaction with the status quo, and the desire to create something new or different. Usually, the creator begins with imitation and

then develops what has been imitated. Completing the deficiency in it and then striving to present it in a new form (Al-Shammari: 2001: 72).

4.5 .Analytical ability: The creative person is the one who is satisfied with a small amount of information when doing any new work because he can simplify and organize his ideas and work according to studied foundations, as the individual who can analyze is described as the individual who can deal with an idea or a work. (Al-Shammari, 2001:73)

4.6. Risk: It means taking the initiative in adopting new ideas and methods and searching for solutions to them at the same time that the individual is capable of bearing the risks resulting from the actions he undertakes and is ready to face the responsibilities arising from that (Al-Shammari, 2001:73).

The second aspect: improving employee performance

1. the concept of employee performance

There are many concepts put forward by researchers about the performance of workers, as the performance of workers is defined as the individual's carrying out the activities and tasks that make up the job (Al Mulla and Waffa, 1996, 121). It is also the degree of achievement and completion of the tasks that make up the job, as this definition reflects how the individual satisfies or achieves the requirements of the job (Al-Barnouti, 2001, 219). While it was defined as an organized process that begins by comparing the current situation and the desired situation for individual and institutional performance and trying to determine the performance gap, here comes the analysis of the causes to know the impact of the work environment on performance. (Harem, 2004, 77).

2. Factors affecting the performance of employees

These factors affecting the performance of workers can be classified into three categories, each category contains a group of sub-influences, namely: (Nibal, 2000, 47-50) (Rawiya, 2000, 211)

2.1 Organizational factors: related to the philosophy of organizations, policies, procedures, and administrative methods used with employees.

2.2 The material conditions of work: These are the material factors that surround the worker while he is doing the work.

2.3 Personal factors: These are the features and characteristics of the working individual.

The third topic: the fieldside

3.1 Description of the research sample

The stratified sample was chosen in the prefabricated building factory in Kirkuk from the category of directors of bodies, departments, people, and their assistants, numbering (39) people, and the following is a description of the research sample as shown by the results of the questionnaire, which are:

3.1.1 Gender: It is clear from Table (1) on the distribution of the research sample by gender, that the percentage of males constituted (56%) of the sample members, and that the percentage of females formed (44%) of the sample members, which indicates that most of the administrative positions are given for males in this company.

Table (1) Distribution of the sample members by sex

No.	gender	the number	The ratio
1	male	22	٥٦%
2	female	17	٤٤%
Total		39	١٠٠%

Source: Prepared by the researchers based on company data

3.1.2 Age: We note from Table (2) that the age groups ranging between (15-20) years constituted 7%, which is the lowest among the mentioned age groups, while the age groups ranging between (25-21) constituted (49%), which is A high percentage compared to other age groups, and about the age group that ranged between (26-30) years, it constituted (18%) and finally the age group that ranged more than (30) years constituted (26%) of the age groups.

Table (2) Distribution of the sample members by age

No.	age	the number	The ratio
1	years (٢٠-١٥)	3	٧%
2	years (٢٥-٢١)	19	٤٩%
3	years (٣٠-٢٦)	7	١٨%
4	More than 30 years	10	٢٦%
Total		39	١٠٠%

Source: Prepared by the researchers based on company data

3.1.3 Qualification

It is clear from Table (3) that the academic achievement of the research sample members and their possession of scientific qualifications, and this reflects the development of their experience and information, as we note that the percentage of holders of a master's degree has reached (5%), and the number of people who hold a higher diploma has reached (8%), While the percentage of people holding a bachelor's degree was very high, it reached (74%), and this is a good indicator, as they can deal with the questionnaire accurately and scientifically and understand its contents. As for the number of people who have a technical diploma, it has reached (13%). This diversity of both sexes and with different academic attainments indicates a diversity of perceptions and orientations, and thus an increase in constructive ideas that contribute to achieving excellence and leadership.

Table (3)

The sample members were distributed according to the certificate

No.	Type of certificate	the number	The ratio
1	Masters	2	٥%
2	Higher Diploma	3	٨%
3	BSC	29	٧٤%
4	Technical Diploma	5	١٣%
Total		39	١٠٠%

Source: Prepared by the researchers based on company data

3.1.4 years of service

It is evident from Table (4) that the number of people whose years of service ranged from (1-to 5) years constituted (26%), while the number of people who had service (5-to 10) years constituted (59%), which is the highest percentage. Compared to the other percentages of years of service for the sample members, the percentage of people whose years of service ranged from (10-15) years, their percentage amounted to (10%), and the number of people whose service ranged between (15-20) years reached Their percentage (5%), we note that there is a clear

difference in the experience of the people in the research sample, which allows them to give a clear perception of the information on the research variables at the company level in general.

Table (4)

Distribution of sample members according to years of service

No,	age	the number	The ratio
1	(٥-١) years	10	26%
2	(١٠-٥) years	23	59%
3	(١٥-١٠) years	4	10%
4	(٢٠-١٥) years	2	5%
Total		39	100%

Source: Prepared by the researchers based on company data

Secondly: the practical aspect of research

Analysis and discussion of the results of the opinions and responses of a sample of respondents (managers) to indicators of administrative creativity.

1. Analysis and discussion of the results of the respondents' opinions and responses to the research variables.

This topic deals with the presentation and analysis of the data included in the questionnaire, by analyzing the opinions and responses of a sample of respondents from the research community represented by (the ready-made building lab) about the research variables related to indicators of managerial creativity.

The responses of the sampled respondents about the administrative creativity variable, table (٥) indicate the general description of the opinions and responses of the research sample members of the managers in the prefabricated building factory and at the detailed level of the indicators of managerial creativity.

Table (5)

The order of relative importance of the average answers of the research sample related to the variables of administrative creativity

No.	administration creativity	standard deviation	Arithmetic mean	The ratio	Verification degree
1	Allergy	.504	4.76	95%	Excellence
2	abundance of ideas	765	4.54	91%	Excellence
3	Flexibility	.535	4.54	91%	Excellence
4	originality	.824	4.43	87%	very good
5	Analytical ability	1.088	4.41	81%	very good
6	risk	1.233	2.80	56%	acceptable

Source: Prepared by the researchers based on company data

It is evident from Table (5) that the indicators of administrative creativity. It was with a varying degree of verification between excellence - very good and acceptable. The sensitivity arrangement ranked first with a degree of good, with a percentage of (95%) and a standard deviation of (0.504), as the index of abundance of ideas, it ranked second with a percentage of (91%). And the arithmetic mean was (4.54) the standard deviation was (0.765), and the flexibility index came in third place, as it got relative importance of (91%), and the arithmetic mean was (4.54), and the standard deviation was (0.5359). It reached (87%), with an arithmetic mean of (4.34) and a deviation of (0.824), and the analysis ability index came in the fifth rank, with relative importance reaching (81%), and the arithmetic mean amounted to (4.41) and standard deviation reached (1.088), and the risk index came in the last rank with a degree of Acceptable, as it obtained relative importance of (56%) and arithmetic mean (2.80) and a standard deviation (1.233), and this is what indicates through the table that the views of each of the managers in the researched company were positive regarding the indicators of administrative creativity because most of the averages and in general are higher than the hypothetical mean of (3).

Table (6)

the order of relative importance to the average answers of the research sample for the variable performance of workers

performance of employees	Arithmetic mean	standard deviation	The ratio	Verification degree
-----------------------------	-----------------	-----------------------	-----------	------------------------

performance of employees	4.42	0.727	88%	very good
--------------------------	------	-------	-----	-----------

Source: Prepared by the researchers based on company data

It is clear from Table (6) that the level of workers' performance was to a very good degree, as it came to a very good degree, with a percentage of (88%) and an arithmetic mean of (4.42), and with a standard deviation of (0.727), and most of the performance indicators of workers were among the good And the very good, and this is evidenced by the table that the views of each of the managers in the company in question were positive regarding indicators of performance improvement for human resources because most of the averages are generally higher than the hypothetical mean of (3) of the test scale.

2 .Correlation hypothesis testing

2.1. Test the first main hypothesis

Table (8) shows the results of the (Spearman) test, which tested the first main hypothesis, which is "there is a statistically significant correlation between administrative creativity and employee performance."

Table (7)

results of the correlation between administrative creativity and employee performance at the overall level

The independent variable X	Dependent variable Y	correlation
0.649	performance of employees	administration creativity

This means the correlation is significant at the significance level.(٠,٠٥)

Source: Prepared by the researchers according to the results of the electronic calculator.

We note from Table (7) that there is a positive significant correlation relationship at the level of significance (0.05) between administrative creativity and the performance of employees, and its values reached (0.649 *), which is a good value that indicates the strength of the relationship between the two variables, and this indicates acceptance of the first main hypothesis, which states There is a statistically significant correlation between administrative creativity and employee performance.

2.2. Sub-hypothesis testing

Table (8)

shows the results of the Spearman test for sub-hypotheses.

Table (8): Results of testing the correlation between administrative creativity and employee performance at the micro-level

dependent variable independent variable	performance of employees
sensitivity to problems	*0.703
abundance of ideas	*0.452
Flexibility	*0.655
originality	*0.441
Analytical ability	*0.715
risk	*0.410

(*)The correlation is significant at the (0.05) level.

Source: Prepared by the researchers according to the results of the electronic calculator.

The results of Spearman's selection according to Table (8) indicated that there is a positive correlation with a moral significance between all dimensions of managerial creativity and the dimensions of employee performance, based on the above. performance of employees.

This result indicates that the increased interest of managers in the company under discussion in the dimensions of administrative creativity will contribute to improving the performance of employees.

3.3 .Impact hypothesis testing

To test the validity of the second hypothesis, statistical tools related to this field were used. A simple linear regression analysis was performed to judge the second main hypothesis. Table (10) shows the effect of administrative creativity as an independent variable on the performance of employees as a dependent variable, as follows:

(9) Table

The effect of administrative creativity in improving the performance of employees at the overall level

F	R ²	administration creativity	in. variable
---	----------------	---------------------------	--------------

tabular	calculated		β_1	β_0	variable / Dep.
٣,٣٩	*٣٨,٦٨	٠,٥٦٢	٠,٦٩٦ *(٦,٢٤)	٠,٨٩٤ *(٢,٠٩)	performance of employees

* P ≤ 0.05 N= 39

Source: Prepared by the researchers according to the results of the electronic calculator

The results of the regression analysis indicate that there is a significant effect of administrative creativity in improving the performance of workers, as the calculated (F) value reached (38.68), which is greater than its tabular value of (3.39) at the level of significance (0.05) and the coefficient of the determination reached R2 (0.562). Following the beta coefficients, it is clear that (1) is (0.894), which is a significant value in terms of (t) calculated, which is (6.24). It is greater than its tabular value of (3.39) at the level of significance (0.05), and thus the second main hypothesis is accepted. Table (10) also shows the testing of the second hypothesis at the partial level, as follows:

Table (10)

The effect of the dimensions of administrative creativity in improving the performance of employees at the micro-level

F		R ²	performance of employees		In. variable / Dep. variable
calculated	calculated		β_1	β_0	
٤,٢٣	*١٧,٩٢	٠,٢٧٧	٠,٤٧٩ *(٤,٢٣)	١,٥٤٧ *(٣,٣٣)	sensitivity to problems
	*١١,٨٨	٠,٢٥٤	٠,٣٥٦ *(٢,٨٥)	٢,٢٨ *(٥,٢٢)	abundance of ideas
	*١٩,٨٢	٠,١٦٥	٠,٤٤٥ *(٤,٣٥)	١,٩٧١ *(٥,٦٧)	for flexibility
	*١٢,٣١	٠,١٨٠	٠,٢٩١ *(٢,٣٥)	٢,٧٧٦ *(٨,٦٩)	originality
	*٤٣,٨٢	٠,٤١٨	٠,٤٨٥ *(٦,٧٢)	١,٧٩٥ *(٦,٨٥)	Analytical ability
	*١٦,٣١	٠,٢١٠	٠,٣٩٢ *(٣,٤٥)	٢,١٧٦ *(٨,٥٩)	risk

* P ≤ 0.05 N= 39 t=3.65

Source: Prepared by the researchers according to the results of the electronic calculator

It is clear from Table (10) that sensitivity has a significant effect on improving the performance of workers, as indicated by the value of the parameter (B1) of (0.479) and the calculated (t) value that exceeds its tabular value of (4.23) at the level of significance (0.05). It was also found that the abundance of ideas significantly affects the improvement of workers' performance, as it reached (B1) (0.356) and the calculated (t) value (2.85), which is greater than its tabular counterpart at the level of significance.(٠,٠٥)

It was also found that flexibility affects significantly in improving the performance of workers, as it reached ((B1) (0.445) and the calculated (t) value that exceeds its tabular value of (0.435) at the level of significance (0.05). As it reached (B1) (0.291) and the calculated (t) value (2.35) which is greater than its tabular counterpart at the level of significance (0.05). It was also found that the ability to analyze significantly affects the improvement of workers' performance, as it reached (B1) (0.485) and the value of (t) calculated that exceeds its tabular value of (6.72) at the level of significance (0.05). It was also found that the risk has a significant effect on improving the performance of workers, as it reached (B1) (0.392) and the calculated (t) value exceeds its tabular value of (3.45), at the level of significance (0.05), thus, the partial hypotheses of the second main hypothesis of the research are accepted.

4. Conclusions and Suggestions

4.1 the conclusions

4.1.1 The organization in question pays great attention to the dimension of sensitivity to problems specialized in administrative creativity, and this is what was indicated by the percentage that this variable possessed compared to the rest of the dimensions.

4.1.2 The organization in question also pays great attention to the dimension of work and production specialized in improving the performance of workers, and this is what was indicated by the percentage that this variable possessed compared to the rest of the dimensions.

4.1.3 The results of the analysis indicated that there is a statistically significant effect of the independent variable, administrative creativity, in the dependent variable, improving the performance of employees.

4.1.4 There is a clear contribution of administrative creativity to improving the performance of employees with value and within the characteristics of good performance.

4.1.5 Adopting administrative creativity in all its dimensions at the core of administrative processes needs increased awareness of the importance of creativity and its active role in improving the performance of employees.

4.1.6 The workers in the prefab factory enjoy a high degree of creativity, although the company's encouragement for creativity is limited.

4.1.7 The process of continuous improvement of the continuous communication service provided to the customer has the effect of supporting the improvement of the performance of employees.

4.1.8 The effectiveness of the information base in the company in question has a very large and highly efficient impact, which is reflected positively on performance levels.

4.1.9 The shares of risk and flexibility for the managers of the company under study in adopting the improvement of the performance of the employees, which strengthened the company's ability to compete in the labor market.

4.1.10 It was found that administrative creativity in all its dimensions and components contributes effectively to achieving all aspects related to improving the performance of employees.

4.2 the suggestions

4.2.1 Encouraging employees to generate new ideas that contribute to increasing their revenues and achieving survival and growth, by focusing on the practical aspects that lead to achieving the best financial return and the best service alike.

4.2.2 Increasing interest in the power of rewards, and offering rewards of all kinds to its creative and distinguished employees to encourage them to generate new ideas and implement the appropriate change that leads to solving problems and thus facing the era with its crises and challenges, by holding celebrations through which the creators are honored.

4.2.3 Emphasizing the importance and role of employee development as one of the strategies that can be adopted by the branches in the field of improving the performance of the employees working in them.

4.2.4 Enhancing the role of a culture of discrimination and creativity, as it is reflected in the performance of workers working in construction companies.

4.2.5 Attracting specialized cadres to implement the work of construction companies to improve the company's performance levels.

4.2.6 Attention to achieving customer satisfaction to achieve a larger market share compared to other construction companies.

4.2.7 The researchers recommend the company in question use contemporary patterns by the management that provide high flexibility for experts and reduce

the restrictions of traditional management on them to enable them to generate creative ideas and allow sufficient time for reading and discussion.

4.2.8 The necessity of adopting the principle of organized thinking and investing in the principle of partnership to face the various environmental changes facing the company in question.

4.2.9 The researchers recommend that the management of the company in question adopt the creative initiatives of its employees, which did not affect improving their performance.

REFERENCES

- 1 -Nibal, Younis Muhammad, 2000, The sequential effect of job design and stress on job satisfaction, unpublished master's thesis, University of Mosul.
- 2 -Arafa, Sayed Salem, 2011. Modern trends in change management, Dar Al-Raya for Publishing and Distribution, Amman.
- 3 -Najm Al-Azzawi, Talal Naseer, "The Impact of Administrative Creativity on Hussein's Management Performance Level in Jordanian Commercial Banks", Saad Dahleb University - Blida - Faculty of Economics and Facilitation Sciences, 2011.
- 4 -Marwan Sharif Ahmed, "Developing the administrative performance in education offices in Lahj governorate in the light of the entrances to administrative creativity", Sana'a University, 2015.
- 5-m. High Jawad Muhammad Ali, m. Saif Al-Din Imad Ahmed College, "The Impact of Empowering Workers in Organizational Development", an exploratory study of the opinions of a sample of workers in the General Company for Woolen Industries in Baghdad, College of Administration and Economics - the University of Baghdad, Journal of Baghdad College of Economic Sciences, University thirty-sixth issue, 2013.
- 6 -Al-Mulla, Abdul Rahman Mustafa and Waftah, Abdul Salam, 1996, measuring and studying the relationship between job satisfaction and organizational performance, Journal of Economic and Administrative Sciences, Volume IV, Issue Ten.
- 7 -Wafiq Al-Agha, Administrative leaders and their role in bringing about development and organizational change in banks operating in the Journal of Al-Azhar University in Gaza, Human Sciences Series, 2010, Vol. 12, No. 2, pp. 297-346.
- 8 -Harem, Hussein. (1997 AD). The behavior of individuals in organizations. Amman: Zahran House for Printing and Publishing.
- 9 -Tawfiq Abdul Rahman (2004), Creativity and Quality Experiences, Professional Management Experience Center, third edition.
- 10 -Al-Shammari, Fahid Ayed (2002). Creative entrance to crisis and disaster management. Riyadh: Najd Trading Company.

- 11 -Al-Faouri Refaat (2005) Administrative Creativity Department, Arab Administrative Development Organization "Research and Studies" Arab Republic of Egypt.
- 12 -Al-Qaryouti, Muhammad Qasim (2000 AD). Organizational Behavior: Study of individual and collective human behavior in different organizations. Amman: Dar Al-Shorouk for Publishing and Distribution.
- 13 -Al-Barghouti, Suad Naif, (2001), Human Resources Management, Wael Publishing House, Amman - Jordan.
- 14- Rawya, Hassan Mohamed, (2000), Human Resources Management: A Future Vision, University House for Publishing and Distribution, Cairo.
- 15-16-Soo, Christine; Timothy Devinney; David Midglers; Anne Deerin, 200٨, Knowledge Management: Philosophy, Processes, and Pitfalls, California Management Review, Vol. 44, No.4, PP: 129-150.
- 16-Sundbo, Jon, 2006 Management of Innovation in Services, The Service Industries Journal, Vol. 17, No. 3, PP:432-455.
- 17-Taylor, C.W.(200٧). Various approaches to and definitions of creativity. New York: Press Syndicate of the University of Cambridge.
- 18-Torrance, E.P.(2005). The nature of creativity is manifest testing. New York: Press Syndicate of the University of Cambridge.

حساب الميل في الاعمدة الاسطوانية و الدائرية ذات الارتفاعات العالية باستخدام التصحيح
بأقل المربعات
وانتاج موديل ثلاثي الابعاد(3D).

**Calculating the slope in high-rise cylindrical and circular columns using the
least squares correction method and producing a three-dimensional (3D)
model.**

Asst. proof. Yousif H. Khalaf¹, Nagham Amer Abdulateef²
Alaa Dawood Salman³, Ayad Abbood Abdulhasan⁴

yousif.hussain1976@gmail.com¹, nagham.amer1984@gmail.com²
a.salman1001@coeng.uobaghdad³, ayad.ce@almustafauniversity.edu.iq⁴

^{1,2,3}Department of Surveying - College of Engineering - University of Baghdad – Iraq.

⁴Department Building and Constructions Engineering Technology , Almustafa University
College, Iraq.

الخلاصة:

تم في هذا البحث مراقبة سارية العلم العراقي الموجودة قرب بوابة جامعة بغداد والتي تعتبر اطول سارية في مدينة بغداد بارتفاع 75م . ونظراً لأهمية هذا الموضوع، تم مراقبة حساب الزحف (الميل العمودي) الحاصل بالسارية باستخدام جهاز المحطة المتكاملة (Total station) نوع (Topcon 105)، حيث تم اخذ عدة رصدات وبأوقات مختلفة لمدة سنتين حيث بدأنا الرصد من شهر تشرين الثاني ٢٠١٦ حتى شهر ايار ٢٠١٧ اي بمعدل اربع رصدات لسنة الواحدة. وبعدها تم معالجة قياسات الرصد باستخدام طريقة أسلوب التصحيح باقل المربعات (least square error) و موائمة الدائرة و (Fitting of circles) ثم تم معالجة البيانات وحساب الميل باستخدام برنامج الـ Matlab مع التطور الكبير لمواصفات الحواسيب واللغات البرمجية تطور علم تصحيح القياسات واصبح استخدامه في حل مسائل تصحيح الشبكات الجيودسية امرا ممكنا ويسيرا. لذلك اعتمدنا في حساب قيم التصحيحات على برنامج Matlab حيث قمنا ببرمجة القوانين الرياضية بالصيغة التي تلائم البرنامج ، حيث تم ادخال الارصادات واجراء التصحيحات عليها وحساب القيم المصححة ومقدار الخطأ بين القيم المرصودة والمحسوبة. حيث كان مقدار الميل ما بين (0.720m الى 0.759) خلال فترة المراقبة ، وبأستخدام برنامج (Auto CAD) وبرنامج الـ (3D MAX) تم رسم السارية بتصميم ثنائي وثلاثي الابعاد.

كلمات الدالة : التصحيح باقل المربعات (least square error) ، موائمة الدائرة (Fitting of circles) ، برنامج الـ Matlab

Abstract

In this research, the Iraqi flag pole located near the gate of the University of Baghdad, which is considered the longest pole in the city of Baghdad with a height of 75 m, was monitored. In view of the importance of this topic, the calculation of the creep (vertical slope) in the mast was monitored using the Total station device (Topcon 105), where several observations were taken at different times for two years, where we started monitoring from November 2016 until May 2017, an average of Four observations per year. Then the monitoring measurements were processed using the least square error method, alignment of the circle and (Fitting of circles), then the data was processed and the slope was calculated using the Matlab program with the great development of computer specifications and programming languages. Problems correcting geodetic networks is possible and easy. Therefore, we relied in calculating the corrections values on Matlab program, where we programmed the mathematical laws in a formula that suits the program, where observations were entered and corrections were made, and the corrected values were calculated and the amount of error

between the observed and calculated values. Where the slope was between (0.720 to 0.759) m during the observation period, and by using Auto CAD program and the 3D MAX program, the mast was drawn with a two- and three-dimensional design.

١- أهداف البحث

حيث يهدف البحث هذا الى حساب الميل العمودي الحاصل بسارية العلم العراقي في بوابة جامعة بغداد وانتاج موديل 3D للسارية وحساب احداثياتها وفق الخطوات التالية:-

١. اختيار خط القاعدة (Base line) لتحديد موقع الرصد المثالي بعد عملية الاستطلاع لسارية.
٢. قياس الاحداثيات 3D المحلية من النقطة المرجعية (OCC) الاولى والثانية في جامعة بغداد بمساعدة جهاز Total Station نوع Topcon 105.
٣. تم توزيع النقاط المرصودة على السارية على شكل دوائر من خطي القاعدة التي تم تحديدهم مسبقا حيث تم تثبيت موقع هذه الدوائر بمعدل ست دوائر من اسفل القاعدة الى اعلى نقطة بالسارية حيث تم رصد السارية بمعدل اربع مرات دورية وبين رصد اخرى شهرين تقريبا لمراقبة التغيرات التي تحدث في الزحف ونتائج الرصدات الاربعه في ٢٠١٦ وكذلك في ٢٠١٧.
٤. ومن ثم تم استخدام لغة (Matlab) لتكوين برنامج خاص لحساب مقدار الزحف العمود لسارية العلم العراقي .
٥. رسم سارية العلم بنموذج ثلاثي الابعاد 3D باستخدام برنامج الاوتوكاد بمنظر امامي (Front view) وكذلك باستخدام برنامج 3D MAX .

٢- المقدمة

جامعة بغداد وهي اكبر الجامعات العراقية، تقع في وسط العاصمة العراقية بغداد. تم تأسيسها وتمويلها من قبل الحكومة العراقية في أواخر الخمسينيات. أقترن اسم جامعة بغداد بتاريخ بغداد وحضارتها، وصارت احدى معالم هذه المدينة. لقد اثبتت جامعة بغداد منذ تأسيسها ولحد اليوم إنها الركن الأساسي والفعال للبناء والتقدم والتطور في هذا البلد وكان ذلك واضحا وجليا من خلال ما ساهمت به من رفد لجميع مدارس ومعاهد وكليات العراق بالأساتذة والمختصين والتربويين الذين قادوا المسيرة العلمية لسنوات طويلة ولا زالوا. ويحق لنا أن نفخر بما حققته هذه الجامعة التي أغنت حركة البحث العلمي والأكاديمي وكان لها الدور المتميز في كل مجال من مجالات البناء والتطور .

تعتبر سارية علم جامعة بغداد بأنها أعلى ساريه علم في العراق، ليصل ارتفاع ساريه العلم العراقي الى أكثر من 75 متر في العاصمة بغداد قرب بوابة الجامعة الشهيرة وبعده فتره من افتتاح السارية ومن خلال الصور لوحظ ان هناك انحراف واضح في السارية.



الشكل (١) يبين سارية العلم العراقي في بوابة جامعة بغداد.

٣- أسلوب التصحيح بأقل المربعات Lease Square

هي مجموعة من المعادلات التي توجد فيها مجهولين او اكثر ، حيث ان "lease square" تعني أن الحل الشامل يقلل من مجموع مربعات الأخطاء التي ارتكبت في نتائج كل معادلة واحدة اي القيام بالتعديل على البيانات او النتائج النهائية بسبب وجود اخطاء عشوائية عند عملية الرصد فيما يزيد في دقة النتائج النهائية. تم تقديم طريقة اقل المربعات و تطبيقها في العديد من الحقول العلمية و الهندسية التي تطورت أخيراً مع ظهور الحاسبات الالكترونية و مع تطور جبر المصفوفات و مع ربطها مع المفاهيم الإحصائية.

[1]

قبل التخطيط للرصد يجب وضع نموذج رياضي عام للمسألة التي ستجمع كلا من الارصادات n و المجاهيل u و العلاقة بينهما. ولا بد من أن نعلم إن هناك دوماً اقل عدد من الارصادات المستقلة عن بعضها

يلزم لحل المسألة n_0 و متى ما كانت n اكبر من n_0 فذلك يعني فائضا في القياسات و الذي يرمز له r الذي يكافئ في الإحصاء ما يسمى بدرجة الحرية degree of freedom حيث: [2]

$$r = n - n_0 \dots\dots\dots (1)$$

نظريا فأن حل مسألة رياضية يتم بقياس كميات معينة في المعادلات و هذه الكميات المقیسة يجب أن تكون كافية لتسمح لنا بالحل للمجاهيل المتبقية في المعادلة.

في مسائل المساحة تكون الأرصادات في اغلب الأحيان فائضة خصوصا في الشبكات الجيودسية و المسح التصويري [3].

١-٣ موائمة الخطوط Fitting

ان تركيب الخطوط او المنحنيات او الدائرة لمجموعة من نقاط البيانات هي مشكلة قديمة كان الدافع وراها كمية كبيرة من التكرار في كثير من الأحيان في مختلف المجالات.

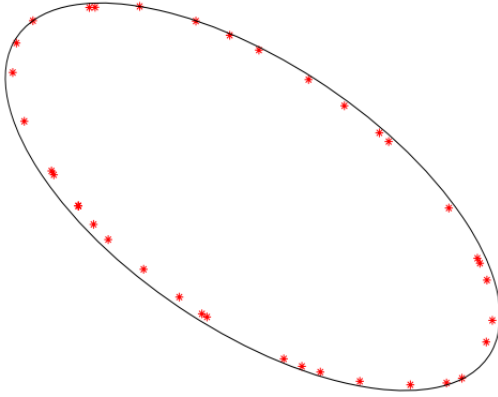
عموما، فإن تركيب الملامح الهندسية لإعطاء $D^2 / 3D$ هو المطلوب من النقاط في مختلف مجالات العلوم والهندسة: علم الفلك، والفيزياء، وعلم الأحياء، والجودة السيطرة، ومعالجة الصور والمقاييس وما إلى ذلك [4].

٢-٣ موائمة الدائرة :

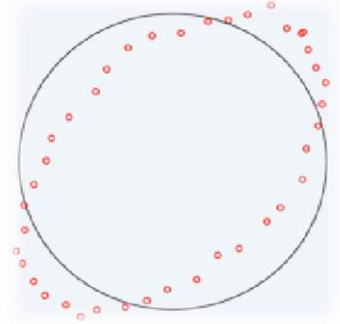
هو محاولة العثور على افضل موائمة للدائرة لمجموعة من النقاط البيانات $2D$ ، وقد تبرز احيانا مسألة موائمة دائرة في بعض التطبيقات المساحية او الهندسية حيث تتبع نفس الاسلوب المتبع مع مسألة موائمة خط مستقيم والمنحنيات باستخدام طريقة اقل المربعات [5].

بالنموذج العام كما تم ذكرها سابقا حيث تعتبر احداثيات النقاط هي الارصادات في المسألة بينما تعتبر معاملات الدائرة (احداثيات المركز ونصف قطرها) هي المجاهيل .

على سبيل المثال مجموعة من $D^2 (y, x)$ النقاط التي كُتبت ولكن لا يقترب بدقة دائرة. ثم هناك نقطة مركز ونصف قطر التي تمثل أفضل دائرة يطابق نقطة. وبالتمثل لخط: يمكن الحصول على التدرج واعتراض المحور y ، والقطع الناقص المركز، المحاور الرئيسية والثانوية والتناوب فهو يعتبر مسقط الدائرة ويكون أفضل لتركيب الأشكال لها استخدامات في مجال الهندسة والمساحة والهندسة الحاسوبية. وافضل حل لاعادة الدائرة او الشكل البيضوي ليكون قريب من الدقه هو باستخدام طريقة least squares [6].



الشكل (3) يمثل موائمة البيضاوي



الشكل (2) يمثل موائمة الدائرة

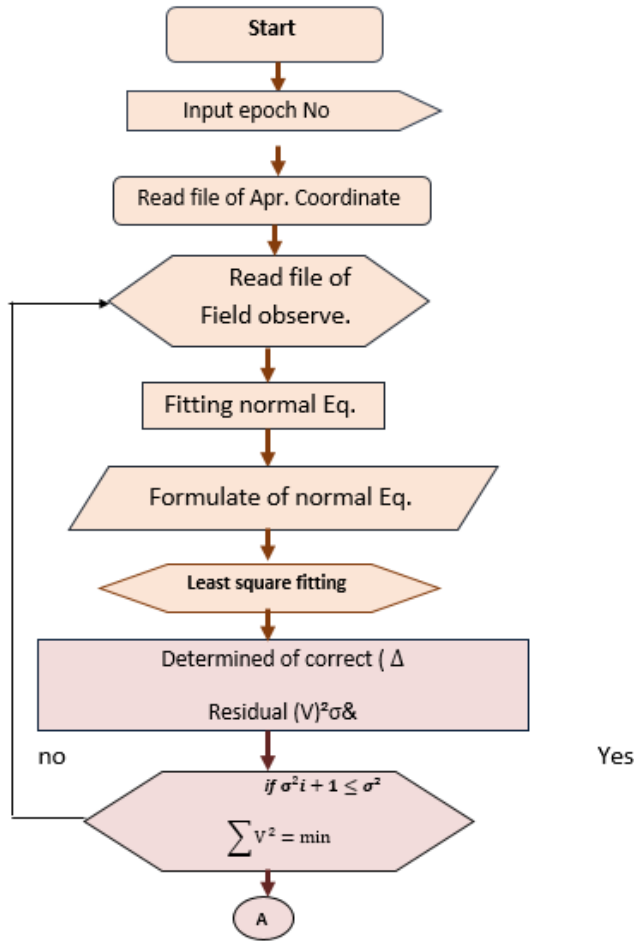
٤- برنامج الـ MatLab

هو برنامج عملاق بما تعنيه الكلمة و يستخدم في الحسابات الرياضية و الهندسية بشكل متقدم .

هو برنامج هندسي وله مجالات اخرى غير هندسيه يقوم بعمليات تحليل وتمثيل البيانات من خلال معالجة تلك البيانات تبعا لقاعدة البيانات الخاصة به ، فمثلا يستطيع البرنامج عمل التفاضل والتكامل وكذلك المعادلات التفاضلية ذات الرتب العليا والتي تكون معقدة جدا ، ليس فقط ذلك بل يستطيع البرنامج عمل التفاصيل الجزئي، ويقوم بعمل عمليات الكسر الجزئي بسهولة ويسر والتي تستلزم وقتا كبيرا لعملها بالطرق التقليدية هذا من الناحية الاكاديمية ، اما من ناحية التطبيقية فيستطيع البرنامج العمل في جميع المجالات الهندسية مثل أنظمة التحكم control system ، وفي مجال الميكانيك Mechanical field، وصناعة السيارات وكذلك مجال الطيران والدفاع الجوي وكذلك الكثير من التطبيقات الهندسية [7].

٤-١ التطبيقات الهندسية .

مع التطور الكبير لمواصفات الحواسيب واللغات البرمجية تطور علم تصحيح القياسات واصبح استخدامه في حل مسائل تصحيح الشبكات الجيودسية امرا ممكنا ويسيرا. لذلك اعتمدنا في حساب قيم التصحيحات على برنامج Matlab حيث قمنا ببرمجة القوانين الرياضية بالصيغة التي تلائم البرنامج ، حيث تم ادخال الارصادات واجراء التصحيحات عليها وحساب القيم المصححة ومقدار الخطأ بين القيم المرصودة والمحسوبة. [8]



الشكل (٣) يمثل مخطط للبرنامج بطريقة الماتلاب

٢-٤ برنامج AutoCAD

البرنامج يحقق للمستخدم التنقل من تخيل التصميم الى تنفيذه ، بالإضافة الى اجراء التعديلات للوصول الى التصميم المطلوب. يستطيع المستخدم انشاء وعمل تصميم ثلاثي الابعاد بطريقة سهلة ومبسطة ، حيث تكون البداية هي تصميم تخيلي للمشروع ثنائي الابعاد ومن ثم تطويره الى تصميم ثلاثي الابعاد. ويتميز بسهولة استخدام البرنامج ، سهولة الرسم ،سهولة التعديل ، تعدد الاصدارات التي تناسب pc او laptop مع ان الاساسيات من اوامر الرسم والتعديل ثابتة مع الاختلاف في الواجهة وبعض الاوامر الاضافية، سهولة حصر الكميات واستخراج المعلومات ، امكانية عمل ملفات نموذجية لتوفير الوقت والجهد ، عمل بلوكات يمكن حفظها لتوفير الوقت ، رسم الرسومات بدقة ، وكذلك يعتبر البرنامج مرآة لافكار وخيال وتصور

المهندس حيث يقوم بزيادة من قدرات المبدعين والمصممين، واطهار موهبتهم في فن التصميم الذي يتحقق من خلال الابعاد الثلاثية. (AutoCAD Exchange Apps) [9]

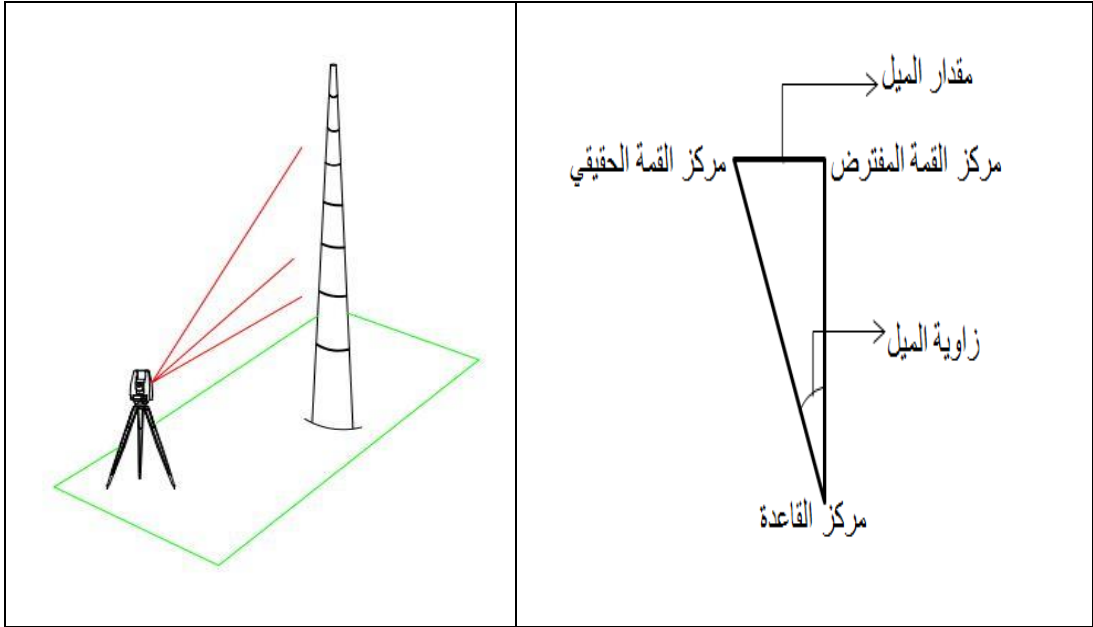
٣-٤ برنامج الـ 3DS MAX

هو إحدى أقوى برامج التصميم الهندسي ثلاثية الأبعاد، قامت بإنشائه شركة Autodesk، يقوم البرنامج على إيجاد بيئة للعمل على أرض واسعة وإنشاء صور كما يتخيّلها المصمّم وتحريكها من منظورٍ ثلاثي كبناء عمارات أو إنشاء سيارات أو أيّ صورةٍ تطرأ في خيال المصمّم، ومن ثم يتمّ التعديل عليها بواسطة الأدوات المتاحة بالبرنامج ويتم إضافة المتريال لإعطاء الصّور إنطباعاً بأنّها حقيقةً وليست تصميماً هندسياً بالغ الإحتراف، ومن ثمّ يضع المصمّم بعض التأثيرات الخارجيّة كالإضاءة الطّبيعية أو الصناعيّة وغيرها من المؤثرات حتّى يطابق تصميمه الواقع وتأتي في المرحلة النهائيّة مرحلة عرض التصميم بصورة ثلاثية الأبعاد (3 DS MAX) [10].

٥- منطقة الدراسة

تعتبر سارية علم جامعة بغداد بأنها أعلى ساريه علم في العراق، ليصل ارتفاع ساريه العلم العراقي الى اكثر من 75 متر في العاصمة بغداد قرب بوابة الجامعة الشهيرة وبعده فتره من افتتاح السارية ومن خلال الصور لوحظ ان هناك انحراف واضح في السارية. تم في هذه البحث مراقبة السارية لمدة سنتين حيث قسمت الى حلقات دائرية وتم تحديد المسح الحقلي من خلال استخدام جهاز المحطات المتكاملة حيث تم الرصد بمعدل اربعة رصدات في العام الواحد وباستخدام معادلات التصحيح (موائمة الدائرة Fitting of circles) وباستخدام طريقة اقل المربعات بالنموذج العام حيث تعتبر احداثيات النقاط هي الارصدات بينما تعتبر معاملات الدائرة (احداثيات المركز ونصف القطرها) هي المجاهيل. تم البدء في العمل الحقلي (الرصد الاولي) في يوم 2014 - 5 - 10 استخدم فيه جهاز (total station) من الجيل الحديث لتوزيع نقاط الضبط الرضي بطريقة الـ Closed Traverse لكي يتم رصد جميع بدن السارية وعمل تقييم لدقة العمل. حيث تم وضع استراتيجية خاصة لضمان الحصول على نتائج دقيقة لاغراض المراقبة خلال فترة تنفيذ البحث وتنفيذها حقليا وبنجاح لضمان مواصفات الدقة التي تفي بمتطلبات البحث والتي تتمثل بتنشيت نقاط ضبط تحيط بالسارية ويمكن من خلالها اجراء قياسات لنقاط منتخبة على بدن السارية بحيث تكون كل مجموعة ترصد على حلقة كاملة بحيث تكون على شكل دائري. ثم تجري عملية تصحيح هذه القياسات فيما بعد مكثيا بالاعتماد على نظرية الـ least squares (موائمة موائمة Fitting). من هذا الاسلوب

بالرصد هو ايجاد احداثيات مركز كل حلقة من السارية وعلى ارتفاعات مختلفة من (Centre line) والتي تشكل بدورها مركز كل حلقة كما موضح في الشكل (٤)



الشكل (٤) يمثل أسلوب الرصد باستخدام جهاز (Total Station) لكل حلقة من السارية.

بعد معرفة احداثيات مركز وقاعدة السارية يمكن حساب الميل واتجاهه وبالاعتماد على المعادلات الرياضية في ادناه:

$$1(x - x_o)^2 + (y - y_o)^2 - r_o = 0 \dots\dots\dots(1)$$

$$((xi + vxi) - (x_o))^2 + ((yi + vyi) - (y_o))^2 - ro^2 = 0 \dots\dots\dots(2)$$

بحيث ستكون المعادلات الارصادية بالنموذج العام بالشكل التالي

$$\dots\dots\dots(3) \dots\dots\dots Av + B\Delta$$

حيث ستكون قيمة المشتقات المكونة لعنصر المصفوفتين في السطر الاول بالشكل التالي.[11]

$$\frac{\partial f_1}{\partial x_1} = 2(x_1 - x_o) \dots\dots\dots(4)$$

$$\frac{\partial f_1}{\partial y_1} = 2(y_1 - y_c^0) \dots \dots \dots (5)$$

$$\frac{\partial f_1}{\partial x_c} = -2(x_1 - x_c^0) \dots \dots \dots (6)$$

$$\frac{\partial f_1}{\partial y_c} = -2(y_1 - y_c^0) \dots \dots \dots (5)$$

$$\frac{\partial f_1}{\partial r} = -2r^0 \dots \dots \dots (6)$$

وهكذا بالنسبة لباقي المشتقات حيث تتغير فقط احداثيات النقطة المعنية.

ومن هنا بدأت فكرة البحث لحساب هذا الزحف العمودي (الميل) وهل هو انحراف ثابت بسبب الاعمال المدنية و الانشائية للسارية او هو انحراف مستمر بسبب عدم ثبات قاعدة السارية بسبب ارتفاعها. وبالتالي تؤدي الى سقوطها مسببه حوادث بشرية وماديه كبيره لانها عند مدخل الجامعة. وبما ان السارية هي عبار عن اسطوانة مقسمة الى 7 حلقات تم اخذ عدة ارصادات لحساب احداثياتها من القاعده الى القمة و لفترات زمنيه متفاوتة بجهاز (TOTAL- STATION) و بوجود الراية مره و بعدم وجودها مره اخرى ومن خلال هذه الارصادات و بالاعتماد على نصف القطر يتم معرفة مقدار الانحراف

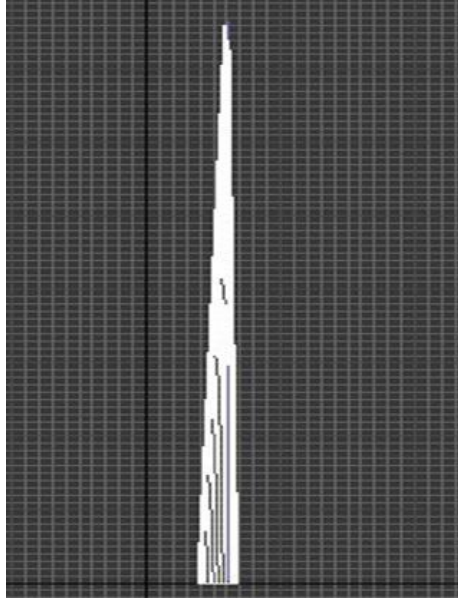
الجدول (١) يمثل حساب الانحراف العمودي لسارية العلم في جامعة بغداد لعام ٢٠١٦

الانحراف العمودي لسارية (m)	اتجاه الميل	نصف قطر الحلقة العليا لسارية (m)	نصف قطر الحلقة الارضية لسارية (m)	فرق الارتفاع (m)	زمن الرصده
0.720	34°44'23"	0.138	0.615	70.650	شهر ايلول
0.756	34°44'32"	0.138	0.615	70.650	كانون الاول
0.742	34°44'29"	0.138	0.615	70.650	شهر اذار
0.725	34°44'24"	0.138	0.615	70.650	شهر حزيران
0.710	34°44'20"	0.138	0.615	70.650	شهر اب بدون الراية

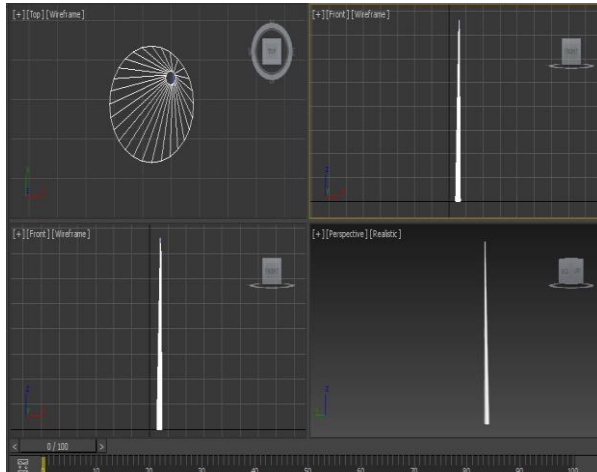
الجدول (٢) يمثل حساب الانحراف العمودي لسارية العلم في جامعة بغداد لعام ٢٠١٧

الانحراف العمودي لسارية (m)	اتجاه الميل	نصف قطر الحلقة العليا لسارية (m)	نصف قطر الحلقة الارضية لسارية (m)	فرق الارتفاع (m)	زمن الرصده
0.725	34°44'24"	0.138	0.615	70.650	شهر ايلول
0.759	34°44'27"	0.138	0.615	70.650	كانون الاول
0.745	34°44'26"	0.138	0.615	70.650	شهر اذار
0.732	34°44'24"	0.138	0.615	70.650	شهر حزيران
0.713	34°44'20"	0.138	0.615	70.650	شهر اب بدون الراية

واخيرا تم رسم سارية العلم بنموذج ثلاثي الابعاد 3D باستخدام برنامج الاوتوكاد بمنظر امامي (Front view) وكذلك باستخدام برنامج 3D MAX كما موضح في الشكل.



الشكل (5) يوضح رسم سارية العلم 3D باستخدام برنامج ال Auto Cad



الشكل (6) يوضح رسم سارية العلم 3D باستخدام برنامج 3D MAX

٦- الاستنتاجات

- تمت الرصدة الاولى في شهر ايلول لسنة ٢٠١٦ باستخدام جهاز المحطات المتكاملة (Total Station) حيث كان مقدار الميل (0.720 m) وهذا الميل كبير بالنسبة للسارية التي لم يمر على افتتاحها فترة طويلة.
- ان مقدار الميل خلال شهر ايلول الى شهر كانون الاول أي مايقارب ثلاثة اشهر وجد ان الميل يتراوح ما بين (0.720 الى 0.756) كما في الجدول رقم (١) قد يكون السبب ان قطر الجزء العلوي للسارية الذي يبلغ حوالي (١٤ cm) اجده لا يتناسب مع ارتفاع السارية حيث توجد حركة اهتزازية واضحة بسبب وجود رياح في هذه الفترة من السنة وخاصة عند الحلقة الاخيرة من السارية.
- ان مقدار الميل خلال شهر اذار الى شهر حزيران أي مايقارب ثلاثة اشهر وجد ان الميل يتراوح ما بين (0.742 الى 0.725) كما في الجدول رقم (١) نلاحظ ان الميل تناقص وهذا يرجع الى سكون الجو وقلة الرياح في هذه الفترة من السنة .
- اما الرصدة في شهر اب فكانت بدون وجود الراية التي تمثل العلم العراقي فلقد تم اختيار هذا الشهر من اجل ان تكون السماء صافية والرياح قليلة نسبيا وكذلك معرفة تأثير حجم الراية على السارية فلقد وجد ان مقدار الزحف هو (0.710m) كما في الجدول رقم (١) وهذا يمثل الميل الحقيقي للسارية لسنة ٢٠١٦.
- اما الرصدات التي تمت خلال فترة سنة ٢٠١٧ فلقد وجد ان الرصدة في شهر ايلول وشهر كانون الاول هي (0.725 , 0.759) حيث نلاحظ ان الميل زاد مع وجود راية العلم العراقي.
- اما الرصدات في شهر اذار وحزيران فكانت كالتالي (0.745 و 0.732) كما في الجدول رقم (٢) وهذه النتائج متقاربة من سنة ٢٠١٦ في نفس الاشهر وهذا مؤشر يدل على ثبات الميل للسارية خلال هذه الفترة.
- اما الرصدة في شهر اب لسنة ٢٠١٧ فكانت بدون وجود الراية التي تمثل العلم العراقي فلقد وجد ان مقدار الزحف هو (0.713m) كما في الجدول رقم (٢) وهذا دليل واضح على ثبات الميل خلال فترة الرصد من سنة ٢٠١٦ الى اخر صدة من سنة ٢٠١٧ وقد يرجع الميل الى حدوث خلل خلال عملية نصب السارية بسبب ارتفاعها العالي وعدم تجانس

اقطارها من القاعدة السفلى التي نصف قطرها حوالي (0.62cm) الى النصف قطر القمة التي هي حوالي (0.14cm).

- استخدام برنامج التصحيح باستخدام موائمة الدائرة من اجل تصحيح النقاط من خلال استخدام برنامج الماتلاب التي من خلالها تم الحصول على النتائج الموجودة في الجداول السابقة التي من خلالها تم احتساب الميل واتجاه الحركة للسارية.
- استخدام برنامج Auto Cad و برنامج 3D MAX لرسم سارية العلم بتقنية الرسم المجسم 3D يوضح شكل الراية والحلقات التي تم الرصد عليها كما في الشكل (5) و الشكل (6).

٧- التوصيات

- ١- الاستمرارية في رصد السارية او مراقبة السارية وذلك لمعرفة هل الميل ثابت ام زيادة في الميل وذلك لما في الموضوع من خطورة من الناحية الهندسية ومايسببها من خسائر واضرار مادية وبشرية ان حدث أي مكروه.
- ٢- استخدام تقنيات اخرى وحديثة اضافة الى جهاز { total station } بحيث يمكن الدمج بين المسح الارضي والمسح التصويري باستخدام جهاز الليزر سكان في عملية الرصد.

٨- المصادر

- 1- Barry, f. Kavanagh, "Surveying Principles and Applications", sixth Upper Saddle River, New Jersey Columbus, Ohio, 2003.
- 2- Bjerhamer, A., "Theory of Errors and Generalized Matrix inverses "1st edition" Elsevier Scientific publishing company Amsterdam-London
- 3- Bomford, G. "Survey adjustments and least squares", 3rd edition, Oxford, (1971).
- 4- Davis, R. D., Foote, F. S., Anderson, J. M. and Mikhail, E. M. , "Surveying Theory and practice", 6th edition, Mc Graw-Hill Book company, (1981).
- 5- Hume, F. Rainsford, "Surveying Adjustment and least Squares", 3rd edition London, (1979).
- 6- Mikhail, E. M., "Observations and Least Squares", 3st edition, Donnelly publisher, New York, (2000).

- 7- Moffitt, F. H. and Bourchard, H., "Surveying". 7th edition, Harper and row, publisher, New York, (1987).
- 8- Topcon Flexline TS02/06/09. (2008). topcon Geosystems. See datasheet for model ES 105 (PDF). Retrieved 27 August 2010
- 9- Wolf, P. R., "Adjustment Computation", Second Edition, P.B.L. Publishing Co., Monona, Wisconsin, 1980.
- 10- Yousif, h. kh., " Displacement Computation of Mosul dam by using Free Geodetic Network Adjustment" M.Sc. thesis, college of Engineering, University of Baghdad, Department of Surveying Engineering, 2009.
- 11- بشار سليم عباس " تصحيح القياسات في المساحة بين النظرية والتطبيق " الطبعة الاولى ٢٠١٠

